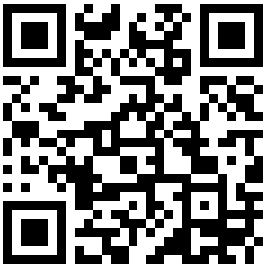

DISTRIBUTED BY:

NTIS

National Technical Information Service
U. S. DEPARTMENT OF COMMERCE
5285 Port Royal Road, Springfield Va. 22151

This document has been approved for public release and sale.

NOTICE: When government or other drawings, specifications or other data are used for any purpose other than in connection with a definitely related government procurement operation, the U. S. Government thereby incurs no responsibility, nor any obligation whatsoever; and the fact that the Government may have formulated, furnished, or in any way supplied the said drawings, specifications, or other data is not to be regarded by implication or otherwise as in any manner licensing the holder or any other person or corporation, or conveying any rights or permission to manufacture, use or sell any patented invention that may in any way be related thereto.

THE BEHAVIOR OF SAND IN ONE-DIMENSIONAL COMPRESSION

Interim Report

October 1963

TECHNICAL DOCUMENTARY REPORT NO. RTD-TDR-63-3089

Research and Technology Division
Air Force Systems Command
AIR FORCE WEAPONS LABORATORY
Kirtland Air Force Base
New Mexico

This research has been funded by the Defense Atomic Support Agency under WEB No. 13.144

Project No. 1080, Task No. 108007

(Prepared under Contract AF 29(601)-5817 by Alfred J. Hendron, Jr., The Department of Civil Engineering, University of Illinois, Urbana, Illinois)

Research and Technology Division
Air Force Systems Command
AIR FORCE WEAPONS LABORATORY
Kirtland Air Force Base
New Mexico

When Government drawings, specifications, or other data are used for any purpose other than in connection with a definitely related Government procurement operation, the United States Government thereby incurs no responsibility nor any obligation whatsoever; and the fact that the Government may have formulated, furnished, or in any way supplied the said drawings, specifications, or other data, is not to be regarded by implication or otherwise as in any manner licensing the holder or any other person or corporation, or conveying any rights or permission to manufacture, use, or sell any patented invention that may in any way be related thereto.

This report is made available for study upon the understanding that the Government's proprietary interests in and relating thereto shall not be impaired. In case of apparent conflict between the Government's proprietary interests and those of others, notify the Staff Judge Advocate, Air Force Systems Command, Andrews AF Base, Washington 25, DC.

This report is published for the exchange and stimulation of ideas; it does not necessarily express the intent or policy of any higher headquarters.

Qualified requesters may obtain copies of this report from DDC. Orders will be expedited if placed through the librarian or other staff member designated to request and receive documents from DDC.

ABSTRACT

The behavior of sand in one-dimensional compression is investigated with both theoretical and experimental studies. The phenomenological aspects of one-dimensional behavior are discussed, such as stress-strain characteristics, energy absorption capacity, and coefficient of earth pressure at rest.

The analytical study deals with the stress-strain relations of an idealized granular medium composed of elastic, equi-radii spheres in a face-centered cubic array. A new solution is derived for the behavior of the array when subjected to a monotonically increasing axial compressive stress for the condition of zero radial strain.

An experimental device is described which is capable of measuring the radial stresses developed in high-pressure, one-dimensional tests. Measurements of both the coefficient of earth pressure at rest and the stress-strain properties are presented for four sands tested to an axial stress of 5,290 psi. Correlations are presented which compare the actual behavior of a rounded, uniform, quartz sand in one-dimensional and triaxial compression with the behavior suggested by the theoretical analysis.

PUBLICATION REVIEW

This report has been reviewed and is approved.

Harry E. Auld
HARRY E. AULD
Capt USAF
Project Officer

Thomas J. Lowry Jr.
THOMAS J. LOWRY, JR.
Col USAF
Chief, Structures Branch

Perry L. Hule
PERRY L. HULE
Col USAF
Chief, Research Division

CONTENTS

	Page
ABSTRACT	i
LIST OF TABLES	v
LIST OF FIGURES	vi
NOTATION	xii
CHAPTER	
1. INTRODUCTION	1
1.1 Statement of Problem	1
1.2 Objectives of Study	2
1.3 Scope	3
2. SUMMARY OF PREVIOUS WORK	5
2.1 General	5
2.2 Theories of Granular Media	5
2.3 Experimental Results	7
3. THEORETICAL APPROACH FOR PREDICTING THE STRESS-STRAIN BEHAVIOR OF AN IDEALIZED GRANULAR MEDIUM	12
3.1 General	12
3.2 The Duffy-Mindlin Theory of Granular Media	13
3.3 One-Dimensional Theory of Granular Media	21
3.4 Equivalent Discrete Mass Model for One-Dimensional Static and Dynamic Behavior	32
3.5 Theoretical Relationship Between the Angle of Internal Friction, Coefficient of Earth Pressure at Rest, and the Coefficient of Friction Between Spheres for a Face-Centered Cubic Array of Uniform Spheres	34
4. THE DEVELOPMENT OF A SPECIAL, HIGH PRESSURE, ONE-DIMENSIONAL COMPRESSION APPARATUS	39
4.1 General	39
4.2 Experimental Apparatus	40
5. EXPERIMENTAL RESULTS	50
5.1 General	50
5.2 Description of Sands	50
5.3 Preparation of Test Specimens	52

	Page
5.4 Experimental Procedure	54
5.5 Test Results	56
6. INTERPRETATION AND DISCUSSION OF EXPERIMENTAL RESULTS	57
6.1 General	57
6.2 Axial Stress-Strain Relationships	57
6.3 The Coefficient of Earth Pressure at Rest	63
6.4 Energy Absorption	69
6.5 General High Pressure Behavior Indicated by Tests on Pennsylvania Sand	72
6.6 Correlation of Experimental Results with the Theory of Granular Media	74
7. SUMMARY AND CONCLUSIONS	79
7.1 Summary	79
7.2 Conclusions	80
7.3 Suggestions for Further Research	88
REFERENCES	90
TABLES	95
FIGURES	99
APPENDIX A - APPLICATION OF THE HERTZ THEORY TO THE BEHAVIOR OF A GRANULAR MEDIUM	266
APPENDIX B - TRIAXIAL TESTS	276
APPENDIX C - EVALUATION OF RING FRICTION	282
DISTRIBUTION	286

LIST OF TABLES

Table No.		Page
3.1	VARIATION OF STRESS AND STRAIN INVARIANTS	95
3.2	EFFECT OF THE COEFFICIENT OF FRICTION ON ONE-DIMENSIONAL STRESS-STRAIN BEHAVIOR OF A FACE-CENTERED ARRAY OF SPHERES	96
6.1	ENERGY LOSSES FOR REPEATED LOADINGS ON MINNESOTA SAND	97
6.2	CORRELATION OF THE COEFFICIENT OF FRICTION, THE COEFFICIENT OF EARTH PRESSURE AT REST AND THE ENERGY ABSORPTION CAPACITY OF A GRANULAR MEDIUM	98

LIST OF FIGURES

Figure No.		Page
1.1	AXIAL STRESS STRAIN CURVES FOR SOIL SUBJECTED TO VARIOUS STATES OF STRESS	99
3.1	CONSTRUCTION OF DENSEST PACKING OF EQUAL SPHERES	100
3.2	TWO SPHERES IN NORMAL CONTACT	101
3.3	DISTRIBUTION OF NORMAL (σ) AND TANGENTIAL (τ) COMPONENTS OF STRESS ON THE CONTACT SURFACE OF TWO LIKE SPHERES SUBJECTED TO A NORMAL FORCE FOLLOWED BY A MONOTONIC TANGENTIAL FORCE	102
3.4	UNIT CUBE OF A FACE-CENTERED CUBIC ARRAY OF EQUAL SPHERES SUBJECTED TO INCREMENT FORCES	103
3.5	FORCES ACTING ON A TYPICAL SPHERE OF A FACE-CENTERED ARRAY	104
3.6	FORCES ACTING ON AN OCTANT OF A SPHERE	105
3.7	COMPONENTS OF FORCE AT A CONTACT AND CORRESPONDING COMPONENTS OF DISPLACEMENT OF THE CENTER OF A SPHERE	106
3.8	VARIATION OF FIRST STRESS INVARIANT WITH FIRST STRAIN INVARIANT	107
3.9	UNIT CUBE OF A FACE-CENTERED CUBIC ARRAY OF EQUAL SPHERES SUBJECTED TO INCREMENTAL FORCES IN ONE-DIMENSIONAL COMPRESSION	108
3.10	FORCES ACTING ON A TYPICAL SPHERE SUBJECTED TO ONE-DIMENSIONAL COMPRESSION	109
3.11	VARIATION OF CONTACT STRESSES UNDER ONE-DIMENSIONAL BEHAVIOR WITH AN INITIAL HYDROSTATIC STRESS	110
3.12	STRESS STRAIN CURVES FOR A FACE-CENTERED ARRAY OF SPHERES SUBJECTED TO HYDROSTATIC AND ONE-DIMENSIONAL STATES OF STRESS	111
3.13	SCHEMATIC REPRESENTATION OF THE DIRECTION OF THE CONTACT FORCES WHEN LOADING AND UNLOADING UNDER ONE-DIMENSIONAL COMPRESSION	112

3.14	LOADING AND UNLOADING ONE-DIMENSIONAL STRESS STRAIN CURVE FOR A FACE-CENTERED ARRAY OF SPHERES	113
3.15	ONE-DIMENSIONAL HORIZONTAL SAND MODEL	114
3.16	ONE-DIMENSIONAL VERTICAL SAND MODEL	115
3.17	A GRANULAR MEDIUM WITH AN INITIAL CONFINING STRESS, σ_o, SUBJECTED TO A STRESS DIFFERENCE σ_{zz}	116
3.18	THEORETICAL VARIATION OF K_o WITH SIN ϕ FOR A FACE-CENTERED CUBIC ARRAY COMPARED WITH A RELATION SUGGESTED FOR SAND BY JAKY	117
4.1	THE EFFECT OF LATERAL MOTION ON THE RATIO OF HORIZONTAL TO VERTICAL PRESSURE	118
4.2	SCHEMATIC CROSS-SECTION THROUGH TESTING APPARATUS	119
4.3	PHOTOGRAPHS OF APPARATUS COMPONENTS	120
4.4	PHOTOGRAPHS OF APPARATUS COMPONENTS	121
4.5	FULL SCALE CROSS-SECTION THROUGH THE ONE-DIMENSIONAL COMPRESSION APPARATUS	123
4.6	FULL SCALE CROSS-SECTION OF THE THIN STEEL RING	125
4.7	FULL SCALE CROSS-SECTION OF THE OUTER THICK-WALLED CYLINDER	127
4.8	FULL SCALE CROSS-SECTION OF THE BASE PLATE	128
4.9	PHOTOGRAPHS OF COMPONENT PARTS AND APPARATUS ASSEMBLED FOR TESTING	129
4.10	SCHEMATIC DIAGRAM ILLUSTRATING THE EFFECT OF SIDE FRICTION IN ONE-DIMENSIONAL COMPRESSION	130
4.11	SCHEMATIC CROSS-SECTION THROUGH TESTING APPARATUS DURING CALIBRATION	131
4.12	CALIBRATION CURVE FOR THE EFFECT OF OIL PRESSURE ON THE METALFILM STRAIN GAGES	132
4.13	CROSS-SECTION OF TESTING HEAD	133
4.14	PHOTOGRAPH OF ONE-DIMENSIONAL COMPRESSION APPARATUS ASSEMBLED FOR TESTING	134

5.1	GRAIN-SIZE DISTRIBUTION CURVES FOR SANDS INVESTIGATED	135
5.2	RELATIONSHIP BETWEEN THE ANGLE OF INTERNAL FRICTION AND INITIAL VOID RATIO FOR SANDS INVESTIGATED	136
5.3-5.22	STRESS STRAIN CURVE FOR MINNESOTA SAND IN ONE-DIMENSIONAL COMPRESSION	137-156
5.23-5.30	STRESS STRAIN CURVE FOR PENNSYLVANIA SAND IN ONE-DIMENSIONAL COMPRESSION	157-164
5.31-5.37	STRESS STRAIN CURVE FOR SANGAMON RIVER SAND IN ONE-DIMENSIONAL COMPRESSION	165-171
5.38-5.45	STRESS STRAIN CURVE FOR WABASH RIVER SAND IN ONE-DIMENSIONAL COMPRESSION	172-179
5.46-5.54	HORIZONTAL STRESS VS. VERTICAL STRESS FOR THE FIRST CYCLE OF LOADING OF MINNESOTA SAND IN ONE-DIMENSIONAL COMPRESSION	180-188
5.55-5.56	HORIZONTAL STRESS VS. VERTICAL STRESS FOR ONE AND ONE-HALF CYCLES OF LOADING OF MINNESOTA SAND IN ONE-DIMENSIONAL COMPRESSION	189-190
5.57-5.65	HORIZONTAL STRESS VS. VERTICAL STRESS FOR THE FIRST CYCLE OF LOADING OF MINNESOTA SAND IN ONE-DIMENSIONAL COMPRESSION	191-199
5.66-5.73	HORIZONTAL STRESS VS. VERTICAL STRESS FOR THE FIRST CYCLE OF LOADING OF PENNSYLVANIA SAND IN ONE-DIMENSIONAL COMPRESSION	200-207
5.74-5.80	HORIZONTAL STRESS VS. VERTICAL STRESS FOR THE FIRST CYCLE OF LOADING OF SANGAMON RIVER SAND IN ONE-DIMENSIONAL COMPRESSION	208-214
5.81-5.88	HORIZONTAL STRESS VS. VERTICAL STRESS FOR THE FIRST CYCLE OF LOADING OF WABASH RIVER SAND IN ONE-DIMENSIONAL COMPRESSION	215-222
6.1	STRESS STRAIN CURVES FOR MINNESOTA SAND IN ONE-DIMENSIONAL COMPRESSION	223
6.2	STRESS STRAIN CURVES FOR PENNSYLVANIA SAND IN ONE-DIMENSIONAL COMPRESSION	224
6.3	STRESS STRAIN CURVES FOR SANGAMON RIVER SAND IN ONE-DIMENSIONAL COMPRESSION	225

6.4	STRESS STRAIN CURVES FOR WABASH RIVER SAND IN ONE-DIMENSIONAL COMPRESSION	226
6.5	RELATIONSHIP BETWEEN CONSTRAINED MODULUS AND VERTICAL STRESS FOR MINNESOTA SAND IN ONE-DIMENSIONAL COMPRESSION	227
6.6	RELATIONSHIP BETWEEN CONSTRAINED MODULUS AND VERTICAL STRESS FOR PENNSYLVANIA SAND IN ONE-DIMENSIONAL COMPRESSION	228
6.7	RELATIONSHIP BETWEEN CONSTRAINED MODULUS AND VERTICAL STRESS FOR SANGAMON RIVER SAND IN ONE-DIMENSIONAL COMPRESSION	229
6.8	RELATIONSHIP BETWEEN CONSTRAINED MODULUS AND VERTICAL STRESS FOR WABASH RIVER SAND IN ONE-DIMENSIONAL COMPRESSION	230
6.9	RELATIONSHIP BETWEEN CONSTRAINED MODULUS AND VERTICAL STRESS AT CONSTANT RELATIVE DENSITY FOR THE FOUR SANDS TESTED IN ONE-DIMENSIONAL COMPRESSION	231
6.10	RELATIONSHIP BETWEEN CONSTRAINED MODULUS AND VERTICAL STRESS AT CONSTANT RELATIVE DENSITY FOR THE FOUR SANDS TESTED IN ONE-DIMENSIONAL COMPRESSION	232
6.11	RELATIONSHIP BETWEEN THE COEFFICIENT OF EARTH PRESSURE AT REST AND INITIAL VOID RATIO FOR MINNESOTA SAND	233
6.12	RELATIONSHIP BETWEEN THE COEFFICIENT OF EARTH PRESSURE AT REST AND INITIAL VOID RATIO FOR PENNSYLVANIA SAND	234
6.13	RELATIONSHIP BETWEEN THE COEFFICIENT OF EARTH PRESSURE AT REST AND INITIAL VOID RATIO FOR SANGAMON RIVER SAND	235
6.14	RELATIONSHIP BETWEEN THE COEFFICIENT OF EARTH PRESSURE AT REST AND INITIAL VOID RATIO FOR WABASH RIVER SAND	236
6.15	RELATIONSHIP BETWEEN THE COEFFICIENT OF EARTH PRESSURE AT REST AND THE ANGLE OF INTERNAL FRICTION FOR THE FOUR SANDS TESTED	237
6.16	RELATIONSHIP BETWEEN THE COEFFICIENT OF EARTH PRESSURE AT REST AND THE OVERCONSOLIDATION RATIO FOR MINNESOTA SAND	238

6.17	RELATIONSHIP BETWEEN THE COEFFICIENT OF EARTH PRESSURE AT REST AND THE OVERCONSOLIDATION RATIO FOR MINNESOTA SAND	239
6.18	RELATIONSHIP BETWEEN THE COEFFICIENT OF EARTH PRESSURE AT REST AND THE OVERCONSOLIDATION RATIO FOR PENNSYLVANIA SAND	240
6.19	RELATIONSHIP BETWEEN THE COEFFICIENT OF EARTH PRESSURE AT REST AND THE OVERCONSOLIDATION RATIO FOR SANGAMON RIVER SAND	241
6.20	RELATIONSHIP BETWEEN THE COEFFICIENT OF EARTH PRESSURE AT REST AND THE OVERCONSOLIDATION RATIO FOR WABASH RIVER SAND	242
6.21	RELATIONSHIP BETWEEN ENERGY ABSORPTION AND INITIAL RELATIVE DENSITY FOR MINNESOTA SAND	243
6.22	RELATIONSHIP BETWEEN ENERGY ABSORPTION AND INITIAL RELATIVE DENSITY FOR PENNSYLVANIA SAND	244
6.23	RELATIONSHIP BETWEEN ENERGY ABSORPTION AND INITIAL RELATIVE DENSITY FOR SANGAMON RIVER SAND	245
6.24	RELATIONSHIP BETWEEN ENERGY ABSORPTION AND INITIAL RELATIVE DENSITY FOR WABASH RIVER SAND	246
6.25	RELATIONSHIP BETWEEN ENERGY ABSORPTION IN THE FIRST CYCLE AND CONSTRAINED MODULUS AT MAXIMUM STRESS IN THE FIRST CYCLE FOR FOUR SANDS TESTED	247
6.26	RELATIONSHIP BETWEEN VERTICAL STRESS AND VOID RATIO FOR PENNSYLVANIA SAND IN ONE-DIMENSIONAL COMPRESSION	248
6.27	RELATIONSHIP BETWEEN VERTICAL STRESS AND VOID RATIO FOR PENNSYLVANIA SAND IN ONE-DIMENSIONAL COMPRESSION	249
6.28	VARIATION OF THE COEFFICIENT OF EARTH PRESSURE AT REST WITH VERTICAL STRESS FOR PENNSYLVANIA SAND	250
6.29	STRESS PATH FOR LOADING OF PENNSYLVANIA SAND IN ONE-DIMENSIONAL COMPRESSION	251
6.30	VARIATION OF THE OCTAHEDRAL SHEARING STRESS WITH THE MEAN PRINCIPAL STRESS FOR PENNSYLVANIA SAND IN ONE-DIMENSIONAL COMPRESSION	252

6.31-6.41	LOGARTHMIC PLOT OF STRESS STRAIN CURVE FOR MINNESOTA SAND IN ONE-DIMENSIONAL COMPRESSION	253-263
6.42	RELATIONSHIP BETWEEN CONSTRAINED MODULUS AND VERTICAL STRESS FOR MINNESOTA SAND IN ONE-DIMENSIONAL COMPRESSION	264
6.43	DILATATIONAL WAVE VELOCITY VERSUS CONFINING PRESSURE FOR OTTAWA SAND	265
A.1	TWO UNSTRESSED SPHERES IN CONTACT	274
A.2	SEGMENT OF A SPHERE TANGENT TO A PLANE	274
A.3	POINT LOAD ON AN INFINITE SURFACE	274
A.4	PLAN VIEW OF THE CONTACT SURVACE OF TWO SPHERES IN HERTZ CONTACT	275
B.1	TYPICAL STRESS STRAIN AND VOLUME CHANGE CURVES FOR TRIAXIAL TESTS ON WABASH RIVER SAND	278
B.2	RELATIONSHIP BETWEEN THE INITIAL TANGENT MODULUS AND CONFINING PRESSURE FOR WABASH RIVER SAND	279
B.3	MODIFIED MOHR-COULOMB DIAGRAM FOR TRIAXIAL TESTS ON WABASH RIVER SAND	280
B.4	RELATIONSHIP BETWEEN THE ANGLE OF INTERNAL FRICTION AND INITIAL VOID RATIO FOR SANDS INVESTIGATED	281
C.1	RELATIONSHIP BETWEEN MEASURED RING FRICTION LOAD AND APPLIED VERTICAL LOAD FOR MINNESOTA SAND	285

NOTATION

Symbol

A	=	constant of integration
a	=	radius of the circular area of contact between two spheres compressed by a normal force, N.
a_0	=	radius of contact between spheres in a face-centered cubic array subjected to a hydrostatic state of stress.
b	=	radius of the adhered portion of the circular area of contact between two spheres initially compressed by a normal force and subsequently subjected to a tangential force in the plane of contact.
C	=	$\frac{da}{dN}$, or the normal (Hertz) compliance for two spheres in contact.
C_0	=	$\frac{da}{dN_0}$, or the normal (Hertz) compliance for spheres in a face-centered cubic array subjected to a hydrostatic state of stress.
C_1	=	a shear strength parameter for a granular medium which is determined by the structural arrangement (relative density).
C_2	=	constant of proportionality in a theoretical relationship between the constrained tangent modulus and the applied axial stress for a face-centered cubic array in one-dimensional compression.
C_3	=	constant of proportionality in an empirical relationship which relates the constrained tangent modulus and the axial stress for sand in one-dimensional compression.
C_u	=	uniformity coefficient, $\frac{D_{60}}{D_{10}}$.
D_r	=	relative density, $\frac{e_{max} - e}{e_{max} - e_{min}}$.
D_{10}	=	the soil grain diameter of which 10 per cent of the soil weight is finer.
D_{60}	=	the soil grain diameter of which 60 per cent of the soil weight is finer.
E_1	=	energy input during loading in one-dimensional compression.
E_2	=	energy given up by the medium during unloading in one-dimensional compression.

e = void ratio

e_0 = initial void ratio

e_{max} = maximum void ratio

e_{min} = minimum void ratio

f = coefficient of static friction

g = acceleration of gravity

H = height of consolidometer ring

I_1 = first stress invariant

J_1 = first strain invariant

K_0 = coefficient of earth pressure at rest

K_2 = $\dfrac{1 - k_1 f}{k_1^{1/3}}$

K_3 = a shear strength parameter of a granular medium which is determined by the structural arrangement (relative density).

k_1 = $\dfrac{2 - \nu}{2(1 - \nu)}$

M_c = constrained tangent modulus

N = normal force between two spheres at the point of contact

N_0 = normal contact force between spheres in a face-centered cubic array subjected to a hydrostatic state of stress

N_1 = normal contact force between spheres in a face-centered cubic array which is perpendicular to the axis about which an axial symmetric load is applied

N_2 = normal contact force between spheres in a face-centered cubic array subjected to one-dimensional compression

N_{ij} = normal contact forces between spheres which are in the plane determined by the i and j axes.

P_H = horizontal force applied to a vertical face of a symmetrical cube from a face-centered cubic array subjected to one-dimensional compression

P_{ij} = force applied to a face of a symmetrical cube from a face-centered cubic array, the plane of the face is normal to a unit vector in the i direction and the force is directed in the j direction.

P_0 = force applied to a face of a symmetrical cube from a face-centered cubic array subjected to hydrostatic compression.

P_{zz} = axial force or vertical force applied along the z axis on the face of a symmetrical cube from a face-centered cubic array subjected to one-dimensional compression.

Q_z = total vertical force applied to a horizontal plane at a depth, z, in a consolidation ring.

---

q = a distributed, flexible load over the contact area between two spheres

q_0 = the pressure at the center of the area of contact between two spheres

R = radius of a sphere

R = radius of a consolidation ring

R_1, R_2 = radii of two different spheres in contact

r = distance from the center of the contact area between two spheres

S = tangential compliance, $\frac{d\delta}{dT}$, between two spheres in contact

T = tangential force between two spheres in contact

T_0 = tangential force between spheres in a face-centered cubic array subjected to a hydrostatic state of stress

T_2 = tangential force between spheres in a face-centered cubic array subjected to one-dimensional compression.

T_{ij} = tangential contact forces between spheres which are in the plane determined by the i and j axes.

T_{kk} = tangential contact forces between spheres which are mutually perpendicular to N_{ij} and T_{ij}

t = slope of the log constrained modulus-log vertical stress relationship for sand in one-dimensional compression

V	=	total volume of soil sample
V_D	=	dilalational wave velocity
V_s	=	volume of soil solids
V_v	=	volume of voids
w	=	vertical deflection of a point load on an infinite elastic half-space
w_1, w_2	=	displacements in the direction of the axis of two spheres in contact
X, Y, Z	=	cartesian coordinates
Z	=	$\left[f - \frac{T_2}{N_2}\right]^{1/3}$
z_1, z_2	=	distances along the Z axis
a	=	relative approach of the centers of two spheres compressed by a normal face
β	=	the angle between the axis of contact between two spheres and a radius drawn to a point on the surface of one of the spheres very close to the point of contact.
γ	=	unit weight of soil
δ	=	relative tangential displacement between the centers of two spheres in contact.
ϵ	=	base of Napierian logarithms, unit strain
ϵ_0	=	strain in any direction as a result of a hydrostatic state of stress.
ϵ_H	=	strain in a horizontal direction
ϵ_{zz}	=	strain in the z direction
ϵ^*_{zz}	=	maximum strain in the z direction during loading
μ	=	shear modulus
ν	=	Poisson's ratio
π	=	constant (3.1416)
ρ	=	distance from the center of the area of contact between two spheres to another point on the contact area
σ	=	normal components of stress
$\sigma_1, \sigma_2, \sigma_3$	=	principal stresses

σ_0	=	all around confining stress
σ_a	=	difference between the major and minor principal stresses
σ_H	=	normal horizontal stress
σ_r	=	normal radial stress
σ_v	=	normal vertical stress
σ_{zz}	=	normal stress in the z direction
τ	=	tangential stress
τ_z	=	shearing stress due to ring friction in a consolidometer
ϕ	=	drained angle of internal friction
ψ	=	the angle between a chord and a fixed radius of a circular area

CHAPTER 1

INTRODUCTION

1.1 Statement of Problem

The design of underground structures to resist the effects of nuclear detonations requires a knowledge of the free-field forces and ground motions transmitted through the soil to the structure. An evaluation of the interaction of the structure and surrounding soil in response to the free-field input is then required. The solution of both the free-field wave propagation problems and soil-structure interaction problems requires a knowledge of the stress-strain properties of soil subjected to various states of stress.

At present, however, a systematic description of the stress-strain behavior of even a dry granular material is not available for static or dynamic loads. The complexity of the stress-strain relations for soil is a consequence of its particulate nature. The stiffness of a granular material is dependent upon the shape, size distribution, and packing arrangement of the particles; the stiffness is also a non-linear function of the applied state of stress.

The dependence of the stress-strain relation on the applied state of stress can be illustrated by considering various states of stress on the cylindrical sample of soil shown in Fig. 1.1. Curve 1 shows an axial stress-strain curve for a sample of soil compressed hydrostatically with $\sigma_a = \sigma_r$. The concave upward stress-strain relationship is exhibited because the resistance to volume change increases as the soil becomes denser. Curve 3 illustrates an axial stress-strain curve for a sample under constant radial stress which is deformed by increasing the axial stress. The resulting stress-strain curve is concave downward indicating that the primary resistance to deformation is a shearing resistance rather than a resistance to volume change. Curve 2 is a one-dimensional compression curve obtained by increasing the axial stress under the

conditions of zero radial strain. In this situation, the lateral stresses are not controlled and are statically indeterminate. The concave upward stress-strain curve shows that the resistance to deformation in one-dimensional compression is primarily a resistance to a change in volume. These examples illustrate the complex, non-linear behavior of soil and point out the difficulties in obtaining a generalized stress-strain relationship.

A useful approximation to many of the problems in protective construction can be obtained by assuming one-dimensional wave propagation. The strata are assumed to be laterally confined such that the only displacement that can occur is in the direction of stress wave propagation. It appears worthwhile, therefore, to investigate the stress-strain behavior and energy absorption mechanisms of soil in one-dimensional compression. The study should prove of value in providing parameters to be used in one-dimensional wave propagation studies. In addition, stress-strain characteristics in one-dimensional compression may be compared with the behavior under other states of stress leading to a more general understanding of the stress-strain relationships of soil.

1.2 Objectives of Study

The objective of this investigation was to study analytically and experimentally the behavior of granular materials in one-dimensional compression. An experimental study was conducted with the purpose of measuring the stress-strain properties and energy absorption characteristics of four sands at various relative densities. The tests were conducted with axial stresses up to 3290 psi in a special one-dimensional compression device; the apparatus allowed the radial stresses necessary to maintain the condition of zero radial strain to be measured. The lateral stress measurements enabled the coefficient of earth pressure at rest to be determined as a function of the type of sand, relative density, and stress history.

An analytical study of a granular medium of equi-radii spheres was conducted in conjunction with the one-dimensional tests. The idealized granular medium was analyzed in one-dimensional compression, hydrostatic compression, and at failure in triaxial compression. The objective of the theoretical analysis was to indicate the significant experimental measurements which should be made, to suggest correlations between the phenomenon exhibited by granular materials subjected to various states of stress, and to contribute to the general understanding of the behavior of granular materials.

1.3 Scope

In the following chapter a survey of the existing literature on the theories of granular media is presented. Previous experimental work on high pressure one-dimensional tests is reviewed and earlier measurements of the coefficient of earth pressure at rest are discussed.

Chapter 3 deals with the analysis of a face-centered cubic array of uniform spheres. The basic framework of the analysis is given and a new solution for the behavior of a face-centered cubic array in one-dimensional compression is presented. The solution gives theoretical relationships for the coefficient of earth pressure at rest, the axial stress-strain relationship, and the energy absorbed in hysteresis. Existing solutions for a face-centered cubic array in hydrostatic compression and in triaxial compression are compared with the one-dimensional solution obtained in this study. The comparison has established relationships among the apparent angle of internal friction, the coefficient of earth pressure at rest, and the coefficient of friction between spheres; a correlation between the hydrostatic and one-dimensional stress-strain relationships has also been developed.

In Chapter 4 the special one-dimensional compression device is described and considerations which affected the design are discussed. Special attention is given to the components of the apparatus which enable a measurement of the radial stresses built up in one-dimensional compression.

In Chapter 5 a description is given of the four sands tested. The method of sample preparation and the testing procedure are discussed. A detailed explanation of the pretest calibration procedure necessary for measuring the radial stresses is also given. Finally, the results of one-dimensional compression tests on four sands at various relative densities are presented.

The test results are summarized and interpreted in Chapter 6. Relationships are presented which show the effect of initial relative density on the constrained tangent modulus, the coefficient of earth pressure at rest, and the energy absorption capacity of the four sands studied. The coefficient of earth pressure is correlated with the angle of internal friction measured in triaxial tests and the effect of stress history on the coefficient of earth pressure at rest is evaluated. Correlations are also presented which qualitatively and quantitatively compare the actual behavior of a rounded, uniform quartz sand in one-dimensional and triaxial compression with the behavior suggested by the theory presented in Chapter 3.

In the final chapter, the summary and conclusions are presented. Future research which appears warranted as a result of this study is also suggested.

CHAPTER 2

SUMMARY OF PREVIOUS WORK

2.1 General

The purpose of this chapter is to present the background for the theory of granular media used in this study and to review some of the significant experimental work on the one-dimensional compression characteristics of sands. All of the work which has contributed to the understanding of the stress-strain relationships in soils is not included; only those investigations which seemed pertinent to this study are reviewed.

2.2 Theories of Granular Media

The idea of using arrays of spheres to model the behavior of sands is not new. In fact, Reynolds (1885) considered a medium of smooth, rigid particles in formulating his concept of "dilatancy". Jenkin (1931) considered rigid circular disks to examine the pressure distribution on the bottom and vertical sides of a container filled with such disks. It was concluded that the center of pressure was indeterminate and could be considerably higher than one-third the height of the wall above the base. An analysis of a uniform array of rigid spheres is cited by Kögler and Scheidig (1928) as a method for qualitatively determining the stress distribution beneath footings on sand. More recently, studies have been conducted on regular and imperfect stackings of rigid cylinders by Trollope (1957), Trollope and Morgan (1959), and Laszlo (1962) to investigate arching and stability in embankments and stress systems in slopes of granular materials. Regular stackings of rigid spheres have also been analyzed by Idel (1960) and Wittke (1962) in an effort to evaluate the effects of porosity, structural arrangement, and the coefficient of friction between spheres on the apparent angle of internal friction. An evaluation of the differences of the angle of internal friction in ordinary triaxial compression and in plane strain for a given array is also given by Wittke.

Arrays of rigid spheres as described above are not satisfactory for the analysis of vibration and wave propagation problems which require stress-strain relationships for the medium. These problems have been handled by the analysis of regular arrays of equi-radii elastic spheres. The object of this type of analysis is to relate the overall stress-strain behavior of the medium to the elastic properties of the spheres. The origin for these theoretical studies dates back to the work of Hertz (1881). Hertz derived a mathematical relationship which relates the normal force compressing two spheres of equal radius with the relative approach of the sphere centers in terms of the radius and elastic constants of the spheres. The radius of the contact area and the distribution of stress over the contact area are also given as a function of the radius and elastic constants of the spheres.

One of the first attempts to use an elastic array of spheres along with the Hertz theory to predict the behavior of soil was given by Iida (1938). Iida predicted that the compressional wave velocity should be proportional to the 1/6 power of the confining pressure on a granular material and independent of the grain size. Vibration tests were conducted on sands by Iida which confirmed the 1/6 power relationship, but indicated a slight increase in velocity with grain size. The Hertz theory was also the basis for the theories developed by Gassman (1953) and Brandt (1955) for studying the propagation of seismic waves through both dry and saturated granular materials.

The shearing forces at the points of contact were neglected in the studies on elastic spheres mentioned above. Cattaneo (1938) and Mindlin (1949) have developed a contact theory for spheres subjected to both normal and shearing forces at a point of contact. These solutions have made possible theories of granular media which take account of both the shearing and normal forces at the points of contact. Therefore, the stress-strain relations for the medium are also a function of the coefficient of friction between spheres as well as the elastic constants of the spheres. If the

shearing forces are accounted for it is found that energy is lost in a load cycle as a result of tangential slip at the contacts. Professor R. D Mindlin and his students at Columbia University have formulated theories for the incremental stress-strain relationships of regular arrays of spheres which take into account the shearing forces at the contacts. The development of these theories are given by Mindlin et al. (1951), Mindlin and Deresiewicz (1953), Mindlin (1954), Duffy and Mindlin (1957), Deresiewicz (1957), and Thurston and Deresiewicz (1959). A very comprehensive review of previous studies of the mechanics of granular media is given by Deresiewicz (1958).

2.3 Experimental Results

Many investigators have studied sand in one-dimensional compression in the low pressure ranges, but the available experimental data for high pressure one-dimensional tests on sand is rather scarce. Tests have been conducted on sands in one-dimensional compression for the purpose of measuring the one-dimensional stress-strain properties and the coefficient of earth pressure at rest. Some of the previous attempts to measure the coefficient of earth pressure at rest are reviewed herein, and the stress-strain measurements pertinent to this study are discussed.

Coefficient of Earth Pressure at Rest Measurements. The term "earth pressure at rest" was introduced by Donath (1891) who made the first attempts to measure its value. The ratio of the horizontal and vertical effective stresses corresponding to the condition of zero lateral strain is termed the coefficient of earth pressure at rest by most soil mechanics investigators, and is represented by the symbol K_o.

Experiments were conducted by Terzaghi (1920) which yielded a K_o value of 0.42 for three different sands at porosities from 42 percent to 44 percent. The sand was prepared in a rigid frame, covered with a rigid slab, and subjected to vertical pressure in a testing machine. The lateral pressure was transmitted to a steel tape

resting against a rigid wall through a piece of paper. The coefficient of friction between the tape and paper was known by calibration and the lateral pressure in the sand was calculated from the force required to overcome the friction of the tape. The coefficient of earth pressure at rest was measured on a sand by Kjellman (1936) in an apparatus which enabled the three principal stresses to be varied on a cube of soil. The metal surfaces enclosing the cubical specimen were divided into small sections separated by gaps which enabled normal stresses and normal strains to be controlled on faces which were free from shear stresses. The significant observation from Kjellman's tests was that the value of K_o was found to increase with increasing over-consolidation ratio for a sand and that it approached a value of 1.5 when the sand was practically unloaded.

The lateral earth pressure meter designed by Bayliss (1948) was used to make measurements of the coefficient of earth pressure at rest at Princeton University and is described in detail by Tschebotarioff (1951). On the basis of these measurements Tschebotarioff claimed that the value of K_o for sands was very close to 0.50 which was somewhat contradictory to the results of previous investigations. Because of the variation of pressure from the top to the bottom of the earth pressure meter, and the dish shaped pattern of settlement which resulted at the top of the sample, it is probable that Tschebotarioff's results are in error.

More recently, an apparatus has been used by Kjellman and Jacobson (1955) which contained a cylindrical sample of soil 50 cm in diameter by 100 cm high. The granular soil was enclosed by a series of steel rings separated by small gaps which allowed axial strain to occur without significant shear due to friction. The lateral deformations resulting from the elastic extension of the rings were measured and the lateral stresses calculated from these measurements. Tests conducted on pebbles and Macadam indicated that K_o was nearly constant during loading and ranged between the values of 0.38 and 0.48 for the materials tested. The value of K_o increased during

unloading for all materials and approached a value of approximately 1.5 as the samples were almost completely unloaded.

A very complete description of the test requirements for the measurement of the coefficient of earth pressure at rest is given by Bishop (1958). Bishop concludes that the only two pieces of experimental apparatus, in addition to the triaxial apparatus, which are suitable for K_o measurements are the devices used by Kjellman (1936) and Kjellman and Jacobson (1955). Two methods of conducting triaxial tests with zero lateral strain are discussed by Bishop; these were originally published by Bishop (1950) and Bishop and Henkel (1957). Bishop gives results obtained by Fraser (1957) from K_o tests conducted on sand in a triaxial apparatus to an axial stress of 310 psi. These results give a constant K_o value of 0.41 during loading for a dry Brasted sand which has a porosity of 40 percent. The value of K_o increases and eventually becomes greater than unity during unloading. Bishop (1958) also presents data which show good agreement between the semi-empirical relationship, $K_o = 1 - \sin \phi$, suggested by Jaky (1944) and available test results on sands and clays. Valuable discussions to Bishop's paper are also given by Rowe (1958), Schmid and Tschebotarioff (1958), Jakobson (1958), and Simons (1958).

The coefficient of earth pressure at rest has also been determined for sands in a triaxial apparatus at the Norwegian Geotechnical Institute. Results are presented by Bjerrum, Kringstad, and Kummeneje (1961) which indicate that the value of K_o increases as the initial porosity increases. The values ranged from 0.25 for dense sand to 0.65 for very loose sand. A similar variation in K_o with porosity is also reported by Chi-in (1958).

One-Dimensional Stress-Strain Measurements. A fairly complete study of the factors which influence the compressibility of sand in one-dimensional compression below an axial stress of 10 kg/cm^2 is given by Schultze and Moussa (1961). Twenty-five different sands are investigated for the purpose of studying the effect of grain

shape, grain size distribution, initial relative density, and the addition of a small amount of cohesive soil on the one-dimensional stress-strain characteristics.

Results of high pressure tests on sands in one-dimensional compression are given by Terzaghi and Peck (1948); these tests were conducted by Urul (1945) in conjunction with another study. Data are given for a loose sand and a dense sand compressed to 100 kg/cm^2 and 2000 kg/cm^2 respectively. These data show that crushing of the grains begins around 100 kg/cm^2 and that even up to considerable pressures the void ratio for the loose sand is greater than the void ratio of the dense sand before loading. Tests were also conducted up to 100 kg/cm^2 for two samples of sand, one with 10 percent mica and the other with 20 percent mica. The experimental results demonstrated that the compressibility increases greatly with increasing percentages of mica.

The results of a single high pressure one-dimensional test on sand is given by Jaky (1948). The test was conducted up to a maximum pressure of 200 kg/cm^2 and a mathematical formulation of the test results were then used to compute geostatic pressures to a depth of 1300 meters.

A series of high pressure tests conducted at the Massachusetts Institute of Technology were reported by Roberts and DeSouza (1958) and Roberts (1959). The tests were carried to pressures as high as 20,000 psi in one-dimensional compression on samples 1.13 and 2.75 inches in diameter and 0.35 to 0.75 inches in initial height. Two different sands and a ground quartz were tested at various initial void ratios. From these tests it was concluded that at sufficiently high pressures sand may be more compressible than clay. The high compressibility of the sand is due to crushing and fracturing of individual grains; the most important factor which influences the pressure at which breakdown occurs for a given sand is the initial void ratio. An angular sand is also shown to be more compressible than a well-rounded sand.

A fairly complete treatment of the behavior of sands in one-dimensional compression is given by Whitman (1962); summaries are given of both high pressure and low pressure work of other investigators. A very interesting study conducted by Roberts (1961) on the one-dimensional energy absorption characteristics of Ottawa sand is summarized by Whitman. The significant aspect of this study is the evaluation of energy absorption in cycles of loading which do not include any permanent deformation.

CHAPTER 3

THEORETICAL APPROACH FOR PREDICTING THE STRESS-STRAIN BEHAVIOR OF AN IDEALIZED GRANULAR MEDIUM

3.1 General

The stress-strain relations for a granular medium cannot be described by two independent elastic constants as in the case of elastic, isotropic, homogeneous materials because the stress-strain relations are extremely dependent upon the stress level, the state of stress, and the displacement conditions at the boundaries of the medium. This complex behavior of a granular medium is due primarily to its particulate nature. An analytical treatment which assumes any form of continuum equations to describe the stress-strain relations of a granular medium circumvents the real problem in the first step, because in reality all that remains is a mathematical exercise after the continuum equations are assumed.

A mechanics approach for predicting the stress-strain relations of a regular stacking of equi-radii spheres is presented in this chapter which accounts for the particulate nature of the medium. The basic elements which must be considered in such an analysis are:

1. The equilibrium of each particle and the medium as a whole.
2. The relationship between the forces at points of contact and the average stresses in the medium.
3. The geometrically admissible conditions on the deformations of the particles (i.e., a set of compatibility equations).
4. The relationship between the normal forces and normal displacements and the relationship between the shearing forces and tangential displacements at each contact point on a particle.
5. The boundary conditions on the medium.

The resulting differential equations which describe the stress-strain behavior of even a regular array of equi-radii spheres by the above approach are extremely complex and closed-form solutions can be obtained for only a few cases. Because some of the tractable problems are important cases, e.g. the hydrostatic, one-dimensional, and triaxial states of stress, this approach has a great deal of merit in that it contributes to the understanding of the behavior of granular materials. It is recognized that the analytical model selected is an oversimplification of a real sand, but it is a useful tool in correlating some of the stress-deformation and strength properties of sand. The model still maintains a particulate nature, however, which is the most important characteristic which distinguishes the behavior of sand from other materials.

The basic framework of this mechanics approach is not original; it is presented as background for a solution describing the behavior of a granular medium in one-dimensional compression which is originally developed by the writer in this thesis.

3.2 The Duffy-Mindlin Theory of Granular Media

Basic Theory. The theory developed here follows that formulated by Duffy and Mindlin (1957), Deresiewicz (1958), and Thurston and Deresiewicz (1959). The granular medium is restricted to a face-centered array of equi-radii spheres as shown in Fig. 3.1. This array has the maximum density for a uniform material and should simulate the behavior of a dense, uniform, well-rounded sand.

Consider the behavior of two spheres pressed together by a normal force. According to Hertz (1881), if two elastic spheres, each having radius R, shear modulus μ, and Poisson's ratio ν, are mutually compressed by a normal force N, the resulting surface of contact is a plane bounded by a circle of radius a, where

$$a = \left[\frac{3(1-\nu)RN}{8\mu}\right]^{1/3} \tag{3.1}$$

The rate of change of the relative approach of the sphere centers, α, with respect to

the normal force N, is

$$C = \frac{da}{dN} = \frac{1 - \nu}{2\mu a} \tag{3.2}$$

where C is defined as the normal compliance. Two spheres in normal contact are shown in Fig. 3.2; Fig. 3.3 shows the distribution of the normal stress across the area of contact. A complete derivation of the Hertz compliance and the assumptions and limitations of the Hertz theory in regard to this study are given in Appendix A.

Suppose now that the two like spheres, initially compressed by a constant normal force N, are subjected to a tangential force T which acts in the plane of contact and whose magnitude increases monotonically from zero to a given value. Because of symmetry, the distribution of normal pressure remains unchanged. If it is assumed that there is no slip* on the contact, then, because of symmetry, the displacement of the contact surface in its plane is that of a rigid body. The solution of the appropriate boundary-value problem, due to Cattaneo (1938) and Mindlin (1949), yields the tangential component of stress, τ, on the contact surface and the tangential displacement, δ, of points in one sphere remote from the contact with respect to similarly situated points in the other sphere. The tangential stress is parallel to the applied force T, axially symmetric in magnitude, and increases to infinity on the bounding curve of the contact area (Fig. 3.3). It is reasonable to suppose that slip is initiated at the edge of the contact because it is there that the shearing stress is infinite in the absence of slip. Since this tangential stress is symmetric without slip, the slip is assumed to progress radially inward, covering an annular area. On this annulus it is assumed, as a first approximation, that the tangential component of stress is in the direction of the applied force and is related to the normal (Hertz) component of stress, σ, in accordance with Coulomb's Law of sliding friction. Hence,

$$\tau = f\sigma \tag{3.3}$$

* The term "slip" is reserved to denote the relative displacement of contiguous points on a portion of the contact surface. The term "sliding" is reserved to denote relative displacement of the entire area of contact.

where f is the coefficient of static friction and σ is given by

$$\sigma = \frac{3N}{2\pi a^3} (a^2 - \rho^2)^{1/2} \tag{3.3a}$$

Here ρ is the distance from the center of the contact circle. The distribution of τ with slip is also shown in Fig. 3.3. Both Cattaneo and Mindlin predicted the relation between the radius of the adhered portion and the applied tangential force as

$$b = a\left(1 - \frac{T}{fN}\right)^{1/3} \tag{3.4}$$

where b is as shown in Fig. 3.3 and where the tangential compliance at the contact is given by

$$S = \frac{d\delta}{dT} = \frac{2 - \nu}{4\mu a} \left(1 - \frac{T}{fN}\right)^{-1/3} \tag{3.5}$$

Equation (3.5) holds only for the case of an increasing T with a constant N at the contact. In the problems considered in this chapter, T and N are both increasing so the tangential compliances appropriate for this problem are (Mindlin and Deresiewicz 1953)

$$S = \frac{2 - \nu}{4\mu a} \left[f\frac{dN}{dT} + \left(1 - f\frac{dN}{dT}\right)\left(1 - \frac{T}{fN}\right)^{-1/3} \right], \quad 0 \leq \frac{dN}{dT} \leq 1/f \tag{3.6}$$

or

$$S = \frac{2 - \nu}{4\mu a}, \quad \frac{dN}{dT} \geq 1/f \tag{3.7}$$

Consider a face-centered cubic array of uniform spheres as shown in Fig. 3.1, where each sphere is in contact with 12 other spheres. A typical element of this packing is shown in Fig. 3.4. If the coordinate system shown in Fig. 3.4 is trarslated to the center of any sphere, Fig. 3.5, the 12 contact points would have the following coordinates in terms of the radius of the sphere.

	X	Y	Z		X	Y	Z
1.	0	$+R/\sqrt{2}$	$+R/\sqrt{2}$	7.	$+R/\sqrt{2}$	$-R/\sqrt{2}$	0
2.	0	$-R/\sqrt{2}$	$+R/\sqrt{2}$	8.	$-R/\sqrt{2}$	$+R/\sqrt{2}$	0
3.	0	$-R/\sqrt{2}$	$-R/\sqrt{2}$	9.	$+R/\sqrt{2}$	0	$+R/\sqrt{2}$
4.	0	$+R/\sqrt{2}$	$-R/\sqrt{2}$	10.	$-R/\sqrt{2}$	0	$-R/\sqrt{2}$
5.	$+R/\sqrt{2}$	$+R/\sqrt{2}$	0	11.	$-R/\sqrt{2}$	0	$+R/\sqrt{2}$
6.	$-R/\sqrt{2}$	$-R/\sqrt{2}$	0	12.	$+R/\sqrt{2}$	0	$-R/\sqrt{2}$

There are two shearing forces and one normal force at each contact point as shown on Fig. 3.5. In index notation it is convenient to identify the various components of normal forces by the symbol, N_{ij}, where the subscripts correspond to the planes in which the components lie. The two tangential force components at each contact are chosen to lie in and normal to the co-ordinate planes, and are identified by T_{ij} and T_{kk}, respectively. At all contacts where the normal has direction cosines of unlike sign the force components are further distinguished by primes. Thus the components at the contact points 1 through 12 are:

1.	N_{yz}	T_{yz}	T_{xx}	7.	N'_{xy}	T'_{xy}	T'_{zz}
2.	N'_{yz}	T'_{yz}	T'_{xx}	8.	N'_{xy}	T'_{xy}	T'_{zz}
3.	N_{yz}	T_{yz}	T_{xx}	9.	N_{xz}	T_{xz}	T_{yy}
4.	N'_{yz}	T_{yz}	T'_{xx}	10.	N_{xz}	T_{xz}	T_{yy}
5.	N_{xy}	T_{xy}	T_{zz}	11.	N'_{xz}	T'_{xz}	T'_{yy}
6.	N_{xy}	T_{xy}	T_{zz}	12.	N'_{xz}	T'_{xz}	T'_{yy}

The equilibrium equations of a representative cube (Fig. 3.4) may now be considered. If an increment in stress is added to an initial state of stress, the forces on the faces of the cube will be increased by corresponding increments dP_{ij}. The unknown increments of force at the contacts between the spheres within the cube which result from the force increments dP_{ij} can be determined. If the stress increment in

the medium is homogeneous, then the contact forces will be equal at contacts having corresponding positions on the surfaces of the spheres. The contact forces diametrically opposed on each sphere are equal, thus only 18 of 36 contact forces on each sphere are independent. Not only must the cube as a whole remain in equilibrium under the action of the increments in applied force, dP_{ij}, but each sphere and each portion of a sphere within the cube must also remain in equilibrium. Since the portions of spheres in the cube are acted on both by applied forces and by contact forces, the equations of equilibrium relate the increments in applied forces to the increments in contact forces. By writing equilibrium equations for various octants of spheres in the cube as shown in Fig. 3.6 it may be shown, (Duffy and Mindlin, 1957), that there are nine independent equations of equilibrium. These equations are the following:

$$
\begin{aligned}
&1.\quad 4dT_{xx} + 2\sqrt{2}\,(dN_{zx} + dN_{xy} - dT_{zx} + dT_{xy}) = dP_{xx} + dP_{xy} + dP_{zx}\\
&2.\quad 4dT_{yy} + 2\sqrt{2}\,(dN_{xy} + dN_{yz} - dT_{xy} + dT_{yz}) = dP_{yy} + dP_{yz} + dP_{xy}\\
&3.\quad 4dT_{zz} + 2\sqrt{2}\,(dN_{yz} + dN_{zx} - dT_{yz} + dT_{zx}) = dP_{zz} + dP_{zx} + dP_{yz}\\
&4.\quad 4dT'_{xx} + 2\sqrt{2}\,(dN'_{zx} + dN_{xy} - dT'_{zx} + dT_{xy}) = dP_{xx} + dP_{xy} + dP_{zx}\\
&5.\quad 4dT'_{yy} + 2\sqrt{2}\,(dN'_{xy} + dN_{yz} - dT'_{xy} + dT_{yz}) = dP_{yy} + dP_{yz} - dP_{xy}\\
&6.\quad 4dT'_{zz} + 2\sqrt{2}\,(dN'_{yz} + dN_{zx} - dT'_{yz} + dT_{zx}) = dP_{zz} + dP_{zx} - dP_{yz}\\
&7.\quad 4dT_{xx} - 2\sqrt{2}\,(dN'_{zx} + dN'_{xy} - dT'_{zx} + dT'_{xy}) = -dP_{xx} + dP_{xy} + dP_{zx}\\
&8.\quad 4dT_{yy} - 2\sqrt{2}\,(dN'_{xy} + dN'_{yz} - dT'_{xy} + dT'_{yz}) = -dP_{yy} + dP_{yz} + dP_{xy}\\
&9.\quad 4dT_{zz} - 2\sqrt{2}\,(dN'_{yz} + dN'_{zx} - dT'_{yz} + dT'_{zx}) = -dP_{zz} + dP_{zx} + dP_{yz}
\end{aligned}
\qquad (3.8)
$$

The nine equilibrium equations given above are not sufficient to uniquely describe the behavior of the medium since the problem is statically indeterminate. A set of compatibility conditions was formulated (Duffy and Mindlin, 1957) by giving consideration to the admissible displacements of the medium which result from the incremental stresses. The components of relative displacements of the centers of spheres are designated by da_{ij}, $d\delta_{ij}$, $d\delta_{kk}$, to correspond, respectively, to the

forces dN_{ij}, dT_{ij}, dT_{kk} (Fig. 3.7). It is required that the displacements of the center of the spheres be single valued, i.e., the vector distance around the closed path through the center of the spheres must vanish both before and after the medium is strained. Hence the sum of the relative displacements of the center of these spheres around the closed path must vanish. Expressions for this condition for all possible paths connecting the center of a sphere in the medium yields 9 independent equations of compatibility as follows:

$$
\begin{aligned}
&\underline{1}. \quad \sqrt{2}d\delta_{zz} = -da'_{yz} + da_{zx} + d\delta'_{yz} + d\delta_{zx} \\
&\underline{2}. \quad \sqrt{2}d\delta_{zz} = da_{yz} - da'_{zx} - d\delta_{yz} - d\delta'_{zx} \\
&\underline{3}. \quad \sqrt{2}d\delta'_{zz} = -da_{yz} + da_{zx} + d\delta_{yz} + d\delta_{zx} \\
&\underline{4}. \quad \sqrt{2}d\delta_{xx} = -da'_{zx} + da_{xy} + d\delta'_{zx} + d\delta_{xy} \\
&\underline{5}. \quad \sqrt{2}d\delta_{xx} = da_{zx} - da'_{xy} - d\delta_{zx} - d\delta'_{xy} \\
&\underline{6}. \quad \sqrt{2}d\delta'_{xx} = da_{zx} - da_{xy} + d\delta_{zx} + d\delta_{xy} \\
&\underline{7}. \quad \sqrt{2}d\delta_{yy} = da'_{xy} + da_{yz} + d\delta'_{xy} + d\delta_{yz} \\
&\underline{8}. \quad \sqrt{2}d\delta_{yy} = da_{xy} - da'_{yz} - d\delta_{xy} - d\delta'_{yz} \\
&\quad\ \sqrt{2}d\delta'_{yy} = -da_{xy} + da_{yz} + d\delta_{xy} + d\delta_{yz}
\end{aligned}
\tag{3.9}
$$

The compatibility equations can be written in terms of force increments by using the compliances

$$
\begin{aligned}
da_{ij} &= C_{ij}dN_{ij} & da'_{ij} &= C_{ij}dN'_{ij} \\
d\delta_{ij} &= S_{ij}dT_{ij} & d\delta_{ij} &= S'_{ij}dT'_{ij} \\
d\delta_{kk} &= S_{kk}dT_{kk} & d\delta'_{kk} &= S'_{kk}dT'_{kk}
\end{aligned}
\tag{3.10}
$$

where the above subscripts identify the contact. Thus Eq. (3.9) together with Eq. (3.8) yield 18 independent equations containing the applied forces dP_{ij}, and 18 independent components of the unknown contact forces, dN_{ij}, dT_{ij}, and dT_{kk}. Unfortunately, these 18 equations are difficult to solve because the equations include the compliances and the compliances are functions of the contact forces. Consequently, a solution to these

equations can be obtained only for a few simple cases.

The incremental extensional and shearing strains in the array, expressed in terms of the compliances, are

$$d\epsilon_{ii} = \frac{1}{4R}(da_{ij} + d\delta_{ij} + da'_{ij} + d\delta'_{ij})$$
$$d\gamma_{ij} = \frac{1}{2R}(da_{ij} - da'_{ij}) \qquad (3.11)$$

Likewise the applied force increments P_{ij} in Fig. 3.4 are related to the stress increments for a face-centered array by

$$dP_{ij} = 8R^2 d\sigma_{ij} \qquad (3.12)$$

Application to a Hydrostatic State of Stress. One problem of interest which can be solved is that of a face-centered array subjected to a hydrostatic state of stress. Under this state of stress symmetry dictates the conditions that all normal forces at the contacts are equal and all shearing forces are equal. If it is designated that

P_o = total force on the face of a differential element

N_o = normal contact force

T_o = tangential contact force

R = radii of spheres

the equilibrium Eqs. (3.8) reduce to

$$4dT_o + 4\sqrt{2}dN_o = dP_o$$
$$4dT_o - 4\sqrt{2}dN_o = dP_o \qquad (3.13)$$

Adding Eqs. (3.13) and considering the initial condition of zero stress yields the expected condition for the tangential force

$$T_o = dT_o = 0$$

Hence, the equilibrium equation becomes

$$dN_o = \frac{1}{4\sqrt{2}}\, dP_o \tag{3.14}$$

If ϵ_o is the hydrostatic strain in any direction, Eq. (3.11) yields

$$d\epsilon_o = \frac{1}{2R}\, da_o \tag{3.15}$$

where da_o is the normal deformation due to dN_o and is related to dN_o by the normal compliance C_o, and

$$da_o = C_o dN_o \tag{3.16}$$

From the Hertz theory

$$C_o = \frac{1 - \nu}{2\mu a_o} \tag{3.17}$$

where a_o is the radius of contact defined by

$$a_o = \left[\frac{3(1 - \nu)\, N_o R}{8\mu}\right]^{1/3} \tag{3.18}$$

By combining Eqs. (3.15), (3.16), (3.17) and (3.18), the incremental strain may be expressed as

$$d\epsilon_o = 1/2 \left[\frac{(1 - \nu)\sqrt{2}}{\mu}\right]^{2/3} \left[3\sigma_o\right]^{-1/3} d\sigma_o \tag{3.19}$$

Integrating Eq. (3.19) and considering zero initial conditions results in

$$\epsilon_o = \left[\frac{3(1 - \nu)\sqrt{2}}{8\mu}\right]^{2/3} \sigma_o^{2/3} \tag{3.20}$$

It should be noted that Eq. (3.20) states that the first stress invariant, I_1, is proportional to the three halves power of the first strain invariant J_1.

It is of interest to compare the results of this theory with some limited experimental results available in the literature. Kjellman (1936) carried out some tests on dry sand subjected to hydrostatic pressure and measured the strains associated with the pressure. Table 3.1 gives the variation of the first stress and strain invariants taken from his experimental results. A plot of these data is shown

in Fig. 3.8. Also shown is a plot of the exponential relationship indicated by the theory discussed, which is fitted to the experimental curve at the 6 kg/cm^2 stress level. The behavior of the sand is not as stiff as the theory indicates in the lower pressure regions whereas it becomes stiffer than the theory predicts in the higher pressure regions. The comparison does point out, however, that the results of the theory associated with the face-centered array of spheres correlate qualitatively with the behavior of dense sand subjected to a hydrostatic state of stress.

3.3 One-Dimensional Theory of Granular Media

Monotonically Increasing Load. The theory of Duffy and Mindlin developed in Section 3.1 will now be extended to solve the stress-strain behavior of an array of spheres subjected to one-dimensional compression. One-dimensional compression is defined as that state of stress resulting from the application of a load in the vertical or z direction when the lateral strains in the x and y directions are zero.

The radial symmetry of the one-dimensional problem greatly simplifies Eqs. (3.8) and (3.9). The representative cube now becomes as shown in Fig. 3.9, and the forces on a sphere reduce to those shown on Fig. 3.10. From symmetry the following simplifications can be made for the forces and displacements:

$$
\begin{aligned}
&N_{xy} = N'_{xy} = N_1 \\
&N_{zy} = N'_{yz} = N_{zx} = N'_{zx} = N_2 \\
&-T_{yz} = -T'_{yz} = T_{zx} = T'_{zx} = T_2 \\
&T_{xx} = T'_{xx} = T_{yy} = T'_{yy} = T_{zz} = T'_{zz} = 0 \\
&T_{xy} = T'_{xy} = 0 \\
&P_{xy} = P_{xz} = P_{zx} = P_{yx} = P_{yz} = P_{zy} = 0 \\
&P_{xx} = P_{yy} = P_H
\end{aligned}
\qquad (3.21)
$$

$$
\begin{aligned}
a_{xy} &= a'_{xy} = a_1 \\
a_{yz} &= a'_{yz} = a_{zx} = a'_{zx} = a_2 \\
-\delta_{yz} &= -\delta'_{yz} = \delta_{zx} = \delta'_{zx} = \delta_2 \\
\delta_{xx} &= \delta'_{xx} = \delta_{yy} = \delta'_{yy} = \delta_{zz} = \delta'_{zz} = 0 \\
\delta_{xy} &= \delta'_{xy} = 0
\end{aligned}
\tag{3.22}
$$

Furthermore, the associated compliances now become

$$
\begin{aligned}
C_{xy} &= C'_{xy} = C_1 \\
C_{yz} &= C'_{yz} = C_{zx} = C'_{zx} = C_2 \\
S_{yz} &= S'_{yz} = S_{zx} = S'_{zx} = S_2
\end{aligned}
\tag{3.23}
$$

Using the above simplifications and considering symmetry reduces the equilibrium Eqs. (3.8) to

$$
\begin{aligned}
dN_2 + dT_2 &= \frac{\sqrt{2}}{8} dP_{zz} \\
dN_1 + dN_2 - dT_2 &= \frac{\sqrt{2}}{4} dP_H
\end{aligned}
\tag{3.24}
$$

In a similar fashion the compatibility Eqs. (3.9) reduce to

$$
da_1 - da_2 + d\delta_2 = 0 \tag{3.25}
$$

where the compliance Eqs. (3.10) now become

$$
\begin{aligned}
da_1 &= C_1 dN_1 \\
da_2 &= C_2 dN_2 \\
d\delta_2 &= S_2 dT_2
\end{aligned}
\tag{3.26}
$$

Substituting Eqs. (3.26) into Eq. (3.25) yields

$$
C_1 dN_1 - C_2 dN_2 + S_2 dT_2 = 0 \tag{3.27}
$$

Equations (3.24) and (3.27) are sufficient to describe the behavior of a granular medium subjected to given vertical and lateral forces P_{zz} and P_H. If, however, only the vertical force is known and the lateral force must also be determined, a further condition is necessary. This condition results from the relationship between the contact displacements and lateral strain.

Due to symmetry the lateral strain ϵ_H determined from Eqs. (3.11) reduces to

$$d\epsilon_H = \frac{da_1}{2R} \tag{3.28}$$

or

$$d\epsilon_H = \frac{C_1 dN_1}{2R} \tag{3.29}$$

Thus the behavior of a face-centered array of spheres subjected to a vertical force P_{zz} and restricted to symmetrical lateral deformations can be obtained from a solution to the following equations:

$$\begin{aligned} dN_2 + dT_2 &= \frac{\sqrt{2}}{8} dP_{zz} \\ dN_1 + dN_2 - dT_2 - \frac{\sqrt{2}}{4} dP_H &= 0 \\ \frac{C_1}{C_2} dN_1 - dN_2 + \frac{S_2}{C_2} dT_2 &= 0 \\ dN_1 &= \frac{2R d\epsilon_H}{C_1} \end{aligned} \tag{3.30}$$

For the case of interest here, namely one-dimensional compression, ϵ_H is required to vanish for all loadings. For this particular state of stress and zero initial conditions, one obtains $N_1 = 0$ and Eqs. (3.30) reduce to

$$dN_2 + dT_2 = \frac{\sqrt{2}}{8} dP_{zz} \tag{3.31a}$$

$$dN_2 - dT_2 - \frac{\sqrt{2}}{4} dP_H = 0 \tag{3.31b}$$

$$dN_2 - \frac{S_2}{C_2} dT_2 = 0 \tag{3.31c}$$

where the expression for $\frac{S_2}{C_2}$ is obtained from Eqs. (3,6) and (3.7) as:

$$\frac{S_2}{C_2} = k_1 \left[f \frac{dN_2}{dT_2} + (1 - f \frac{dN_2}{dT_2}) (1 - \frac{T_2}{fN_2}) \right]^{-1/3} \tag{3.32a}$$

where

$$k_1 = \frac{2 - \nu}{2(1 - \nu)} \tag{3.32b}$$

It should be noted that Eqs. (3,31) are simultaneous differential equations and are non-linear because of the compliances in the third equation.

The vertical strains ϵ_{zz} associated with the behavior of this medium can be obtained from Eqs. (3,11) as

$$d\epsilon_{zz} = \frac{1}{2R} (da_2 + d\delta_2) \tag{3.33}$$

The compatibility Eq. (3.31c) states that

$$da_2 = d\delta_2$$

Hence for the one-dimensional case Eq. (3.32) reduces to

$$d\epsilon_{zz} = \frac{da_2}{R} = \frac{C_2 dN_2}{R} \tag{3.34}$$

For the solution of Eqs. (3.31), consider first the compatibility Eq. (3.31c). Substituting Eqs. (3.32) into Eq. (3.31c) and rearranging yields

$$\frac{dT_2}{dN_2} = f + \frac{1 - k_1 f}{k_1} (1 - \frac{T_2}{fN_2})^{1/3} \tag{3.35}$$

Introducing the new variable

$$Z^3 = f - \frac{T_2}{N_2} \tag{3.36a}$$

and

$$N_2 Z^3 = N_2 f - T_2$$

one obtains

$$dN_2 Z^3 + 3 N_2 Z^2 dZ = f dN_2 - dT_2$$

or

$$\frac{dT_2}{dN_2} = f - Z^3 - 3N_2 Z^2 \frac{dZ}{dN_2} \tag{3.36b}$$

By using Eqs. (3.36), Eq. (3.35) can be transformed into the form

$$-\frac{3ZdZ}{Z^2+K_2} = \frac{dN_2}{N_2} \tag{3.37}$$

where

$$K_2 = \frac{1-k_1 f}{k_1^{1/3}} \tag{3.38}$$

Integrating both sides results in

$$\ln N_2 - \ln A = -3/2 \ln (Z^2 + K_2)$$

or

$$\frac{N_2}{A} = (Z^2 + K_2)^{-3/2} \tag{3.39}$$

where A is a constant of integration.

From Eq. (3.36a), Eq. (3.39) becomes

$$\frac{N_2}{A} = \left[(f - \frac{T_2}{N_2})^{2/3} + K_2 \right]^{-3/2} \tag{3.40}$$

Equation (3.40) is the general solution to Eq. (3.31c) and a particular solution may be obtained by evaluating the constant of integration.

Because the initial conditions, $P_{zz} = N_2 = T_2 = 0$, are obvious one is inclined to evaluate A from these conditions. Although this is a true boundary condition, a singularity point occurs at the origin. The equation is, however, well behaved at

other points and the following technique will be used to evaluate A.

Imagine a small hydrostatic state of stress initially holding the spheres in contact before the one dimensional state is imposed. This hydrostatic stress produced no initial tangential force at the contacts but it does cause a normal force of $N_2 = N_o$.

From eq. (3.40)

$$N_o = A(f^{2/3} + K_2)^{-3/2}$$

or solving for A, the constant of integration

$$A = \frac{N_o}{(K_2 + f^{2/3})^{-3/2}} \tag{3.41}$$

Substituting A into Eq. (3.40) yields after some rearranging and taking into account Eq. (3.38).

$$T_2 = fN_2 \left[1 - \left(\frac{1}{fK_1} \left[\left(\frac{N_o}{N_2} \right)^{2/3} - 1 \right] + 1 \right)^{3/2} \right] \tag{3.42}$$

A plot of a family of curves representing Eq. (3.42) with various values of the initial hydrostatic stress N_o is given in Fig. 3.11. The paths of loading are indicated by arrows on the curves. For convenience the coefficient of friction f was taken as 0.3 and Poisson's ratio ν as 0.2.

If an initial hydrostatic stress is imposed the value of N_2 can be determined at which sliding begins. For this condition Eq. (3.42) yields

$$\frac{1}{fK_1} \left[\left(\frac{N_o}{N_2} \right)^{2/3} - 1 \right] + 1 = 0$$

Rewriting and taking account of (3.32b) yields

$$N_2 = \frac{N_o}{\left[1 - \frac{f(2-\nu)}{2(1-\nu)} \right]^{3/2}} \tag{3.43}$$

The reader will recall that the problem was to define the relation between N_2 and T_2 for a granular medium in one-dimensional compression which was loaded from an unstressed condition. It was noted that the solution contained a singularity at the zero stress and it was necessary to provide an initial hydrostatic stress N_o to hold the spheres in contact when loading. If N_o is now allowed to approach zero we obtain the solution desired. On investigating Fig. 3.11 or Eq. (3.42) it is clear that if one-dimensional loading commences from a completely unstressed condition ($N_o = 0$), the relation between N_2 and T_2 is that of a straight line with a slope of $1/f$. Thus, the relationship between N_2 and T_2 for a face-centered array subjected to one-dimensional compression is

$$T_2 = fN_2$$

This means that sliding (differentiated from slip in Section 3.1) at the contacts occurs immediately on initiation of loading. This is extremely important in that the theory developed to date along the lines of Mindlin et al does not allow sliding at the contacts. It will be shown herein that the stress-strain relationships in the one-dimensional granular medium can be described mathematically even though sliding occurs throughout the application of a monotonically increasing load.

From compatibility, even in the case of sliding, the geometrical relationship still holds for the displacements at the contacts, i.e.

$$da_2 - d\delta_2 = 0 \tag{3.44}$$

It must be emphasized, however, that the tangential displacement δ_2 is no longer related to the tangential contact force T_2 by the tangential compliance S_2 because of sliding at the contacts. The tangential displacement is now made up of two effects, a sliding effect and a contribution due to slip. On the other hand, the normal forces and displacements are still connected by the compliances.

Furthermore, because Eq. (3.44) is a geometrical relationship, it also holds for total displacements in the problem at hand; hence,

$$a_2 = \delta_2 \tag{3.45}$$

The vertical strain Eq. (3.33) is also purely geometrical and can be written as

$$d\epsilon_{zz} = \frac{da_2}{R} = \frac{C_2 dN_2}{R} \tag{3.46}$$

The equilibrium Eqs. (3.31a) and (3.31b), which were originally written in terms of differential stresses, also hold for total stresses. Hence,

$$N_2 + T_2 = \frac{\sqrt{2}}{8} P_{zz} \tag{3.47a}$$

$$N_2 - T_2 - \frac{\sqrt{2}}{4} P_H = 0 \tag{3.47b}$$

It has already been determined that N_2 and T_2 are related by the coefficient of friction throughout the entire loading, i.e.

$$fN_2 - T_2 = 0 \tag{3.47c}$$

The behavior of the granular medium subjected to one-dimensional compression can now be described by Eqs. (3.44, (3.54), (3.46), and (3.47).

Equations (3.47) may be combined to eliminate T_2 resulting in

$$N_2 (1+f) = \frac{\sqrt{2}}{8} P_{zz} \tag{3.48a}$$

$$N_2 (1-f) = \frac{\sqrt{2}}{4} P_H \tag{3.48b}$$

In theoretical soil mechanics a quantity of major interest in one-dimensional compression is K_o, the ratio between the horizontal and vertical stresses at rest. From Eqs. (3.48) this ratio is clearly

$$K_o = \frac{P_H}{P_{zz}} = \frac{1}{2} \left(\frac{1-f}{1+f}\right) \tag{3.49}$$

Some indication of the variation of K_o with the coefficient of friction f is shown in Table 3.2.

The strains resulting from one-dimensional compression may now be investigated. The substitution of Eq. (3.2) into Eq. (3.46) yields

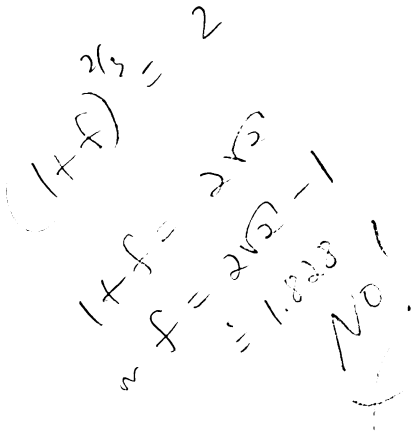

$$d\epsilon_{zz} = \frac{(1-\nu)}{2\mu R}\left[\frac{3(1-\nu)\,RN_2}{8\mu}\right]^{-1/3} dN_2 \qquad (3.50)$$

Combining Eqs. (3.50) and (3.48a) and noting from Fig. 3.9 that

$$\sigma_{zz} = \frac{P_{zz}}{8R^2} \qquad (3.51)$$

gives

$$d\epsilon_{zz} = \frac{1}{2}\left[\frac{(1-\nu)\sqrt{2}}{\mu(1+f)}\right]^{2/3}\left[3/8\,\sigma_{zz}\right]^{-1/3} d\sigma_{zz} \qquad (3.52)$$

Integration of Eq. (3.52) yields

$$\epsilon_{zz} = \left[\frac{(1-\nu)\,(3)\sqrt{2}}{\mu\,(1+f)\,(8)}\right]^{2/3} 2\sigma_{zz}^{2/3} \qquad (3.53)$$

An interesting result of Eq. (3.53) is that the stress-strain behavior is independent of the radii of the particles. A comparison of the stress-strain curves for hydrostatic and one-dimensional compression shows that the curves are similar in shape, but turn up at different rates. The ratio of the one-dimensional strain to the hydrostatic strain at the same level of stress, σ_{zz}, is a ratio of Eqs. (3.53) to (3.20), which reduces to

$$\frac{\epsilon_{zz}}{\epsilon_o} = \frac{2}{(1+f)^{2/3}} \qquad (3.54)$$

Values of f of 0.1 and 0.2 give values for ϵ_{zz}/ϵ_o of 1.88 and 1.77, respectively. This indicates that the hydrostatic and one-dimensional stress-strain curves are related as shown in Fig. 3.12.

Unloading Cycle. When the medium is loaded the tangential forces tend to resist the sliding motion. During unloading the tangential forces tend to resist the sliding movement which is now in the opposite direction. Hence, the tangential forces reverse their direction on unloading. The cases of loading and unloading are illustrated

schematically in Fig. 3.13. The normal and tangential forces are still related by the coefficient of friction; only now the direction of the tangential force is changed.

The new equilibrium equations become

$$N_2 - T_2 = \frac{\sqrt{2}}{8} P_{zz}$$

$$N_2 + T_2 = \frac{\sqrt{2}}{4} P_H \tag{3.55}$$

where

$$fN_2 - T_2 = 0 \tag{3.56}$$

Consider the medium to be loaded from 0 to σ^*_{zz}, Fig. 3.14, according to Eqs. (3.53). If equilibrium Eqs. (3.55) become valid at the instant ϵ_{zz} begins to decrease from ϵ^*_{zz}, then σ_{zz} will decrease instantaneously from σ^*_{zz} to some value σ'_{zz}. At the end of loading N_2 and σ^*_{zz} are related by

$$\sigma^*_{zz} = N_2 \frac{(1+f)}{\sqrt{2}R^2} \tag{3.57}$$

whereas the stress σ'_{zz} is related to the contact forces by Eqs. (3.54) and Eq. (3.51) by

$$\sigma'_{zz} = \frac{N_2 (1-f)}{2R^2} \tag{3.58}$$

The relation between σ^*_{zz} and σ'_{zz} at the instant when ϵ_{zz} just begins to decrease is

$$\sigma'_{zz} = \sigma^*_{zz} \left(\frac{1-f}{1+f}\right) \tag{3.59}$$

because the value of N_2 has essentially the same value while the shearing stress has changed directions. Combining Eqs. (3.55), (3.51), (3.46) and (3.2) yields for unloading

$$d\epsilon_{zz} = 1/2 \left[\frac{(1-\nu)\sqrt{2}}{\mu (1-f)}\right]^{2/3} \left[3/8\, \sigma_{zz}\right]^{-1/3} d\sigma_{zz} \tag{3.60}$$

which by integration becomes

$$\epsilon_{zz} = \left[\frac{(1-\nu)\, 3\sqrt{2}}{\mu\,(1-f)\, 8}\right]^{2/3} 2\,\sigma_{zz}^{2/3} \tag{3.61}$$

The entire stress-strain history for one cycle of loading in one-dimensional compression is shown in Fig. 3.14 in terms of σ^*_{zz} and σ'_{zz}. The derivations above are based upon the assumption that the tangential contact forces immediately reverse directions when unloading begins. This assumption is not quite true, however, because each sphere must exhibit a small elastic tangential displacement before the tangential forces can change direction. This effect, however, is small with respect to the tangential displacement due to sliding and was neglected in the analysis. Because of the above assumption, the stress-strain curve reflects a vertical drop in stress from A to B without any change in strain. If the small elastic tangential displacement due to slip were accounted for, the stress-strain curve would follow a smooth relationship such as the dotted line suggested in Fig. 3.14.

The stress-strain behavior shown in Fig. 3.14 exhibits an energy loss after a cycle of loading and unloading but has no residual strain. Hence, this medium can absorb energy without any permanent displacements.

Energy Absorption. The amount of energy absorbed by the medium on loading and subsequent unloading can now be determined.

The energy E_1 required to load up to an applied vertical stress of σ^*_{zz} and the strain of ϵ^*_{zz} is

$$E_1 = \int_0^{\epsilon^*_{zz}} \sigma_{zz}\, d\epsilon_{zz} \tag{3.62}$$

$$E_1 = \frac{4}{5}\,(1+f)\,\epsilon^{*5/2}_{zz}$$

The energy taken out of the medium E_2 during unloading back to zero from a stress of σ'_{zz} and strain ϵ^*_{zz} is

$$E_2 = \frac{4}{5}(1 - f)\epsilon^{*5/2}_{zz} \tag{3.63}$$

Thus, the energy lost is

$$\Delta E = E_1 - E_2 = \frac{8}{5} f\epsilon^{*5/2}_{zz} \tag{3.64}$$

The ratio of the energy loss to the energy input is

$$\frac{\Delta E}{E_1} = \frac{2f}{1+f} \tag{3.65}$$

Thus, a very significant property of the one-dimensional stress-strain curve is that the per cent of energy absorbed due to loading and unloading is always constant for a material and depends only on the coefficient of friction at the contacts. Hence, the ratio of the area between the loading and unloading curves to the area under the loading curve is a constant given by Eq. (3.65). The per cent energy absorbed for various coefficients of friction is given in Table 3.2.

The relationship between normal and tangential contact forces determines the relationship between the recoverable and dissipated energies. The work done by the normal forces during deformation $\int N_2 da_2$ is stored in the form of recoverable strain energy. On the other hand, the work done by the tangential forces $\int T_2 d\delta_2$ is a non-recoverable energy and is dissipated as heat into the medium. As seen from Table 3.2 this energy loss during one cycle can be quite significant. In fact, with a coefficient of friction of 0.15, the dissipated energy is 26.1% of the energy put into the system.

3.4 Equivalent Discrete Mass Model for One-Dimensional Static and Dynamic Behavior

In recent years, an increasing effort has been devoted to studying the static and dynamic behavior of soils using discrete mass-spring models. These models have taken many shapes with various components from models such as the standard Voigt and Maxwell models. These model studies have been particularly useful in wave

propagation studies, such as the work of Smith and Newmark (1958). The dynamic equations of motion can be integrated numerically with a digital computer using the β-method (Newmark, 1959); it is a fairly straightforward approach to modify soil parameters or spring stiffnesses as the need arises.

As might be expected from such an approach, there are certain aspects of the soil behavior which escape the mass-spring model. Part of this inaccuracy is due to the discreteness of the system and part can be attributed to choice of the model itself. A study of the problems associated with the choice of various models for investigating the propagation of stress waves in a one-dimensional medium has been carried out by Murtha (1961).

In spite of the inherent difficulties associated with the use of models, there are some cases where the model is the only hope for obtaining even an approximate solution. Therefore, the writer would like to suggest a one-dimensional model which seems to exhibit the behavior expected of dry cohesionless sand, and is based upon the theory presented in Section 3.2.

If a pressure on the surface of the earth extends over a large area, it may be reasonable to consider the soil completely confined. If this condition is satisfied, and the soil composition is similar to sand, the one-dimensional behavior discussed herein may very well be a good approximation to the in-situ soil behavior.

Horizontal Model. Figure 3.15 gives a model representation of the granular system described in Section 3.2. This model yields the same stress-strain curve as the spheres for a static load as the load increases or decreases. The model consists of non-linear spring elements and Coulomb damping elements which dissipate energy by the same mechanism as the spheres. The reason that the model depicts horizontal behavior is that there are no initial stresses in the model before the load is applied. Such an assumption might be reasonable for a vertical column if the weight of the soil is negligible compared to the applied stresses.

Vertical Model. The vertical model is slightly more complex than the horizontal one in that the weight of the material produces initial stresses in the model. Since the stress-strain curve for the material is non-linear, the stiffness is a function of the stress, and consequently, a function of the height of overburden. The overburden pressure increases linearly with depth and it can therefore be incorporated in the equations of motion.

A vertical model which includes the initial stresses due to the overburden of the material is given in Fig. 3.16. It includes a change in stiffness associated with the increased initial stress and follows the stress-strain behavior consistent with the analysis of the granular medium in Section 3.2.

3.5 Theoretical Relationship Between the Angle of Internal Friction, Coefficient of Earth Pressure at Rest, and the Coefficient of Friction Between Spheres for a Face-Centered Cubic Array of Uniform Spheres.

The relationship between the principal stresses at failure for a face-centered cubic array has been investigated by Thurston and Deresiewicz (1959). The analysis applies to an array as shown in Fig. 3.9 which is initially under an isotropic confining pressure, σ_o, and subsequently subjected to a uniaxial stress difference, σ_{zz}, as shown in Fig. 3.17. When σ_{zz} approaches the ultimate value, failure planes are formed by a series of shearing displacements of individual layers of spheres. The failure is initiated in layers containing planes in which the density of sphere centers is greatest, i.e., the (111) planes or octahedral planes with respect to the co-ordinate axis in Fig. 3.9. It is also interesting to note that Smith (1961) reports exactly the same phenomena for yielding in steel crystals which have a crystal arrangement such that the atoms have exactly the same location as the centers of the spheres in Fig. 3.9. A single relative shearing displacement of parallel (111) layers would translate sphere A, Fig. 3.9, from the hollow between spheres B, C, and E to the hollow between spheres B, C, and D. The translation of sphere A would be a distance of $R\sqrt{4/3}$ in the $[1\bar{1}2]$ direction. The

expression given by Thurston and Deresiewicz for the maximum stress difference that can be maintained without failure between octahedral layers of spheres is

$$\frac{\sigma_{zz}}{\sigma_o} = \frac{\sqrt{6} + 8f}{\sqrt{6} - 4f} \tag{3.66}$$

Since the major principal stress, σ_1, is given by

$$\sigma_1 = \sigma_{zz} + \sigma_o \tag{3.67}$$

and the minor principal stress, σ_3, is equal to σ_o, then equation 3.66 may be written as

$$\frac{\sigma_1 - \sigma_3}{\sigma_3} = \frac{\sqrt{6} + 8f}{\sqrt{6} - 4f} \tag{3.68}$$

If Eq. 3.68 is examined for the limiting condition of $f \Leftarrow 0$, then it is found that a stress difference equal to the confining stress can be maintained in this array even if the spheres are frictionless. The writer was initially disturbed by this result and analyzed several simple geometrical arrangements of frictionless spheres. It was found by the method of virtual displacements that the stress difference that could be maintained with a given confining stress was a function of the structural arrangement of the frictionless spheres. At the point of failure, the principal stresses and the kinematically possible virtual displacements in the principal directions are such that the change in potential energy is zero. Because the structural arrangement controls the displacements which are kinematically possible, then it follows that the structure also controls the principal stress ratio at failure in a frictionless array of spheres. For a given structural arrangement the stress difference at failure is governed by the boundary displacement conditions, such as the boundary restrictions in plane strain. The change in kinematically possible displacements imposed by the condition of plane strain accounts for the increased apparent angle of internal friction observed for granular materials sheared in plane strain.

The ratio of the principal stresses at failure for a dry granular material is defined by

$$\frac{\sigma_1}{\sigma_3} = \frac{1 + \sin \phi}{1 - \sin \phi} \tag{3.69}$$

where ϕ is the angle of internal friction of the material. The elimination of σ_1 and σ_3 from equation 3.68 and 3.69 yields

$$\sin \phi = \frac{8f + \sqrt{6}}{3\sqrt{6}} \tag{3.70}$$

Eq. (3.70) is more meaningful if it is written in the form

$$\sin \phi = \frac{1}{3} + \frac{8}{3\sqrt{6}} f \tag{3.71}$$

Eq. (3.71) clearly shows that part of the angle of internal friction is due to friction and the remainder is due to the structural arrangement. Eqs. (3.70) and (3.68) are correct only for a face-centered array of uniform spheres but the relationships suggest that the following relation should apply to any granular medium

$$\sin \phi = K_3 + C_1 f \tag{3.72}$$

where K_3 is a portion of sin ϕ due only to structure (relative density) and C_1 is a constant determined by the structural arrangement (relative density) which governs how efficiently the coefficient of friction is in increasing sin ϕ. It should be pointed out that the conclusions drawn above by the writer are contradictory to equations published by Bishop (1954) and Caquot (1934). The equation published for triaxial stress conditions, where $\sigma_2 = \sigma_3 < \sigma_1$, by A. W. Bishop was

$$\sin \phi = \frac{15f}{10 + 3f} \tag{3.73}$$

and the equations published by Caquot (1934) and Bishop (1954) for plane strain were respectively

$$\tan \phi = \pi/2\, f \tag{3.73}$$

and

$$\sin \phi = 3/2\, f$$

All of the relationships suggested by Bishop and Caquot show that ϕ reduces to zero when f reduces to zero. Thus the equations do not include a term which shows a component of the angle of internal friction which is a function only of structure, (relative density), and independent of the coefficient of friction between grains. It is therefore concluded that the equations given by Bishop and Caquot cannot explain the variation of ϕ with relative density.

Studies of the strength characteristics of uniform spheres in various packings are presented by Idel (1960) and Wittke (1962) which support the opinion of the writer. In fact, relationships between porosity and tan ϕ are presented in each study for the special case of the coefficient of friction between spheres equal to zero. Therefore the studies of Idel and Wittke also point out that part of the shear strength of a granular medium is due to structural arrangement, (relative density), and is independent of the coefficient of friction between particles. For the case of triaxial compression of a medium of frictionless spheres in the densest packing, Idel (1960) gives a value of 0.38 for tan ϕ whereas the value tan ϕ calculated from Eq. (3.71) for f = 0 is 0.35. The agreement is very good and the difference is due to the fact that the densest packing considered in this study was a face-centered cubic array whereas the densest stacking considered by Idel was a closed-packed hexagonal array.

The coefficient of earth pressure at rest and the angle of internal friction for a face-centered array can be related by combining Eqs. (3.49) and (3.70) to give

$$K_o = \frac{1}{2}\left[\frac{1+\sqrt{6/8}-3\sqrt{6/8}\sin\phi}{1-\sqrt{6/8}+3\sqrt{6/8}\sin\phi}\right] \qquad (3.76)$$

A plot of Eq. (3.76) is shown in Fig. 3.18 and a relationship between K_o and sin ϕ as suggested by Jaky (1944) is shown for comparison. The relationship given in Eq. (3.76) suggests that K_o decreases as ϕ increases, which is similar qualitatively to Jaky's relationship but not numerically identical. The coefficient of friction f was

eliminated between Eqs. (3.49) and (3.70) to obtain Eq. (3.76) because, although the coefficient of friction is a useful tool in relating ϕ and K_o, it cannot be measured reliably for grains with roughness and small radii of curvature. Eq. (3.76) can be checked, however, in the above form by measuring K_o and ϕ for a granular material.

CHAPTER 4

THE DEVELOPMENT OF A SPECIAL, HIGH PRESSURE, ONE-DIMENSIONAL COMPRESSION APPARATUS

4.1 General

A device was designed and built to investigate the one-dimensional behavior of sand in the high pressure regions. The apparatus can measure the lateral stress under conditions of zero lateral strain, and provides one of the best means yet developed for attaining the condition of "zero" lateral strain. Previous investigators have generally assumed that the effects of small lateral strains are negligible, particularly when the sample is enclosed in steel rings. Research by Speer (1944), which was recently pointed out by Fulton and Hendron (1962) shows that lateral motion significantly affects the ratio of σ_H/σ_V. The results of Speer's research is presented in graphical form in Fig. 4.1 and shows that a lateral displacement of 4×10^{-6} inches will cause a 10% reduction in the value of σ_H/σ_V. Since Speer's work was with a sand sample 7 5/8 inches in diameter, the above diameter change corresponds to a unit strain of approximately $.5 \times 10^{-6}$ in./in. It is doubtful to the writer that Speer really achieved an accuracy of $\pm 1 \times 10^{-6}$ in./in. since slight electrical instabilities in the circuit would cause minor variations of at least that magnitude in the strain gage readings. However, his work does in general point out that the ratio of σ_H/σ_V is very sensitive to lateral movements. This phenomenon had already been observed by Terzaghi (1934) in connection with his "Large Retaining Wall Tests" at MIT. Terzaghi concluded that an outward movement of the wall of .0007 h in the case of a well compacted dense sand was enough to fully mobilize the shear strength or, in other words, reduce the ratio of σ_H/σ_V to the coefficient of active earth pressure. This outward movement corresponds approximately to a lateral strain of about 12×10^{-4} in./in. Thus for a truly one-dimensional test, whereby one also wishes to measure the

magnitude of the lateral stresses which are concomitant with the vertical load, it is extremely important to closely control the lateral displacements. In fact, preliminary calculations revealed that an extremely thick walled cylinder subjected to an internal pressure of 7,500 psi (which is an approximation to the lateral soil pressure due to a vertical load of 15,000 psi) would experience a radial strain of 3.25×10^{-4} in./in. if the specimen were 7 inches in diameter and the containing cylinder were assumed to have an infinite external radius. This strain is of the same order of magnitude as the tolerable strains listed by Speer and Terzaghi. Thus, in order to study one-dimensional compression, a new experimental apparatus had to be designed which would restrict the lateral deformations. The apparatus developed in this study is discussed in the following sections.

4.2 Experimental Apparatus

General Description of the Apparatus. An experimental apparatus designed to determine the stress-strain relations for soil under one-dimensional compression and to measure the lateral stress necessary to completely restrain the sample is shown schematically in Fig. 4.2. The apparatus consists essentially of a thin steel ring, which contains a soil sample, surrounded by an annular space. The annular space is filled with oil which communicates freely with hydraulic jacks. The flexible ring and oil space are enclosed in a thick hollow cylinder bolted to a baseplate in order to withstand the high fluid pressures. The vertical load is applied to the sample by the testing head shown in Fig. 4.2 which is mounted in a 120,000 lb Baldwin testing machine.

The principle upon which the device is based is relatively simple. As the vertical load is applied by the testing head there are lateral pressures built up in the sand which tend to increase the diameter of the thin steel ring. Any slight increase in the diameter of the ring is immediately indicated by the strain gages mounted on the flexible ring as shown in Figs. 4.2 and 4.3a. In order to keep the lateral strains zero, the oil pressure

is modified with changes in the vertical load in such a manner that the strain indicator remains balanced at all times during the test. When the strain indicator remains balanced, there are no lateral strains and the oil pressure is equal to the lateral soil pressure acting against the inside of the container.

The apparatus consists of the following four basic elements:

(1) A thin steel ring monitored with strain gages, Fig. 4.3a.

(2) A testing head, Fig. 4.3b.

(3) A baseplate, Fig. 4.4a.

(4) A thick walled cylinder, Fig. 4.4b.

A detailed assembly drawing of the test cell is shown drawn to full scale in Fig. 4.5. The three component parts of the cell are drawn to full scale in Figs. 4.6, 4.7, and 4.8. The apparatus setup for testing in a 120,000 lb. hydraulic testing machine is shown in Fig. 4.9a.

Design of the Thin Steel Ring. The key sensing device, upon which the measurement of the coefficient of earth pressure at rest is dependent, is the instrumented steel ring. The steel ring is essentially a thin tube which has an internal diameter of 6.812 inches and an external diameter of 7.000 inches over most of its length, except at the upper and lower ends where special provisions are made to accommodate "O" ring seals. Four Budd Metalfilm Strain Gages (Type C6-1161) are mounted at the mid-height of the soil sample at 90° intervals and connected in series as shown in Fig. 4.3a. In this arrangement, the strains sensed by the four gages are averaged since the change in resistance balanced by the indicator is the sum of the changes in all four gages.

The strain gages are "foil" gages with a gage length of one inch and a grid width of 0.09 inches. The backing of the gages is epoxy and the gages are temperature compensated for steel. Tatnall G-5 adhesive was used for cementing the gages to the ring. The gages were baked on for 2 hours at 175°F and cured for an additional 2 hours at 170°F. The specific reasons for the choice of gages, backing, and cement are given below:

1. The metalfilm gages were chosen because the foil grid is constructed so that the strands parallel to the axis of the gage have a very small cross-sectional area whereas the end loops transverse to the axis of the gage have a large cross-sectional area. This type of construction renders the gage practically insensitive to strains transverse to the axis of the gage. Transverse sensitivity is of paramount importance in this study because the purpose of the gages is to measure only the strains in a circumferential direction. Since there are axial strains in the ring arising from friction between the soil and the ring, it is mandatory that the effect of the axial strains on the output of the gages be minimized.

2. The foil gages were also desirable because the experimental apparatus is constructed such that the gages are required to function in oil up to pressures approaching 2000 psi. This type of gage is relatively insensitive to ambient stresses perpendicular to the plane of the gage.

3. A gage length of one inch was selected for two reasons. First, averaging the circumferential strain over one inch reduces the probability of obtaining an erroneous reading because of a flaw. Secondly, the gage length of 1 inch and a grid width of .09 inches were chosen because this proportion tends to minimize the sensitivity to transverse strains. A study of transverse sensitivity of bonded strain gages is presented by Wu (1962) which supports this choice. One definite conclusion of the study was that the transverse sensitivity decreased from 1% to 0.1% for epoxy-backed foil gages as the gage length increased from 0.1 inch to 1 inch. The writer would like to point out, however, that the gages used in the study cited above were Baldwin gages rather than the Budd gages used on the thin steel ring; therefore, the exact numerical values do not apply. The evidence, however, does point out that transverse sensitivity can be greatly reduced by increasing the gage length.

4. The epoxy backing was selected because it was thought that this backing would be competent enough to perform satisfactorily under the high oil pressures.

5. Tatnall G-5 adhesive was used because it is a competent epoxy cement which was thought to be superior to other cements for functioning under oil pressure. This cement has the additional advantage that it can tolerate strains as large as 15% without unbonding. The cement was baked and cured at around 175°F. If adhesives are not cured at temperatures well above the temperature they are used, it is possible that a rise in temperature during the life of the gages will start a new curing cycle which will cause the gages to record an apparent strain.

The dimensions of the thin steel ring were determined by three considerations: ring friction effects, sensitivity of the ring for measuring the coefficient of earth pressure at rest, and accuracy in vertical strain measurement. The overall dimensions of the ring selected are such that a soil sample approximately 7 inches in diameter by 2 inches high can be accommodated. These proportions were selected in an effort to minimize ring friction. The theoretical basis for the above statement is presented in the following analysis from Taylor (1942).

Consider a confining ring of radius R and height H as shown in Fig. 4.10. At any arbitrary depth z below the surface loaded by the force P, the vertical force supported by the soil is designated as Q_z. The force Q_z may be expressed in terms of the shearing stress τ_z and the applied load P as:

$$Q_z = P - \int_0^z 2\pi R \tau_z dz \qquad (4.1)$$

The shearing stress is also related to Q_z by

$$\tau_z = \frac{Q_z}{A} \cdot K_o \cdot f \qquad (4.2)$$

where A is the area of the sample, K_o is the ratio of the horizontal to vertical stress, and f is the coefficient of friction between the soil and the ring.

Substituting Eq. (4.2) into Eq. (4.1) yields

$$Q_Z = P - \int_o^z 2\pi R \frac{Q_Z}{A} \cdot K_o \cdot f \, dz \qquad (4.3)$$

Differentiating both sides of Eq. (4.3) and rearranging gives

$$\frac{dQ_Z}{Q_Z} = \frac{-2\pi R K_o f}{A} dz \qquad (4.4)$$

Integrating the above equation between the appropriate limits yields

$$\int_P^{Q_H} [\ell n Q_Z] = \int_o^H \left[\frac{-2\pi R K_o f z}{A} \right] = \ell n \frac{Q_H}{P} = \frac{-2\pi R K_o f h}{A} \qquad (4.5)$$

Rearranging Eq. (4.5) gives

$$Q_H = P\epsilon^{\frac{-2\pi R K_o f H}{A}} = P\epsilon^{\frac{-2K_o f H}{R}} \qquad (4.6)$$

where ϵ is the base of Napierian logarithms. Equation (4.6) implies that if $\epsilon^{\frac{-2K_o f H}{R}}$ approaches 1, then $Q_H = P$, and the frictional effects become negligible. This relationship shows that the R/H ratio should be as large as possible to reduce the effect of friction. In fact, increasing the R/H ratio by a factor of 2 has the same effect as reducing the coefficient of friction by 50%.

It is obvious that the R/H ratio may be increased by either increasing the diameter or decreasing the height of the ring. There are practical considerations, however, which limit both of these alternatives. The diameter becomes limited by the

capacity of loading machines available if one desires to attain pressures up to 3000 psi or more. A practical limit is also reached in reducing the height of the sample since the height of the sample influences the accuracy of the vertical strain measurement. If the sample becomes too thin, the increments in vertical displacement can become too small for the Ames dials to sense, especially in the 2000-3000 psi pressure ranges where the constrained modulus of one of the sands tested approaches 250,000 psi. A sample height of 2 inches was selected for giving the required vertical strain sensitivity and a diameter of 7 inches was selected because that is the largest diameter that could be used to obtain at least 3000 psi on the sample with a 120,000 lb. Baldwin testing machine. This combination also gives a desirable diameter to height ratio of 3.5.

The wall thickness of the ring was also determined by compromising two conflicting considerations. The accuracy of the lateral pressure measurement is enhanced by making the ring thin since very small differential pressures across the ring can be detected by the circumferential strain gages. The ring wall, however, cannot be designed too thin since the ring friction could possibly cause a permanent set in the ring or could cause high enough axial strains that the circumferential gage readings would be affected by axial strains even though they are relatively insensitive to transverse strains. A thickness of .094 inches was selected for the design, but the overall design of the apparatus was made so that the wall thickness of the ring could be changed if the .094 thickness proved to be unsatisfactory. The final dimensions of the ring are shown in Fig. 4.6. A pressure differential across this ring of .80 psi produces a calculated circumferential strain of 1 microinch on the outside of the ring. Since the Baldwin strain indicator can only be read accurately to the nearest 5 microinches, the ring is accurate in measuring the lateral stress to 4 psi. This degree of accuracy was thought to be satisfactory for measurement of lateral pressures from 50 - 2000 psi, but is not accurate enough for determining the lateral pressures with less than 10% error for lateral pressures below 50 psi.

The dimensions of the ring were also selected so that when the oil in the annular space is under pressure there is a net upward oil pressure on the ring which holds the ring in a position as shown in the assembled drawing in Fig. 4.5. The purpose of this feature is to keep the ring suspended from the top so that ring friction will put a tensile axial stress rather than a compressive axial stress in the ring. This arrangement also limits the friction because when the frictional force exceeds a certain value the ring will start to move downward, which in turn tends to decrease the friction because the ring begins to act like a floating ring rather than a fixed ring. The net area over which the oil pressure acts upward is 2.32 square inches. Since the oil pressure is equal to the lateral earth pressure, the pressure in the oil is given by:

$$p_o = \sigma_v K_o \tag{4.7}$$

where p_o is the pressure in the oil, σ_v is the average vertical stress on the soil sample, and K_o is the coefficient of earth pressure at rest. The fraction of the total vertical load in friction needed to make the ring of internal radius, R, move down is:

$$\frac{\sigma_v K_o (2.32)\text{in.}^2}{\sigma_v \pi R^2} = \frac{(K_o)(2.32)\text{in.}^2}{(36.5)\text{in.}^2} = 0.064\, K_o \tag{4.8}$$

A sand with a K_o of 0.4 would then move the ring downward with only 2.55% of the vertical load arched into the ring. This movement would in turn tend to reduce the frictional effects by causing the ring to act like a floating ring.

Calibration of the Thin Steel Ring. The effect of the high oil pressure on the strain gages could not be assumed to be negligible even though the gages were selected to minimize these effects. Calibration of the strain gages was accomplished with the apparatus assembled as shown in Fig. 4.11. The significant feature of this assembly is that the lower "O" ring between the bottom of the steel ring and the baseplate has been removed so that the oil in the annular space can communicate freely with the oil inside the sample chamber. A steel plug 1-inch thick is also inserted into the sample chamber

to confine the oil and a testing head is lowered flush with the top of the plug to supply a reaction of sufficient magnitude to keep the plug in place during calibration.

The gages were calibrated by increasing the oil pressure in increments up to 2,500 psi. Since the "O" ring at the bottom of the steel ring was omitted, the oil pressure in the annular space was equal to the pressure in the sample chamber, thus giving zero net pressure differential across the ring. Hence any change in gage reading is due to the effects of the all around oil pressure on the gages. This calibration procedure was conducted several times and the calibration curve obtained is shown in Fig. 4.12. The curve was reproducible within $\pm$ 4 x 10^{-6} in./in. and the pressure effect amounts to 7 x 10^{-6} in./in. per 500 psi of oil pressure. Compensation for these pressure effects was made when the tests were conducted on sands.

The ring was calibrated several times during the testing period and no change in the calibration curve could be detected. Since the first calibration described above, however, a better procedure has been developed which eliminates the necessity of removing the lower "O" ring for calibration. This is important because the cell then does not have to be dismantled for calibration. A steel plug with a hydraulic fitting as shown in Fig. 4.9b is employed in the improved method. The hydraulic jack is then connected to both the hydraulic fitting leading to the annular space around the ring and the hydraulic fitting leading into the sample chamber filled with oil. Since both the inside and outside of the ring are connected to the same pressure source, there is no pressure differential across the ring. This procedure proved to give the same results as the first procedure described above with the advantage of greater efficiency.

Technique for Getting the Gage Wires Out of the Cell. One of the most challenging problems in the design of the cell was devising a method of bringing the strain gage wires out of the cell without cutting the wires or getting an oil leak. The wires also had to be taken out of the cell so that the cell could be taken apart and put

back together without requiring a new seal each time. The final design of the outlet for the gage wires provided an outlet through a 1/8" tapered hole in the base plate as shown in Fig. 4.5. The wires are sealed in the hole with an epoxy cement with a shear strength of 3000 psi which was an excellent dialectric material. The hole was tapered so that the seal would become even tighter at high pressures. In the first stages of the assembly of the cell the wires are fed through the hole in the baseplate. The wires are then sealed in the epoxy cement and about 6 inches of slack wire is left between the point where the wires enter the baseplate to where the wires hook onto the thin steel ring. This slack wire is necessary in order to prevent the wires from being broken when the cell is dismantled. The slack wire is then taped to the outside of the thin steel ring and the thick walled cylinder is lowered around the ring and baseplate and bolted in place. The cell is then ready for use. This method has proven very satisfactory in the pressure ranges of current testing, but it is expected that for extremely high pressures the insulation will have to be stripped from the wires where they pass through the epoxy seal or oil may leak through past the insulation on the wires. This should be no problem, however, if an epoxy is used which is also an excellent dialectric.

Description of the Testing Head. The load was applied to the soil sample by means of a heavy, internally stiffened piston, mounted in a 120,000-lb. hydraulic testing machine as shown in Fig. 4.3. The testing head is 6.800 inches in diameter and 8.125 inches high. The device consists of two rigid steel plates which are welded on two concentric steel cylinders. Figure 4.13 also shows the manner in which a dynamometer is incorporated into the device to measure the pressure over the center square inch of the loaded area. This feature enables one to check the load on the center square inch against the average load over the entire area. The piston and the dynamometer were designed with approximately the same relative stiffness in order to maintain a uniform deflection of the specimen across the face of the loading device as the sample is compressed.

The vertical displacement of the sand during compression was measured by two Ames Dials mounted at 180° to each other on the loading piston as shown in Fig. 4.14. The dials measure the relative displacement between the moving piston and the thick walled cylinder designated as Part A in Fig. 4.5. This measured relative displacement is actually the sum of the vertical displacement of the soil plus the strain in the testing head from the surface of loading to the point where the dials are connected. The strains in the head were so small compared to the strains in the soil that they were neglected and the measurement was taken to represent the vertical displacement of the soil sample. The dials are accurate to 1/10,000 of an inch and have a 0.4 inch travel. When the two dials read differently, the average reading of the two dials was taken as the vertical displacement of the soil.

CHAPTER 5

EXPERIMENTAL RESULTS

5.1 General

One-dimensional compression tests were conducted on four different sands up to a maximum vertical stress of 3290 psi with the apparatus discussed in Chapter 4. Axial stress-strain properties and the coefficient of earth pressure at rest K_o were measured on all tests. The energy absorption capacity of the sands was also measured by means of cyclic loading.

Each sand was tested at a variety of initial void ratios in order to cover the complete range of behavior for each sand. The four sands selected for this study were chosen because they are extremely dissimilar with respect to grain shape and grain-size distribution characteristics. It was hoped that the sands selected would manifest a wide range of one-dimensional properties so that the extreme limits of the various measured quantities could be defined. Descriptions of the sands are given in subsequent sections of this chapter.

Triaxial tests were also conducted on the four sands to document fully the engineering description of the sands and to determine if any of the properties measured in one-dimensional compression could be correlated with index properties defined by well established routine tests. The triaxial test procedure and results are presented in Appendix B.

5.2 Description of Sands

Minnesota Sand. One sand used in this investigation was a uniform, rounded, silica sand obtained from the Gopher State Silica Co. in LeSeur, Minnesota. The sand is a coarse fraction obtained from the St. Peter Formation, a marine sand of Ordovician age. Because of the frosted nature of the sand it is thought to be of eolian origin. The transportation of this sand by wind and the additional working of this sand under marine

forces dN_{ij}, dT_{ij}, dT_{kk} (Fig. 3.7). It is required that the displacements of the center of the spheres be single valued, i.e., the vector distance around the closed path through the center of the spheres must vanish both before and after the medium is strained. Hence the sum of the relative displacements of the center of these spheres around the closed path must vanish. Expressions for this condition for all possible paths connecting the center of a sphere in the medium yields 9 independent equations of compatibility as follows:

$$
\begin{aligned}
&\underline{1}. \quad \sqrt{2}d\delta_{zz} = -da'_{yz} + da_{zx} + d\delta'_{yz} + d\delta_{zx} \\
&\underline{2}. \quad \sqrt{2}d\delta_{zz} = da_{yz} - da'_{zx} - d\delta_{yz} - d\delta'_{zx} \\
&\underline{3}. \quad \sqrt{2}d\delta'_{zz} = -da_{yz} + da_{zx} + d\delta_{yz} + d\delta_{zx} \\
&\underline{4}. \quad \sqrt{2}d\delta_{xx} = -da'_{zx} + da_{xy} + d\delta'_{zx} + d\delta_{xy} \\
&\underline{5}. \quad \sqrt{2}d\delta_{xx} = da_{zx} - da'_{xy} - d\delta_{zx} - d\delta'_{xy} \\
&\underline{6}. \quad \sqrt{2}d\delta'_{xx} = da_{zx} - da_{xy} + d\delta_{zx} + d\delta_{xy} \\
&\underline{7}. \quad \sqrt{2}d\delta_{yy} = da'_{xy} + da_{yz} + d\delta'_{xy} + d\delta_{yz} \\
&\underline{8}. \quad \sqrt{2}d\delta_{yy} = da_{xy} - da'_{yz} - d\delta_{xy} - d\delta'_{yz} \\
&\qquad \sqrt{2}d\delta'_{yy} = -da_{xy} + da_{yz} + d\delta_{xy} + d\delta_{yz}
\end{aligned}
\tag{3.9}
$$

The compatibility equations can be written in terms of force increments by using the compliances

$$
\begin{aligned}
da_{ij} &= C_{ij}dN_{ij} & da'_{ij} &= C_{ij}dN'_{ij} \\
d\delta_{ij} &= S_{ij}dT_{ij} & d\delta_{ij} &= S'_{ij}dT'_{ij} \\
d\delta_{kk} &= S_{kk}dT_{kk} & d\delta'_{kk} &= S'_{kk}dT'_{kk}
\end{aligned}
\tag{3.10}
$$

where the above subscripts identify the contact. Thus Eq. (3.9) together with Eq. (3.8) yield 18 independent equations containing the applied forces dP_{ij}, and 18 independent components of the unknown contact forces, dN_{ij}, dT_{ij}, and dT_{kk}. Unfortunately, these 18 equations are difficult to solve because the equations include the compliances and the compliances are functions of the contact forces. Consequently, a solution to these

equations can be obtained only for a few simple cases.

The incremental extensional and shearing strains in the array, expressed in terms of the compliances, are

$$d\epsilon_{ii} = \frac{1}{4R}\left(da_{ij} + d\delta_{ij} + da'_{ij} + d\delta'_{ij}\right)$$

$$d\gamma_{ij} = \frac{1}{2R}\left(da_{ij} - da'_{ij}\right) \tag{3.11}$$

Likewise the applied force increments P_{ij} in Fig. 3.4 are related to the stress increments for a face-centered array by

$$dP_{ij} = 8R^2 d\sigma_{ij} \tag{3.12}$$

Application to a Hydrostatic State of Stress. One problem of interest which can be solved is that of a face-centered array subjected to a hydrostatic state of stress. Under this state of stress symmetry dictates the conditions that all normal forces at the contacts are equal and all shearing forces are equal. If it is designated that

P_o = total force on the face of a differential element

N_o = normal contact force

T_o = tangential contact force

R = radii of spheres

the equilibrium Eqs. (3.8) reduce to

$$4dT_o + 4\sqrt{2}dN_o = dP_o$$

$$4dT_o - 4\sqrt{2}dN_o = dP_o \tag{3.13}$$

Adding Eqs. (3.13) and considering the initial condition of zero stress yields the expected condition for the tangential force

$$T_o = dT_o = 0$$

Hence, the equilibrium equation becomes

$$dN_o = \frac{1}{4\sqrt{2}}\, dP_o \tag{3.14}$$

If ϵ_o is the hydrostatic strain in any direction, Eq. (3.11) yields

$$d\epsilon_o = \frac{1}{2R}\, da_o \tag{3.15}$$

where da_o is the normal deformation due to dN_o and is related to dN_o by the normal compliance C_o, and

$$da_o = C_o dN_o \tag{3.16}$$

From the Hertz theory

$$C_o = \frac{1 - \nu}{2\mu a_o} \tag{3.17}$$

where a_o is the radius of contact defined by

$$a_o = \left[\frac{3(1 - \nu)\, N_o R}{8\mu}\right]^{1/3} \tag{3.18}$$

By combining Eqs. (3.15), (3.16), (3.17) and (3.18), the incremental strain may be expressed as

$$d\epsilon_o = 1/2 \left[\frac{(1 - \nu)\sqrt{2}}{\mu}\right]^{2/3} \left[3\sigma_o\right]^{-1/3} d\sigma_o \tag{3.19}$$

Integrating Eq. (3.19) and considering zero initial conditions results in

$$\epsilon_o = \left[\frac{3(1 - \nu)\sqrt{2}}{8\mu}\right]^{2/3} \sigma_o^{2/3} \tag{3.20}$$

It should be noted that Eq. (3.20) states that the first stress invariant, I_1, is proportional to the three halves power of the first strain invariant J_1.

It is of interest to compare the results of this theory with some limited experimental results available in the literature. Kjellman (1936) carried out some tests on dry sand subjected to hydrostatic pressure and measured the strains associated with the pressure. Table 3.1 gives the variation of the first stress and strain invariants taken from his experimental results. A plot of these data is shown

in Fig. 3.8. Also shown is a plot of the exponential relationship indicated by the theory discussed, which is fitted to the experimental curve at the 6 kg/cm^2 stress level. The behavior of the sand is not as stiff as the theory indicates in the lower pressure regions whereas it becomes stiffer than the theory predicts in the higher pressure regions. The comparison does point out, however, that the results of the theory associated with the face-centered array of spheres correlate qualitatively with the behavior of dense sand subjected to a hydrostatic state of stress.

3.3 One-Dimensional Theory of Granular Media

Monotonically Increasing Load. The theory of Duffy and Mindlin developed in Section 3.1 will now be extended to solve the stress-strain behavior of an array of spheres subjected to one-dimensional compression. One-dimensional compression is defined as that state of stress resulting from the application of a load in the vertical or z direction when the lateral strains in the x and y directions are zero.

The radial symmetry of the one-dimensional problem greatly simplifies Eqs. (3.8) and (3.9). The representative cube now becomes as shown in Fig. 3.9, and the forces on a sphere reduce to those shown on Fig. 3.10. From symmetry the following simplifications can be made for the forces and displacements:

$$
\begin{aligned}
&N_{xy} = N'_{xy} = N_1 \\
&N_{zy} = N'_{yz} = N_{zx} = N'_{zx} = N_2 \\
&-T_{yz} = -T'_{yz} = T_{zx} = T'_{zx} = T_2 \\
&T_{xx} = T'_{xx} = T_{yy} = T'_{yy} = T_{zz} = T'_{zz} = 0 \\
&T_{xy} = T'_{xy} = 0 \\
&P_{xy} = P_{xz} = P_{zx} = P_{yx} = P_{yz} = P_{zy} = 0 \\
&P_{xx} = P_{yy} = P_H
\end{aligned}
\qquad (3.21)
$$

$$
\begin{aligned}
a_{xy} &= a'_{xy} = a_1 \\
a_{yz} &= a'_{yz} = a_{zx} = a'_{zx} = a_2 \\
-\delta_{yz} &= -\delta'_{yz} = \delta_{zx} = \delta'_{zx} = \delta_2 \\
\delta_{xx} &= \delta'_{xx} = \delta_{yy} = \delta'_{yy} = \delta_{zz} = \delta'_{zz} = 0 \\
\delta_{xy} &= \delta'_{xy} = 0
\end{aligned}
\tag{3.22}
$$

Furthermore, the associated compliances now become

$$
\begin{aligned}
C_{xy} &= C'_{xy} = C_1 \\
C_{yz} &= C'_{yz} = C_{zx} = C'_{zx} = C_2 \\
S_{yz} &= S'_{yz} = S_{zx} = S'_{zx} = S_2
\end{aligned}
\tag{3.23}
$$

Using the above simplifications and considering symmetry reduces the equilibrium Eqs. (3.8) to

$$
\begin{aligned}
dN_2 + dT_2 &= \frac{\sqrt{2}}{8} dP_{zz} \\
dN_1 + dN_2 - dT_2 &= \frac{\sqrt{2}}{4} dP_H
\end{aligned}
\tag{3.24}
$$

In a similar fashion the compatibility Eqs. (3.9) reduce to

$$
da_1 - da_2 + d\delta_2 = 0 \tag{3.25}
$$

where the compliance Eqs. (3.10) now become

$$
\begin{aligned}
da_1 &= C_1 dN_1 \\
da_2 &= C_2 dN_2 \\
d\delta_2 &= S_2 dT_2
\end{aligned}
\tag{3.26}
$$

Substituting Eqs. (3.26) into Eq. (3.25) yields

$$
C_1 dN_1 - C_2 dN_2 + S_2 dT_2 = 0 \tag{3.27}
$$

Equations (3.24) and (3.27) are sufficient to describe the behavior of a granular medium subjected to given vertical and lateral forces P_{zz} and P_H. If, however, only the vertical force is known and the lateral force must also be determined, a further condition is necessary. This condition results from the relationship between the contact displacements and lateral strain.

Due to symmetry the lateral strain ϵ_H determined from Eqs. (3.11) reduces to

$$d\epsilon_H = \frac{da_1}{2R} \tag{3.28}$$

or

$$d\epsilon_H = \frac{C_1 dN_1}{2R} \tag{3.29}$$

Thus the behavior of a face-centered array of spheres subjected to a vertical force P_{zz} and restricted to symmetrical lateral deformations can be obtained from a solution to the following equations:

$$\begin{aligned} dN_2 + dT_2 &= \frac{\sqrt{2}}{8} dP_{zz} \\ dN_1 + dN_2 - dT_2 - \frac{\sqrt{2}}{4} dP_H &= 0 \\ \frac{C_1}{C_2} dN_1 - dN_2 + \frac{S_2}{C_2} dT_2 &= 0 \\ dN_1 &= \frac{2R d\epsilon_H}{C_1} \end{aligned} \tag{3.30}$$

For the case of interest here, namely one-dimensional compression, ϵ_H is required to vanish for all loadings. For this particular state of stress and zero initial conditions, one obtains $N_1 = 0$ and Eqs. (3.30) reduce to

$$dN_2 + dT_2 = \frac{\sqrt{2}}{8} dP_{zz} \tag{3.31a}$$

$$dN_2 - dT_2 - \frac{\sqrt{2}}{4} dP_H = 0 \tag{3.31b}$$

$$dN_2 - \frac{S_2}{C_2} dT_2 = 0 \tag{3.31c}$$

where the expression for $\frac{S_2}{C_2}$ is obtained from Eqs. (3.6) and (3.7) as:

$$\frac{S_2}{C_2} = k_1 \left[f \frac{dN_2}{dT_2} + (1 - f \frac{dN_2}{dT_2}) (1 - \frac{T_2}{fN_2})^{-1/3} \right] \tag{3.32a}$$

where

$$k_1 = \frac{2 - \nu}{2(1 - \nu)} \tag{3.32b}$$

It should be noted that Eqs. (3.31) are simultaneous differential equations and are non-linear because of the compliances in the third equation.

The vertical strains ϵ_{zz} associated with the behavior of this medium can be obtained from Eqs. (3.11) as

$$d\epsilon_{zz} = \frac{1}{2R} (da_2 + d\delta_2) \tag{3.33}$$

The compatibility Eq. (3.31c) states that

$$da_2 = d\delta_2$$

Hence for the one-dimensional case Eq. (3.32) reduces to

$$d\epsilon_{zz} = \frac{da_2}{R} = \frac{C_2 dN_2}{R} \tag{3.34}$$

For the solution of Eqs. (3.31), consider first the compatibility Eq. (3.31c). Substituting Eqs. (3.32) into Eq. (3.31c) and rearranging yields

$$\frac{dT_2}{dN_2} = f + \frac{1 - k_1 f}{k_1} (1 - \frac{T_2}{fN_2})^{1/3} \tag{3.35}$$

Introducing the new variable

$$Z^3 = f - \frac{T_2}{N_2} \tag{3.36a}$$

and

$$N_2 Z^3 = N_2 f - T_2$$

one obtains

$$dN_2 Z^3 + 3 N_2 Z^2 dZ = f dN_2 - dT_2$$

or

$$\frac{dT_2}{dN_2} = f - Z^3 - 3N_2 Z^2 \frac{dZ}{dN_2} \tag{3.36b}$$

By using Eqs. (3.36), Eq. (3.35) can be transformed into the form

$$-\frac{3ZdZ}{Z^2+K_2} = \frac{dN_2}{N_2} \tag{3.37}$$

where

$$K_2 = \frac{1-k_1 f}{k_1^{1/3}} \tag{3.38}$$

Integrating both sides results in

$$\ln N_2 - \ln A = -3/2 \ln (Z^2 + K_2)$$

or

$$\frac{N_2}{A} = (Z^2 + K_2)^{-3/2} \tag{3.39}$$

where A is a constant of integration.

From Eq. (3.36a), Eq. (3.39) becomes

$$\frac{N_2}{A} = \left[(f - \frac{T_2}{N_2})^{2/3} + K_2 \right]^{-3/2} \tag{3.40}$$

Equation (3.40) is the general solution to Eq. (3.31c) and a particular solution may be obtained by evaluating the constant of integration.

Because the initial conditions, $P_{zz} = N_2 = T_2 = 0$, are obvious one is inclined to evaluate A from these conditions. Although this is a true boundary condition, a singularity point occurs at the origin. The equation is, however, well behaved at

other points and the following technique will be used to evaluate A.

Imagine a small hydrostatic state of stress initially holding the spheres in contact before the one dimensional state is imposed. This hydrostatic stress produced no initial tangential force at the contacts but it does cause a normal force of $N_2 = N_o$.

From eq. (3.40)

$$N_o = A(f^{2/3} + K_2)^{-3/2}$$

or solving for A, the constant of integration

$$A = \frac{N_o}{(K_2 + f^{2/3})^{-3/2}} \tag{3.41}$$

Substituting A into Eq. (3.40) yields after some rearranging and taking into account Eq. (3.38).

$$T_2 = fN_2 \left[1 - \left(\frac{1}{fK_1} \left[\left(\frac{N_o}{N_2} \right)^{2/3} - 1 \right] + 1 \right)^{3/2} \right] \tag{3.42}$$

A plot of a family of curves representing Eq. (3.42) with various values of the initial hydrostatic stress N_o is given in Fig. 3.11. The paths of loading are indicated by arrows on the curves. For convenience the coefficient of friction f was taken as 0.3 and Poisson's ratio ν as 0.2.

If an initial hydrostatic stress is imposed the value of N_2 can be determined at which sliding begins. For this condition Eq. (3.42) yields

$$\frac{1}{fK_1} \left[\left(\frac{N_o}{N_2} \right)^{2/3} - 1 \right] + 1 = 0$$

Rewriting and taking account of (3.32b) yields

$$N_2 = \frac{N_o}{\left[1 - \frac{f(2-\nu)}{2(1-\nu)} \right]^{3/2}} \tag{3.43}$$

The reader will recall that the problem was to define the relation between N_2 and T_2 for a granular medium in one-dimensional compression which was loaded from an unstressed condition. It was noted that the solution contained a singularity at the zero stress and it was necessary to provide an initial hydrostatic stress N_o to hold the spheres in contact when loading. If N_o is now allowed to approach zero we obtain the solution desired. On investigating Fig. 3.11 or Eq. (3.42) it is clear that if one-dimensional loading commences from a completely unstressed condition ($N_o = 0$), the relation between N_2 and T_2 is that of a straight line with a slope of 1/f. Thus, the relationship between N_2 and T_2 for a face-centered array subjected to one-dimensional compression is

$$T_2 = fN_2$$

This means that sliding (differentiated from slip in Section 3.1) at the contacts occurs immediately on initiation of loading. This is extremely important in that the theory developed to date along the lines of Mindlin et al does not allow sliding at the contacts. It will be shown herein that the stress-strain relationships in the one-dimensional granular medium can be described mathematically even though sliding occurs throughout the application of a monotonically increasing load.

From compatibility, even in the case of sliding, the geometrical relationship still holds for the displacements at the contacts, i.e.

$$da_2 - d\delta_2 = 0 \tag{3.44}$$

It must be emphasized, however, that the tangential displacement δ_2 is no longer related to the tangential contact force T_2 by the tangential compliance S_2 because of sliding at the contacts. The tangential displacement is now made up of two effects, a sliding effect and a contribution due to slip. On the other hand, the normal forces and displacements are still connected by the compliances.

Furthermore, because Eq. (3.44) is a geometrical relationship, it also holds for total displacements in the problem at hand; hence,

$$a_2 = \delta_2 \tag{3.45}$$

The vertical strain Eq. (3.33) is also purely geometrical and can be written as

$$d\epsilon_{zz} = \frac{da_2}{R} = \frac{C_2 dN_2}{R} \tag{3.46}$$

The equilibrium Eqs. (3.31a) and (3.31b), which were originally written in terms of differential stresses, also hold for total stresses. Hence,

$$N_2 + T_2 = \frac{\sqrt{2}}{8} P_{zz} \tag{3.47a}$$

$$N_2 - T_2 - \frac{\sqrt{2}}{4} P_H = 0 \tag{3.47b}$$

It has already been determined that N_2 and T_2 are related by the coefficient of friction throughout the entire loading, i.e.

$$fN_2 - T_2 = 0 \tag{3.47c}$$

The behavior of the granular medium subjected to one-dimensional compression can now be described by Eqs. (3.44, (3.54), (3.46), and (3.47).

Equations (3.47) may be combined to eliminate T_2 resulting in

$$N_2 (1+f) = \frac{\sqrt{2}}{8} P_{zz} \tag{3.48a}$$

$$N_2 (1-f) = \frac{\sqrt{2}}{4} P_H \tag{3.48b}$$

In theoretical soil mechanics a quantity of major interest in one-dimensional compression is K_o, the ratio between the horizontal and vertical stresses at rest. From Eqs. (3.48) this ratio is clearly

$$K_o = \frac{P_H}{P_{zz}} = \frac{1}{2} \left(\frac{1-f}{1+f}\right) \tag{3.49}$$

Some indication of the variation of K_o with the coefficient of friction f is shown in Table 3.2.

The strains resulting from one-dimensional compression may now be investigated. The substitution of Eq. (3.2) into Eq. (3.46) yields

$$d\epsilon_{zz} = \frac{(1-\nu)}{2\mu R}\left[\frac{3(1-\nu)\,RN_2}{8\mu}\right]^{-1/3} dN_2 \qquad (3.50)$$

Combining Eqs. (3.50) and (3.48a) and noting from Fig. 3.9 that

$$\sigma_{zz} = \frac{P_{zz}}{8R^2} \qquad (3.51)$$

gives

$$d\epsilon_{zz} = \frac{1}{2}\left[\frac{(1-\nu)\sqrt{2}}{\mu(1+f)}\right]^{2/3}\left[3/8\,\sigma_{zz}\right]^{-1/3} d\sigma_{zz} \qquad (3.52)$$

Integration of Eq. (3.52) yields

$$\epsilon_{zz} = \left[\frac{(1-\nu)\,(3)\sqrt{2}}{\mu\,(1+f)\,(8)}\right]^{2/3} 2\sigma_{zz}^{2/3} \qquad (3.53)$$

An interesting result of Eq. (3.53) is that the stress-strain behavior is independent of the radii of the particles. A comparison of the stress-strain curves for hydrostatic and one-dimensional compression shows that the curves are similar in shape, but turn up at different rates. The ratio of the one-dimensional strain to the hydrostatic strain at the same level of stress, σ_{zz}, is a ratio of Eqs. (3.53) to (3.20), which reduces to

$$\frac{\epsilon_{zz}}{\epsilon_o} = \frac{2}{(1+f)^{2/3}} \qquad (3.54)$$

Values of f of 0.1 and 0.2 give values for ϵ_{zz}/ϵ_o of 1.88 and 1.77, respectively. This indicates that the hydrostatic and one-dimensional stress-strain curves are related as shown in Fig. 3.12.

Unloading Cycle. When the medium is loaded the tangential forces tend to resist the sliding motion. During unloading the tangential forces tend to resist the sliding movement which is now in the opposite direction. Hence, the tangential forces reverse their direction on unloading. The cases of loading and unloading are illustrated

schematically in Fig. 3.13. The normal and tangential forces are still related by the coefficient of friction; only now the direction of the tangential force is changed.

The new equilibrium equations become

$$N_2 - T_2 = \frac{\sqrt{2}}{8} P_{zz}$$

$$N_2 + T_2 = \frac{\sqrt{2}}{4} P_H \tag{3.55}$$

where

$$fN_2 - T_2 = 0 \tag{3.56}$$

Consider the medium to be loaded from 0 to σ^*_{zz}, Fig. 3.14, according to Eqs. (3.53). If equilibrium Eqs. (3.55) become valid at the instant ϵ_{zz} begins to decrease from ϵ^*_{zz}, then σ_{zz} will decrease instantaneously from σ^*_{zz} to some value σ'_{zz}. At the end of loading N_2 and σ^*_{zz} are related by

$$\sigma^*_{zz} = N_2 \frac{(1+f)}{\sqrt{2}R^2} \tag{3.57}$$

whereas the stress σ'_{zz} is related to the contact forces by Eqs. (3.54) and Eq. (3.51) by

$$\sigma'_{zz} = \frac{N_2 (1-f)}{2R^2} \tag{3.58}$$

The relation between σ^*_{zz} and σ'_{zz} at the instant when ϵ_{zz} just begins to decrease is

$$\sigma'_{zz} = \sigma^*_{zz} \left(\frac{1-f}{1+f}\right) \tag{3.59}$$

because the value of N_2 has essentially the same value while the shearing stress has changed directions. Combining Eqs. (3.55), (3.51), (3.46) and (3.2) yields for unloading

$$d\epsilon_{zz} = 1/2 \left[\frac{(1-\nu)\sqrt{2}}{\mu (1-f)}\right]^{2/3} \left[3/8\, \sigma_{zz}\right]^{-1/3} d\sigma_{zz} \tag{3.60}$$

which by integration becomes

$$\epsilon_{zz} = \left[\frac{(1-\nu)\, 3\sqrt{2}}{\mu\,(1-f)\, 8}\right]^{2/3} 2\,\sigma_{zz}^{2/3} \tag{3.61}$$

The entire stress-strain history for one cycle of loading in one-dimensional compression is shown in Fig. 3.14 in terms of σ^*_{zz} and σ'_{zz}. The derivations above are based upon the assumption that the tangential contact forces immediately reverse directions when unloading begins. This assumption is not quite true, however, because each sphere must exhibit a small elastic tangential displacement before the tangential forces can change direction. This effect, however, is small with respect to the tangential displacement due to sliding and was neglected in the analysis. Because of the above assumption, the stress-strain curve reflects a vertical drop in stress from A to B without any change in strain. If the small elastic tangential displacement due to slip were accounted for, the stress-strain curve would follow a smooth relationship such as the dotted line suggested in Fig. 3.14.

The stress-strain behavior shown in Fig. 3.14 exhibits an energy loss after a cycle of loading and unloading but has no residual strain. Hence, this medium can absorb energy without any permanent displacements.

Energy Absorption. The amount of energy absorbed by the medium on loading and subsequent unloading can now be determined.

The energy E_1 required to load up to an applied vertical stress of σ^*_{zz} and the strain of ϵ^*_{zz} is

$$E_1 = \int_0^{\epsilon^*_{zz}} \sigma_{zz} d\epsilon_{zz}$$

$$E_1 = \frac{4}{5}\,(1+f)\,\epsilon^{*5/2}_{zz} \tag{3.62}$$

The energy taken out of the medium E_2 during unloading back to zero from a stress of σ'_{zz} and strain ϵ^*_{zz} is

$$E_2 = \frac{4}{5}(1 - f)\epsilon^{*5/2}_{zz} \tag{3.63}$$

Thus, the energy lost is

$$\Delta E = E_1 - E_2 = \frac{8}{5} f\epsilon^{*5/2}_{zz} \tag{3.64}$$

The ratio of the energy loss to the energy input is

$$\frac{\Delta E}{E_1} = \frac{2f}{1+f} \tag{3.65}$$

Thus, a very significant property of the one-dimensional stress-strain curve is that the per cent of energy absorbed due to loading and unloading is always constant for a material and depends only on the coefficient of friction at the contacts. Hence, the ratio of the area between the loading and unloading curves to the area under the loading curve is a constant given by Eq. (3.65). The per cent energy absorbed for various coefficients of friction is given in Table 3.2.

The relationship between normal and tangential contact forces determines the relationship between the recoverable and dissipated energies. The work done by the normal forces during deformation $\int N_2 da_2$ is stored in the form of recoverable strain energy. On the other hand, the work done by the tangential forces $\int T_2 d\delta_2$ is a non-recoverable energy and is dissipated as heat into the medium. As seen from Table 3.2 this energy loss during one cycle can be quite significant. In fact, with a coefficient of friction of 0.15, the dissipated energy is 26.1% of the energy put into the system.

3.4 Equivalent Discrete Mass Model for One-Dimensional Static and Dynamic Behavior

In recent years, an increasing effort has been devoted to studying the static and dynamic behavior of soils using discrete mass-spring models. These models have taken many shapes with various components from models such as the standard Voigt and Maxwell models. These model studies have been particularly useful in wave

propagation studies, such as the work of Smith and Newmark (1958). The dynamic equations of motion can be integrated numerically with a digital computer using the β-method (Newmark, 1959); it is a fairly straightforward approach to modify soil parameters or spring stiffnesses as the need arises.

As might be expected from such an approach, there are certain aspects of the soil behavior which escape the mass-spring model. Part of this inaccuracy is due to the discreteness of the system and part can be attributed to choice of the model itself. A study of the problems associated with the choice of various models for investigating the propagation of stress waves in a one-dimensional medium has been carried out by Murtha (1961).

In spite of the inherent difficulties associated with the use of models, there are some cases where the model is the only hope for obtaining even an approximate solution. Therefore, the writer would like to suggest a one-dimensional model which seems to exhibit the behavior expected of dry cohesionless sand, and is based upon the theory presented in Section 3.2.

If a pressure on the surface of the earth extends over a large area, it may be reasonable to consider the soil completely confined. If this condition is satisfied, and the soil composition is similar to sand, the one-dimensional behavior discussed herein may very well be a good approximation to the in-situ soil behavior.

Horizontal Model. Figure 3.15 gives a model representation of the granular system described in Section 3.2. This model yields the same stress-strain curve as the spheres for a static load as the load increases or decreases. The model consists of non-linear spring elements and Coulomb damping elements which dissipate energy by the same mechanism as the spheres. The reason that the model depicts horizontal behavior is that there are no initial stresses in the model before the load is applied. Such an assumption might be reasonable for a vertical column if the weight of the soil is negligible compared to the applied stresses.

Vertical Model. The vertical model is slightly more complex than the horizontal one in that the weight of the material produces initial stresses in the model. Since the stress-strain curve for the material is non-linear, the stiffness is a function of the stress, and consequently, a function of the height of overburden. The overburden pressure increases linearly with depth and it can therefore be incorporated in the equations of motion.

A vertical model which includes the initial stresses due to the overburden of the material is given in Fig. 3.16. It includes a change in stiffness associated with the increased initial stress and follows the stress-strain behavior consistent with the analysis of the granular medium in Section 3.2.

3.5 Theoretical Relationship Between the Angle of Internal Friction, Coefficient of Earth Pressure at Rest, and the Coefficient of Friction Between Spheres for a Face-Centered Cubic Array of Uniform Spheres.

The relationship between the principal stresses at failure for a face-centered cubic array has been investigated by Thurston and Deresiewicz (1959). The analysis applies to an array as shown in Fig. 3.9 which is initially under an isotropic confining pressure, σ_o, and subsequently subjected to a uniaxial stress difference, σ_{zz}, as shown in Fig. 3.17. When σ_{zz} approaches the ultimate value, failure planes are formed by a series of shearing displacements of individual layers of spheres. The failure is initiated in layers containing planes in which the density of sphere centers is greatest, i.e., the (111) planes or octahedral planes with respect to the co-ordinate axis in Fig. 3.9. It is also interesting to note that Smith (1961) reports exactly the same phenomena for yielding in steel crystals which have a crystal arrangement such that the atoms have exactly the same location as the centers of the spheres in Fig. 3.9. A single relative shearing displacement of parallel (111) layers would translate sphere A, Fig. 3.9, from the hollow between spheres B, C, and E to the hollow between spheres B, C, and D. The translation of sphere A would be a distance of $R\sqrt{4/3}$ in the $[1\bar{1}2]$ direction. The

expression given by Thurston and Deresiewicz for the maximum stress difference that can be maintained without failure between octahedral layers of spheres is

$$\frac{\sigma_{zz}}{\sigma_o} = \frac{\sqrt{6} + 8f}{\sqrt{6} - 4f} \tag{3.66}$$

Since the major principal stress, σ_1, is given by

$$\sigma_1 = \sigma_{zz} + \sigma_o \tag{3.67}$$

and the minor principal stress, σ_3, is equal to σ_o, then equation 3.66 may be written as

$$\frac{\sigma_1 - \sigma_3}{\sigma_3} = \frac{\sqrt{6} + 8f}{\sqrt{6} - 4f} \tag{3.68}$$

If Eq. 3.68 is examined for the limiting condition of $f \leq 0$, then it is found that a stress difference equal to the confining stress can be maintained in this array even if the spheres are frictionless. The writer was initially disturbed by this result and analyzed several simple geometrical arrangements of frictionless spheres. It was found by the method of virtual displacements that the stress difference that could be maintained with a given confining stress was a function of the structural arrangement of the frictionless spheres. At the point of failure, the principal stresses and the kinematically possible virtual displacements in the principal directions are such that the change in potential energy is zero. Because the structural arrangement controls the displacements which are kinematically possible, then it follows that the structure also controls the principal stress ratio at failure in a frictionless array of spheres. For a given structural arrangement the stress difference at failure is governed by the boundary displacement conditions, such as the boundary restrictions in plane strain. The change in kinematically possible displacements imposed by the condition of plane strain accounts for the increased apparent angle of internal friction observed for granular materials sheared in plane strain.

The ratio of the principal stresses at failure for a dry granular material is defined by

$$\frac{\sigma_1}{\sigma_3} = \frac{1 + \sin \phi}{1 - \sin \phi} \tag{3.69}$$

where ϕ is the angle of internal friction of the material. The elimination of σ_1 and σ_3 from equation 3.68 and 3.69 yields

$$\sin \phi = \frac{8f + \sqrt{6}}{3\sqrt{6}} \tag{3.70}$$

Eq. (3.70) is more meaningful if it is written in the form

$$\sin \phi = \frac{1}{3} + \frac{8}{3\sqrt{6}} f \tag{3.71}$$

Eq. (3.71) clearly shows that part of the angle of internal friction is due to friction and the remainder is due to the structural arrangement. Eqs. (3.70) and (3.68) are correct only for a face-centered array of uniform spheres but the relationships suggest that the following relation should apply to any granular medium

$$\sin \phi = K_3 + C_1 f \tag{3.72}$$

where K_3 is a portion of sin ϕ due only to structure (relative density) and C_1 is a constant determined by the structural arrangement (relative density) which governs how efficiently the coefficient of friction is in increasing sin ϕ. It should be pointed out that the conclusions drawn above by the writer are contradictory to equations published by Bishop (1954) and Caquot (1934). The equation published for triaxial stress conditions, where $\sigma_2 = \sigma_3 < \sigma_1$, by A. W. Bishop was

$$\sin \phi = \frac{15f}{10 + 3f} \tag{3.73}$$

and the equations published by Caquot (1934) and Bishop (1954) for plane strain were respectively

$$\tan \phi = \pi/2\, f \tag{3.73}$$

and

$$\sin \phi = 3/2\, f$$

All of the relationships suggested by Bishop and Caquot show that ϕ reduces to zero when f reduces to zero. Thus the equations do not include a term which shows a component of the angle of internal friction which is a function only of structure, (relative density), and independent of the coefficient of friction between grains. It is therefore concluded that the equations given by Bishop and Caquot cannot explain the variation of ϕ with relative density.

Studies of the strength characteristics of uniform spheres in various packings are presented by Idel (1960) and Wittke (1962) which support the opinion of the writer. In fact, relationships between porosity and tan ϕ are presented in each study for the special case of the coefficient of friction between spheres equal to zero. Therefore the studies of Idel and Wittke also point out that part of the shear strength of a granular medium is due to structural arrangement, (relative density), and is independent of the coefficient of friction between particles. For the case of triaxial compression of a medium of frictionless spheres in the densest packing, Idel (1960) gives a value of 0.38 for tan ϕ whereas the value tan ϕ calculated from Eq. (3.71) for f = 0 is 0.35. The agreement is very good and the difference is due to the fact that the densest packing considered in this study was a face-centered cubic array whereas the densest stacking considered by Idel was a closed-packed hexagonal array.

The coefficient of earth pressure at rest and the angle of internal friction for a face-centered array can be related by combining Eqs. (3.49) and (3.70) to give

$$K_o = \frac{1}{2}\left[\frac{1 + \sqrt{6}/8 - 3\sqrt{6}/8 \sin\phi}{1 - \sqrt{6}/8 + 3\sqrt{6}/8 \sin\phi}\right] \qquad (3.76)$$

A plot of Eq. (3.76) is shown in Fig. 3.18 and a relationship between K_o and sin ϕ as suggested by Jaky (1944) is shown for comparison. The relationship given in Eq. (3.76) suggests that K_o decreases as ϕ increases, which is similar qualitatively to Jaky's relationship but not numerically identical. The coefficient of friction f was

iminated between Eqs. (3.49) and (3.70) to obtain Eq. (3.76) because, although the
efficient of friction is a useful tool in relating ϕ and K_o, it cannot be measured
liably for grains with roughness and small radii of curvature. Eq. (3.76) can be
ecked, however, in the above form by measuring K_o and ϕ for a granular material.

CHAPTER 4

THE DEVELOPMENT OF A SPECIAL, HIGH PRESSURE, ONE-DIMENSIONAL COMPRESSION APPARATUS

4.1 General

A device was designed and built to investigate the one-dimensional behavior of sand in the high pressure regions. The apparatus can measure the lateral stress under conditions of zero lateral strain, and provides one of the best means yet developed for attaining the condition of "zero" lateral strain. Previous investigators have generally assumed that the effects of small lateral strains are negligible, particularly when the sample is enclosed in steel rings. Research by Speer (1944), which was recently pointed out by Fulton and Hendron (1962) shows that lateral motion significantly affects the ratio of σ_H/σ_V. The results of Speer's research is presented in graphical form in Fig. 4.1 and shows that a lateral displacement of 4×10^{-6} inches will cause a 10% reduction in the value of σ_H/σ_V. Since Speer's work was with a sand sample 7 5/8 inches in diameter, the above diameter change corresponds to a unit strain of approximately $.5 \times 10^{-6}$ in./in. It is doubtful to the writer that Speer really achieved an accuracy of $\pm 1 \times 10^{-6}$ in./in. since slight electrical instabilities in the circuit would cause minor variations of at least that magnitude in the strain gage readings. However, his work does in general point out that the ratio of σ_H/σ_V is very sensitive to lateral movements. This phenomenon had already been observed by Terzaghi (1934) in connection with his "Large Retaining Wall Tests" at MIT. Terzaghi concluded that an outward movement of the wall of .0007 h in the case of a well compacted dense sand was enough to fully mobilize the shear strength or, in other words, reduce the ratio of σ_H/σ_V to the coefficient of active earth pressure. This outward movement corresponds approximately to a lateral strain of about 12×10^{-4} in./in. Thus for a truly one-dimensional test, whereby one also wishes to measure the

magnitude of the lateral stresses which are concomitant with the vertical load, it is extremely important to closely control the lateral displacements. In fact, preliminary calculations revealed that an extremely thick walled cylinder subjected to an internal pressure of 7,500 psi (which is an approximation to the lateral soil pressure due to a vertical load of 15,000 psi) would experience a radial strain of 3.25×10^{-4} in./in. if the specimen were 7 inches in diameter and the containing cylinder were assumed to have an infinite external radius. This strain is of the same order of magnitude as the tolerable strains listed by Speer and Terzaghi. Thus, in order to study one-dimensional compression, a new experimental apparatus had to be designed which would restrict the lateral deformations. The apparatus developed in this study is discussed in the following sections.

4.2 Experimental Apparatus

General Description of the Apparatus. An experimental apparatus designed to determine the stress-strain relations for soil under one-dimensional compression and to measure the lateral stress necessary to completely restrain the sample is shown schematically in Fig. 4.2. The apparatus consists essentially of a thin steel ring, which contains a soil sample, surrounded by an annular space. The annular space is filled with oil which communicates freely with hydraulic jacks. The flexible ring and oil space are enclosed in a thick hollow cylinder bolted to a baseplate in order to withstand the high fluid pressures. The vertical load is applied to the sample by the testing head shown in Fig. 4.2 which is mounted in a 120,000 lb Baldwin testing machine.

The principle upon which the device is based is relatively simple. As the vertical load is applied by the testing head there are lateral pressures built up in the sand which tend to increase the diameter of the thin steel ring. Any slight increase in the diameter of the ring is immediately indicated by the strain gages mounted on the flexible ring as shown in Figs. 4.2 and 4.3a. In order to keep the lateral strains zero, the oil pressure

is modified with changes in the vertical load in such a manner that the strain indicator remains balanced at all times during the test. When the strain indicator remains balanced, there are no lateral strains and the oil pressure is equal to the lateral soil pressure acting against the inside of the container.

The apparatus consists of the following four basic elements:

(1) A thin steel ring monitored with strain gages, Fig. 4.3a.

(2) A testing head, Fig. 4.3b.

(3) A baseplate, Fig. 4.4a.

(4) A thick walled cylinder, Fig. 4.4b.

A detailed assembly drawing of the test cell is shown drawn to full scale in Fig. 4.5. The three component parts of the cell are drawn to full scale in Figs. 4.6, 4.7, and 4.8. The apparatus setup for testing in a 120,000 lb. hydraulic testing machine is shown in Fig. 4.9a.

Design of the Thin Steel Ring. The key sensing device, upon which the measurement of the coefficient of earth pressure at rest is dependent, is the instrumented steel ring. The steel ring is essentially a thin tube which has an internal diameter of 6.812 inches and an external diameter of 7.000 inches over most of its length, except at the upper and lower ends where special provisions are made to accommodate "O" ring seals. Four Budd Metalfilm Strain Gages (Type C6-1161) are mounted at the mid-height of the soil sample at 90° intervals and connected in series as shown in Fig. 4.3a. In this arrangement, the strains sensed by the four gages are averaged since the change in resistance balanced by the indicator is the sum of the changes in all four gages.

The strain gages are "foil" gages with a gage length of one inch and a grid width of 0.09 inches. The backing of the gages is epoxy and the gages are temperature compensated for steel. Tatnall G-5 adhesive was used for cementing the gages to the ring. The gages were baked on for 2 hours at 175°F and cured for an additional 2 hours at 170°F. The specific reasons for the choice of gages, backing, and cement are given below:

1. The metalfilm gages were chosen because the foil grid is constructed so that the strands parallel to the axis of the gage have a very small cross-sectional area whereas the end loops transverse to the axis of the gage have a large cross-sectional area. This type of construction renders the gage practically insensitive to strains transverse to the axis of the gage. Transverse sensitivity is of paramount importance in this study because the purpose of the gages is to measure only the strains in a circumferential direction. Since there are axial strains in the ring arising from friction between the soil and the ring, it is mandatory that the effect of the axial strains on the output of the gages be minimized.

2. The foil gages were also desirable because the experimental apparatus is constructed such that the gages are required to function in oil up to pressures approaching 2000 psi. This type of gage is relatively insensitive to ambient stresses perpendicular to the plane of the gage.

3. A gage length of one inch was selected for two reasons. First, averaging the circumferential strain over one inch reduces the probability of obtaining an erroneous reading because of a flaw. Secondly, the gage length of 1 inch and a grid width of .09 inches were chosen because this proportion tends to minimize the sensitivity to transverse strains. A study of transverse sensitivity of bonded strain gages is presented by Wu (1962) which supports this choice. One definite conclusion of the study was that the transverse sensitivity decreased from 1% to 0.1% for epoxy-backed foil gages as the gage length increased from 0.1 inch to 1 inch. The writer would like to point out, however, that the gages used in the study cited above were Baldwin gages rather than the Budd gages used on the thin steel ring; therefore, the exact numerical values do not apply. The evidence, however, does point out that transverse sensitivity can be greatly reduced by increasing the gage length.

4. The epoxy backing was selected because it was thought that this backing would be competent enough to perform satisfactorily under the high oil pressures.

5. Tatnall G-5 adhesive was used because it is a competent epoxy cement which was thought to be superior to other cements for functioning under oil pressure. This cement has the additional advantage that it can tolerate strains as large as 15% without unbonding. The cement was baked and cured at around 175°F. If adhesives are not cured at temperatures well above the temperature they are used, it is possible that a rise in temperature during the life of the gages will start a new curing cycle which will cause the gages to record an apparent strain.

The dimensions of the thin steel ring were determined by three considerations: ring friction effects, sensitivity of the ring for measuring the coefficient of earth pressure at rest, and accuracy in vertical strain measurement. The overall dimensions of the ring selected are such that a soil sample approximately 7 inches in diameter by 2 inches high can be accommodated. These proportions were selected in an effort to minimize ring friction. The theoretical basis for the above statement is presented in the following analysis from Taylor (1942).

Consider a confining ring of radius R and height H as shown in Fig. 4.10. At any arbitrary depth z below the surface loaded by the force P, the vertical force supported by the soil is designated as Q_z. The force Q_z may be expressed in terms of the shearing stress τ_z and the applied load P as:

$$Q_z = P - \int_0^z 2\pi R \tau_z dz \qquad (4.1)$$

The shearing stress is also related to Q_z by

$$\tau_z = \frac{Q_z}{A} \cdot K_o \cdot f \qquad (4.2)$$

where A is the area of the sample, K_o is the ratio of the horizontal to vertical stress, and f is the coefficient of friction between the soil and the ring.

Substituting Eq. (4.2) into Eq. (4.1) yields

$$Q_Z = P - \int_o^z 2\pi R \frac{Q_Z}{A} \cdot K_o \cdot f \, dz \qquad (4.3)$$

Differentiating both sides of Eq. (4.3) and rearranging gives

$$\frac{dQ_Z}{Q_Z} = \frac{-2\pi R K_o f}{A} dz \qquad (4.4)$$

Integrating the above equation between the appropriate limits yields

$$\int_P^{Q_H} [\ell n Q_Z] = \int_o^H \left[\frac{-2\pi R K_o f z}{A}\right] = \ell n \frac{Q_H}{P} = \frac{-2\pi R K_o f h}{A} \qquad (4.5)$$

Rearranging Eq. (4.5) gives

$$Q_H = P\epsilon^{\frac{-2\pi R K_o f H}{A}} = P\epsilon^{\frac{-2K_o f H}{R}} \qquad (4.6)$$

where ϵ is the base of Napierian logarithms. Equation (4.6) implies that if $\epsilon^{\frac{-2K_o f H}{R}}$ approaches 1, then $Q_H = P$, and the frictional effects become negligible. This relationship shows that the R/H ratio should be as large as possible to reduce the effect of friction. In fact, increasing the R/H ratio by a factor of 2 has the same effect as reducing the coefficient of friction by 50%.

It is obvious that the R/H ratio may be increased by either increasing the diameter or decreasing the height of the ring. There are practical considerations, however, which limit both of these alternatives. The diameter becomes limited by the

capacity of loading machines available if one desires to attain pressures up to 3000 psi or more. A practical limit is also reached in reducing the height of the sample since the height of the sample influences the accuracy of the vertical strain measurement. If the sample becomes too thin, the increments in vertical displacement can become too small for the Ames dials to sense, especially in the 2000-3000 psi pressure ranges where the constrained modulus of one of the sands tested approaches 250,000 psi. A sample height of 2 inches was selected for giving the required vertical strain sensitivity and a diameter of 7 inches was selected because that is the largest diameter that could be used to obtain at least 3000 psi on the sample with a 120,000 lb. Baldwin testing machine. This combination also gives a desirable diameter to height ratio of 3.5.

The wall thickness of the ring was also determined by compromising two conflicting considerations. The accuracy of the lateral pressure measurement is enhanced by making the ring thin since very small differential pressures across the ring can be detected by the circumferential strain gages. The ring wall, however, cannot be designed too thin since the ring friction could possibly cause a permanent set in the ring or could cause high enough axial strains that the circumferential gage readings would be affected by axial strains even though they are relatively insensitive to transverse strains. A thickness of .094 inches was selected for the design, but the overall design of the apparatus was made so that the wall thickness of the ring could be changed if the .094 thickness proved to be unsatisfactory. The final dimensions of the ring are shown in Fig. 4.6. A pressure differential across this ring of .80 psi produces a calculated circumferential strain of 1 microinch on the outside of the ring. Since the Baldwin strain indicator can only be read accurately to the nearest 5 microinches, the ring is accurate in measuring the lateral stress to 4 psi. This degree of accuracy was thought to be satisfactory for measurement of lateral pressures from 50 - 2000 psi, but is not accurate enough for determining the lateral pressures with less than 10% error for lateral pressures below 50 psi.

The dimensions of the ring were also selected so that when the oil in the annular ɔace is under pressure there is a net upward oil pressure on the ring which holds the ıng in a position as shown in the assembled drawing in Fig. 4.5. The purpose of this ıature is to keep the ring suspended from the top so that ring friction will put a tensile xial stress rather than a compressive axial stress in the ring. This arrangement also ımits the friction because when the frictional force exceeds a certain value the ring will tart to move downward, which in turn tends to decrease the friction because the ring egins to act like a floating ring rather than a fixed ring. The net area over which the ıil pressure acts upward is 2.32 square inches. Since the oil pressure is equal to the ateral earth pressure, the pressure in the oil is given by:

$$p_o = \sigma_v K_o \tag{4.7}$$

where p_o is the pressure in the oil, σ_v is the average vertical stress on the soil sample, and K_o is the coefficient of earth pressure at rest. The fraction of the total vertical load in friction needed to make the ring of internal radius, R, move down is:

$$\frac{\sigma_v K_o (2.32)\text{in.}^2}{\sigma_v \pi R^2} = \frac{(K_o)(2.32)\text{in.}^2}{(36.5)\text{in.}^2} = 0.064\, K_o \tag{4.8}$$

A sand with a K_o of 0.4 would then move the ring downward with only 2.55% of the vertical load arched into the ring. This movement would in turn tend to reduce the frictional effects by causing the ring to act like a flo ·ing ring.

Calibration of the Thin Steel Ring. The effect of the high oil pressure on the strain gages could not be assumed to be negligible even though the gages were selected to minimize these effects. Calibration of the strain gages was accomplished with the apparatus assembled as shown in Fig. 4.11. The significant feature of this assembly is that the lower "O" ring between the bottom of the steel ring and the baseplate has been removed so that the oil in the annular space can communicate freely with the oil inside the sample chamber. A steel plug 1-inch thick is also inserted into the sample chamber

to confine the oil and a testing head is lowered flush with the top of the plug to supply a reaction of sufficient magnitude to keep the plug in place during calibration.

The gages were calibrated by increasing the oil pressure in increments up to 2,500 psi. Since the "O" ring at the bottom of the steel ring was omitted, the oil pressure in the annular space was equal to the pressure in the sample chamber, thus giving zero net pressure differential across the ring. Hence any change in gage reading is due to the effects of the all around oil pressure on the gages. This calibration procedure was conducted several times and the calibration curve obtained is shown in Fig. 4.12. The curve was reproducible within $\pm$ 4 x 10^{-6} in./in. and the pressure effect amounts to 7 x 10^{-6} in./in. per 500 psi of oil pressure. Compensation for these pressure effects was made when the tests were conducted on sands.

The ring was calibrated several times during the testing period and no change in the calibration curve could be detected. Since the first calibration described above, however, a better procedure has been developed which eliminates the necessity of removing the lower "O" ring for calibration. This is important because the cell then does not have to be dismantled for calibration. A steel plug with a hydraulic fitting as shown in Fig. 4.9b is employed in the improved method. The hydraulic jack is then connected to both the hydraulic fitting leading to the annular space around the ring and the hydraulic fitting leading into the sample chamber filled with oil. Since both the inside and outside of the ring are connected to the same pressure source, there is no pressure differential across the ring. This procedure proved to give the same results as the first procedure described above with the advantage of greater efficiency.

Technique for Getting the Gage Wires Out of the Cell. One of the most challenging problems in the design of the cell was devising a method of bringing the strain gage wires out of the cell without cutting the wires or getting an oil leak. The wires also had to be taken out of the cell so that the cell could be taken apart and put

ıck together without requiring a new seal each time. The final design of the outlet for ıe gage wires provided an outlet through a 1/8" tapered hole in the base plate as shown ı Fig. 4.5. The wires are sealed in the hole with an epoxy cement with a shear strength f 3000 psi which was an excellent dialectric material. The hole was tapered so that the eal would become even tighter at high pressures. In the first stages of the assembly of ıe cell the wires are fed through the hole in the baseplate. The wires are then sealed in he epoxy cement and about 6 inches of slack wire is left between the point where the vires enter the baseplate to where the wires hook onto the thin steel ring. This slack vire is necessary in order to prevent the wires from being broken when the cell is lismantled. The slack wire is then taped to the outside of the thin steel ring and the thick walled cylinder is lowered around the ring and baseplate and bolted in place. The cell is then ready for use. This method has proven very satisfactory in the pressure ranges of current testing, but it is expected that for extremely high pressures the insulation will have to be stripped from the wires where they pass through the epoxy seal or oil may leak through past the insulation on the wires. This should be no problem, however, if an epoxy is used which is also an excellent dialectric.

Description of the Testing Head. The load was applied to the soil sample by means of a heavy, internally stiffened piston, mounted in a 120,000-lb. hydraulic testing machine as shown in Fig. 4.3. The testing head is 6.800 inches in diameter and 8.125 inches high. The device consists of two rigid steel plates which are welded on two concentric steel cylinders. Figure 4.13 also shows the manner in which a dynamometer is incorporated into the device to measure the pressure over the center square inch of the loaded area. This feature enables one to check the load on the center square inch against the average load over the entire area. The piston and the dynamometer were designed with approximately the same relative stiffness in order to maintain a uniform deflection of the specimen across the face of the loading device as the sample is compressed.

The vertical displacement of the sand during compression was measured by two Ames Dials mounted at 180° to each other on the loading piston as shown in Fig. 4.14. The dials measure the relative displacement between the moving piston and the thick walled cylinder designated as Part A in Fig. 4.5. This measured relative displacement is actually the sum of the vertical displacement of the soil plus the strain in the testing head from the surface of loading to the point where the dials are connected. The strains in the head were so small compared to the strains in the soil that they were neglected and the measurement was taken to represent the vertical displacement of the soil sample. The dials are accurate to 1/10,000 of an inch and have a 0.4 inch travel. When the two dials read differently, the average reading of the two dials was taken as the vertical displacement of the soil.

CHAPTER 5

EXPERIMENTAL RESULTS

5.1 General

One-dimensional compression tests were conducted on four different sands up to a maximum vertical stress of 3290 psi with the apparatus discussed in Chapter 4. Axial stress-strain properties and the coefficient of earth pressure at rest K_o were measured on all tests. The energy absorption capacity of the sands was also measured by means of cyclic loading.

Each sand was tested at a variety of initial void ratios in order to cover the complete range of behavior for each sand. The four sands selected for this study were chosen because they are extremely dissimilar with respect to grain shape and grain-size distribution characteristics. It was hoped that the sands selected would manifest a wide range of one-dimensional properties so that the extreme limits of the various measured quantities could be defined. Descriptions of the sands are given in subsequent sections of this chapter.

Triaxial tests were also conducted on the four sands to document fully the engineering description of the sands and to determine if any of the properties measured in one-dimensional compression could be correlated with index properties defined by well established routine tests. The triaxial test procedure and results are presented in Appendix B.

5.2 Description of Sands

Minnesota Sand. One sand used in this investigation was a uniform, rounded, silica sand obtained from the Gopher State Silica Co. in LeSeur, Minnesota. The sand is a coarse fraction obtained from the St. Peter Formation, a marine sand of Ordovician age. Because of the frosted nature of the sand it is thought to be of eolian origin. The transportation of this sand by wind and the additional working of this sand under marine

conditions account for the fact that it is rounded. This sand was selected primarily because it is rounded and highly spherical; a sphericity of 0.95 has been determined for this sand by a method suggested by Rittenhouse, (1943). Therefore, test results on this sand should provide an experimental check for the theory developed in Chapter 3. The sand is 100 per cent silica and 95 per cent of the material is between the No. 10 and No. 20 U. S. Bureau of Standards sieve. The effective size, (D_{10}), of the sand is 0.89 mm and the uniformity coefficient is 1.18. A grain-size distribution curve for the Minnesota Sand is shown in Fig. 5.1. The specific gravity of the Minnesota Sand is 2.65 and the void ratios for the loosest and densest states are $e_{max.} = 0.675$ and $e_{min.} = 0.455$, respectively. The procedure used for determining the maximum and minimum void ratios was the method suggested by Bauer and Thornburn (1962). The loosest state was obtained by placing the sand in a brass measure of known volume, 205 cc, with a glass funnel held about 1 inch above the free surface. The excess material was then carefully trimmed with a straight edge. The densest state was obtained by filling the measure through the funnel while tapping the measure continuously with a wooden tamper and it was also achieved by placing the sand in the measure in 1/2-inch layers and tapping the sides with a mallet until the free surface was no longer settling. Both methods yielded the same results. The relationship between the initial void ratio and the angle of internal friction was obtained for Minnesota Sand from the drained triaxial tests described in Appendix B and is shown in Fig. 5.2.

Pennsylvania Sand. A coarse, angular, silica sand obtained from the Pennsylvania Glass Sand Corp., Pittsburgh, Pennsylvania, was also used. The sand is obtained from the Sharon Formation of Lower Pennsylvania age in a quarry near Geauga Lake, Ohio. The sand was selected primarily because it is a pure silica sand in the same size range as the Minnesota Sand; however, it is angular in contrast to the rounded Minnesota Sand. It was thought that these two sands would more or less define the extreme limits of the

behavior of coarse sands in one-dimensional compression. The sand is 99 per cent pure silica and 93 per cent is retained between the No. 10 and No. 20 U.S. Bureau of Standards sieves. The effective size is 0.92 mm and the uniformity coefficient, C_u, is 1.48. The grain-size distribution for this material is shown in Fig. 5.1. The specific gravity of the sand is 2.64 and the sphericity as defined by the method of Rittenhouse (1943) is 0.89. Values of the void ratio for the densest and loosest states were determined by the method described previously and were found to be 0.880 and 0.595, respectively. The relationship between the angle of internal friction and the initial void ratio for Pennsylvania Sand is shown in Fig. 5.2.

Sangamon River Sand. Sangamon River sand obtained from the Pontiac Stone Co., Mahomet, Illinois, was also used in this investigation. Figure 5.1 gives the grain-size distribution for this sand. The sand has an effective size (D_{10}) of 0.18 mm and a uniformity coefficient, C_u, of 1.83. The sand may be described as sub-angular; the sphericity is 0.87, and the specific gravity is 2.67. The maximum and minimum void ratios are 0.875 and 0.540 respectively. The relationship between the angle of internal friction and the initial void ratio for the Sangamon River Sand is shown in Fig. 5.2.

Wabash River Sand. A fairly well-graded sand was used in this study which was obtained from the Wabash River near Attica, Indiana. The sand may be described as sub-angular to sub-rounded and has a sphericity of 0.85; the effective size, D_{10}, is 0.26 mm and the uniformity coefficient, C_u, is 3.0. The grain-size distribution curve for Wabash River Sand is shown in Fig. 5.1. The Wabash River Sand has a specific gravity of 2.67 and maximum and minimum void ratios of 0.694 and 0.434, respectively. The variation of the angle of internal friction with the initial void ratio is shown for Wabash Sand in Fig. 5.2.

5.3 Preparation of Test Specimens

The accurate control and measurement of the initial void ratio of all specimens were of extreme importance since the relative density significantly affects the stress

deformation properties of sand. Each sample of sand used in the one dimensional tests consisted of 2,000 grams of oven-dry material; thus the volume of the sand solids was constant for each test. Since the void ratio, e, is by definition $\frac{V_v}{V_s}$, where V_v is the volume of the voids and V_s is the volume of the soil solids, the void ratio may also be written as:

$$e = \frac{V}{V_s} - 1$$

where V represents the total volume of the sample. Since V_s was constant, the void ratio was determined by controlling the total volume, V. The Sample chamber of the device described in Chapter 4 was cylindrically shaped so this was easily accomplished by controlling the height of the sample.

Each test specimen was prepared by placing 2,000 grams of oven-dry sand into the sample chamber and inserting a metal plug into the chamber above the sand. This steel plug fits into the chamber as shown in Fig. 4.11. A vibrator was then set on the metal plug and the sand was vibrated until the plug settled to the desired height. The height was measured to the nearest 0.01 inch by measuring the distance between the top of the steel plug and the top surface of the cell. The sample was considered adequately prepared only when the vertical height of the specimen was measured to be the same at 4 points at 90° to each other around the periphery of the sample. This method of sample preparation has proven to be rather simple and convenient and the test results indicate that very good reproducibility has been achieved by the employment of this technique.

It was noted throughout the tests that the maximum densities that could be attained in the one-dimensional device were not as high as the maximum densities defined by the relative density tests described previously. The samples were then placed in layers in an effort to get denser samples, but higher densities than those reported could not be obtained. The most probable reason for this phenomenon is that in a confined condition in a heavy apparatus the particles were not free to rearrange as in the relative

density mold, and due to the heavy mass of the cell (approximately 500 lbs.) the amplitude of vibration applied to the soil would not be as large as the amplitude of vibration put into the light mold used in the relative density tests.

5.4 Experimental Procedure

General. The objective of these one-dimensional tests was to obtain curves of vertical stress versus vertical strain and to obtain measurements of the lateral stresses which are concomitant with the vertical stress throughout the history of loading under the conditions of zero lateral strain. The procedures described herein were intended to accomplish this objective by utilizing the equipment described in Chapter 4 with a 120,000-lb hydraulic testing machine for supplying a measurable controlled load.

Pretest Procedure. Immediately after a sample is prepared, the zero reading is obtained for the circumferential strain gages on the flexible steel ring for the conditions of atmospheric pressure in the hydraulic system. A calibration chart similar to Fig. 4.12 is then constructed by drawing a straight line through the zero reading with a slope of -7 microinches per 500 psi to obtain the relationship of strain indicator reading versus oil pressure for zero circumferential strain in the ring. The strain indicator is then balanced on this calibration line throughout the test. This procedure must be followed for each test because the zero reading may change from one test set-up to another due to temperature changes affecting the resistance of the dummy gages and changes in the strain indicator. Since it is the slope of the straight line calibration that accounts for the effect of the changes in oil pressure on the gages throughout the test, the magnitude of the initial zero reading has no significance. It is important however that the zero reading before and after any one test be the same, otherwise a zero shift has occurred during the test and the error in the calibration curve is exactly equal to the magnitude of the zero shift. The zero readings before and after each test should be within 5 microinches.

A seating load of about 5 psi is then applied to the sample and the strain dials on the testing head are secured in approximately the correct position to give maximum travel. The seating load is then reduced until it is almost exactly zero and the Ames dials on the testing head are adjusted to zero. The equipment is then completely ready for testing.

Testing Procedure. The sample is loaded by a vertical load applied at a constant strain rate while the horizontal pressure on the flexible ring is adjusted continuously by hydraulic jacks in order to maintain the condition of zero lateral strain. Readings of the oil pressure and the Ames dial readings are taken simultaneously at predetermined intervals of vertical stress. During unloading, however, the Baldwin hydraulic testing machine had no provisions for maintaining a constant rate of strain. Therefore the unloading portion of the test was conducted at a constant rate of stress. Occasional tests were run of each sand, however, which were designated as "consolidated type" tests. These samples were loaded and unloaded in stress increments as in ordinary consolidation tests on clay and each increment was left on the sample until the movement of the Ames dials became imperceptible. The horizontal pressure reading recorded in the "consolidated" tests was the horizontal pressure at the same time the final dial reading was recorded for each increment.

The vertical stress on the sample was taken as the total load registered on the testing machine divided by the area of the specimen. There were no corrections for ring friction reducing the average load on the sample. An attempt to assess the importance of ring friction in these tests is presented in Appendix C.

The vertical strain was measured by the Ames dials mounted on the testing head at 180° as shown in Fig. 4.14. The two dial readings were averaged because the testing machine allowed some tilting of the testing head. The vertical displacement indicated by the dials was taken as the displacement of the top of the sample because the strain between the surface of the testing head and the point where the dials were connected was negligible.

.5 Test Results

The vertical stress-strain data from this series of tests has been plotted for he entire history of loading for each test. A plot of the horizontal stress versus the ertical stress was also made for each test. These plots therefore show the relationship etween the three quantities measured in these tests and thus incorporate all of the xperimental data for each test into two diagrams.

The stress-strain curves for tests on Minnesota Sand, Pennsylvania Sand, Sangamon River Sand, and Wabash River Sand are shown in Figs. 5.3 through 5.22, Figs. 5.23 through 5.30, Figs. 5.31 through 5.37, and in Figs. 5.38 through 5.45, respectively. The relationship of horizontal stress to vertical stress for the same tests on Minnesota, Pennsylvania, Sangamon River, and Wabash River sands are given in Figs. 5.46 through 5.65, Figs. 5.66 through 5.73, Figs. 5.74 through 5.80, and Figs. 5.81 through 5.88 respectively.

CHAPTER 6

INTERPRETATION AND DISCUSSION OF EXPERIMENTAL RESULTS

6.1 General

The experimental data presented in the previous chapter are summarized and interpreted in this chapter. Generally, the stress-strain behavior is qualitatively similar to that observed by previous investigators such as Roberts and De Souza (1958). Due to the sample dimensions used in this test series, however, the numerical results are believed to be more precise than any previous one-dimensional stress-strain data published for sands up to 3290 psi. However, many of the conclusions drawn below concerning the coefficient of earth pressure at rest are given for the first time. The experimental data on the coefficient of earth pressure at rest also give actual numerical support to relationships suggested by other investigators, such as Jaky (1944). Summary graphs are shown for all four sands where the consolidation of data clearly shows the effect of a significant variable. A special effort is made throughout to correlate the experimental results on Minnesota Sand with the theoretical analysis presented in Chapter 3.

6.2 Axial Stress-Strain Relationships

The one-dimensional stress-strain measurements on all four sands are presented in Figs. 5.3, through 5.45 in which both quantities have been plotted to an arithmetic scale. The stress-strain curves in general for all tests are nonlinear curves which are concave upward on the loading portion of the curve unless significant crushing of the soil grains causes the curvature to become concave downward. The unloading curves, however, are all concave upward. If the sand sample is subjected to subsequent cycles of load with a maximum stress well below the peak value of the first cycle, both the loading and unloading curves are concave upward.

Summary graphs are shown in Figs. 6.1 - 6.4 which show families of stress-strain curves for samples of Minnesota, Pennsylvania, Sangamon River, and Wabash River sands tested at various initial relative densities. All four graphs show the obvious effect of the initial relative density. The denser the sand the more steeply the stress-strain curve turns up giving less strain for a dense sample than a loose sample at a given vertical stress. The initial relative density also affects the shape of the stress-strain curves. Figure 6.1 shows four tests on Minnesota Sand at four different void ratios. The tests with initial void ratios of 0.54 and 0.62 manifest stress-strain curves with a concave upward curvature throughout the entire range of loading. The two tests with initial void ratios of 0.66 and 0.77 have stress-strain curves which initially are concave upward but display a concave downward curvature at higher pressures. It should also be noted that the stress-strain curve begins to turn concave downward at a lower vertical stress for the sample with an initial void ratio of 0.77 than for the sample with an initial void ratio of 0.66. The family of stress-strain curves for Pennsylvania sand shown in Fig. 6.2 are similar in shape because they are all initially concave upward but become concave downward at higher levels of vertical stress. The curves for the Pennsylvania Sand also show the trend that the higher the initial relative density, the higher is the vertical stress at which the curvature becomes concave downward. The tests on Sangamon River Sand given in Fig. 6.3 show that the densest sample has a stress-strain curve which is concave upward throughout the entire range of loading; the three looser samples, however, display stress-strain curves which are initially concave upward and become concave downward at higher stresses. Tests on Wabash River Sand presented in Fig. 6.4 also show that increasing the initial relative density increases the slope of the stress-strain curves. These test results are different than those for the other three sands because tests at all initial relative densities have stress-strain curves which are concave upward throughout the entire range of loading.

The non-linearity of the stress-strain curves discussed above demonstrates the well-known phenomenon that the stiffness of a given sand is highly dependent upon the stress level. This stiffness in the case of one-dimensional compression is usually designated as the "constrained modulus" of deformation. The "constrained" tangent modulus of deformation which, by definition, is the rate of change of vertical stress with respect to vertical strain under conditions of zero lateral strain, will be used hereafter in this discussion. Values of the constrained tangent modulus have been calculated at intervals in the vertical stress of 275 psi for the initial loading of all tests. The variation of the constrained tangent modulus with vertical stress is shown for all four sands at various initial relative densities in Figs. 6.5 - 6.8.

The general trend shown in all four summary graphs is that the constrained tangent modulus increases with pressure for a given specimen until crushing of the grains causes the modulus to decrease with further increase in pressure. This phenomenon is illustrated best by the angular Pennsylvania Sand, for which the constrained tangent modulus initially increases with vertical stress and then decreases at higher pressures for the entire family of curves shown in Fig. 6.6. A decrease in constrained modulus with pressure occurs only for the tests on loose samples of Minnesota and Sangamon River Sands shown in Figs. 6.5 and 6.7, respectively. The denser samples of Minnesota and Sangamon River sands, however, manifested a monotonically increasing constrained modulus with increasing stress up to the maximum pressure; therefore, crushing of the grains in the dense samples was not significant enough to cause a decrease in constrained modulus. The constrained modulus-vertical stress relationships for the fairly well graded Wabash River Sand are shown for three initial void ratios in Fig. 6.8. The constrained modulus increases with increasing vertical stress until a vertical stress of about 2000 psi; then, the moduli for the three different curves appear to remain constant up to the maximum vertical stress of 3290 psi. Thus significant crushing did not occur in either the dense or loose samples of well graded Wabash River Sand because

the constrained tangent modulus did not decrease with additional vertical stress at any stage of the loading.

In summary, the families of stress-strain curves and constrained tangent modulus vertical stress curves for the Minnesota, Pennsylvania, and Sangamon River Sands indicate that the initial relative density of the sand governs the stress level at which crushing of the grains causes the constrained tangent modulus to begin to decrease with additional vertical stress. In general, as the initial relative density increases, the stress level at which the constrained modulus peaks also increases. Therefore the stress level at which significant crushing occurs for a given sand also increases as the initial relative density increases. This behavior can be explained in the following manner. A sand with a higher void ratio or lower relative density is free to rearrange as a small amount of crushing takes place at points of contact, and the strains from this rearrangement are reflected in a decreasing constrained tangent modulus. The sands with a lower void ratio, however, are not free to rearrange to a great degree when crushing initiates and thus no significant strains due to rearrangement occur. Even the denser samples will show a decreasing modulus at some stage due to crushing but, in general, one would expect crushing to occur at a higher average stress level in a dense sand than in a loose sand. A dense sand has more contact points per unit volume than a loose sand and thus for the same average applied stress, the loose sand has higher grain to grain contact stresses than a dense sand. Therefore, the loose sand begins crushing at a lower stress than the dense sand. The explanation above is consistent with the experimental results presented for the Minnesota and Sangamon River sands which showed crushing of the loose specimens but did not show crushing of the dense sands within the range of vertical stress applied in these tests. The trend which would be predicted from the above explanation was definitely exhibited for the Pennsylvania Sand which showed crushing for specimens tested at both high and low initial void ratios.

These experimental results are given in Fig. 6.6 and definitely show that the vertical stress level at which significant crushing occurs increases for a given sand as the relative density increases. The Wabash River Sand did not show significant crushing for either the dense or loose samples within the pressure ranges of these tests. This behavior can be explained by the fact that the sand is fairly well graded which provides many contact points per unit of volume. Therefore the contact stresses for a given average stress on the medium are reduced.

The significance of relative density in determining the constrained modulus for a given sand is definitely indicated in Figs. 6.5-6.8. These data show that the constrained modulus for a given sand at a given level of vertical stress may be 8 or 9 times higher for a dense sand than for a loose sand. This is not enough evidence, however, to draw the conclusion that relative density is the unifying index property which determines the stiffness of all sands at a given level of stress. Figures 6.9 and 6.10 show constrained tangent modulus versus vertical stress curves for tests on all four sands at approximately the same relative density. These data indicate that the constrained modulus for the rounded Minnesota Sand may be 9 or 10 times greater than the constrained modulus for the angular Pennsylvania Sand at approximately the same relative density. The rounded Minnesota Sand and the Angular Pennsylvania Sand define the upper and lower limits of the constrained modulus while the Sangamon and Wabash River Sands fall closely together between the two extreme limits. Thus the angularity of the particles is just as significant in affecting the constrained modulus as the initial relative density. A rounded sand has had most of the incompetent pieces weathered out and consists entirely of rounded quartz grains that experience much less local crushing and permanent deformation at points of contact than a more angular sand. Therefore the rounded sands are stiffer during loading and exhibit a higher strain recovery during unloading. Since the angularity is a function of the transportation

history of the sand, the constrained modulus at a given relative density is indirectly related to the geologic processes which acted to produce the natural sand deposit. It is probable that the Sangamon River Sand and Wabash River Sand show almost identical constrained tangent modulus - vertical stress curves in Figs. 6.9 and 6.10 because they are both from recent river channels and have similar mineralogical content.

The effect of time on the one-dimensional stress strain relationships was not part of this study. The strain rate was varied however between the limits of 0.005 inches per minute and 0.04 inches per minute on the initial test series on Minnesota Sand. This small range of strain rate was not enough to materially effect the constrained modulus. Values of the constrained tangent modulus in the 2,500-3,000 psi vertical stress range are shown below for different testing rates on samples of Minnesota Sand with an initial void ratio of 0.54.

Testing Rate, in/min	Constrained Modulus, psi
0.005	262,500
0.010	262,500
0.020	269,500
0.040	270,000
Consolidated Type Test	245,000

The constrained modulus appears to increase slightly with increasing strain rate; however, in the range of constant strain rates considered, this difference is only about 8,000 psi which is not significant. There is a slightly greater difference, however, between the consolidated type test and tests run at a constant strain rate because the consolidated type test includes more deformation due to creep. Even this difference is less than 10% and not significant compared with the changes in constrained moduli caused by small changes in initial relative densities.

6.3 The Coefficient of Earth Pressure at Rest

The results of the lateral earth pressure measurements for the first cycle of loading on all four sands are shown in Figs. 5.46 - 5.88. The lateral earth pressure required for zero lateral strain is plotted in these graphs as ordinate versus the vertical stress as abscissa. All of the curves show the same general qualitative characteristics even though they are quantitatively different. The relationship between the horizontal and vertical stresses in the low pressure ranges gives a straight line through the origin for all tests and the coefficient of earth pressure at rest, K_o, is numerically equal to the slope of the straight line. As the pressure increases some of the tests show that the relationship between the vertical and the horizontal stress continue on the same straight line up to the maximum pressure. Most of the data indicate, however, that as the pressure increases there is a tendency for the coefficient of earth pressure at rest to increase which is reflected in an increase in slope of the curve at higher pressures. Throughout most of the unloading the horizontal stresses decrease at a lower rate than the vertical stresses which gives a flatter curve located above the loading curve. In fact, near the end of unloading the horizontal pressure exceeds the vertical pressure which gives a coefficient of earth pressure at rest greater than 1.0.

Because all of the tests give a straight-line relationship between horizontal stress and vertical stress up to about 1000 psi, the values of the coefficient of earth pressure at rest have been computed for all tests in this range for the purposes of comparison. Thus the values of the coefficient of earth pressure at rest discussed in this paragraph are for normally loaded sands up to 1000 psi. The value of the coefficient of earth pressure at rest is found to be dependent upon the type of sand and the initial relative density of the sand. Summary graphs of the coefficient of earth pressure at rest versus the initial void ratio are shown for the four sands in Figs. 6.11 - 6.14. These data consistently show that the coefficient of earth pressure at rest increases as the

initial void ratio increases for all four sands. This trend in the data was expected because previous investigators such as Jaky (1944) have reported that the coefficient of earth pressure at rest is inversely proportional to the angle of internal friction. Because the angle of internal friction increases as the initial relative density increases, it follows that the coefficient of earth pressure at rest should decrease with increasing relative density as observed. A series of drained triaxial tests was conducted on all four of the sands at various relative densities. The object of the triaxial testing program was to define the relationship between the angle of internal friction and the initial void ratio. This relationship was used to establish a correlation between the angle of internal friction and the coefficient of earth pressure at rest. The experimental relationships between the drained angle of internal friction and the initial void ratio for the sands are presented in Fig. 5.2. The relationship between the angle of internal friction and the coefficient of earth pressure at rest was obtained for Minnesota Sand by taking a value of K_o from Fig. 6.11 corresponding to a given initial void ratio; a value of ϕ is then picked off Fig. 5.2 corresponding to the same initial void ratio. This procedure is repeated for several values of the initial void ratio and the values of the coefficient of earth pressure at rest are plotted against the sine of the angle of internal friction as shown in Fig. 6.15. The relationships for the other sands were obtained by the same procedure and are also shown in Fig. 6.15. The experimental results for the Pennsylvania, Sangamon River and Wabash River sands conform almost exactly to the relationship suggested by Jaky (1944), whereas the experimental results for rounded Minnesota Sand fit very closely the relationship obtained from the theoretical investigation in Chapter 3. Because the Minnesota Sand is composed of almost spherical particles of uniform size, it is reasonable that the Minnesota Sand should fit the theoretical relationship derived for a medium of uniform spheres more closely than the other three sands.

The experimental data definitely indicate that the coefficient of earth pressure at rest for a given sand is inversely related to the angle of internal friction. This relationship may also explain the tendency for the coefficient of earth pressure at rest to increase with pressure as typically illustrated by the relationship of the horizontal and vertical pressures during loading for a sample of Sangamon River Sand (Fig. 5.77). It is well known that the angle of internal friction of a given sand decreases as the confining pressure increases. Thus the coefficient of earth pressure at rest should be expected to increase with pressure because it is inversely related to the angle of internal friction. The above explanation accounts for the value of K_o increasing with pressure, but according to this mechanism the transition should be gradual and continuous. Test results are given in Figs. 5.57 and 5.58 for loose Minnesota Sand at void ratios of 0.64 and 0.66 which show a rather sharp break in the relationship between the lateral and vertical pressures during loading. The curves make a transition from an initial straight line into another straight line with a steeper slope. An abrupt change of this type is thought to be caused by crushing of the grains. This abrupt change is manifested by loose Minnesota Sand, Figs. 5.57 and 5.58, but dense Minnesota Sand gives a straight-line relationship throughout loading as shown in Figs. 5.64 and 5.65. Figure 6.5 shows that it is also the loose Minnesota Sand which gives a decrease in constrained tangent modulus at higher pressures due to crushing and rearrangement.

Graphs of lateral pressure versus vertical pressure for Pennsylvania Sand are shown in Figs. 5.66 - 5.73. All of the graphs show abrupt changes in the curves during loading. Figure 6.6 also shows that the constrained tangent modulus decreases due to crushing for tests at all initial relative densities for Pennsylvania Sand.

The lateral stress versus vertical stress plots for Wabash River Sand are given in Figs. 5.81 - 5.88. These data indicate that the lateral stress-vertical stress relationship for loading is almost a straight line through the origin for all tests, and no abrupt changes in slope are shown. This phenomenon is consistent with the idea that

crushing is important in causing an abrupt change in the σ_H versus σ_v relationship because the constrained tangent modulus versus vertical stress graph in Fig. 6.8 indicates that significant crushing has not occurred within the pressure ranges of testing for the Wabash River Sand.

The lateral stress measurements for Test 2 on Pennsylvania Sand are given in Fig. 5.67 and will be used here as a specific example to illustrate the mechanism which causes the fairly abrupt changes in the horizontal stress-vertical stress relationships. The first break in the loading curve given in Fig. 5.67 occurs at a vertical stress of approximately 1200 psi. The constrained tangent modulus versus vertical stress relationship for Test 2 is given in Fig. 6.6 by the curve shown for an initial void ratio of 0.70; it is observed that the constrained modulus begins to decrease with pressure at approximately 1200 psi. This behavior indicates that at 1200 psi some of the contacts have disintegrated and have transferred enough load to the remaining contacts so that a large number of contacts are near the point of failure. Additional vertical stress causes a sufficient number of contacts to fail which results in rearrangement and large strains. Therefore, the constrained modulus decreases with additional vertical stress as observed in Fig. 6.6. These contacts which are crushed were contributing to the average shearing stresses necessary to maintain the difference between the lateral and vertical stresses. When the rearrangement described above occurs, the value of K_o will have a tendency to increase because the sand grains will tend to move such that shear stresses on them are relieved rather than increased. The value of K_o for Test 2 on Pennsylvania Sand continues to increase up to about 2600 psi where the horizontal stress-vertical stress curve flattens out and the value of K_o begins to decrease with pressure. Figure 6.6 indicates that the constrained modulus for Test 2 ($e_o = 0.70$), is beginning to approach a constant value in the 2600-3000 psi range. Therefore, at a stress of about 2600 psi the sand has rearranged until many more new contact points have been made which permits a larger principal effective stress ratio and thus a lower value of K_o.

The relationship between the lateral pressure and the vertical pressure for unloading is shown for all tests in Figs. 5.46 - 5.88. The typical unloading curve for all tests is a concave downward curve which is very flat at high pressures and increases in curvature and slope as the vertical stress approaches zero. Throughout most of the unloading portion the vertical stresses are relieved at a faster rate than the horizontal stresses. Thus, as unloading proceeds the value of the coefficient of earth pressure at rest increases. The test results show that for some sands the value of the coefficient of earth pressure ranges from about 0.40 to 2.90 during unloading. Therefore, depending upon the stress history, the coefficient of earth pressure at rest can be very close to either the active or passive earth pressure coefficients. The most commonly accepted number, at least for clays, that is utilized for expressing the stress history is the overconsolidation ratio, which will hereafter be referred to as the OCR. The OCR, by definition, is the ratio of the maximum previous stress to which a soil has been subjected to the present stress on the soil. The OCR is 1.0 during loading up to the maximum pressure, but if the specimen is unloaded the OCR becomes greater than 1 and increases to infinity when the specimen is completely unloaded. A typical variation of K_o with OCR is illustrated in Fig. 6.16 for Tests 3 and 4 on Minnesota Sand. This graph clearly shows that K_o increases at a decreasing rate with OCR and appears to be approaching a horizontal asymptote. The K_o value at an OCR of 37 is almost 2.0 and still increasing such that the curve will probably become asymptotic to a straight horizontal line where K_o is equal to the coefficient of passive earth pressure. Curves of K_o versus OCR have been plotted for all specimens loaded to the same maximum vertical stress for purposes of comparison. Summary graphs of K_o versus OCR are shown in Figs. 6.17 - 6.20. Each graph with the exception of Fig. 6.17, gives a rather narrow band within which all test results for a given sand fall regardless of the initial relative density. This band is especially narrow for the Wabash River Sand (Fig. 6.20) and the Sangamon River Sand (Fig. 6.19). The influence of initial relative density is

more pronounced for the Minnesota Sand, however, since the band within which all the data in Fig. 6.17 fall is somewhat broader. The experimental results shown for Pennsylvania Sand in Fig. 6.18 show a very narrow band within which five tests fall. Because the void ratio varies only between the narrow limits of 0.68 and 0.74 for tests with the same maximum pressure on Pennsylvania Sand, it cannot be said that samples tested over a wide range of initial relative densities would necessarily fall in the narrow band shown in Fig. 6.18. The data presented in all the figures do indicate, however, that the stress history as expressed by the overconsolidation ratio is more significant in determining the value of K_o during unloading than the initial relative density of the sand. In fact the K_o versus OCR graphs for Sangamon River and Wabash River sands in Fig. 6.19 and 6.20 show results of six and eight tests respectively conducted at different relative densities which indicate that the coefficient of earth pressure at rest during unloading is almost a unique function of stress history and nearly independent of the initial relative density. However, the summary plots for the Minnesota, Sangamon River, and Wabash River sands consistently indicate that the upper limit of the band is given by the experimental results from the loose sands and the lower limit of the band is given by the data from the denser specimens.

Figures 5.55 and 5.56 show the variation of lateral earth pressure with vertical stress for 1 1/2 cycles of loading in tests 12 and 13 on Minnesota Sand. These curves show that cyclic loading can gradually build up the coefficient of lateral earth pressure if the load is cycled in the range between 1650 psi and 3290 psi. The data for Test 13 in Fig. 5.56 show that the value of K_o at point a is higher than at point b even though the computed overconsolidation ratio is identical for these two points. Thus, the value of K_o for a given sand is not only a function of the stress history as expressed by the OCR, but it also depends on the number of preceding cycles.

6.4 Energy Absorption

The energy absorption characteristics of the four dry sands were investigated by means of cyclic loading. In general, the procedure was to load the specimen to 3290 psi and unload to zero on the first cycle. A second and sometimes a third cycle of loading was then applied with a maximum stress of about one-third the maximum stress applied in the first cycle so that the subsequent hysteresis loops would be practically recoverable.

The deformations in the first cycle are only about 10-20 percent recoverable for tests on the Pennsylvania, Sangamon River and Wabash River sands (Figs. 5.23 - 5.45). The denser samples of Minnesota sand, however, are as much as 75% recoverable; in general, the recoverable strain becomes lower as the initial relative density of the samples decreases. These irrecoverable strains, however, are expected on the first cycle of loading because energy is absorbed as the stresses do work when rearrangement of the grains causes a permanent decrease in volume and energy is expended in creating new surfaces as crushing of the grains takes place. When crushing of the grains occurs, further rearrangement also takes place and both mechanisms are responsible for energy absorption. The two mechanisms cannot be distinctly separated but both contribute significantly to the area of the hysteresis loop on the first cycle.

Generally, the deformations in the second cycle are almost entirely recoverable, but energy is still lost because the loading and unloading paths are different. If the second cycle is followed by a third cycle identical to the second (such as in Tests 3, 5, 6, 7, and 8 on Minnesota Sand) it is found that the third cycle traverses essentially the same loop with very little irrecoverable strain. However, a significant amount of energy is still dissipated due to the difference between the paths of loading and unloading.

The energy lost in hysteresis for various tests on all four sands was evaluated by computing the areas enclosed in the loops traversed in the first cycle which includes considerable permanent deformation, and in the second and third cycles which are essentially recoverable. The energy absorbed is then expressed as a percentage of the input energy.

The experimental data on the energy absorption characteristics of the sands are presented in Figs. 6.21 - 6.24. Results for the Minnesota Sand in Fig. 6.21 show that the energy absorbed on the first cycle decreases from about 60 percent for samples at a low relative density to as low as 35 percent for relatively dense samples. The angular Pennsylvania Sand which manifested significant crushing in the first cycle of load dissipated about 95 percent of the energy input for all relative densities as shown in Fig. 6.22. Tests on both the Sangamon River and Wabash River sands show that the energy absorption in the first cycle decreases as the initial relative density increases. Figures 6.23 and 6.24 give the experimental results for Sangamon River and Wabash River sands which have energy absorption ratios in the first cycle of 90 to 70 percent and 95 to 80 percent, respectively, as the relative density increases from the loosest to the densest states. The amount of crushing and rearrangement are indirectly included in the constrained tangent modulus because the constrained modulus decreases in general as the amount of permanent deformation increases. Therefore, the constrained tangent modulus at the maximum load should be inversely related to the percent energy absorbed in the first cycle of loading. Figure 6.25 gives a plot of constrained tangent modulus at 3290 psi versus the percent energy absorbed on the first cycle. This graph shows that the energy absorption is definitely a function of the constrained tangent modulus at the maximum load in the cycle; the experimental data from all four sands fall generally along the trend given in Fig. 6.25.

The energy dissipated in the small hysteresis loops on the second and third cycles was also measured. The ratio of energy absorbed to input energy expressed as a percentage is plotted against the initial relative density for the four sands in Figs. 6.21 - 6.24. Energy losses in these small hysteresis loops are considerably smaller than the first cycle for all sands tested because most of the permanent deformation has already taken place in the first cycle of loading. It should also be observed that in the Minnesota, Sangamon River, and Wabash River sands the percent energy absorbed is

relatively independent of the initial relative density because the best straight lines through the experimental points have very flat slopes. The experimental results given for Pennsylvania Sand (Fig. 6.22), however, show a variation of percent energy absorbed with initial relative density in which the energy absorption appears to increase from about 25 to 53 percent as the initial relative density increases. The energy dissipated in the small hysteresis loops for Minnesota Sand ranges from 33 to 27 percent of the input energy whereas the Sangamon River sand and Wabash River sand absorbed 38-50 percent and 38-49 percent of the input energy respectively.

In general, the study of energy absorption from the hysteresis loops indicates that there are three mechanisms which dissipate energy in dry sand. Energy is dissipated by work which is done by the stresses in producing an irrecoverable change in volume due to rearrangement of the grains; energy is absorbed in the form of surface energy as crushing creates new surfaces. The third mechanism, which was manifested in the small hysteresis loops and which was indicated by the theory in Chapter 3, is the absorption of energy due to a difference in loading and unloading path even though the deformations are fully recoverable. The energy lost in the first cycle is dissipated by all three mechanisms whereas energy is dissipated in the small hysteresis loops, primarily by the third mechanism. The method of cyclic loading employed in these tests provides a means of separating the third energy absorbing mechanism from the first two mechanisms; the effects of the first two mechanisms, however, cannot be separated. A method has been suggested by Hendron, Fulton, and Mohraz (1963) for separating the energy losses due to the first two mechanisms. The method involves a statistical evaluation of the new surface area created by crushing from changes in the grain-size distribution curve. The results of laboratory experiments which evaluate the energy required to produce a unit area of new surface for a given mineral can then be applied to give the total amount of energy expended in the creation of new surfaces. However, there is only limited laboratory data of this type available and most of the

data is for quartz, (Axelson, 1949), (Heney, 1951), (Kenny, 1954), and (Zeleny, 1959), The method is most severely restricted, however, by the statistical procedure which requires that the grain-size distribution before and after crushing plot as two straight lines on log probability paper. Unfortunately, most real sands do not satisfy these requirements and the deviations from the straight lines can cause large errors in the statistical evaluation of the new surface area. Therefore this method is of no use until more experimental data are obtained on surface energies of minerals and until statistical methods are developed to the point where the assumption of such idealized grain-size distribution curves is not required.

6.5 General High Pressure Behavior Indicated by Tests on Pennsylvania Sand

The family of curves in Fig. 6.6 define the constrained tangent modulus versus vertical stress relationship for Pennsylvania Sand at various initial relative densities. All of the curves show a decreasing constrained modulus after crushing of the grains begins, but the most interesting phenomenon is the tendency for all tests to approach the same constrained modulus, (20,000 psi), at a vertical stress of about 3200 psi. This behavior suggests that a stress level has been reached for the angular Pennsylvania Sand where the effects of the initial relative density have been completely erased. Therefore, the physical behavior beyond this critical stress should be the same for all specimens of Pennsylvania Sand regardless of the initial void ratio. The vertical stress-void ratio relationships for four specimens of Pennsylvania Sand with initial void ratios between the limits of 0.86 and 0.67 are shown in Fig. 6.26. It is apparent that all four specimens are approaching the void ratio of approximately 0.55 at the maximum pressure of 3290 psi; the four pressure-void ratio curves are merging to give a single relationship at higher stresses for all initial relative densities. These same data are shown in Fig. 6.27 in the form of a conventional void ratio-log pressure diagram. The specimens with different initial relative densities merge into a "virgin" slope which is common to all four samples. These data are very much analogous to

consolidation data published by Olson (1962) which showed a family of void ratio - log pressure curves for samples of Calcium Illite consolidated from different initial liquidity indices. Another interesting observation from the void ratio-log pressure plot is that the compression index of the "virgin" portion of the curve is about 0.49, which exceeds that of most normally loaded clays.

Further experimental evidence to support the prognostication that the physical properties of specimens with different initial relative densities become the same at higher pressures is given in Figs. 6.28 - 6.30. Fig. 6.28 shows the variation of the coefficient of earth pressure at rest with vertical stress throughout the loading of the first cycle for loose, medium, and dense specimens of Pennsylvania Sand. At higher pressures the value of the coefficient of earth pressure at rest is 0.50 for all three tests shown. A plot of the stress paths of the top point on a Mohr circle as loading progresses is given in Fig, 6.29 for the same three tests which indicates that the stress trajectories of the three different specimens merge at a stress of about 2000 psi. Figure 6.30 shows a continuous plot of one-third the first stress invariant as abscissa versus the octahedral shearing stress as ordinate for the first loading in Tests 3, 5, and 7 on Pennsylvania Sand. The data interpreted in this manner also show that at higher pressures all three specimens have the same physical properties even though the initial relative densities are greatly different.

It is the opinion of the writer that all sands will reach a certain void ratio at high pressures in one-dimensional compression at which the effects of initial relative density will be erased and the physical properties exhibited with further increase in pressure will be the same for all samples of a particular sand. This opinion is supported by the measurements presented for Pennsylvania Sand. The other three sands should behave in a similar fashion but the pressure range of this series of tests was not high enough to reach these "critical" void ratios for the Minnesota, Sangamon River and Wabash River sands.

6.6 Correlation of Experimental Results with the Theory of Granular Media

The theory presented in Chapter 3 is applicable to a granular medium composed of equi-radii spheres arranged in a face-centered cubic array. Since the Minnesota Sand is a uniform, rounded, highly spherical sand, the results from the tests conducted on Minnesota Sand will be compared with the predicted behavior from theory.

The stress-strain data from Tests 3 - 1 on Minnesota Sand are presented on log-log graphs in Figs. 6.31 - 6.41. The stress-strain relationship for the initial loading plots as a straight line on these graphs which means that the axial stress may be expressed in terms of the axial strain by

$$\epsilon_{zz} = m \sigma_{zz}^{n} \tag{6.1}$$

The above expression may also be written

$$\log_{10} \epsilon_{zz} = \log_{10} m + n \log_{10} \sigma_{zz} \tag{6.2}$$

Thus, from Eq. (6.2) it is apparent that the parameter n is the reciprocal of the slope of the straight line and m is the value of the strain at which the straight line intersects the strain axis. The values of n ranges from 0.38 to 0.53 for these tests as compared to the value of 0.67 which is predicted for n from the theoretical analysis presented in Chapter 3. The results do show, however, that the relationship between stress and strain is an exponential relationship as predicted by theory, but the value of n from tests seems to be consistently less than 0.67.

The constrained tangent modulus, M_c, is the continuous derivative of the theoretical one-dimensional stress-strain curve given in Chapter 3 and can be expressed in terms of the vertical stress, σ_{zz} by

$$M_c = \frac{d\sigma_{zz}}{d\epsilon_{zz}} = C_2 \sigma_{zz}^{1/3} \tag{6.3}$$

where C_2 is a constant, Figure 6.42 gives the variation of log M_c versus log σ_{zz} for all tests with an initial void ratio of 0.54. Since the relationship is a straight line the constrained tangent modulus may be expressed in terms of the vertical stress as

$$M_c = C_3 \sigma_{zz}^t \tag{6.4}$$

where t is the slope of the line and C_3 is a constant. The value of t for this set of experiments on Minnesota Sand at an initial void ratio of 0.54 is 1/2 whereas the theory from Chapter 3 predicted that t should be 1/3. An interesting comparison can also be made with data compiled by Whitman (1962) for Standard Ottawa Sand. The Minnesota Sand and Standard Ottawa Sand are both obtained from the St. Peter Sandstone formation and are very similar in every respect except that the Minnesota Sand is comprised of No. 10-No. 20 sieve-size material and the Ottawa Sand is composed of the No. 20-No. 30 size fraction. Figure 6.43 gives the variation of dilatational wave velocity with confining pressure for Standard Ottawa Sand at a void ratio of 0.53. The dilatational wave velocity is given by

$$V_D = \sqrt{\frac{M_c g}{\gamma}} \tag{6.5}$$

where V_D is the dilatational wave velocity, g is the acceleration of gravity, and γ is the unit weight of the soil. Therefore the data for Minnesota Sand at a void ratio of 0.54 presented in Fig. 6.42 can be compared with the seismic data presented by Whitman if the seismic velocity is calculated by Eq. (6.5) for given values of the constrained tangent modulus in Fig. 6.42. Calculated values of the seismic velocities versus vertical stress from values of the constrained tangent modulus given in Fig. 6.42 are shown in Fig. 6.43 by curve A; the same calculated velocities are shown plotted versus the horizontal stress in curve B by applying a K_o factor of 0.35 to the vertical stress. Curves A and B are parallel to and below the band given by Whitman which rises at a slope of 1/4. Since the theory of Chapter 3 predicts that the constrained tangent

modulus is proportional to the cube root of the confining pressure and the dilatational wave velocity is proportional to the square root of the constrained tangent modulus, then it follows that the theory would predict the wave velocity to vary as the sixth root of the confining pressure. Therefore the theory predicts that the straight lines shown in Fig. 6.43 should rise at a slope of 1/6 rather than the slope of 1/4 observed. One of the most interesting aspects of the data presented in Fig. 6.43 is that it gives a correlation between seismic results and stress-strain properties measured at higher stresses. It is observed that the pseudo-wave velocities calculated from the constrained tangent moduli measured at high pressure levels are about 1/2 to 3/4 of the seismic velocities for lines A and B respectively. The result is consistent with Sauer (1959) who has suggested that the "effective" wave velocity for use in predicting the ground motion for high overpressures produced by a nuclear weapon should be taken as approximately equal to 3/4 of the seismic wave velocity.

An energy absorption mechanism is predicted for a dense granular medium by the theory given in Chapter 3 whereby energy is dissipated due to a difference between the loading and unloading paths even when the strains are fully recoverable. The energy absorption characteristics of Minnesota Sand have been investigated as described in Section 6.4. It was found that the second and third hysteresis loops were essentially completely recoverable for Minnesota Sand. In fact, the second and third cycles traversed exactly the same path for Tests 3, 5, and 7 on Minnesota Sand given in Figs. 5.3, 5.5, and 5.7; the small loops shown on each stress-strain curve for these tests actually represent both the second and third cycles. Energy was dissipated on these recoverable hysteresis loops, however, due to a difference in loading and unloading paths in a manner very similar to the mechanism suggested by the theory of Chapter 3. The energy absorbed in the second or third hysteresis loops expressed as a percentage of the input energy was computed for Tests 3-9 and 11 on Minnesota Sand (Table 6.1).

In general, it is found that the ratio of energy lost to energy input is practically a constant regardless of the magnitude of the vertical stress range of the loop, and varies between the narrow limits of 0.275 and 0.334. These results correlate very well with the conclusions based upon the theory from Chapter 3 which indicates that the ratio of energy absorbed to input energy for a hysteresis loop from a stress of zero to any stress below the crushing stress should be a constant related to the coefficient of friction between grains.

The laboratory measurements also provide another check on the theory presented in Chapter 3. The coefficient of earth pressure at rest is predicted from the theory to be related to the coefficient of friction by

$$K_o = 1/2 \left(\frac{1-f}{1+f}\right) \tag{3.49}$$

and the ratio of energy absorbed to energy input is given as

$$\frac{\Delta E}{E_1} = \frac{2f}{1+f} \tag{3.65}$$

Since K_o and the ratio of energy lost to energy input have been independently measured in the laboratory tests, the coefficient of friction, or more appropriately, the pseudo coefficient of friction can be evaluated by two independent calculations for each test. These calculations were made for tests on Minnesota Sand with an initial void ratio of 0.54 and 0.62 (Table 6.2). Tests 3 and 4 do not show good agreement for the two calculated values of the coefficient of friction. Tests 5 - 9 and 11, however, show a very good correlation between the two independently calculated values of the coefficient of friction. The latter group of tests were placed at an initial void ratio of 0.54 as compared to 0.62 for Tests 3 and 4. Because the theory of Chapter 3 assumes the granular medium in the densest possible state, it is not surprising that the tests on sand in the denser state should give a better correlation with the theory than tests at higher initial void ratios. The average value of the coefficient of friction calculated

rom the denser samples was 0.18 which is not unrealistic since a value of 0.16 has een reported for polished specimens of air equilibriated milky quartz from Wisconsin y Horn and Deere (1962).

An expression which relates the angle of internal friction and the coefficient of arth pressure at rest was derived in Chapter 3 and presented in Fig. 3.18. An xperimental relationship between the coefficient of earth pressure at rest and the ngle of internal friction has been determined from one-dimensional and triaxial tests n Minnesota Sand. The experimental values and the theoretical curve are shown in ig. 6.15 for comparison and excellent agreement is observed.

CHAPTER 7

SUMMARY AND CONCLUSIONS

7.1 Summary

An analytical and experimental investigation has been conducted with the objective of explaining and describing qualitatively and quantitatively the behavior of granular materials in one-dimensional compression. The analytical investigation applies only for pressures below that at which crushing of the grains begins, and deals with the stress-strain relations of a granular medium consisting of elastic, equi-radii spheres in a face-centered cubic array. The analysis utilizes the Hertz compliance, which relates the normal forces to the normal displacements between centers of spheres, and the Mindlin compliance which relates the tangential forces to the tangential displacements between centers of spheres. The basic framework of the analysis uses the equilibrium and compatibility equations for a face-centered cubic array as developed by Duffy and Mindlin (1957). A new solution is presented in Chapter 3 which gives the stress-strain behavior of a face-centered cubic array subjected to a monotonically increasing axial compressive stress for the conditions of zero radial strain, the case of one-dimensional compression. The new solution gives a theoretical expression for the axial stress-strain curve, the constrained tangent modulus as a function of pressure, and the coefficient of earth pressure at rest as a function of the coefficient of friction between grains. An expression is also obtained which relates the absorbed energy to input energy for a cycle of loading with recoverable deformations as a function of the coefficient of friction between grains. This expression, however, is dependent upon an approximation which was made in deriving the equation of the unloading curve. An analysis of a face-centered cubic array at failure in a triaxial state of stress for $\sigma_2 = \sigma_3 < \sigma_1$ was used from Thurston and Deresiewicz (1959) in Chapter 3 to

correlate the phenomenological behavior of the same granular medium in both one-dimensional and triaxial states of stress. A theoretical relationship between the coefficient of earth pressure at rest and the angle of internal friction was obtained by this correlation. A relationship between the angle of internal friction and the coefficient of friction between spheres was also obtained.

An experimental apparatus was designed and built which is capable of measuring the lateral stresses built up in one-dimensional compression into the high pressure ranges. The apparatus was used to measure the coefficient of earth pressure at rest and the stress-strain properties of four sands up to a maximum vertical stress of 3290 psi. Each sand was tested at a variety of initial densities and cyclic loading was employed to evaluate the energy absorption characteristics of each sand. The conclusions from these test results and the correlations of the one-dimensional tests with the theoretical analysis and triaxial test results are given in the following section.

7.2 Conclusions

The following major conclusions can be made from the test results, theoretical analysis, and the preceding discussion of the behavior of granular material in one-dimensional compression.

Conclusions from the Theoretical Analysis. A new solution for the stress-strain behavior of a face-centered cubic array of uniform spheres in one-dimensional compression has been presented. The results of this solution have been compared with an existing solution for the same array at failure in a triaxial state of stress with $\sigma_2 = \sigma_3 < \sigma_1$. The following conclusions have resulted from this analysis.

1) The axial stress-strain relations of a granular medium in one-dimensional compression become stiffer as the pressure increases which gives a concave upward curve on a conventional stress-strain plot. The equation derived for the stress-strain relation gives the axial stress as a linear function of the three halves power of the

axial strain; the constant of proportionality is determined by the coefficient of friction between spheres and the elastic properties of the spheres. The slope of the one-dimensional stress-strain curve is the constrained tangent modulus which is proportional to the cube root of the vertical stress; the constant of proportionality is a function of the coefficient of friction between spheres and the elastic properties of the spheres. The stress-strain relationships have been compared for the face-centered array subjected to a hydrostatic state of stress and one-dimensional compression. For a given level of axial stress the axial strains in one-dimensional compression are greater than in the hydrostatic case. The ratio between the axial strains for hydrostatic and one-dimensional compression is a constant which is only dependent upon the coefficient of friction between spheres.

2) The new one-dimensional solution also gives the lateral stress required to give the condition of zero lateral strain. A ratio of the lateral stress to the vertical stress is the classical coefficient of earth pressure at rest. The coefficient of earth pressure at rest given by the theory is

$$K_o = 1/2 \left(\frac{1-f}{1+f}\right) \qquad (3.49)$$

which indicates that the coefficient of earth pressure at rest for the array considered is only a function of the coefficient of friction and therefore the value of K_o should be inversly related to the strength of the granular medium.

3) The analysis given in Chapter 3 also indicates that the deformations of a face-centered cubic array in one-dimensional compression are fully recoverable when the medium is unloaded. Energy is dissipated, however, because the loading and unloading paths are different. The ratio of energy lost to energy input has been derived for one cycle of loading, assuming a reasonable approximation in the derivation of the unloading curve, which yielded

$$\frac{\Delta E}{E_1} = \frac{2f}{1+f} \qquad (3.65)$$

aus the energy absorbed in elastic hysteresis in one-dimensional compression is only
:pendent upon the coefficient of friction between spheres.

4) An analysis of the strength of a face-centered cubic array as given by
hurston and Deresiewicz (1959) was interpreted in terms of the angle of internal
iction as used in soil mechanics. This strength analysis is applicable to a triaxial
tate of stress where $\sigma_2 = \sigma_3 < \sigma_1$ and the angle of internal friction for a face-centered
ubic array was related to the coefficient of friction between grains by

$$\sin \phi = 1/3 + \frac{8}{3\sqrt{6}} f \qquad (3.71)$$

Therefore it is concluded that even when the coefficient of friction between spheres is
ero there is still a definite angle of internal friction due to the structural arrangement.
: is suggested by the writer that the angle of internal friction for a granular medium is
elated to the coefficient of friction by a general relationship of the form,

$$\sin \phi = K_3 + C_1 f \qquad (3.72)$$

Where K_3 is that fraction of sin ϕ due only to structure and C_1 is a constant determined
y the structural arrangement which determines the efficiency of the coefficient of
riction in contributing to the angle of internal friction.

5) The angle of internal friction and the coefficient of earth pressure at rest for
face-centered cubic array were both related to the coefficient of friction between
spheres. Therefore a relationship between the coefficient of earth pressure at rest and
he angle of internal friction was derived by eliminating the coefficient of friction to give

$$K_o = 1/2 \left[\frac{1 + \sqrt{6}/8 - 3\sqrt{6}/8 \sin \phi}{1 - \sqrt{6}/8 + 3\sqrt{6}/8 \sin \phi} \right] \qquad (3.76)$$

Therefore it is concluded that the coefficient of earth pressure at rest is definitely
elated to the strength parameters of a granular medium. In general, the coefficient of
arth pressure at rest decreases as the angle of internal friction increases.

The coefficient of earth pressure at rest is a statically indeterminate quantity which is dependent upon the stress-strain properties of the medium. Therefore the relationship given above which theoretically relates the coefficient of earth pressure at rest with a strength parameter emphasizes the fact that the stress-deformation and strength properties of a particulate medium such as soil are interrelated.

Conclusions from the Experimental Program. The development of a new one-dimensional compression device has been discussed and test data has been presented for four sands tested up to high pressure in one-dimensional compression. These tests have been analyzed in the light of triaxial test results for the four sands and the experimental results have been compared with the one-dimensional behavior predicted from the theory presented in Chapter 3. The following conclusions have resulted from this analysis.

1) The axial stress-strain curves for the high pressure one-dimensional tests show a concave upward curvature; the initial relative density of the sand is the significant variable which determines the slope of the stress-strain curve for a given sand at a given level of vertical stress. As higher pressures are applied, however, a point is reached where significant crushing of the grains causes the stress-strain curve to become concave downward. The initial relative density is also the significant variable which determines the stress level at which significant crushing will commence in a given sand. In general, the stress level at which crushing of the grains becomes significant increases as the initial relative density increases. Although the initial relative density is a significant variable in determining the behavior of a given sand in one-dimensional compression, the relative density is not a unifying index property for relating the behavior of different sands in one-dimensional compression. Data were presented for four different sands at the same initial relative density from which it was concluded that the stiffness at a given level of stress as expressed by the constrained tangent modulus could vary by a factor of 8 or 9 for the different sands. Therefore, it was concluded that the angularity and grain-size distribution were just as significant in determining

the one-dimensional behavior over a large range of pressures as the initial relative density.

2) In general, the initial relative density is the most important variable which affects the coefficient of earth pressure at rest for the initial loading of a given sand. The denser the sand, the lower is the coefficient of earth pressure at rest. The coefficient of earth pressure at rest varies inversely with the angle of internal friction as determined from drained triaxial tests. Three of the sands tested follow very closely the relationship

$$K_o = 1 - \sin \phi \qquad (7.1)$$

as suggested by Jaky (1944), and the test results on Minnesota sand agreed very well with the theoretical relationship between K_o and ϕ as suggested by the theory for spheres presented in Chapter 3 of this thesis. As the vertical stress became higher, the value of the coefficient of earth pressure at rest had a tendency to increase. It was concluded that this phenomenon was probably due to the angle of internal friction decreasing with pressure and was also a consequence of crushing of the grains.

The coefficient of earth pressure was found to be related to stress history as expressed by the overconsolidation ratio. As the overconsolidation ratio increases, the coefficient of earth pressure at rest increases and was observed to be between the limits of about 1.8 and 2.75 for an overconsolidation ratio of 48. The relationship between the overconsolidation ratio and the coefficient of earth pressure for three sands showed that during unloading, tests at all initial relative densities gave practically the same unique relationship of K_o versus OCR within narrow limits. The Minnesota Sand however, showed a different K_o versus OCR relationship for each initial relative density. Since the value of K_o still appeared to be increasing at an overconsolidation ratio of 48, it is the opinion of the writer that the coefficient of earth pressure at rest will approach the coefficient of passive earth pressure.

3) The mechanisms of energy absorption exhibited by sand loaded to high pressures in one-dimensional compression are:

a) Work done by the stresses due to permanent volume changes caused by rearrangement of the grains.

b) Energy absorbed in the form of surface energy in the creation of new surfaces during crushing of the grains.

c) Energy absorbed by an elastic hysteresis mechanism due to friction, even when the strains are recoverable.

Energy absorbed on the first cycle of loading in these tests is due to all three mechanisms; the energy absorption is quite high in the first cycle because of the irrecoverable deformations due to crushing and rearrangement. It is concluded from a unique correlation for all four sands that the constrained tangent modulus at the maximum stress on the first cycle is a good indication of the energy which is dissipated during the entire first cycle. The energy absorption per unit of energy input decreases as the constrained tangent modulus at the maximum stress in the cycle increases. The deformations in the second and third cycles of loading were practically 100 percent recoverable because the maximum stress was only one-third the maximum stress in the first cycle. A considerable amount of energy, however, was dissipated due to a difference in loading and unloading paths. This mechanism of energy dissipation is the mechanism listed under (c) above and is the type of mechanism predicted by the theory presented in Chapter 3. The energy lost in the second and third cycles varied from about 27 percent to 50 percent depending on the type of sand. It is concluded, therefore, that a significant amount of energy can be dissipated in sands even when the deformations are apparently almost 100 percent recoverable. The energy absorbed by this mechanism is dissipated into heat by a Coulombic type of damping as indicated in the theory presented in Chapter 3. It is suggested, therefore, that discrete lumped-mass models, which are

used to study the propagation of stress waves through soil, include a type of Coulomb damping element such as the one given in Section 3.4. It is obvious that an ordinary viscous damping element does not include a major mechanism which dissipates energy in soil because a viscous damper would not dissipate energy under a static load. It has been found on this study that a considerable amount of energy is absorbed by a granular medium loaded statically in one-dimensional compression even when the strains are fully recoverable. Therefore, it is felt that such models would more realistically represent a soil if Coulomb damping elements were included in the system.

4) The independent measurement of the coefficient of earth pressure at rest and the ratio of energy lost to energy absorbed for samples of Minnesota Sand have provided an experimental check to the theory presented in Chapter 3. The coefficient of friction between grains was back-calculated by formulas from the theory from both the measured energy absorption and the measured coefficient of earth pressure at rest. The theory was found to be at least consistent because the back-calculated values of the coefficient of friction between grains by both methods showed good agreement for the series of tests run on Minnesota Sand at an initial void ratio of 0.54. The back calculated values ranged from 0.16 to 0.20 and the average was 0.18. These values for the coefficient of friction are not unrealistic since a value of 0.16 has been reported for an air equilibriated sample of polished milky quartz from Wisconsin by Horn and Deere (1962).

5) The series of tests conducted on the angular Pennsylvania Sand showed that specimens with different initial relative densities tended to behave as the same material in all respects in the high pressure ranges. This conclusion is based upon the following observations: the pressure-void ratio curves merged into one curve at higher pressures; the constrained tangent moduli of all samples approached the same value at high pressures; the coefficient of earth pressure at rest for samples at various relative densities became the same value above the 2000 psi level; the stress paths of the top point on a Mohr circle

were initially different paths at low pressures for different initial relative densities, but paths for dense, loose, and medium samples merged into one path at higher pressure; a continuous plot of octahedral shearing stress versus one-third the first stress invariant as the tests progressed from low to high pressures showed different curves for dense, loose, and medium sands at low pressures which merged into one curve at higher stresses.

It is concluded from these tests that all sands will eventually manifest the same type of behavior as Pennsylvania Sand if high enough pressures are reached. The pressure level for the effects of initial relative density to be erased, however, is beyond the stress level of crushing for the densest specimen and therefore much higher for most sands than the stress levels investigated in these tests.

The results of the tests conducted on Pennsylvania Sand at different relative densities give various void ratio-log pressure curves which merge on a straight line which is usually called the "virgin" slope for clays. The compression index, C_c, of this slope is 0.49, which is substantially higher than the value of C_c for most clays. The family of void ratio-log pressure curves obtained by varying the initial relative density for sand is very similar to the family of curves obtained for clays consolidated in one-dimensional compression from different initial liquidity indices. These similarities between the phenomenological behavior of sands and clays cited above emphasize the fact that clays and sands qualitatively manifest the same behavior in many respects even though the physical make up of the particles in each is entirely different. It is the writer's opinion, however, that they each have in common the one main common denominator of all soils which make the stress-strain and strength properties of soils different from continuous elastic solids. This common denominator is the particulate nature of clays and sands. A particulate nature is also the most important common property that the sands tested and the idealized theoretical model of uniform spheres possess; it is because of this common property that the model predicted reasonably well the qualitative behavior of the sands and it is the only

tification for analyzing in detail such an idealized medium which is supposed to present soil.

Suggestions for Further Research

The foregoing investigation appears to warrant several lines of future research.

1) High pressure triaxial and hydrostatic compression tests should be conducted the same four sands used in this series of one-dimensional tests with lateral earth essure measurements. The data from these three types of tests should then be intereted in terms of the first, second, and third stress and strain invariants, as suggested Newmark (1960), in an effort to define more general stress-strain relations for a anular medium. Such an investigation was initiated for low pressure by the late ofessor D. W. Taylor of the Massachusetts Institute of Technology and published in finished form by Whitman (1960).

2) After the high pressure characteristics of the four sands have been measured der various states of stress these same four sands should be used as aggregates for ncrete specimens. The effects of the cement paste can then be evaluated because the operties of the aggregate under the same level of stress will be known. A study of this ture should lead to a clearer understanding of the stress-strain and strength behavior plain concrete.

3) The results of the tests on Pennsylvanian Sand suggest that a series of one-mensional tests should be run at high enough pressures to define the stress level at which e effect of the initial relative density is erased for a number of sands. The lateral resses built up in these one-dimensional tests should be measured so that the stress ith of the top point on a Mohr circle can be defined throughout the range of testing essures. A point of practical significance to look for is the point at which the stress ith becomes horizontal. When the path becomes horizontal the stress difference which n be maintained becomes a constant. This point is important to investigators working

on the mechanics of cratering and direct ground shock. The classical hydrodynamic equations used by the physicists assume that the behavior of the material is essentially like a fluid since the level of the hydrostatic component of stress is assumed to be very much larger than the shearing stresses. Therefore the lower limit of the pressure range for which the hydrodynamic equations apply must be defined by tests on real materials such as those outlined above.

4) Because the initial relative density of a sand is such an important index property, a standard method should be developed for determining the values of e_{max} and e_{min}.

5) A technique should be devised for using the apparatus developed on this investigation to test undisturbed samples of soil and intact specimens of rock up to high pressures in one-dimensional compression.

6) The model developed in Chapter 3 with the frictional damping elements should be analyzed for several types of dynamic stress pulses. This type of energy dissipation is probably more realistic for sand than viscous damping.

7) A very extensive list of suggestions for further research in the area of the theoretical mechanics of granular media is given by Deresiewicz (1958). The writer feels that there is further work in this area which can be used in conjunction with experimental tests to develop a more general and systematic description of the stress-strain and strength relationships in granular materials.

REFERENCES

xelson, J. W., (1949), "Energy-New Surface Relationship in the Crushing of Solids, V Application of Slow Compression to an Investigation of the Crushing of Crystalline luartz," Ph.D. Thesis, University of Minnesota.

auer, E. E., and Thornburn, T. H., (1962), "Introductory Soil Testing," Stipes ublishing Company, Champaign, Illinois.

ayliss, J R., (1948), "Design, Calibration, and Use of the Lateral Earth Pressure leter," M.S. Thesis, Princeton University.

lishop, A. W., (1950), "Summarized Proceedings of a Conference on Stress Analysis," lritish Journal of Applied Physics, I. 241:251.

lishop, A. W., (1954), Correspondence, Geotechnique, Vol. IV, No. 1, March.

lishop, A. W., (1958), "The Test Requirements for Measuring the Coefficient of Earth Pressure at Rest," Brussels Conference on Earth Pressure Problems, Vol. I, pp. 2-14.

lishop, A. W., and Henkel, D. J., (1957), "The Measurement of Soil Properties in the Triaxial Test," Edward Arnold, London, 190 pp.

Bjerrum, (1962), Personal Correspondence to Professor R. B. Peck.

Bjerrum, L., Kringstad, S., and Kunmeneje, O., (1961), "The Shear Strength of a Fine Sand," Proceedings of the Fifth International Conference on Soil Mechanics and Foundation Engineering, Vol. I, pp. 29-37.

Brandt, H., (1955), "A Study of the Speed of Sound in Porous Granular Media," Journal of Applied Mechanics, Vol. 22, No. 4, December.

Cattaneo, C., (1938), "Sul Contatto di due corpi elastici," Accademi dei Lincei, Rendiconti, Series 6, Vo. 27, pp. 342-348, 434-436 and 474-478.

Caquot, A., (1934), "Equilibre des Massifs à Frottement Interne. Stabilité des Terres Pulvérulents et Cohérentes," Gauthier-Villars, Paris, 91 pp.

Chi-in, H., (1958), "A New Apparatus for the Determination of the Coefficient of Lateral Earth Pressure at Rest," Scientia Sinica, Vol. VII, No. 6.

Deresiewicz, H., (1957), "Stress-Strain Relations for a Simple Model of a Granular Medium," Journal of Applied Mechanics, Paper No. 57-A-90, or Office of Naval Research Project NR-064-388, Contract Nonr-266(09) Technical Report No. [illegible], April.

Deresiewicz, H., (1958), "Mechanics of Granular Matter," Advances in Applied Mechanics, Vol. 5, Academic Press, Inc., New York, New York, p. 233.

Donath, A. D., (1891), "Untersuchungen ueber den Erddruck auf Stuetzwaende," Zeitschrift fuer Bauwesen, Berlin.

Duffy, J. and Mindlin, R. D., (1957), "Stress-Strain Relations and Vibrations of a Granular Medium," Journal of Applied Mechanics, Vol. 24, Trans. ASME, Vol. 79, pp. 585-593.

Fraser, A. M., (1957), "The Influence of Stress Ratio on Compressibility and Pore Pressure Coefficients in Compacted Soils," Ph. D. Thesis, University of London.

Fulton, R. E. and Hendron, A. J., (1962), "Discussion to Impact Waves in Sand: Theory Compared with Experiments on Sand Columns," Transactions ASCE, Vol. 127, Part I, pp. 1301-1305.

Gassman, F., (1953), "Elastic Waves Through a Packing of Spheres," Geophysics 18, pp. 268.

Hendron, A. J., Fulton, R. E. and Mohraz, B., "The Energy Absorption Capacity of Granular Materials in One-Dimensional Compression," Technical Documentary Report Number, AFSWC-TDR-62-91, Air Force Special Weapons Center, Air Force Systems Command, Kirtland Air Force Base, New Mexico.

Heney, L. J., (1951), "Energy-New Surface Relationship in the Crushing of Solids, V Impact Crushing of Single Particles of Crystalline Quartz," Ph. D. Thesis, University of Minnesota.

Hertz, H., (1881), "Über die Beruhrung fester elastischer Körper, J. F. reine u. angew. Math. (Creele's J.), Vol. 92, p. 155.

Horn, H. M. and Deere, D. U., (1962), "Frictional Characteristics of Minerals," Geotechnique, Vol. XII, No. 4, December.

Idel, K. H., (1960), "Die Scherfestigkeit rolliger Erdstoffe," Veröffentlichungen des Institutes für Bodenmechnik und Grundbau der Technischen Hochschule Fridericiana in Karlsruhe, Heft 2.

Iida, K., (1938), "The Velocity of Elastic Waves in Sand," Bulletin Earthquake Research Institute, Tokyo University, 16, pp. 131-144.

Jakobson, B., (1958), Discussion, Brussels Conference on Earth Pressure Problems, Vol. III, pp. 46-48.

Jaky, J., (1944), "The Coefficient of Earth Pressure at Rest," Journal of the Society of Hungarian Architects and Engineers, Budapest, pp. 355-358.

Jaky, J., (1948), "State of Stress in Great Depth," Proceedings of the Second International Conference on Soil Mechanics and Foundation Engineering, Vol. 1, pp. 90-93.

Jenkin, C. F., (1931), "The Pressure Exerted by Granular Material: An Application of the Principle of Dilatancy," Proceedings of the Royal Society, (London), Ser. A. 131, pp. 53-89.

Kenny, W. J., (1954), "Energy-New Surface Relationship in the Crushing of Solids, VII Slow Compression Crushing of Single Particles of Glass," Ph. D. Thesis, University of Minnesota.

Jellman, W., (1936), "Report on an Apparatus for Consummate Investigation of the echanical Properties of Soils," First International Conference on Soil Mechanics and oundation Engineering, Cambridge, Vol. 2, pp. 16-20.

Jellman, W., and Jakobson, B., (1955), "Some Relations Between Stress and Strain in oarse-Grained Cohesionless Materials," Bulletin No. 9, Proceedings of the Royal wedish Geotechnical Institute, Stockholm.

Ögler, F., and Sheidig, A., (1928), "Pressure Distribution in Soil," Die Bautechnik, lo. 15, p. 205-209.

Laszlo, F. V., (1962), "Stability of Granular Masses," Proceedings of the American ociety of Civil Engineers, Journal of the Engineering Mechanics Division, Vol. 88, lo. EM6, December, Part I.

Mindlin, R. D., (1949), "Compliance of Elastic Bodies in Contact," Journal of Applied Mechanics, Vol. 16, Trans. ASME, Vol. 71, p. A-259,

Mindlin, R. D., (1954), "Mechanics of Granular Media," Proceedings of the Second J.S. National Congress of Applied Mechanics, Ann Arbor, pp. 13-20.

Mindlin, R. D. and Deresiewicz, H., (1953), "Elastic Spheres in Contact Under Varying Oblique Forces," Journal of Applied Mechanics, Vol. 20, Trans. ASME, Vol. 75, pp. 327-344.

Mindlin, R. D., and Deresiewicz, H., (1953), "Elastic Spheres in Contact Under Varying Oblique Forces," Journal of Applied Mechanics, Vol. 20, pp. 327-344.

Mindlin, R. D., Mason, W. P., Osmer, T. F., and Deresiewicz, H., (1951), "Effects of an Oscillating Tangential Force on the Contact Surfaces of Elastic Spheres," Proceedings of the First National Congress of Applied Mechanics, Chicago, pp. 203-208.

Murtha, J. P., (1961), "Discrete Mass Mathematical Models for One-Dimensional Stress Waves," Ph.D. Thesis, University of Illinois.

Newmark, N. M., (1959), "A Method of Computation for Structural Dynamics," Proceedings of the American Society of Civil Engineers, Journal of the Engineering Mechanics Division, Vol. 85, No. EM3, Part 1, pp. 67-94.

Newmark, N. M., (1960), "Failure Hypotheses for Soils," American Society of Civil Engineers Research Conference on Shear Strength of Cohesive Soils, University of Colorado, Boulder, Colorado, June, pp. 17-32.

Olson, R. E., (1962), "The Shear Strength Properties of Calcium Illite," Geotechnique, Vol. XII, March, No. 1, pp. 23-44.

Reynolds, O., (1885), "On the Dilatancy of Media Composed of Rigid Particles in Contact," Philosophical Magazine (5. Series) 20, pp. 469-481.

Rittenhouse, G., (1943), "A Visual Method of Estimating Two Dimensional Sphericity, Journal of Sedimentary Petrology, Vol. 13, pp. 79-81.

Roberts, J. E., (1959), "Study of Soils Consolidated Under High Pressure," Report for the Creole Petroleum Corp., Maracaibo, Venezuela, Massachusetts Institute of Technology, October.

Roberts, J. E., and De Souza, J. M., (1958), "The Compressibility of Sands," Proceedings of the American Society for Testing Materials, Vol. 58, pp. 1269-1277.

Roberts, J. M., (1961), "A Study of Hysteresis in Granular Soils," M. S. Thesis, Massachusetts Institute of Technology, June.

Rowe, P. W., (1958), "General Report on Papers in Section I," Brussels Conference on Earth Pressure Problems, Vol. III, pp. 25-30.

Sauer, F. M., (1959), "Ground Motion Produced by Above-Ground Nuclear Explosions," Air Force Special Weapons Center, AFSWC-TR-59-71 (Secret), Air Force Special Weapons Center, Kirtland Air Force Base, Albuquerque, New Mexico.

Schmid, W. E., and Tschebotariof, G. P., (1958), Discussion, Brussels Conference on Earth Pressure Problems, Vol. III, pp. 40-43.

Schultze, E., and Moussa, A., (1961), "Factors Affecting the Compressibility of Sand," Proceedings of the Fifth International Conference on Soil Mechanics and Foundation Engineering, Vol. I, pp. 335-340.

Simons, N., (1985), Discussion, Brussels Conference on Earth Pressure Problems, Vol. III, pp. 50-53.

Smith, J. O., (1961), "A Resolved Shearing Stress Energy Theory of Failure by Slip of a Polycrystalline Metal with Face-Centered Cubic Lattice Crystals," Theoretical and Applied Mechanics Report No. 189, University of Illinois.

Smith, R. H. and Newmark, N. M., (1958), "Numerical Integration for One-Dimensional Stress Waves," Civil Engineering Studies, Structural Research Series No. 162, University of Illinois, August.

Speer, T. L., (1944), Personal files of R. B. Peck, Professor of Foundation Engineering, University of Illinois.

Taylor, D. W., (1942), "Research on Consolidation of Clays," Publication No. 82, Publications of the Department of Civil and Sanitary Engineering, Massachusetts Institute of Technology, Cambridge, Massachusetts.

Terzaghi, K., (1920), "Old Earth-Pressure Theories and New Test Results," Engineering News-Record, Vol. 85, No. 14, September 30, pp. 632-637.

Terzaghi, K., (1934), "Large Retaining-Wall Tests," Engineering News-Record, February 1, pp. 136-140.

Terzaghi, K., and Peck, R. B., (1948), "Soil Mechanics in Engineering Practice," John Wiley & Sons, New York, 566 pp.

Thurston, C. W. and Deresiewicz, H., (1959), "Analysis of a Compression Test of a Face-Centered Cubic Array of Elastic Spheres," Journal of Applied Mechanics, Vol. 26, Trans. ASME, Vol. 81, pp. 251-258.

Timoshenko, S., and Goodier, J. N., (1951), "Theory of Elasticity," Second Edition, McGraw-Hill, New York, 506 pp.

Trollope, D. H., (1957), "The Systematic Arching Theory Applied to the Stability Analysis of Embankments," Proceedings of the Fourth International Conference on Soil Mechanics and Foundation Engineering, Vol. II, p. 382.

Trollope, D. H. and Morgan, J. R., (1959), "Stress Systems Within Simple Slopes of Granular Materials," The Institute of Engineers, Australia, Civil Engineering Transactions, Vol. CEI, No. 1, March, p. 18.

Tschebotarioff, G. P., (1948), Discussion of "Earth Pressure on Horizontal Conduits," Proceedings of the Second International Conference on Soil Mechanics and Foundation Engineering, Vol. VI, pp. 108-111.

Tschebotarioff, G. P., (1951), "Soil Mechanics, Foundations, and Earth Structures," McGraw-Hill Book Company, Inc., New York, 655 pp.

Urul, M. V., (1945), "An Experimental Study of the Compressibility of Remolded Clay at High Pressure," M. S. Thesis, University of Illinois, Department of Civil Engineering.

Whitman, R. V., (1960), Discussion, American Society of Civil Engineers Research Conference on the Shear Strength of Cohesive Soils, University of Colorado, Boulder, Colorado, June, pp. 1062-1065.

Whitman, R. V., (1962), Nuclear Geoplosics, Part Two - Mechanical Properties of Earth Materials. 3203 (11) Draft (Unpublished) Prepared for the Defense Atomic Support Agency, Washington 25, D. C., under Contract Nos. DA-22-079-eng-224 and DA-49-146-xz-030, June.

Wittke, W., (1962), "Über die Scherfestigkeit rollinger Erdstaffe, Rechnerische und Experimentelle Untersuchung von Kugelschüttungen," Veröffentlichungen des Institutes fur Bodenmechanik und Grundbau der Technischen Hochschule Fridericiana in Karlsruhe, Heft 11.

Wu, C. T., (1962), "Transverse Sensitivity of Bonded Strain Gages," Experimental Mechanics, Vol. 2, No. 11, pp. 338-344.

Zeleny, R. A., and Piret, E. L., (1959), "Studies of the Energy Requirements for Crushing," Third Symposium on Rock Mechanics, Colorado School of Mines, Quarterly Colorado School of Mines, Vol. 54, No. 3, July.

TABLE 3.1

VARIATION OF STRESS AND STRAIN VARIANTS

After Kjellman (1936)

$I_{\frac{1}{3}} = \frac{1}{3}(\sigma_1 + \sigma_2 + \sigma_3)$	$\Delta v/v = (\epsilon_1 + \epsilon_2 + \epsilon_3) = J_1$	$J_{\frac{1}{3}}$
kg/cm^2	10^{-2} cm/cm	10^{-2} cm/cm
1	0.12	0.04
2	0.24	0.08
4	0.38	0.13
6	0.47	0.16
8	0.54	0.18
10	0.62	0.21
12	0.69	0.23

I_1 = First stress invariant

J_1 = First strain invariant

TABLE 3.2

EFFECT OF THE COEFFICIENT OF FRICTION ON ONE-DIMENSIONAL STRESS-STRAIN BEHAVIOR OF A FACE-CENTERED ARRAY OF SPHERES

f	K_o $\frac{1}{2}\left(\frac{1-f}{1+f}\right)$	$\Delta E/E_1$ percent $\frac{2f}{1+f} \times 100$
0	0.5	0
0.05	0.45	9.5
0.10	0.41	18.2
0.15	0.37	26.1
0.20	0.33	33.3
0.25	0.30	40.0
0.30	0.27	46.2

f = coefficient of friction at contact points

K_o = coefficient of earth pressure at rest, P_H/P_{zz}

$\frac{\Delta E}{E_1} \times 100\%$ = percent energy absorbed due to loading and unloading

TABLE 6.1

ENERGY LOSSES FOR REPEATED LOADINGS ON MINNESOTA SAND

Test No.	Stress Range for Hysteresis Loop psi	Mean Stress psi	Energy Lost / Energy Input %
3	0-1100	550	33.4
4	0-1100	550	33.1
5	0-1100	550	32.8
6	0-1100	550	30.2
7	0-1100	550	27.9
8	0-1100	550	27.5
9	0-3290	1645	27.8
10	0-1100	550	28.7
11	0-2195	1098	28.5

TABLE 6.2

CORRELATION OF THE COEFFICIENT OF FRICTION, THE COEFFICIENT OF EARTH PRESSURE AT REST AND THE ENERGY ABSORPTION CAPACITY OF A GRANULAR MEDIUM

Test	e_o	$f = \frac{1 - 2K_o}{2K_o + 1}$	$f = \frac{1/2 \frac{\Delta E}{E_I}}{(1 - 1/2 \frac{\Delta E}{E_I})}$
3	.62	.12	.20
4	.62	.09	.20
5	.54	.18	.20
6	.54	.16	.18
7	.54	.20	.16
8	.54	.20	.16
9	.54	.19	.17
10	.54	(no hysteresis loop on this test)	
11	.54	.18	.17

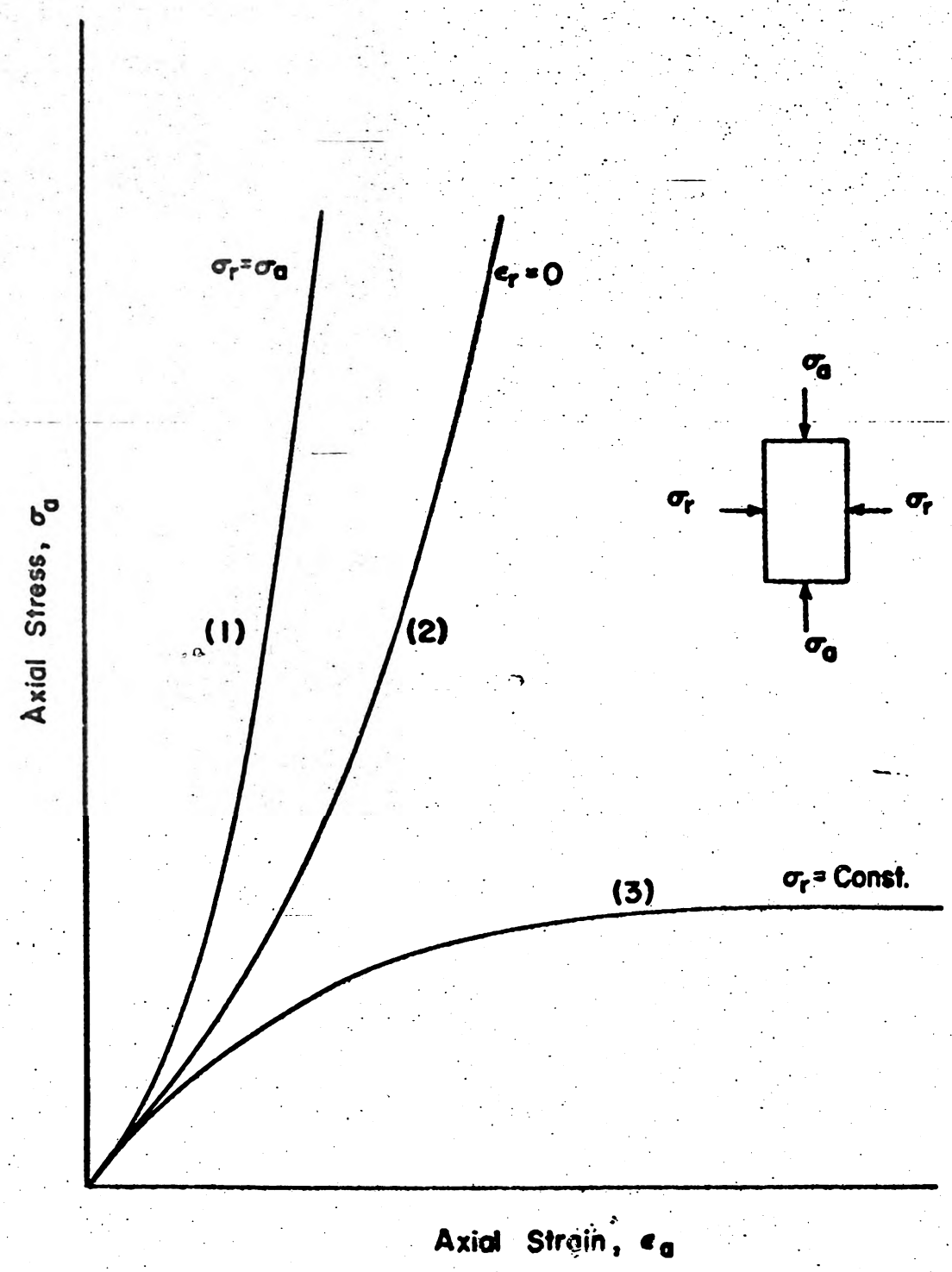

Fig. 1.1 AXIAL STRESS STRAIN CURVES FOR SOIL SUBJECTED TO VARIOUS STATES OF STRESS

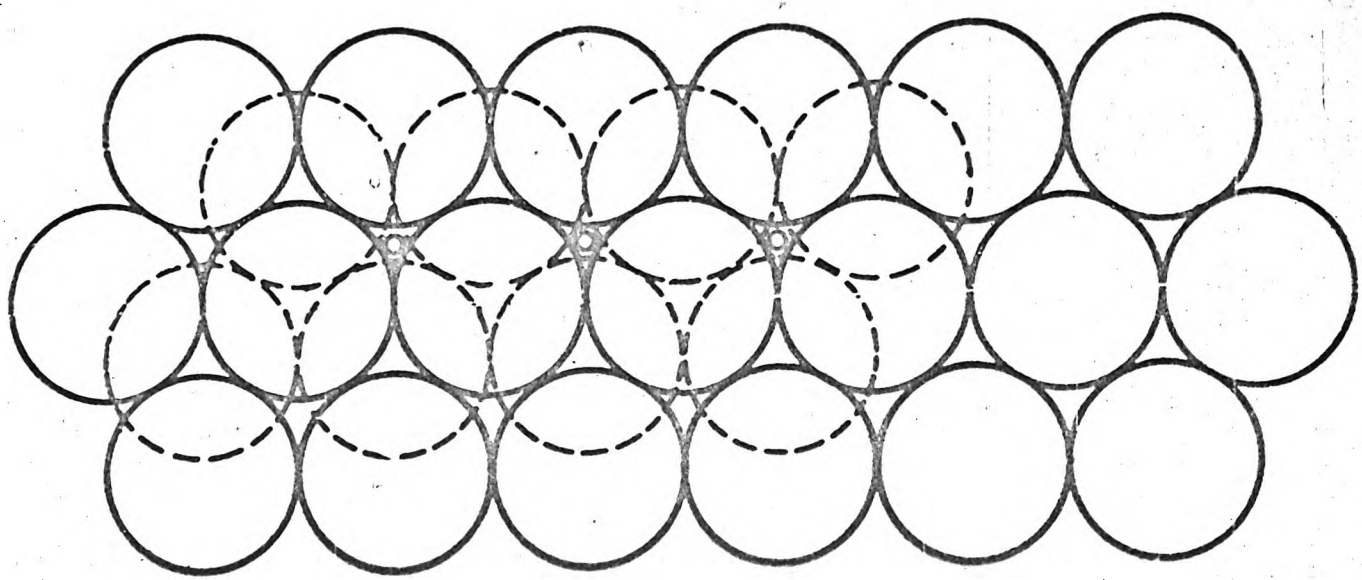

O: Location of sphere centers in third layer resulting in a face-centered cubic array

Fig. 3.1 CONSTRUCTION OF DENSEST PACKING OF EQUAL SPHERES AFTER DERESIEWICZ (1958)

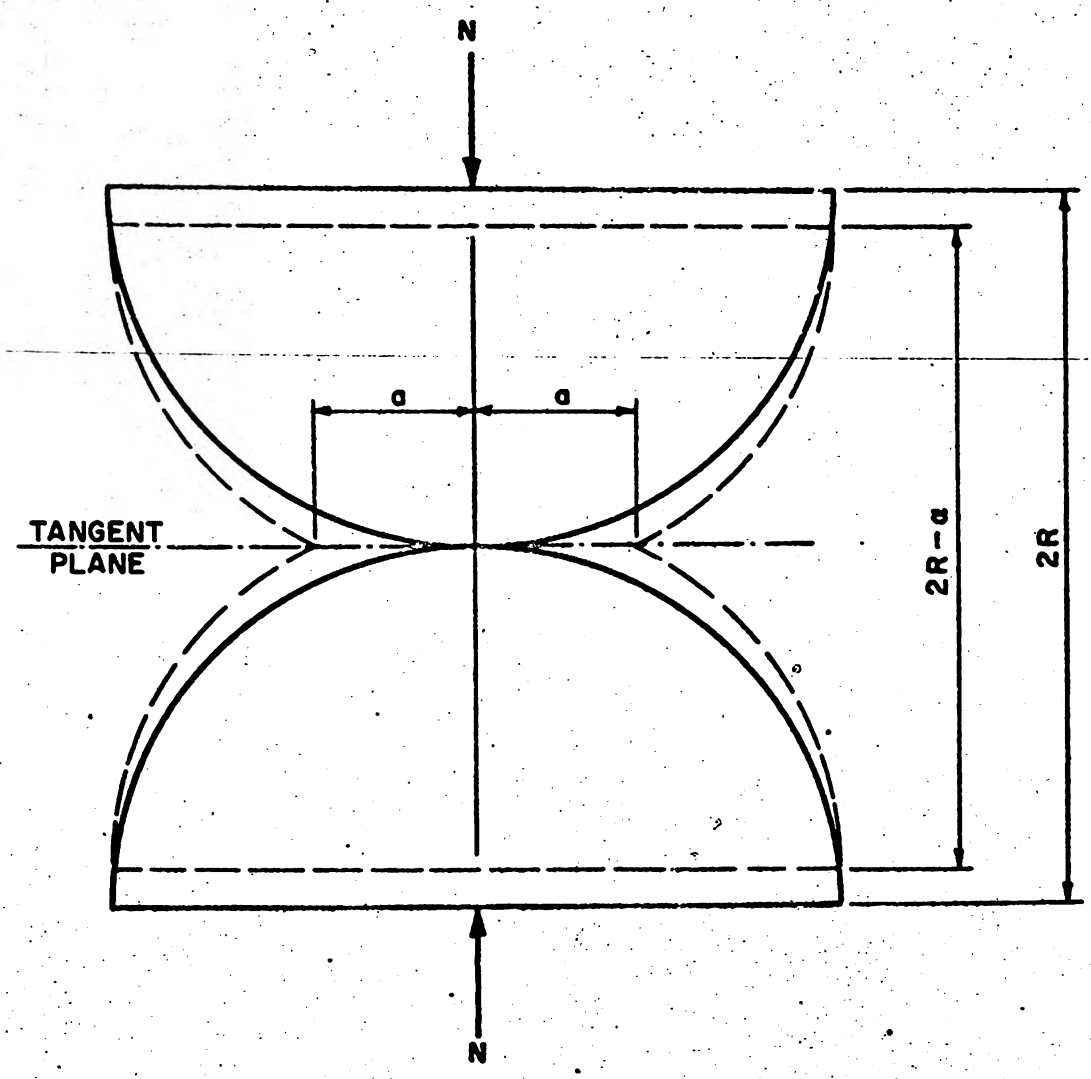

Fig. 3.2 TWO SPHERES IN NORMAL CONTACT

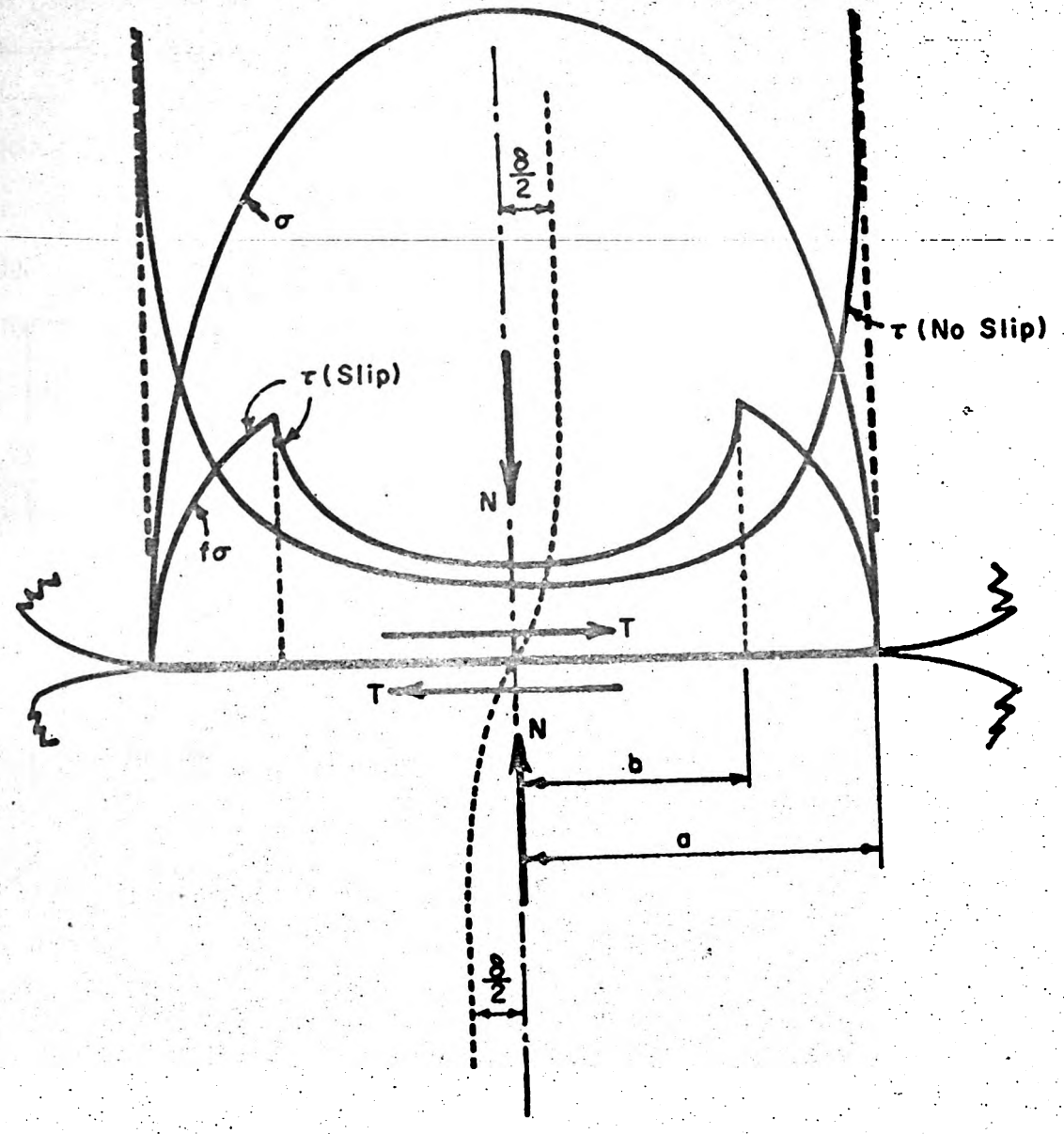

Fig. 3.3 DISTRIBUTIONS OF NORMAL (σ) AND TANGENTIAL (τ) COMPONENTS OF STRESS ON THE CONTACT SURFACE OF TWO LIKE SPHERES SUBJECTED TO A NORMAL FORCE FOLLOWED BY A MONOTONIC TANGENTIAL FORCE AFTER MINDLIN (1949)

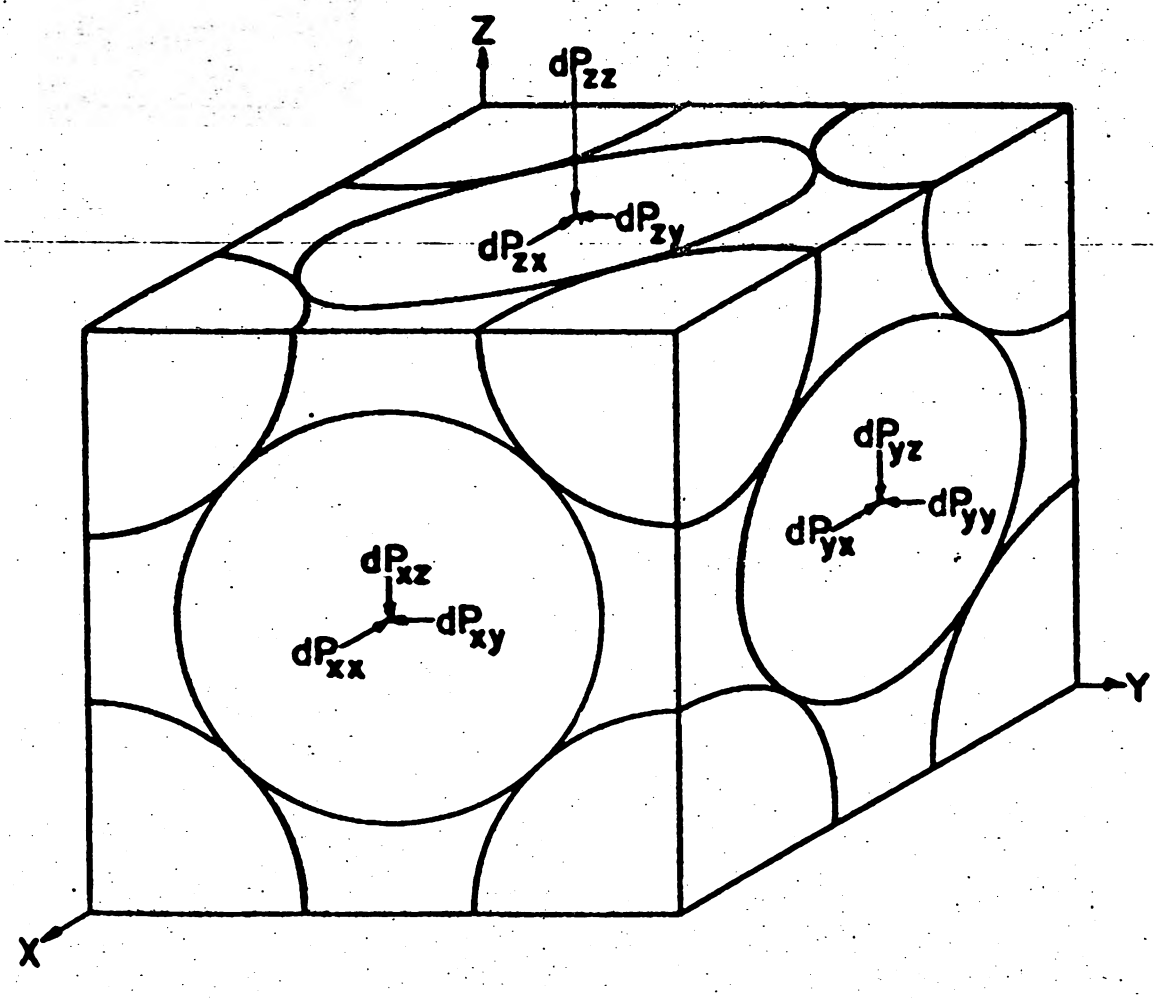

Fig. 3.4 UNIT CUBE OF A FACE-CENTERED CUBIC ARRAY OF EQUAL SPHERES SUBJECTED TO INCREMENT FORCES AFTER DERESIEWICZ (1958)

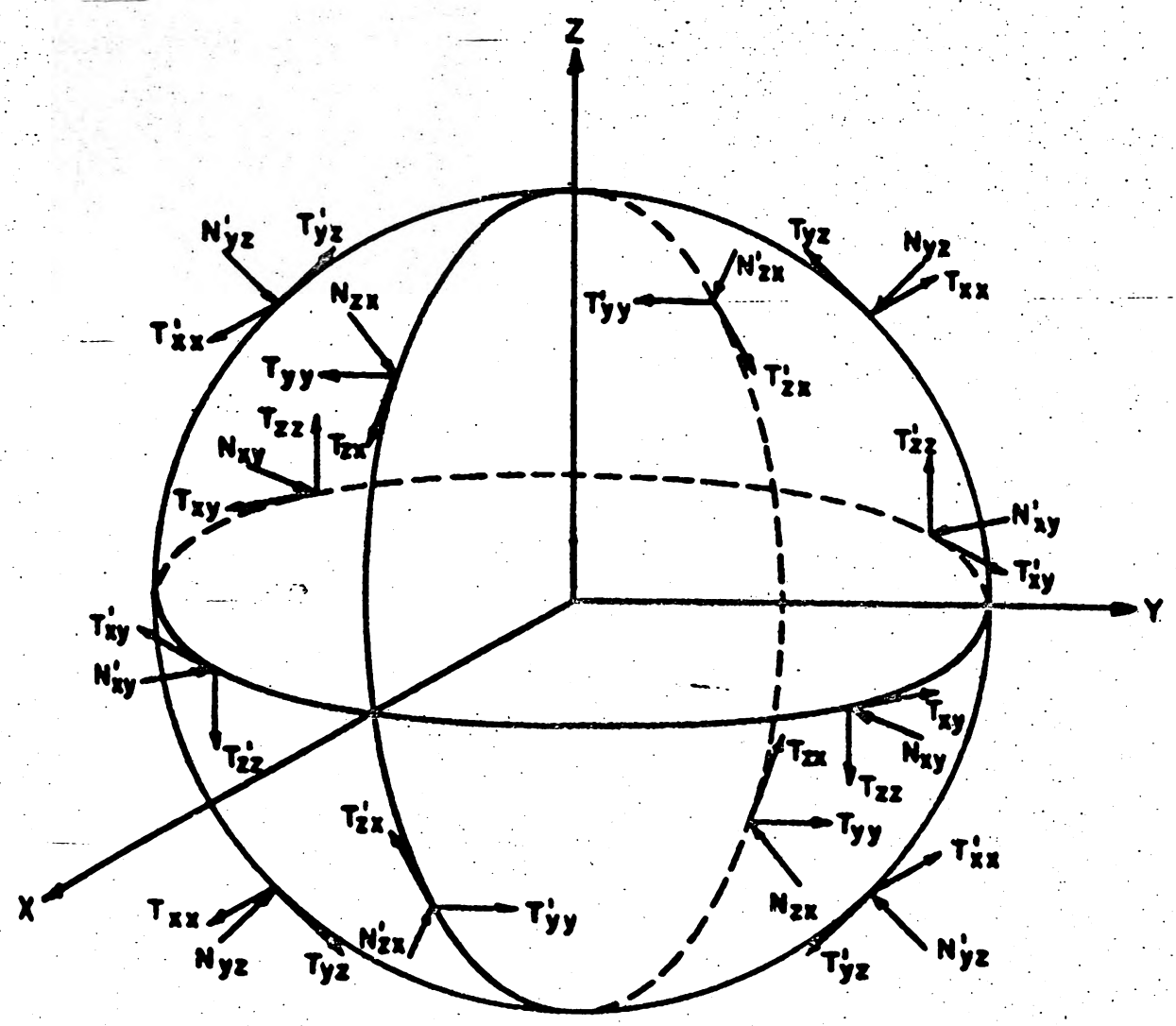

Fig. 3.5 FORCES ACTING ON A TYPICAL SPHERE OF A FACE-CENTERED ARRAY AFTER THURSTON AND DERESIEWICZ (1959)

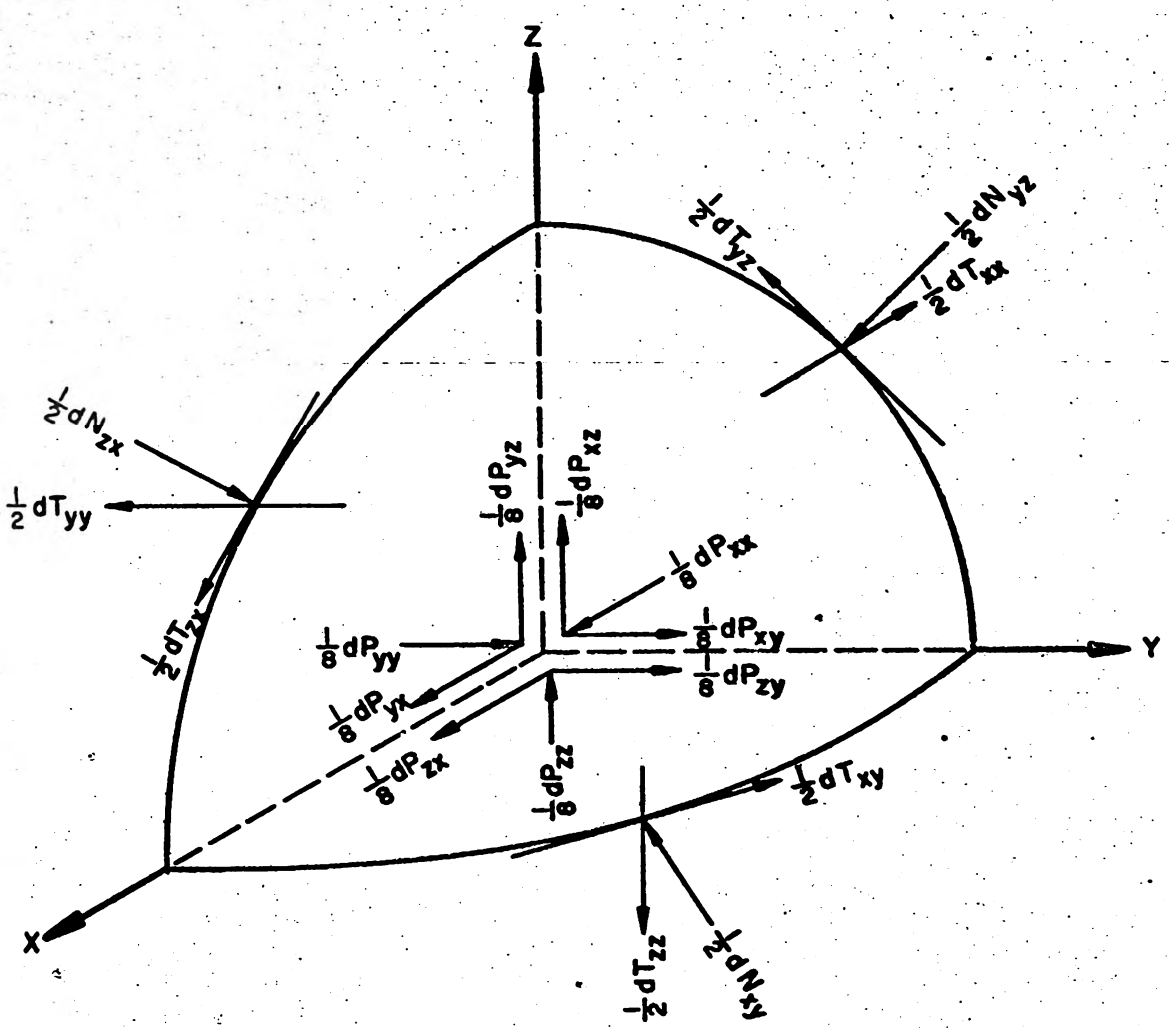

Fig. 3.6 FORCES ACTING ON AN OCTANT OF A SPHERE
(Octant Shown Here is Located at Origin in Fig. 3.5)
AFTER DUFFY AND MINDLIN (1957)

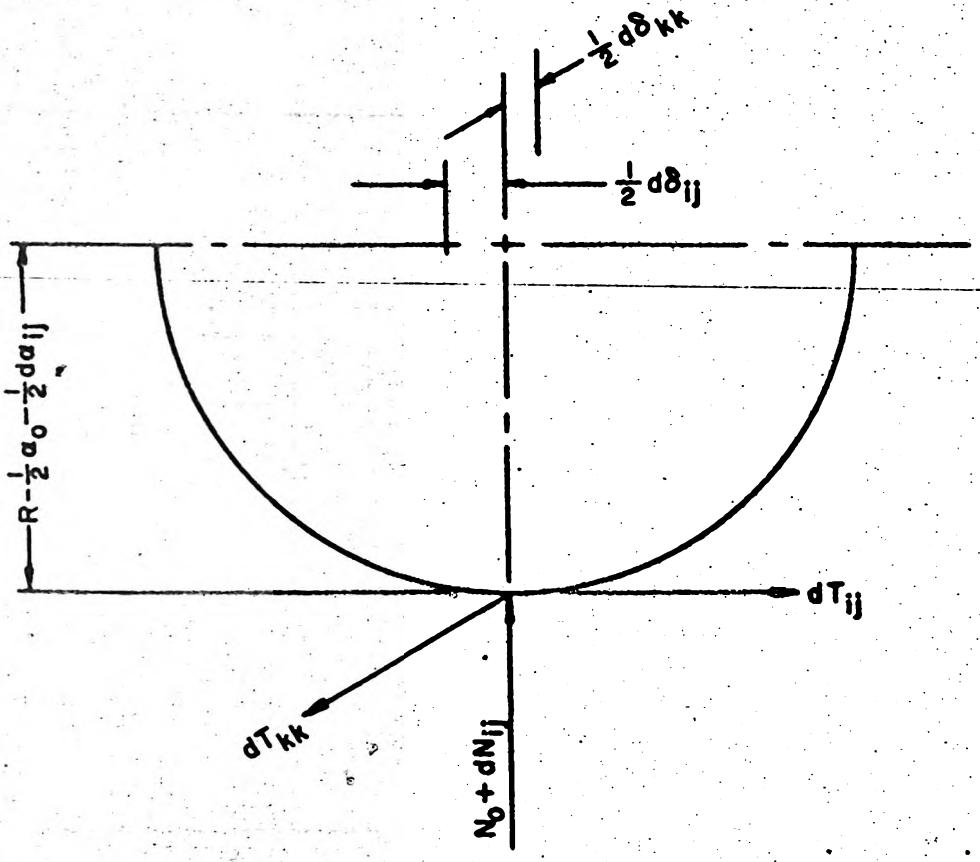

Fig. 3.7 COMPONENTS OF FORCE AT A CONTACT AND CORRESPONDING COMPONENTS OF DISPLACEMENT OF THE CENTER OF A SPHERE AFTER DUFFY AND MINDLIN (1957)

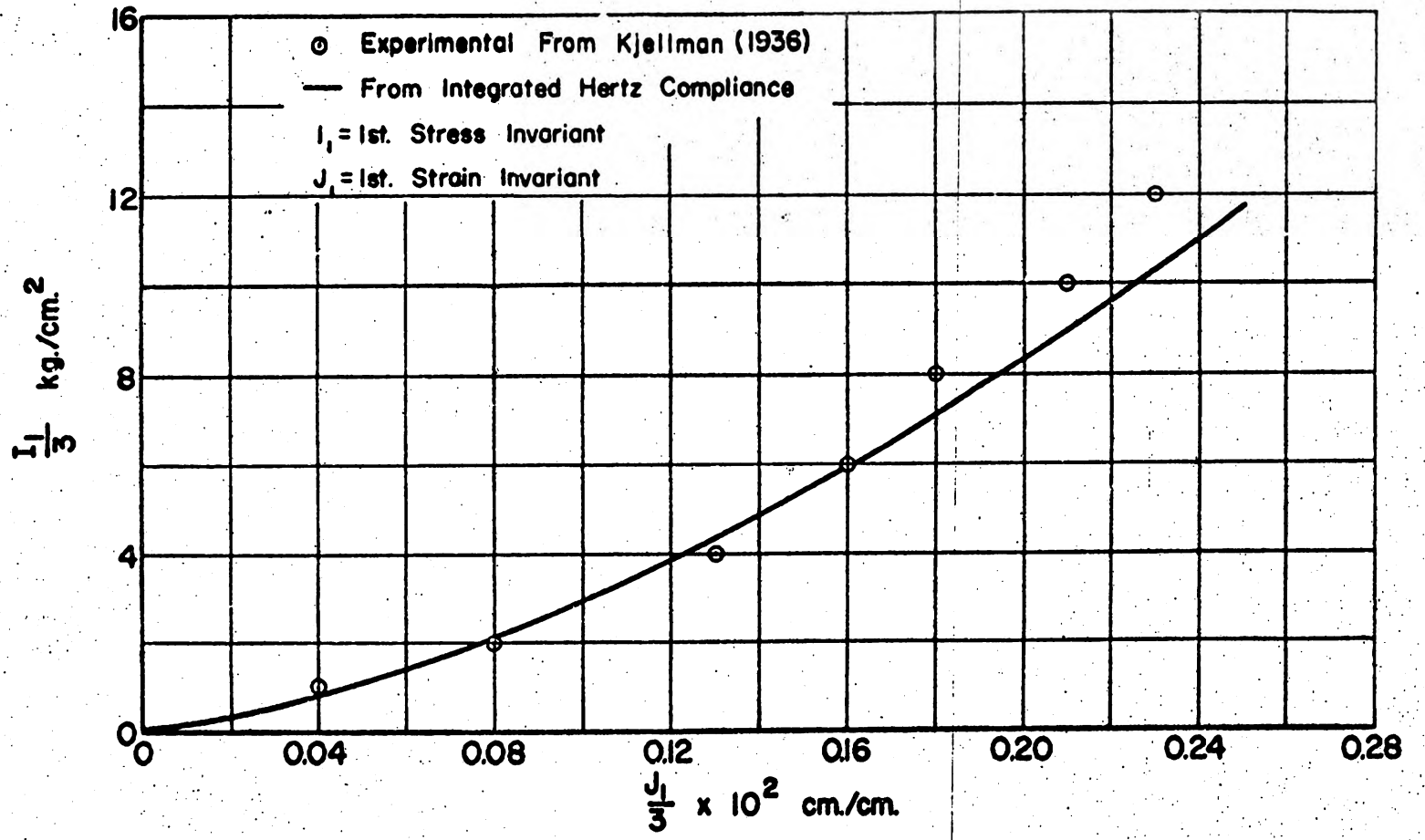

Fig. 3.8 VARIATION OF FIRST STRESS INVARIANT WITH FIRST STRAIN INVARIANT

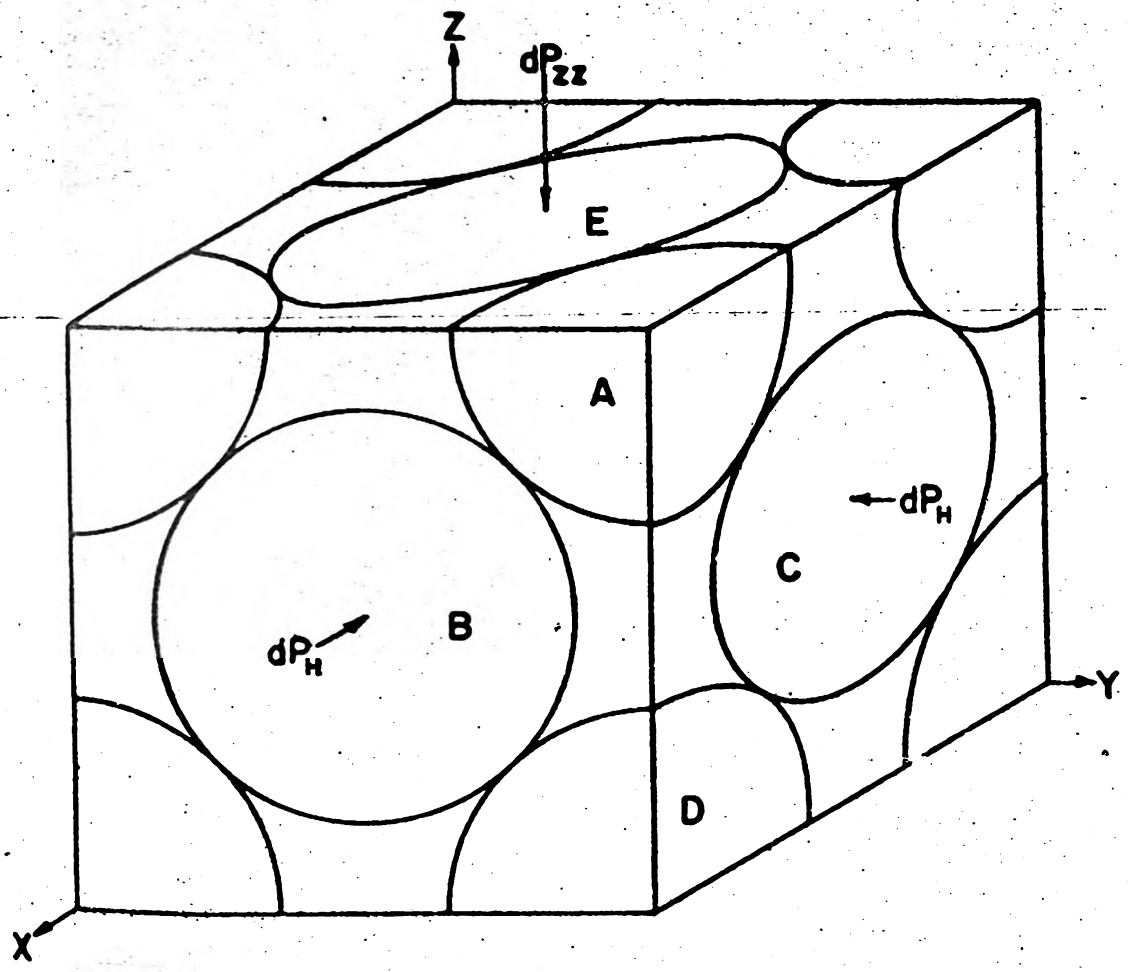

Fig. 3.9 UNIT CUBE OF A FACE-CENTERED CUBIC ARRAY OF EQUAL SPHERES SUBJECTED TO INCREMENTAL FORCES IN ONE-DIMENSIONAL COMPRESSION

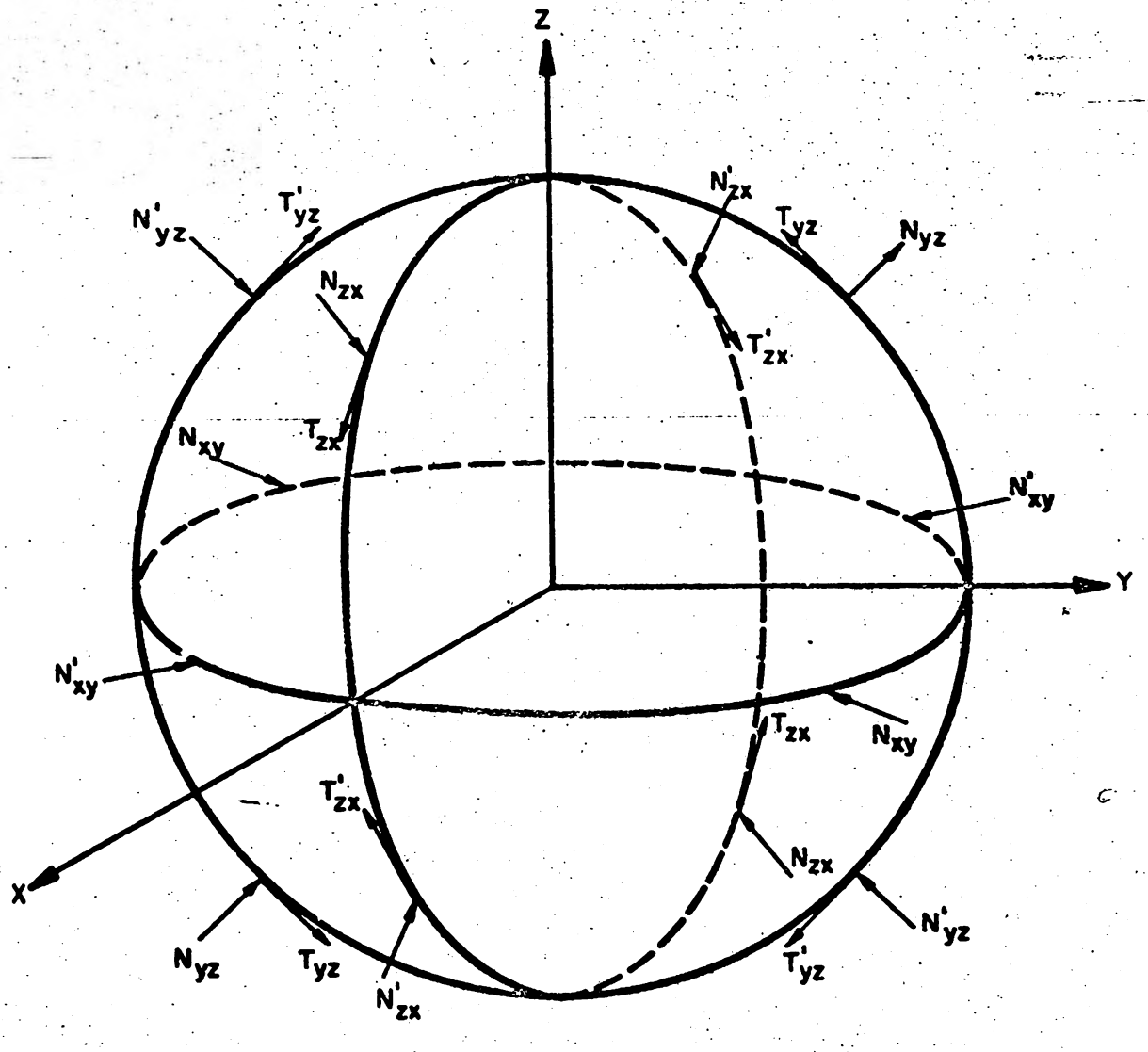

Note That Due To Symmetry

$$T_{zx} = T'_{zx} = -T_{yz} = -T'_{yz} = T_2$$

$$N_{yz} = N'_{yz} = N_{zx} = N'_{zx} = N_2$$

$$N_{xy} = N'_{xy} = N_1$$

Fig. 3.10 FORCES ACTING ON A TYPICAL SPHERE SUBJECTED TO ONE-DIMENSIONAL COMPRESSION

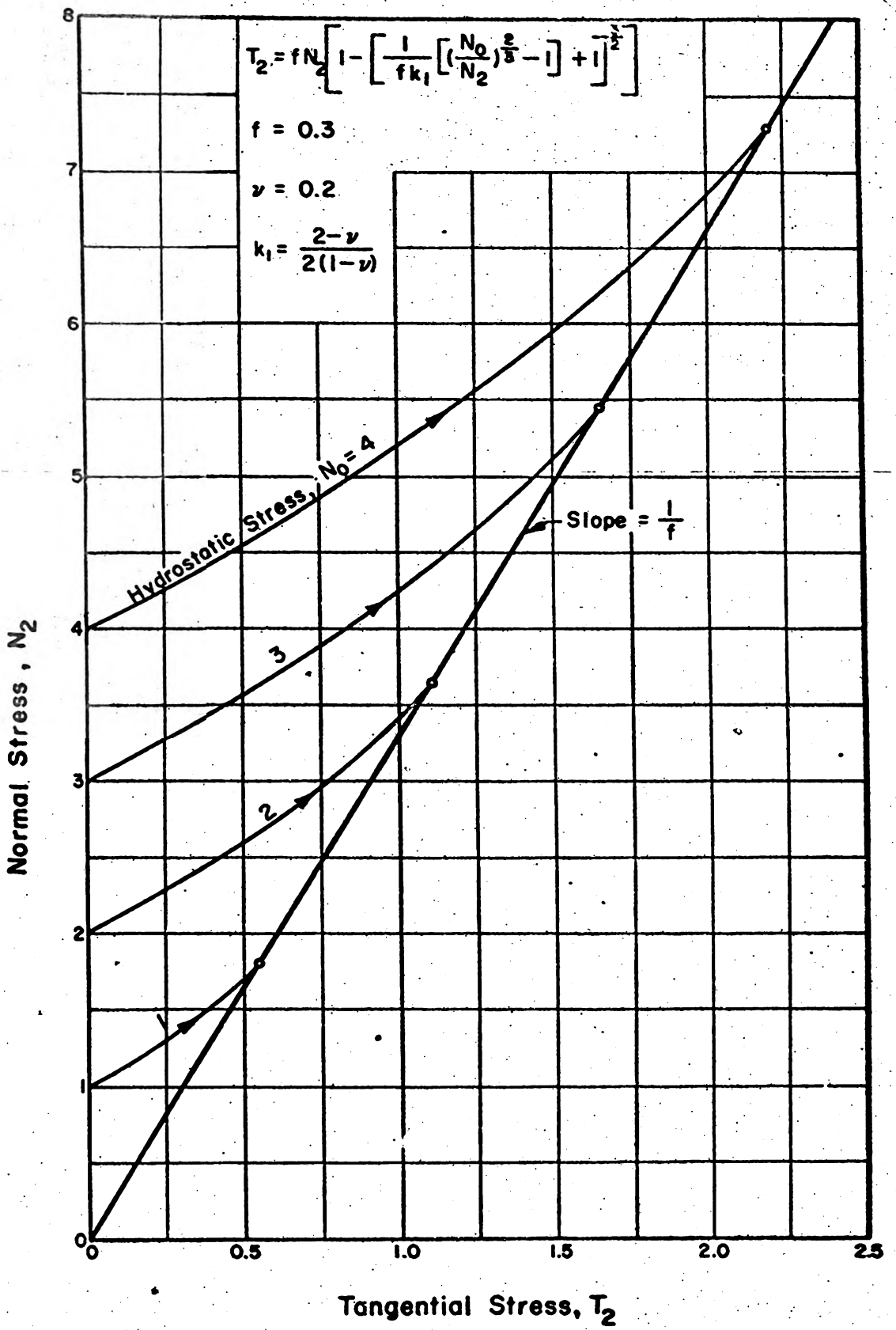

Fig. 3.11 VARIATION OF CONTACT STRESSES UNDER ONE-DIMENSIONAL BEHAVIOR WITH AN INITIAL HYDROSTATIC STRESS

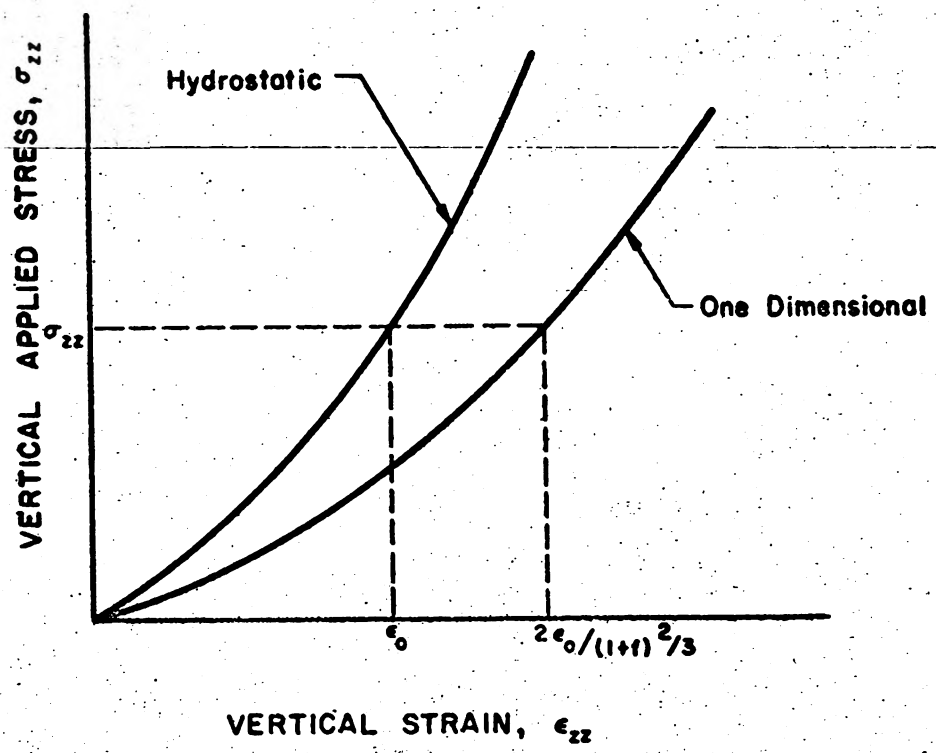

Fig. 3.12 STRESS STRAIN CURVES FOR A FACE-CENTERED ARRAY OF SPHERES SUBJECTED TO HYDROSTATIC AND ONE-DIMENSIONAL STATES OF STRESS

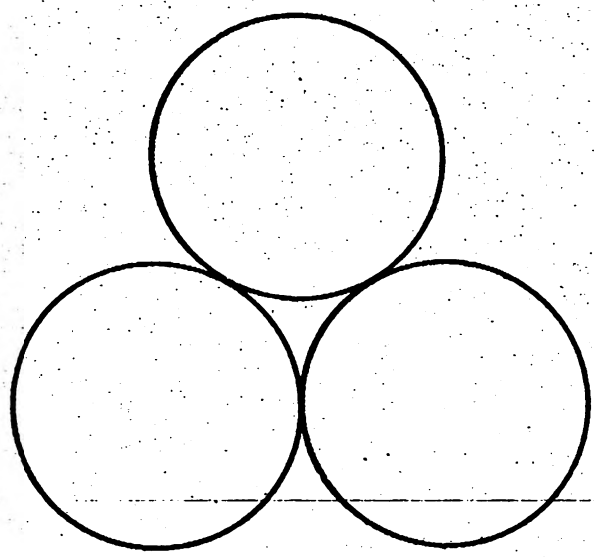

(a) Unloaded State

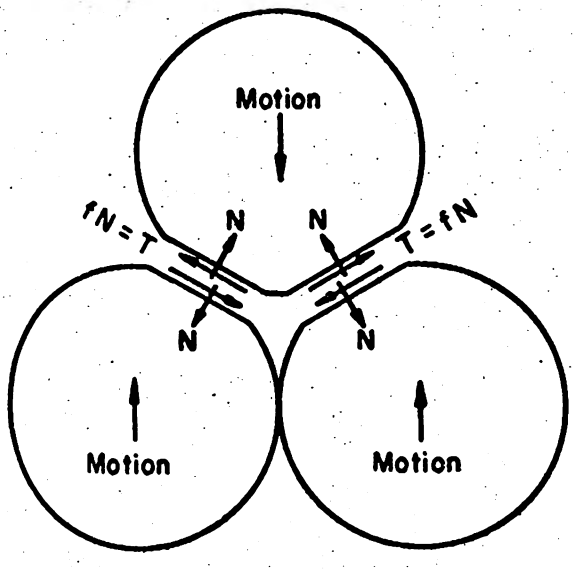

(b) Loading Cycle

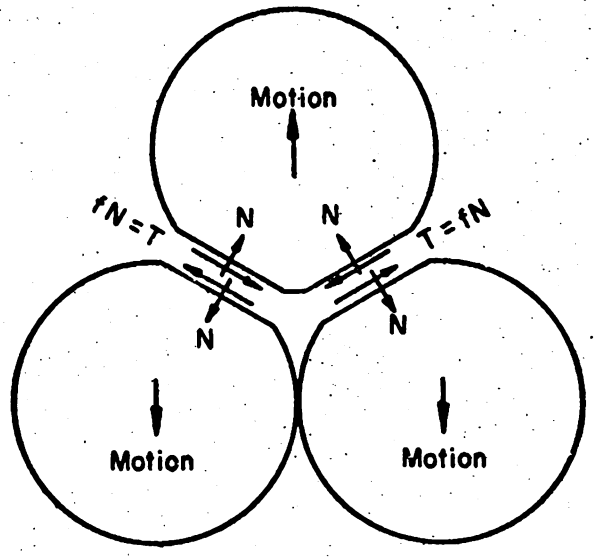

(c) Unloading Cycle

Fig. 3.13 SCHEMATIC REPRESENTATION OF THE DIRECTION OF THE CONTACT FORCES WHEN LOADING AND UNLOADING UNDER ONE-DIMENSIONAL COMPRESSION

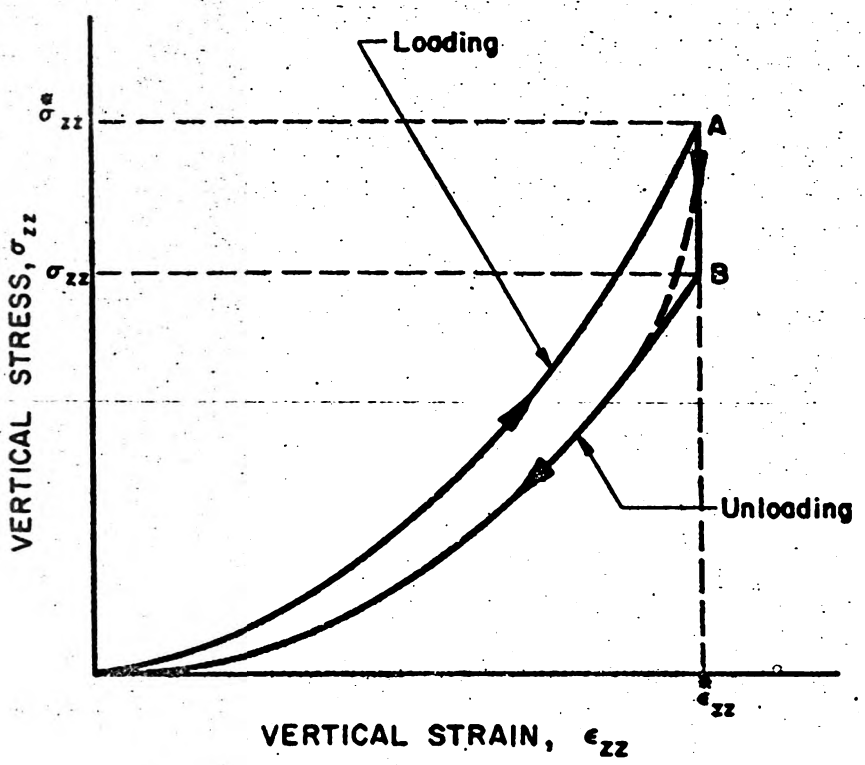

Fig. 3.14 LOADING AND UNLOADING ONE-DIMENSIONAL STRESS STRAIN CURVE FOR A FACE-CENTERED ARRAY OF SPHERES

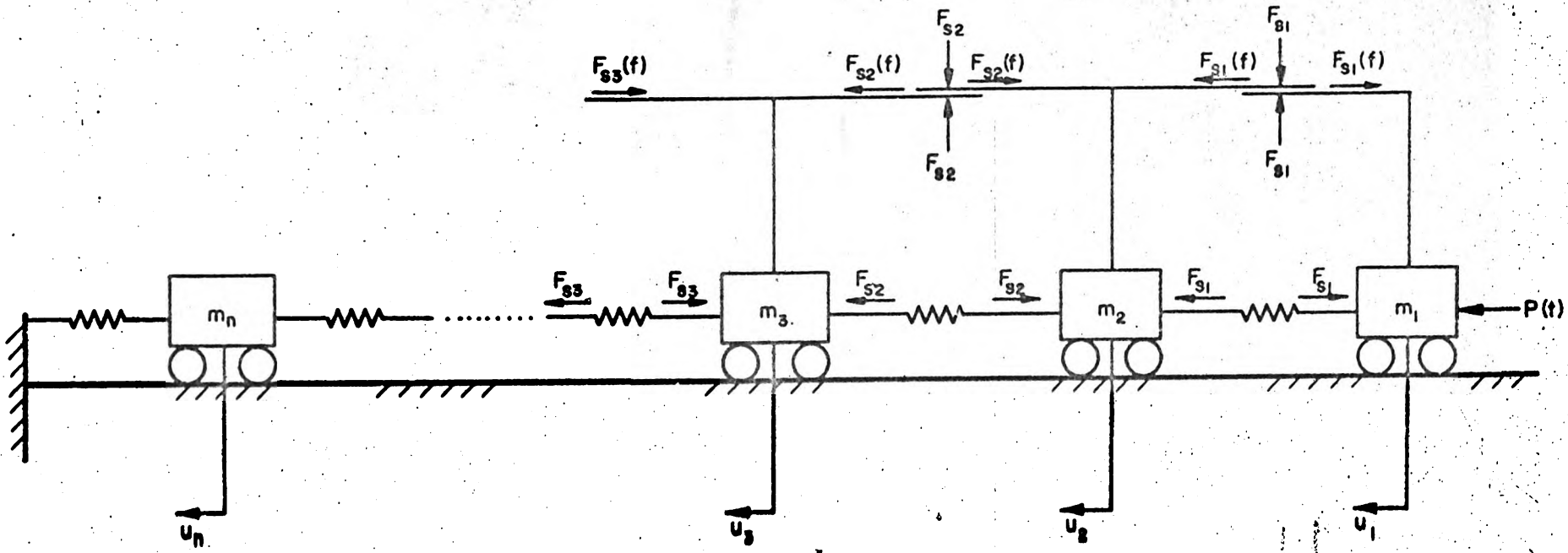

$$F_{s3} = k(u_3 - u_4)^{\frac{3}{2}} \qquad F_{s2} = k(u_2 - u_3)^{\frac{3}{2}} \qquad F_{s1} = k(u_1 - u_2)^{\frac{3}{2}}$$

In General, $F_{sn} = k(u_n - u_{n+1})^{\frac{3}{2}}$

Fig. 3.15 ONE-DIMENSIONAL HORIZONTAL SAND MODEL

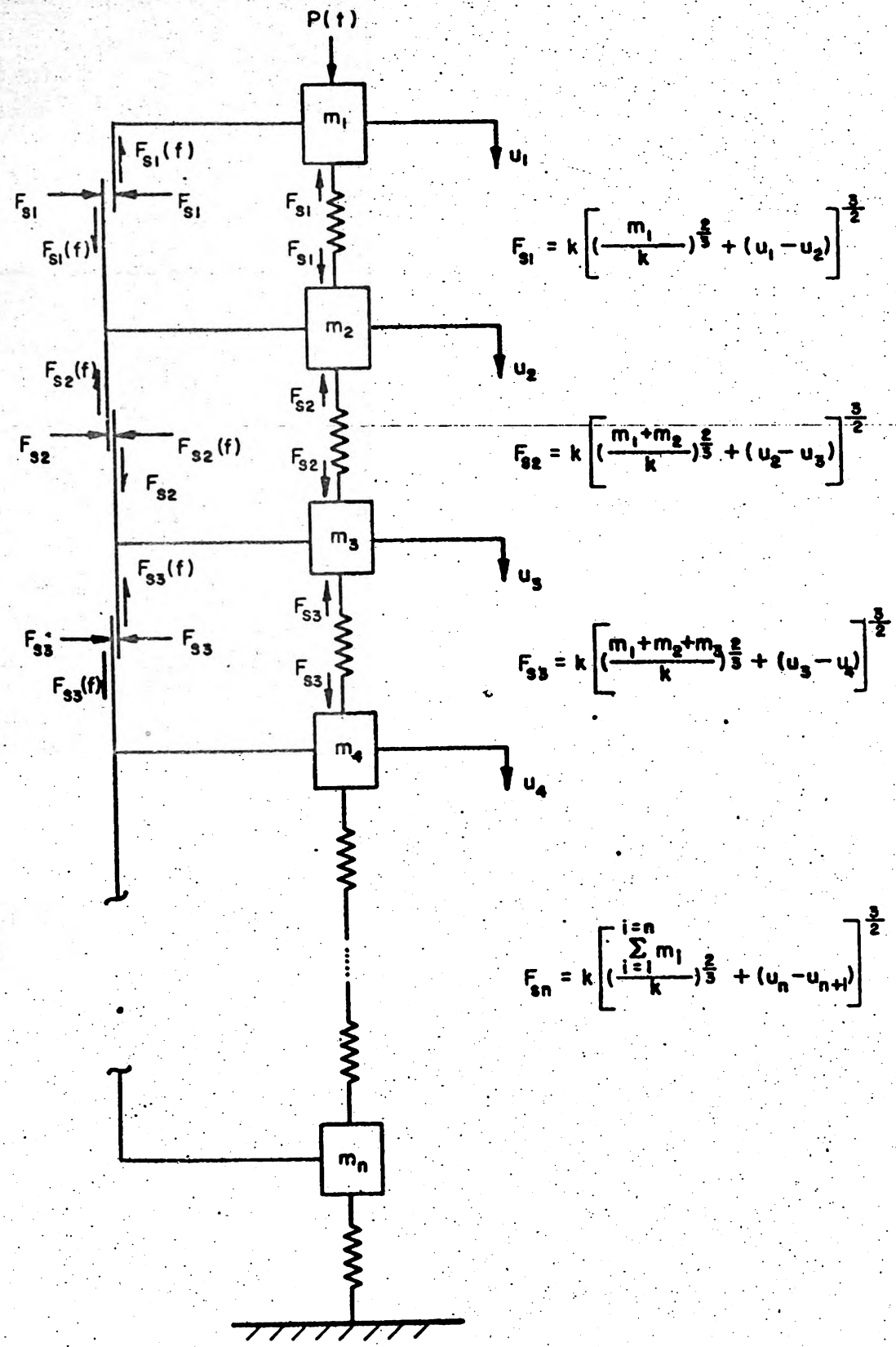

Fig. 3.16 ONE-DIMENSIONAL VERTICAL SAND MODEL

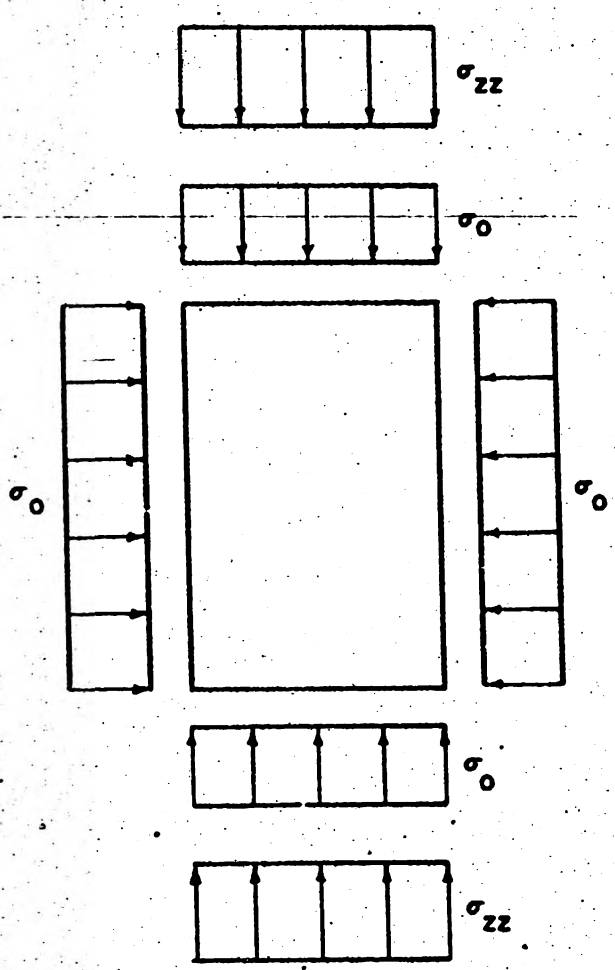

Fig. 3.17 A GRANULAR MEDIUM WITH AN INITIAL CONFINING STRESS, σ_o, SUBJECTED TO A STRESS DIFFERENCE σ_{zz}

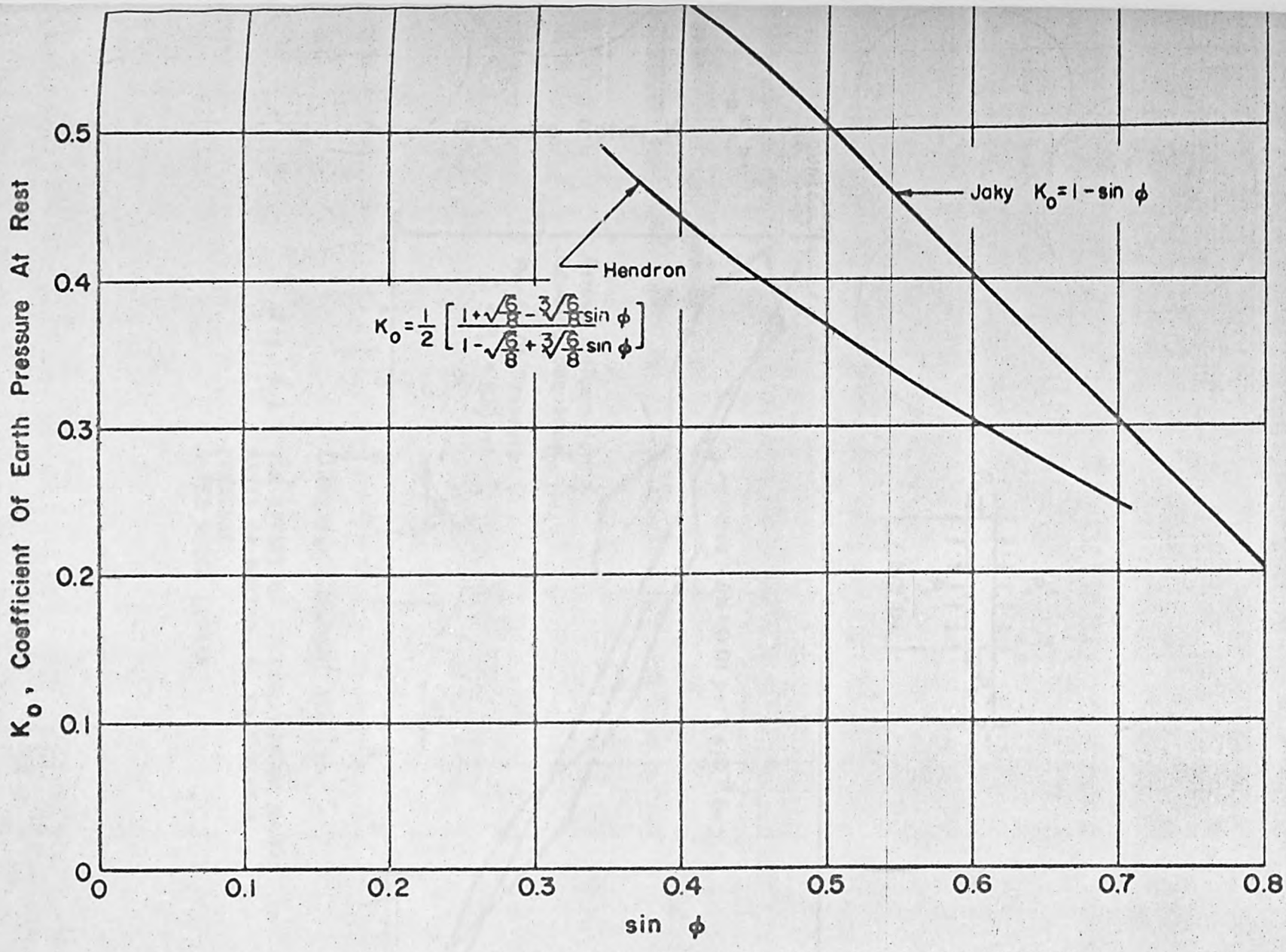

Fig. 3.18 THEORETICAL VARIATION OF K_o WITH SIN ϕ FOR A FACE-CENTERED CUBIC ARRAY COMPARED WITH A RELATION SUGGESTED FOR SAND BY JAKY

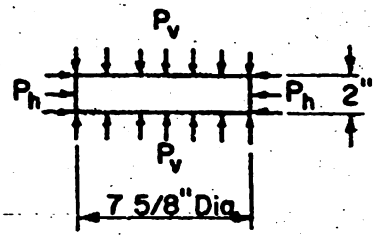

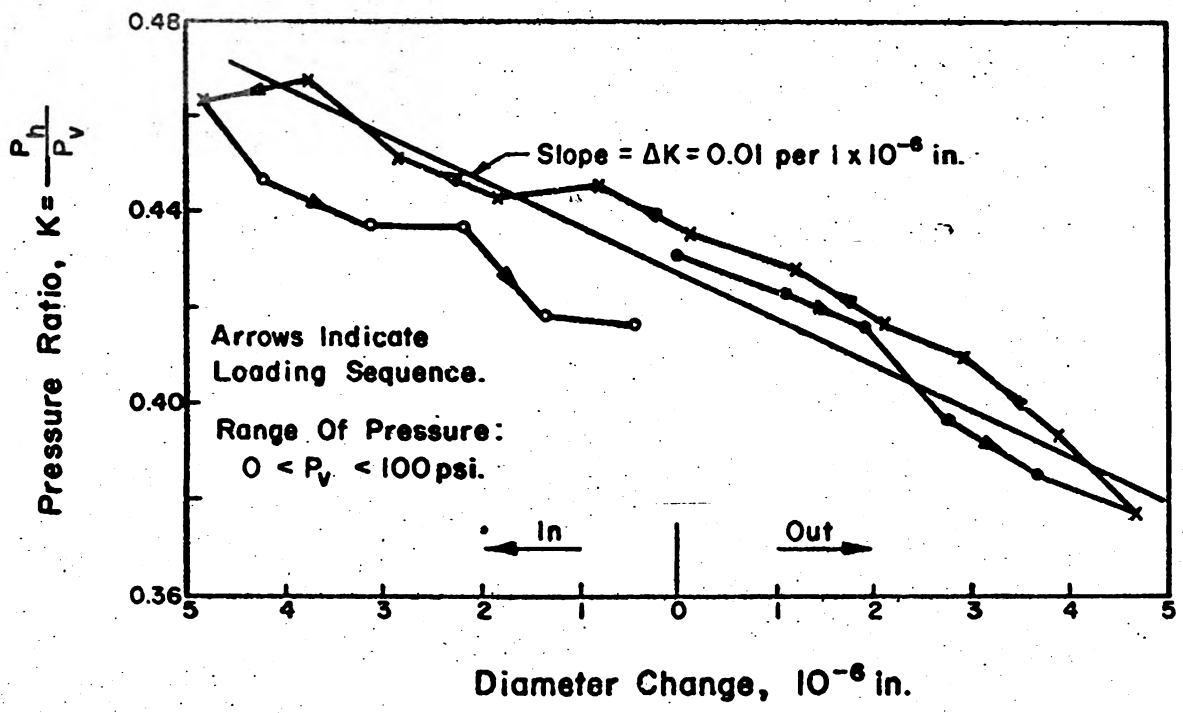

Fig. 4.1 THE EFFECT OF LATERAL MOTION ON THE RATIO OF HORIZONTAL TO VERTICAL PRESSURE
AFTER SPEER (1944)

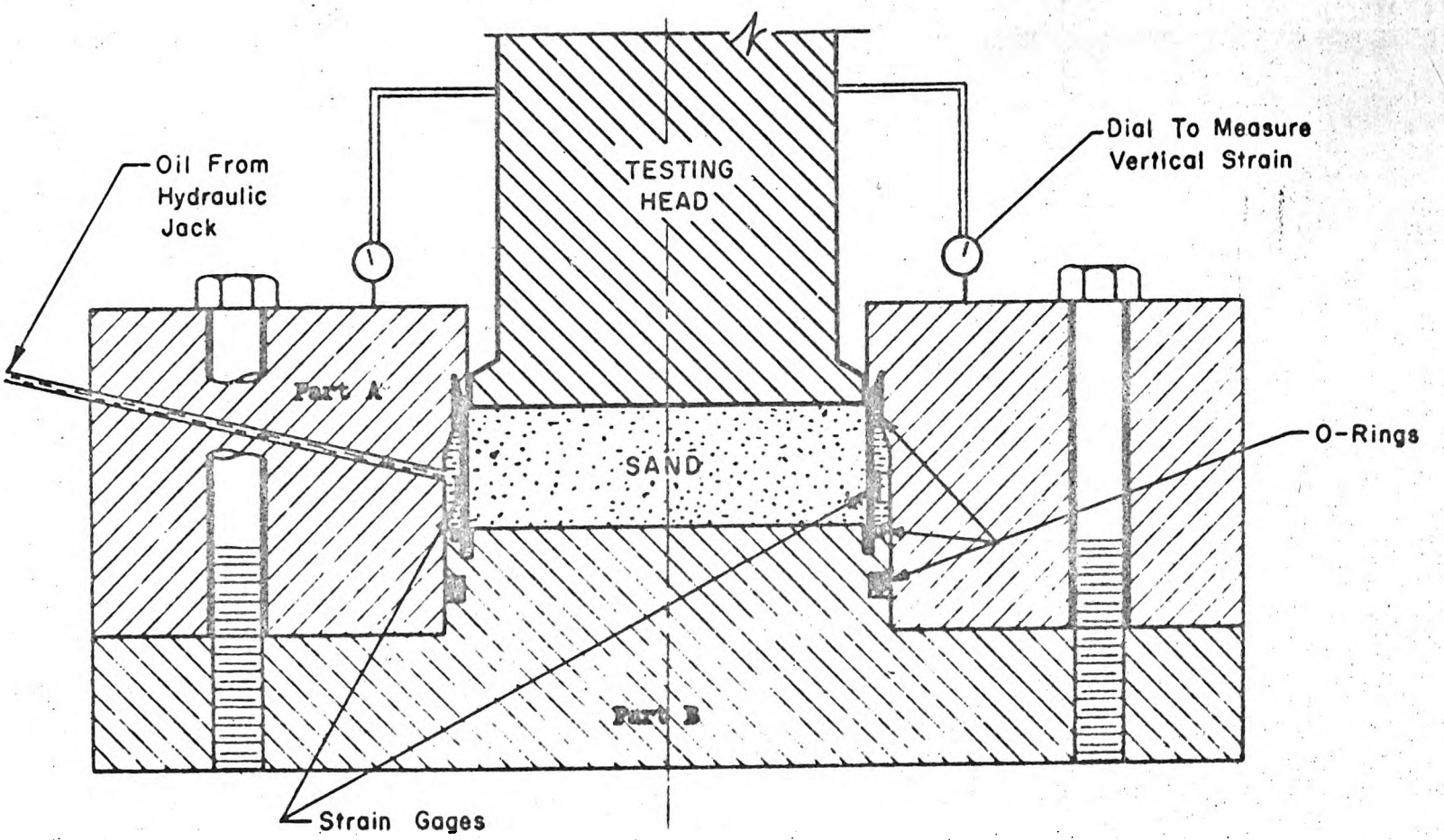

Fig. 4.2 SCHEMATIC CROSS-SECTION THROUGH TESTING APPARATUS

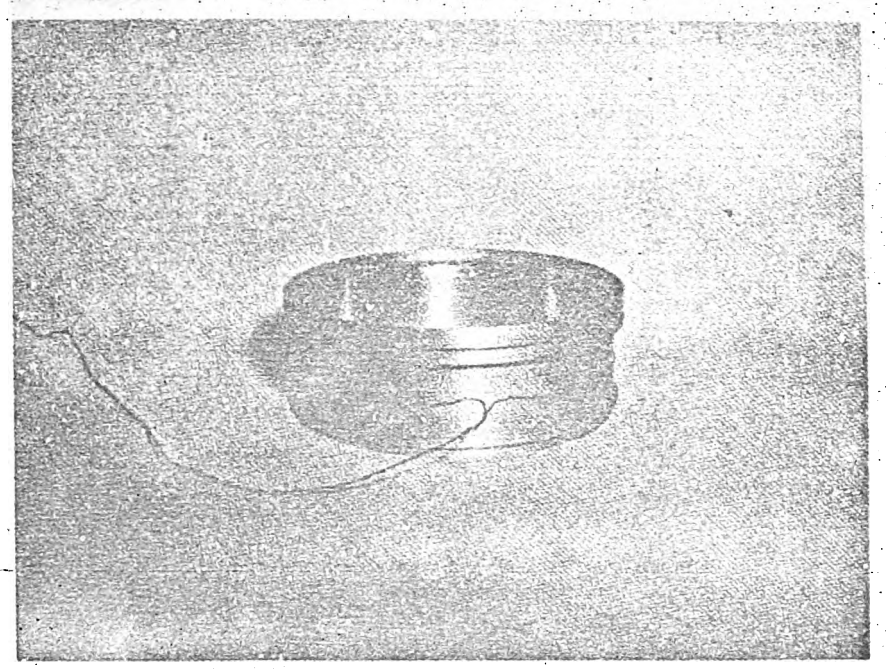

(a) THIN STEEL RING

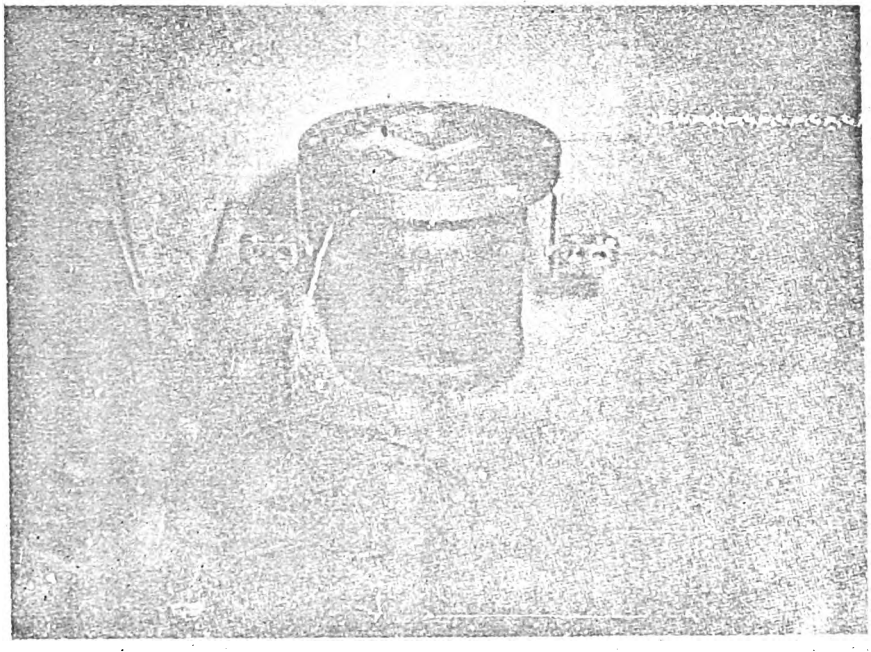

(b) TESTING HEAD

Fig. 4.3 PHOTOGRAPHS OF APPARATUS COMPONENTS

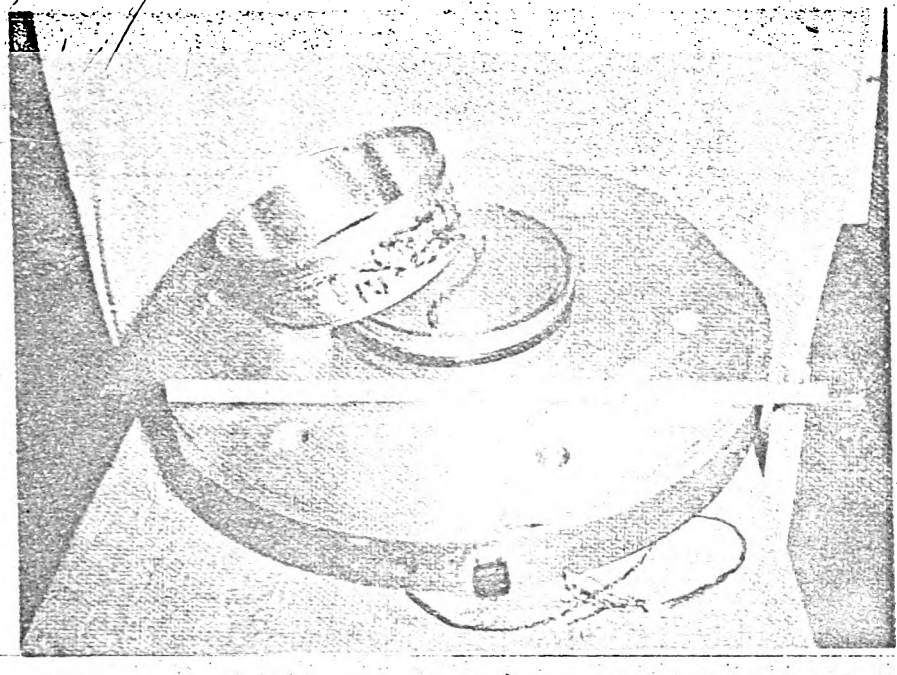

(a) VIEW OF STEEL RING ON BASEPLATE WHICH SHOWS OUTLET FOR GAGE WIRES

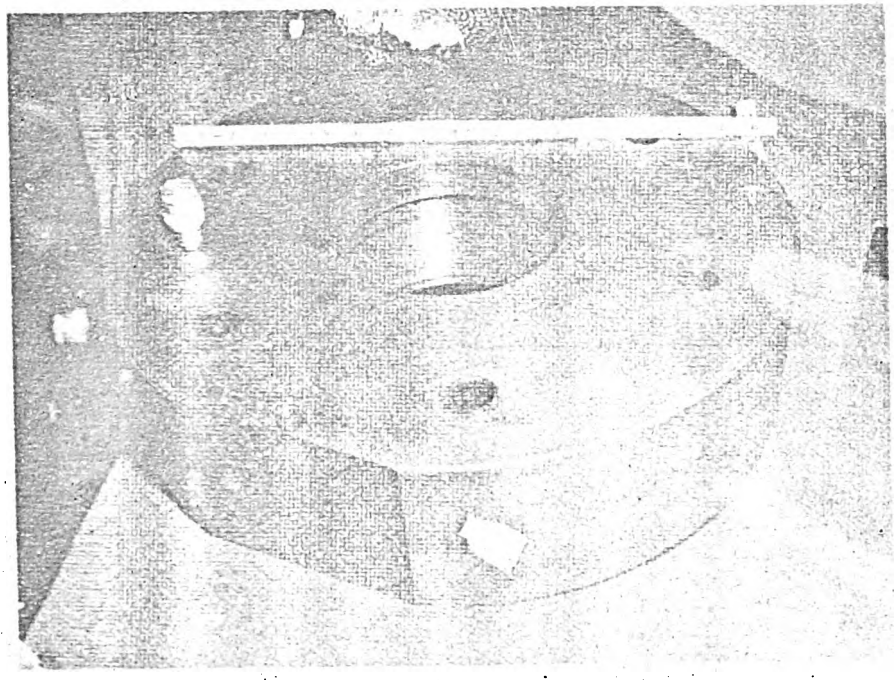

(b) OUTER CYLINDER OF APPARATUS

Fig. 4.4 PHOTOGRAPHS OF APPARATUS COMPONENTS

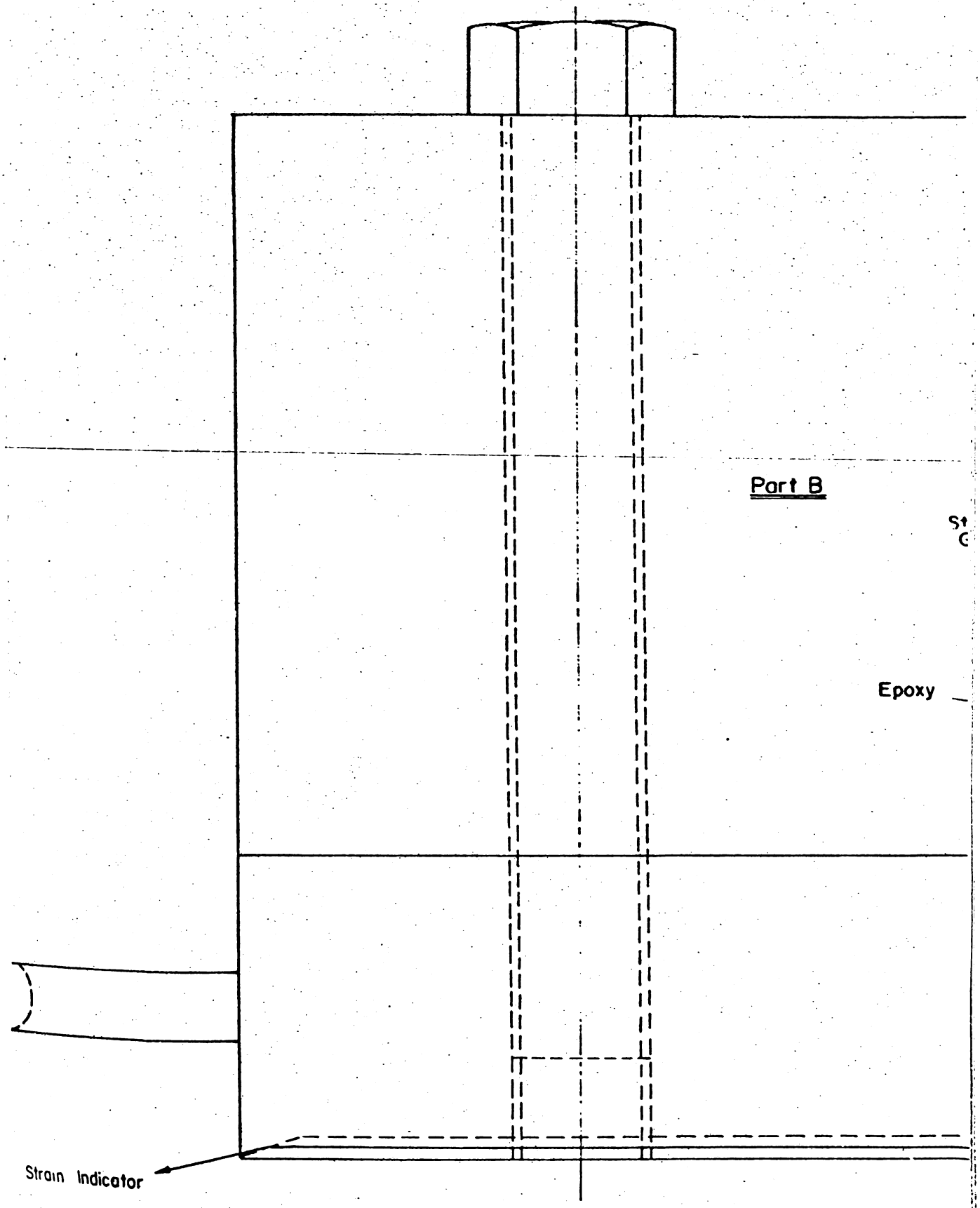

Fig. 4.5 FULL SCALE CROSS-SECTION THROUGH THE ONE-DIMENSION

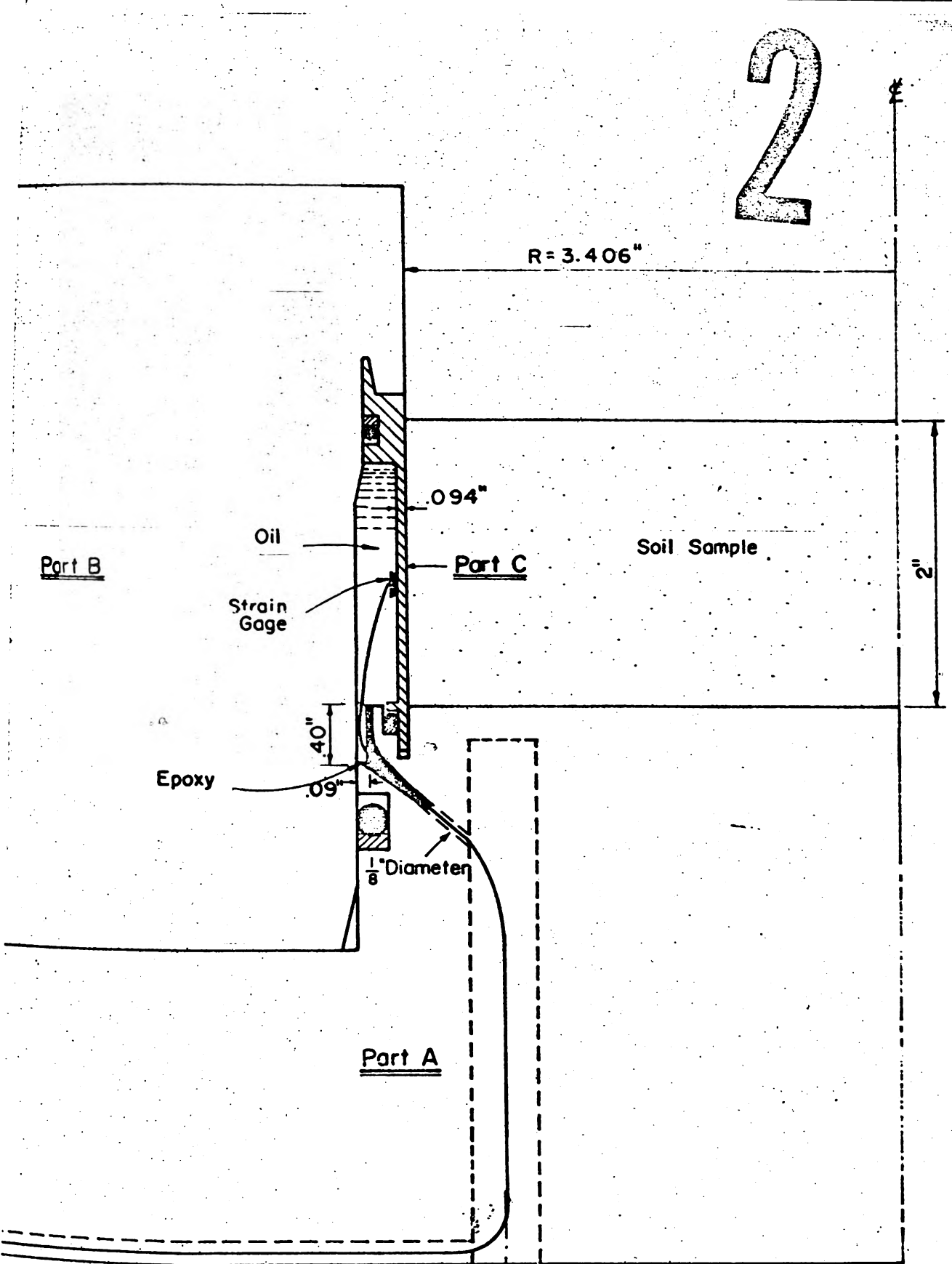

HROUGH THE ONE-DIMENSIONAL COMPRESSION APPARATUS

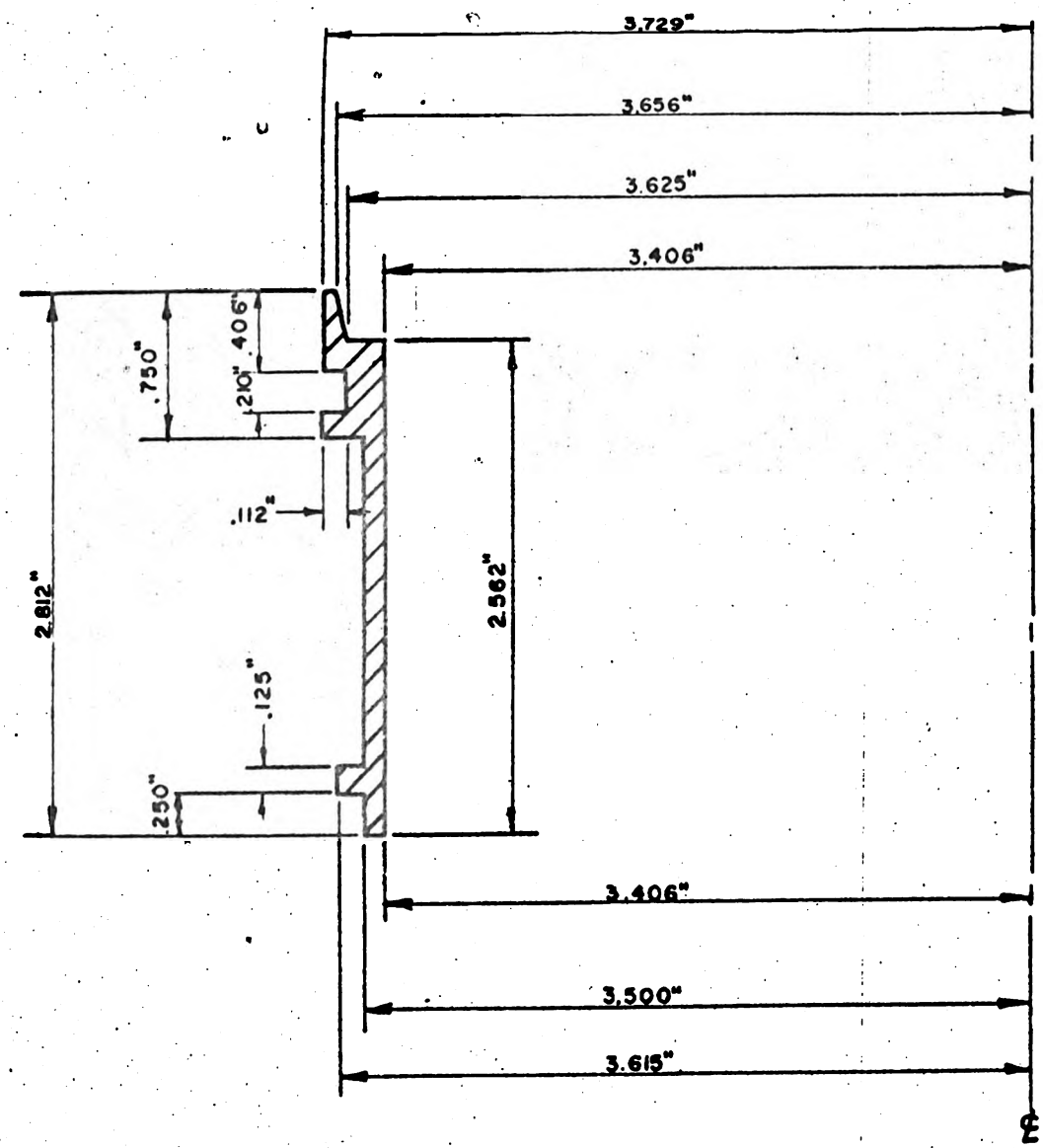

Fig. 4.6 FULL SCALE CROSS-SECTION OF THE THIN STEEL RING

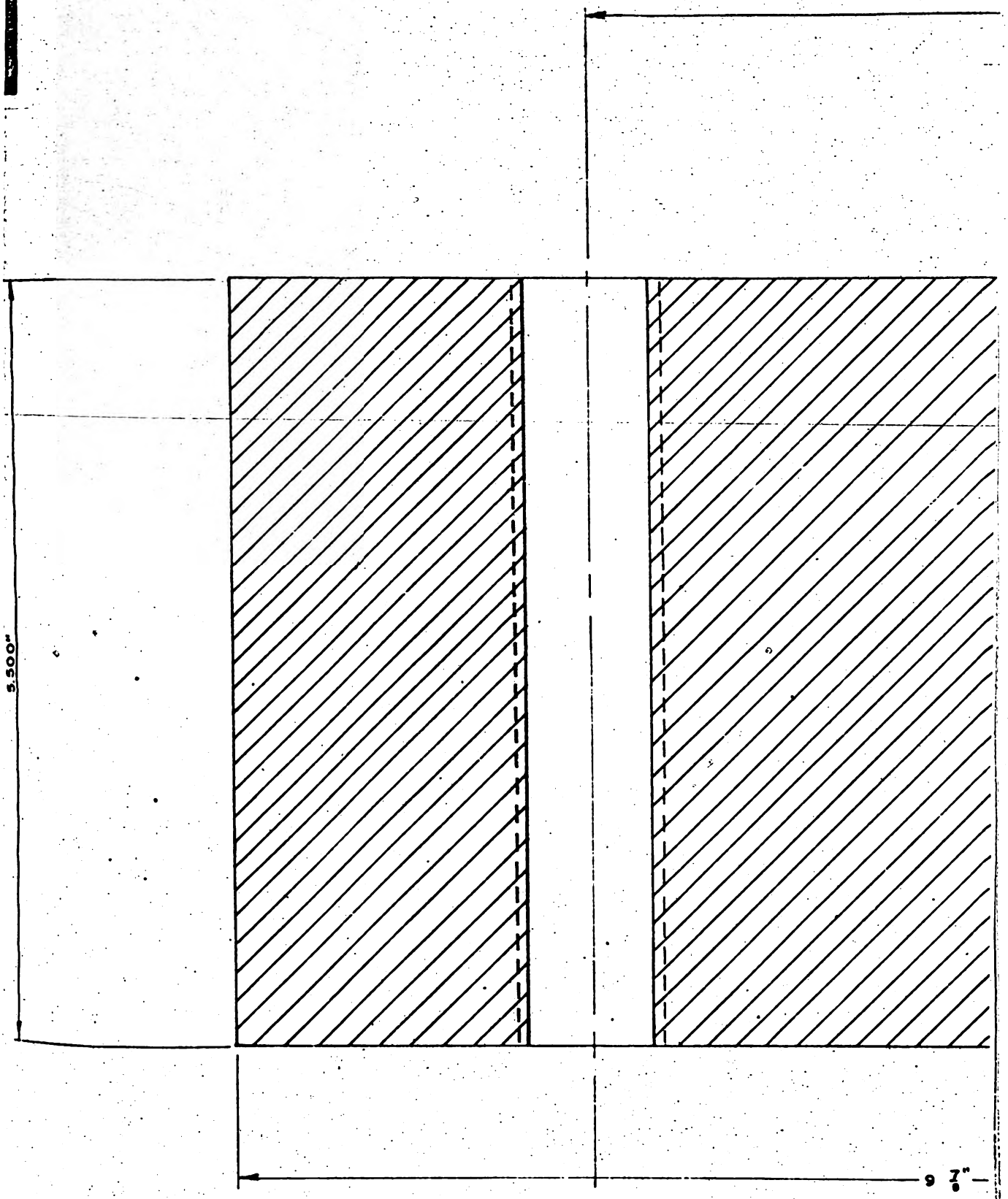

Fig. 4.7 FULL SCALE CROSS-SECTION OF THE OUTER THICK-

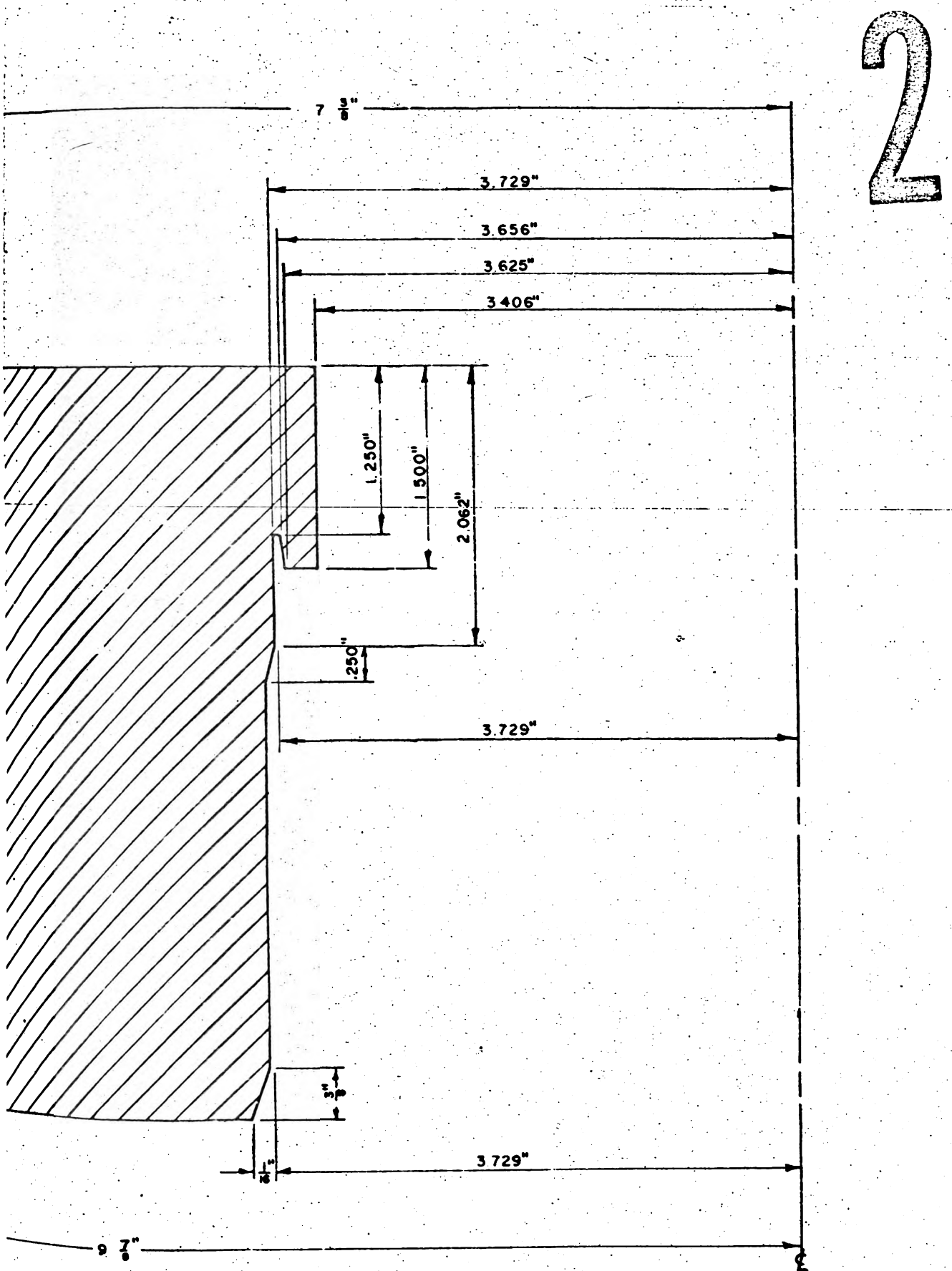

: THE OUTER THICK-WALLED CYLINDER

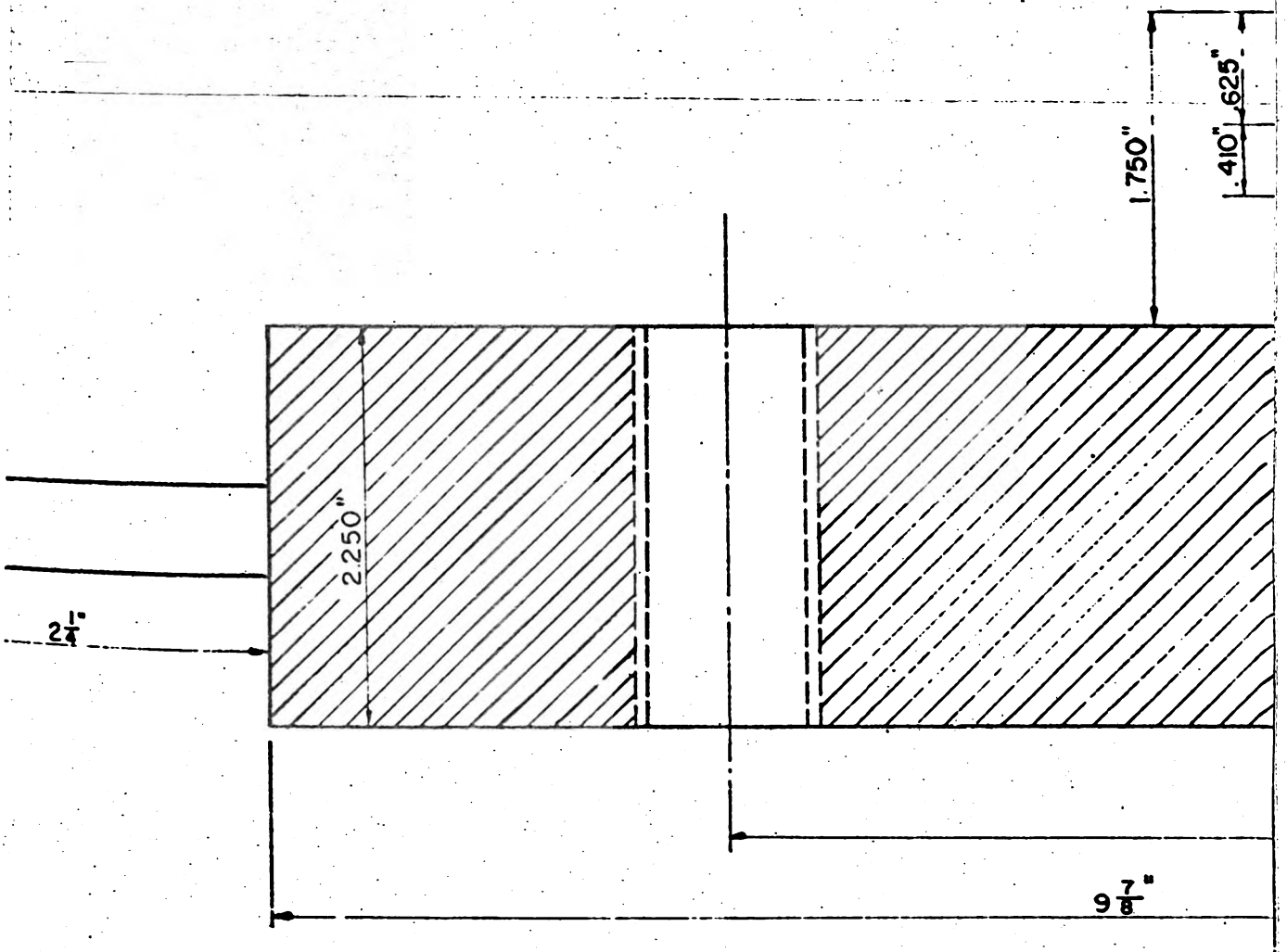

Fig. 4.8 FULL SCALE CROSS-SECTION OF THE BASE

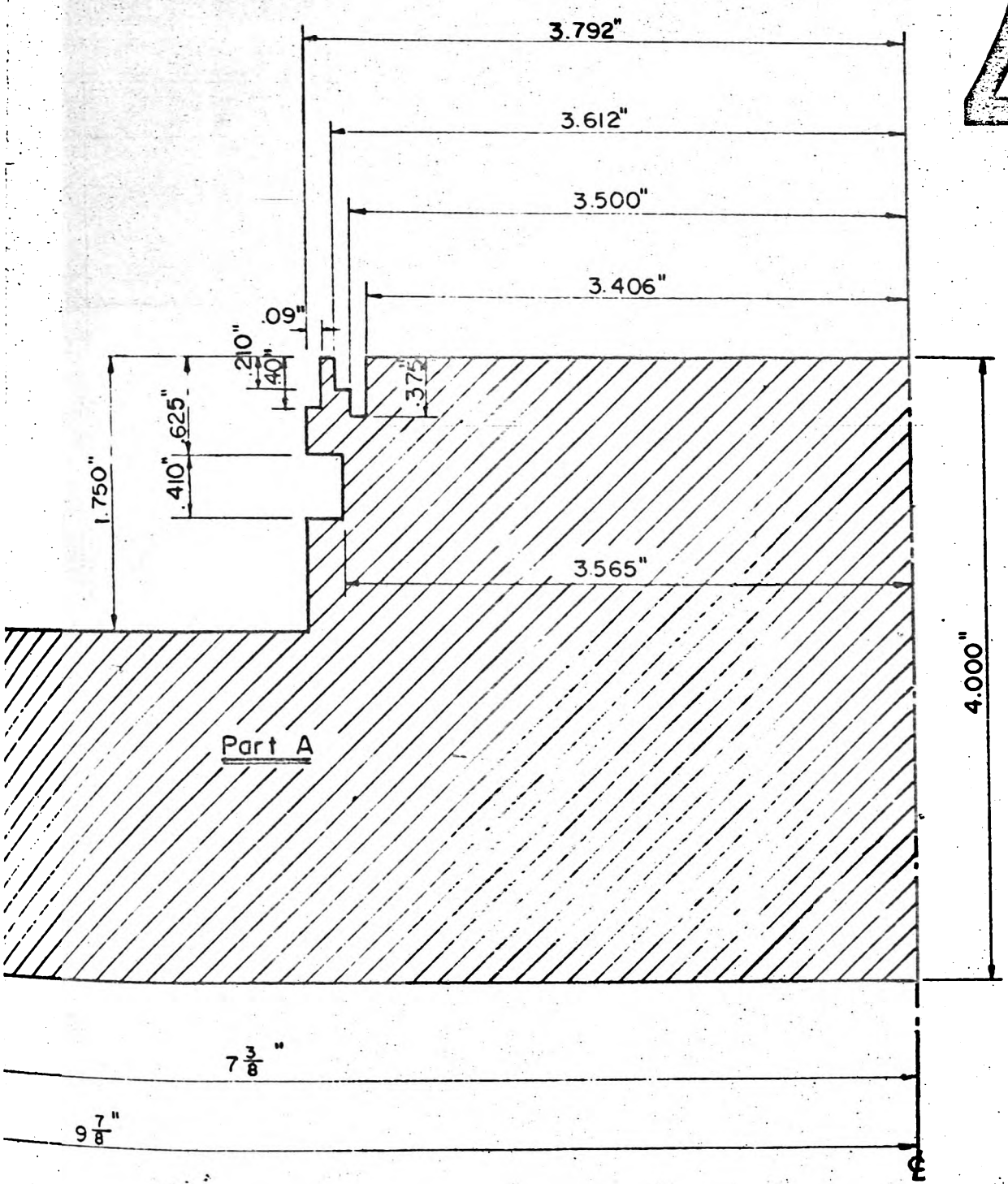

ECTION OF THE BASE PLATE

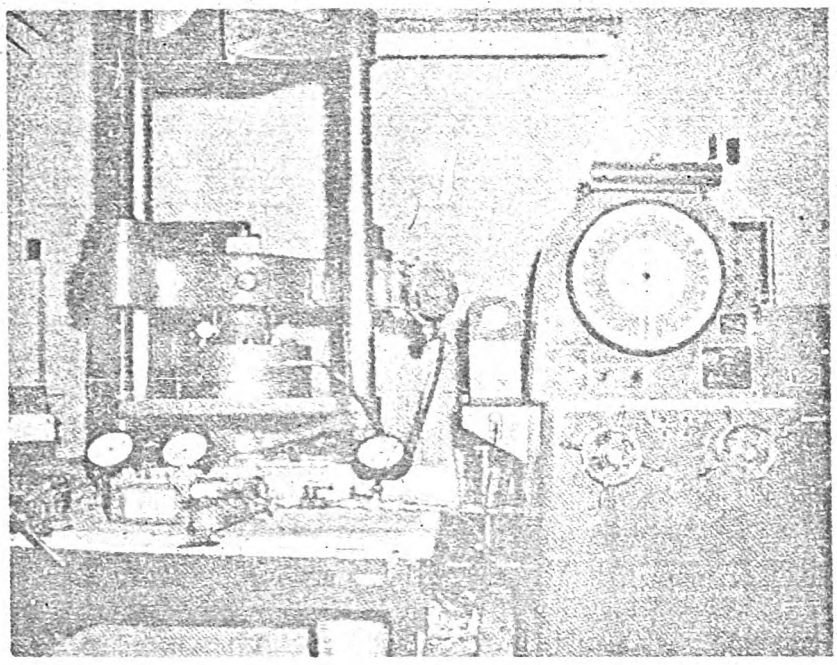

(a) ONE-DIMENSIONAL COMPRESSION APPARATUS ASSEMBLED IN TESTING MACHINE

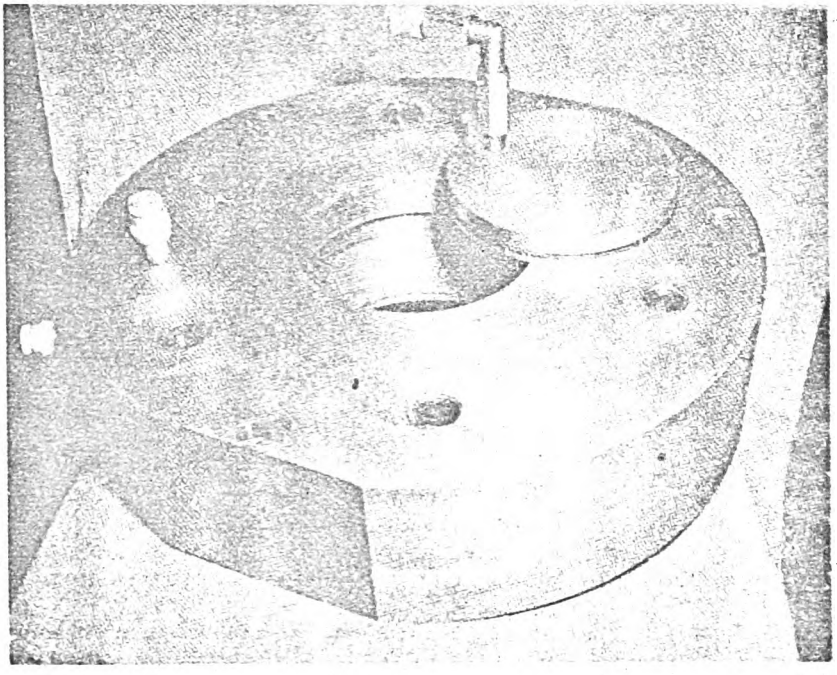

(b) OUTER THICK-WALLED CYLINDER AND STEEL CALIBRATION PLUG

Fig. 4.9 PHOTOGRAPHS OF COMPONENT PARTS AND APPARATUS ASSEMBLED FOR TESTING

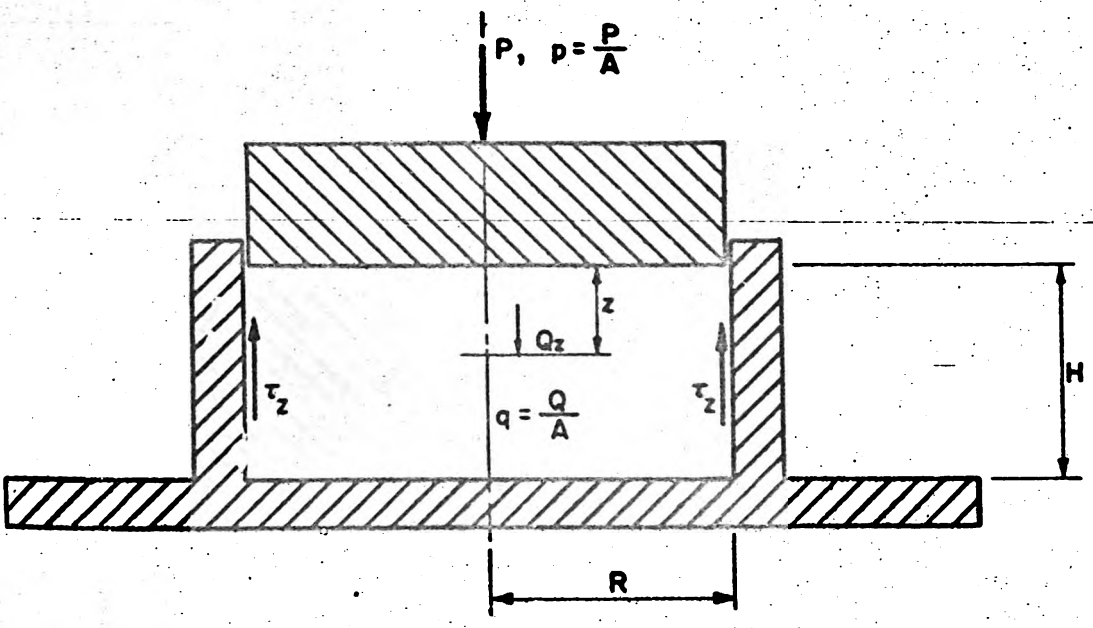

$$K_0 = \frac{\sigma_H}{\sigma_V} \quad , \quad A = \pi R^2$$

f = Coefficient Of Friction Between Soil And Ring

Fig. 4.10 SCHEMATIC DIAGRAM ILLUSTRATING THE EFFECT OF SIDE FRICTION IN ONE-DIMENSIONAL COMPRESSION

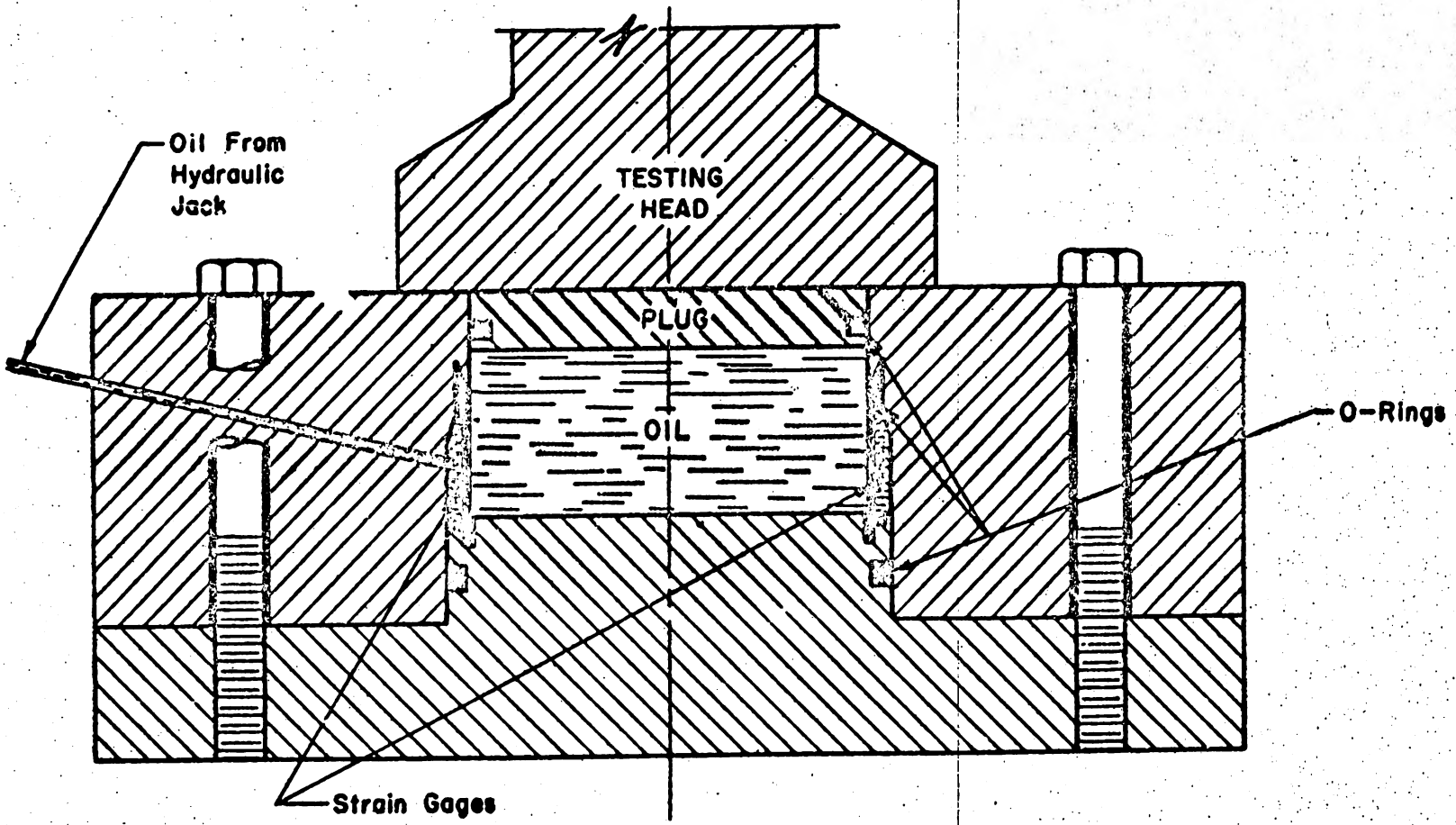

Fig. 4.11 SCHEMATIC CROSS-SECTION THROUGH TESTING APPARATUS DURING CALIBRATION

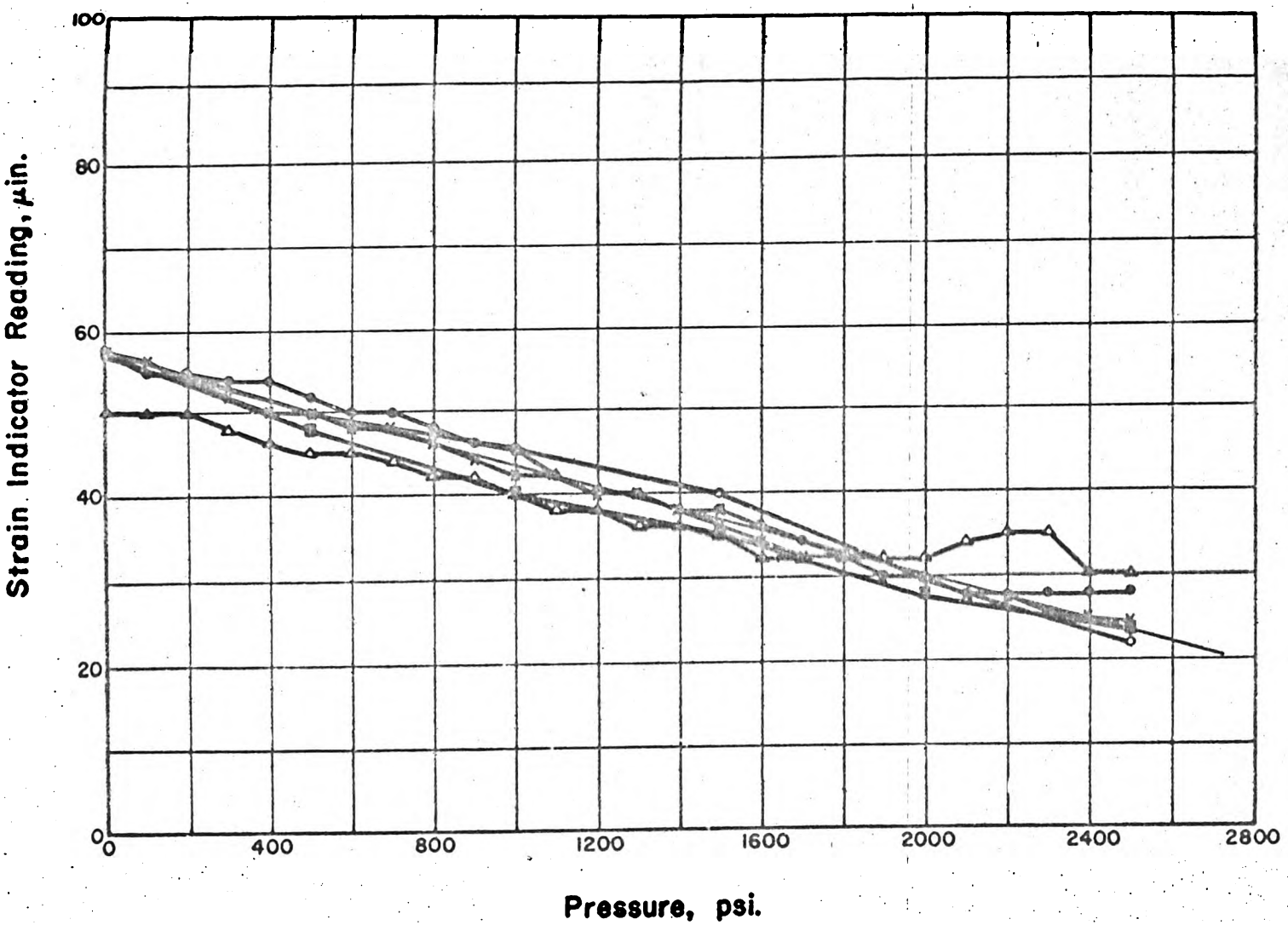

Fig. 4.12 CALIBRATION CURVE FOR THE EFFECT OF OIL PRESSURE ON THE METALFILM STRAIN GAGES

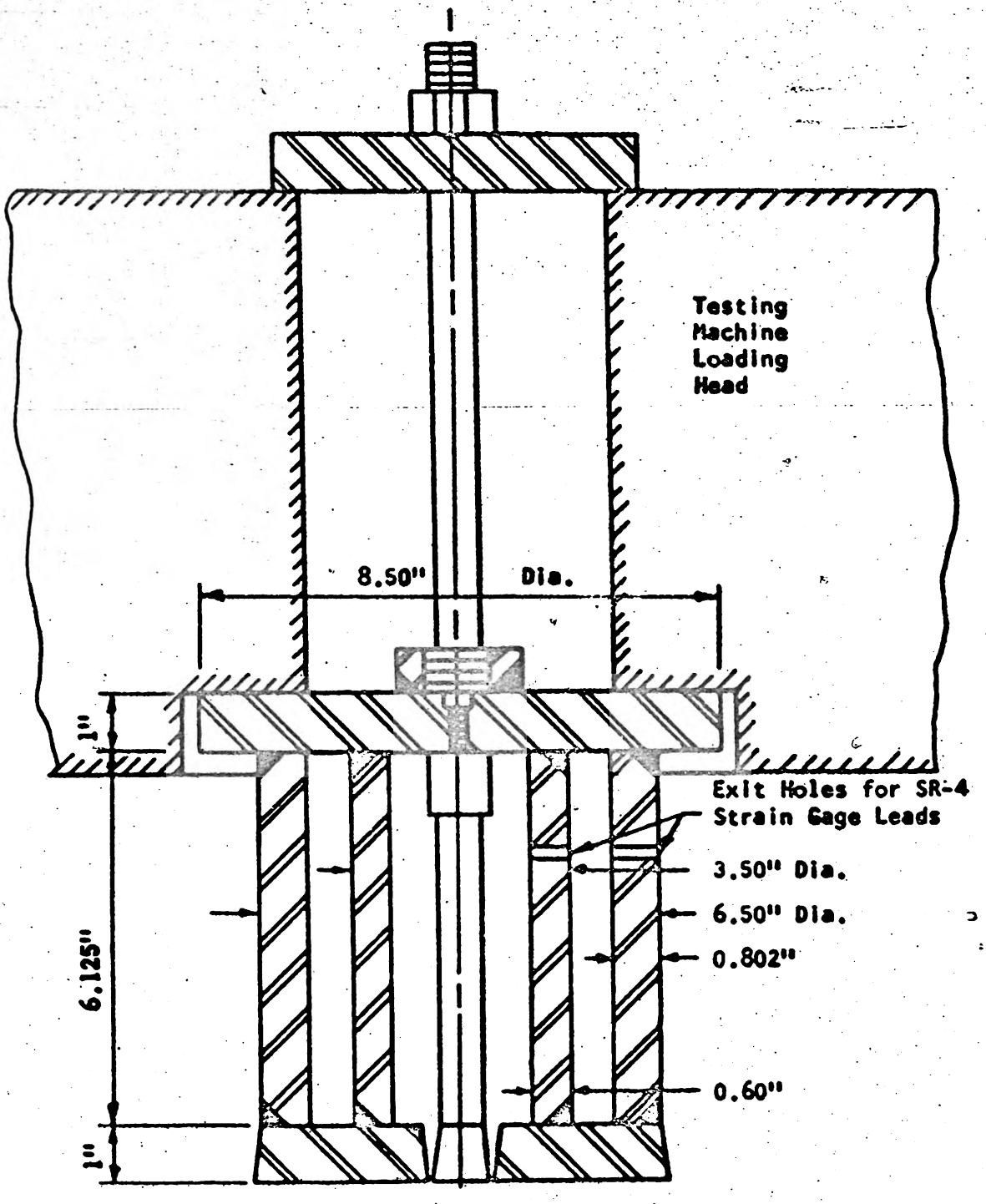

Fig. 4.13 CROSS-SECTION OF TESTING HEAD

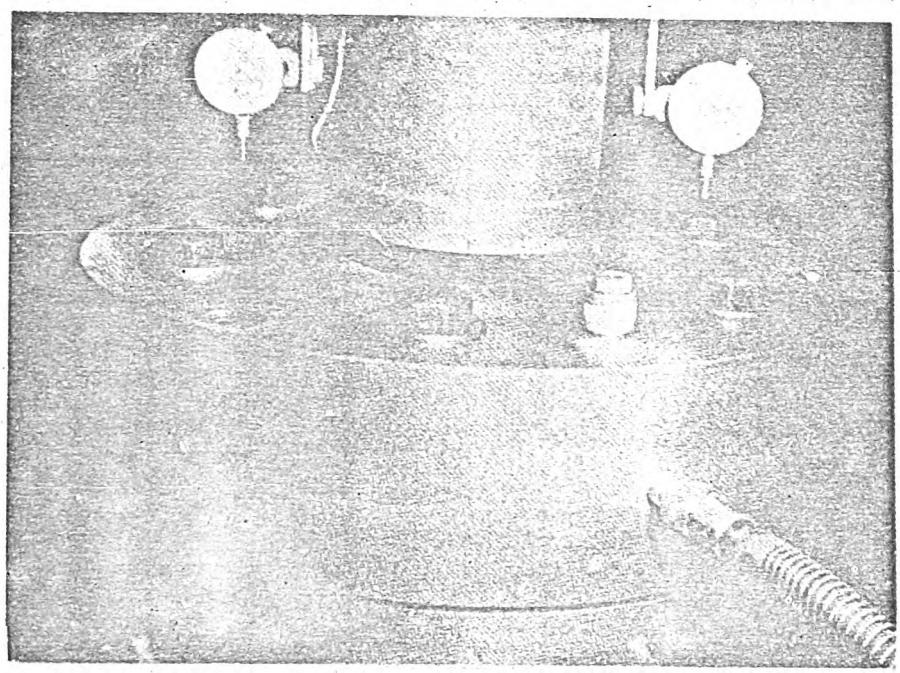

Fig. 4.14 PHOTOGRAPH OF ONE-DIMENSIONAL COMPRESSION APPARATUS ASSEMBLED FOR TESTING

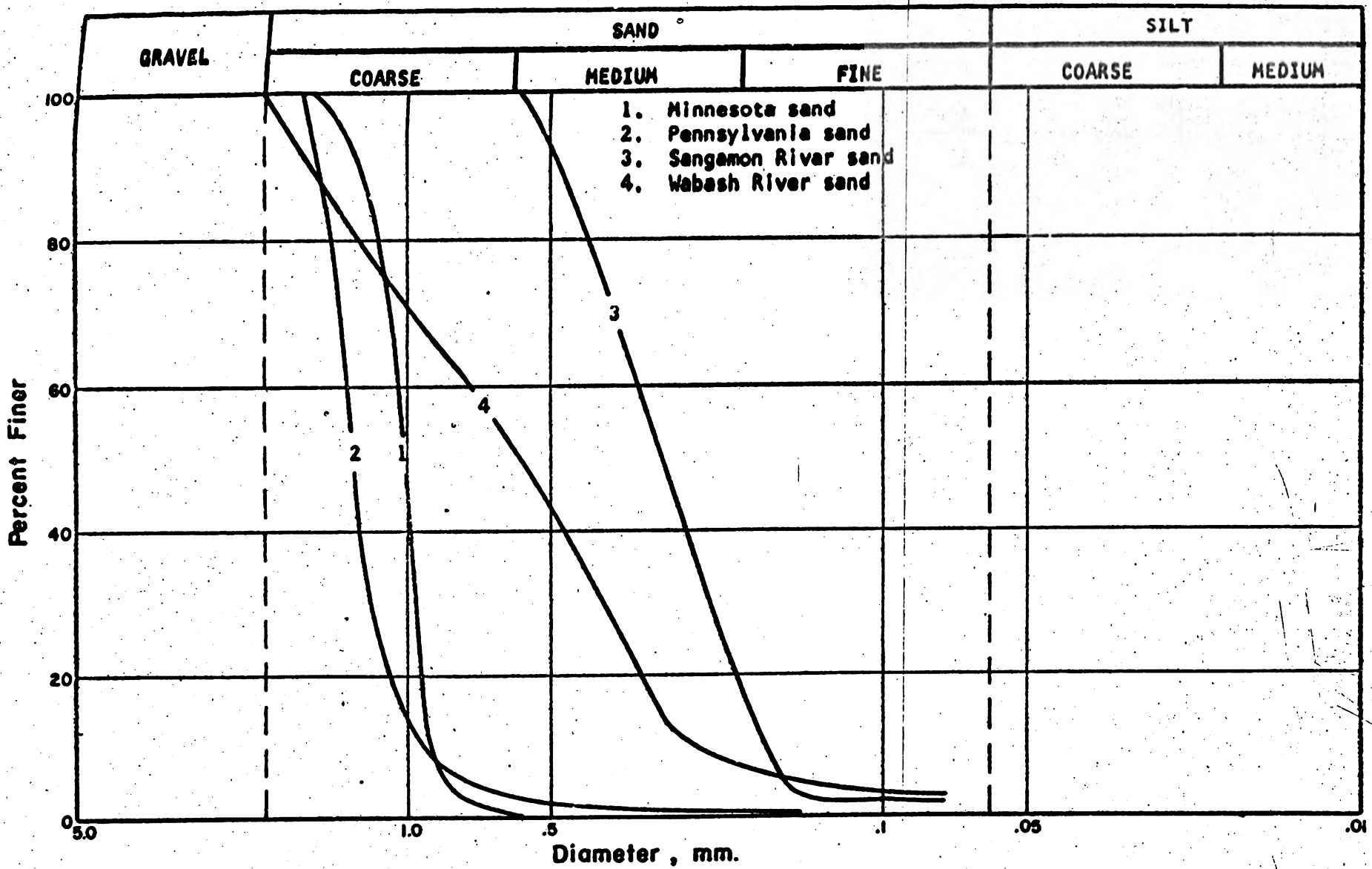

Fig. 5.1 GRAIN-SIZE DISTRIBUTION CURVES FOR SANDS INVESTIGATED

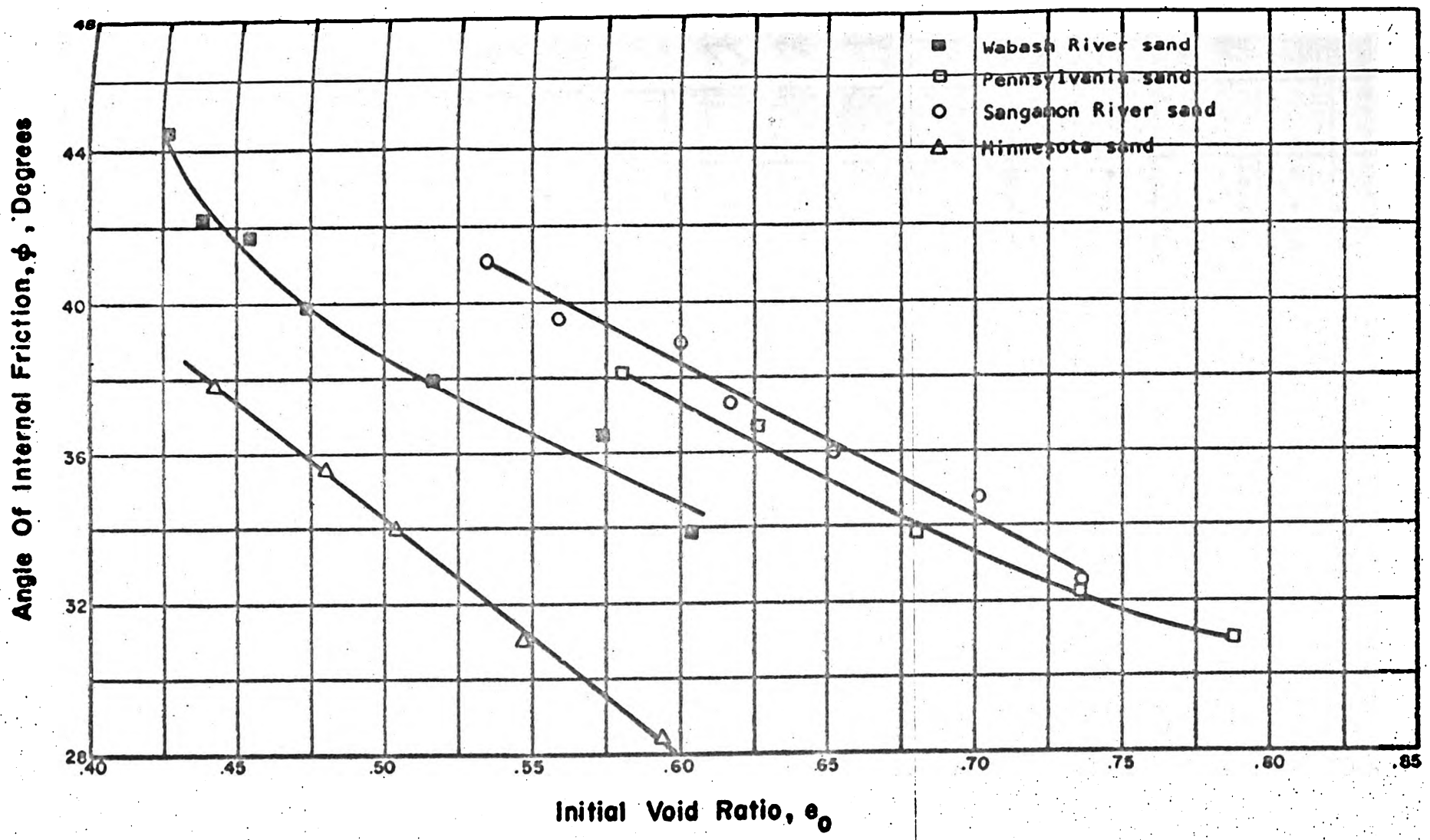

Fig. 5.2 RELATIONSHIP BETWEEN THE ANGLE OF INTERNAL FRICTION AND INITIAL VOID RATIO FOR SANDS INVESTIGATED

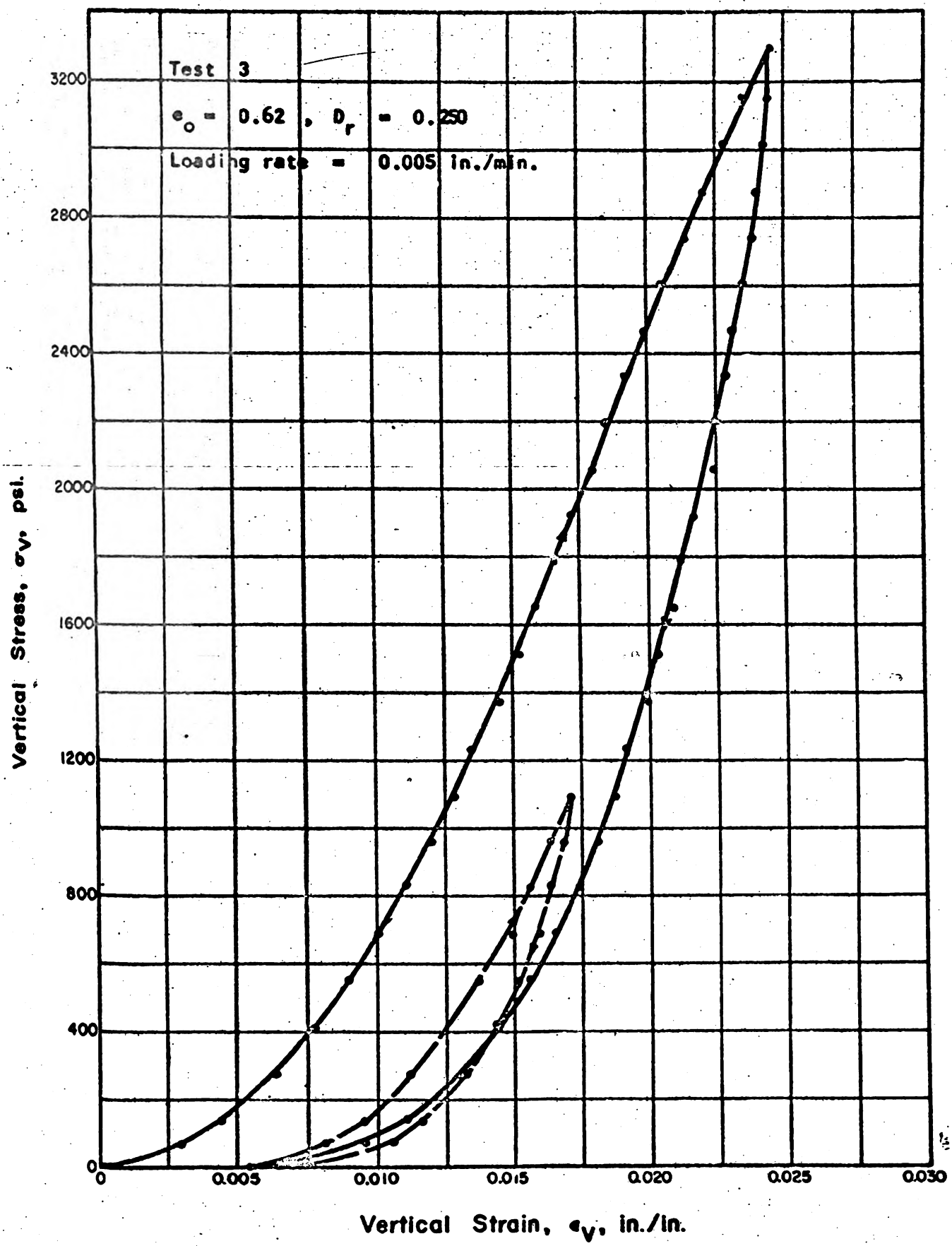

Fig. 5.3 STRESS STRAIN CURVE FOR MINNESOTA SAND IN ONE-DIMENSIONAL COMPRESSION

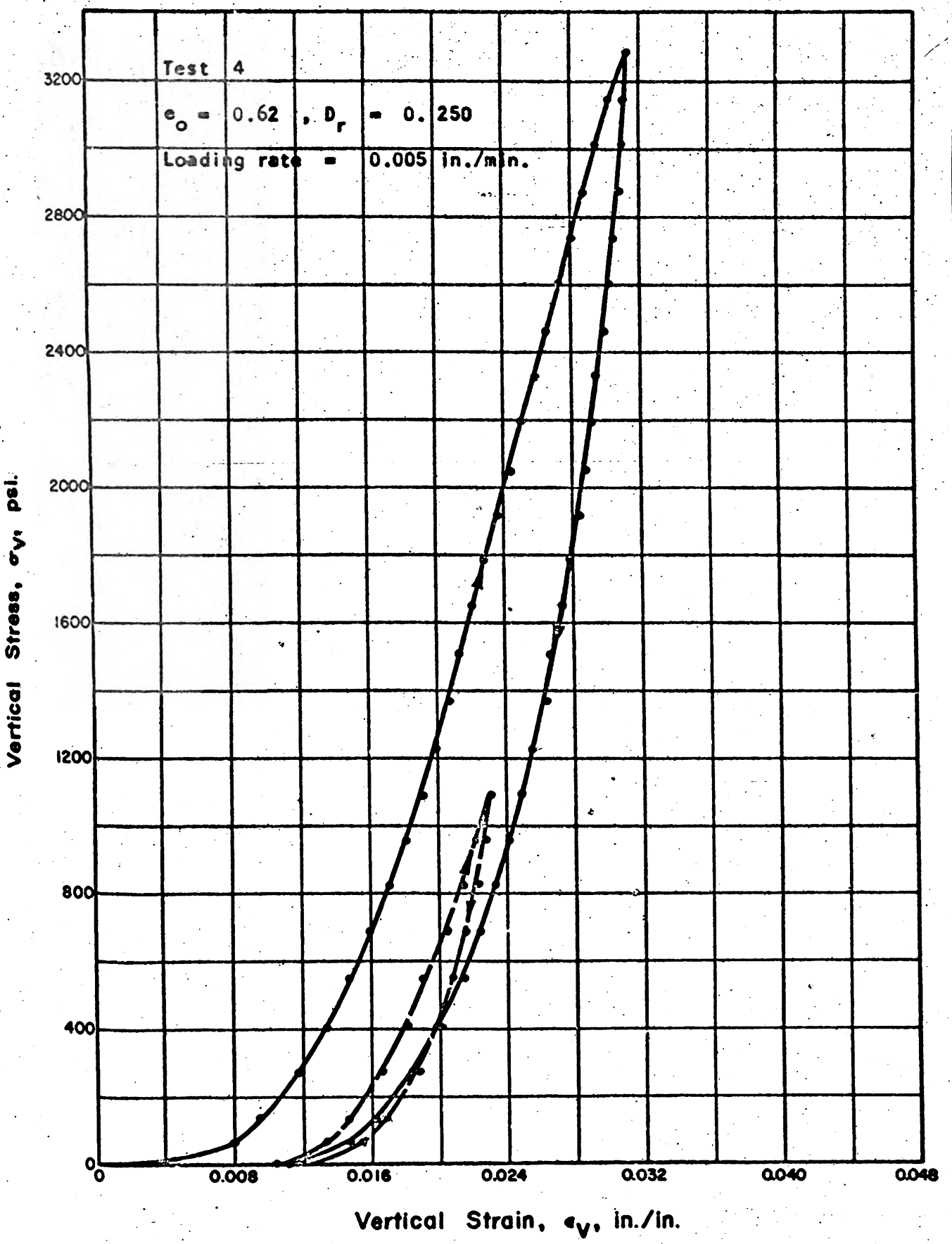

Fig. 5.4 STRESS STRAIN CURVE FOR MINNESOTA SAND IN ONE-DIMENSIONAL COMPRESSION

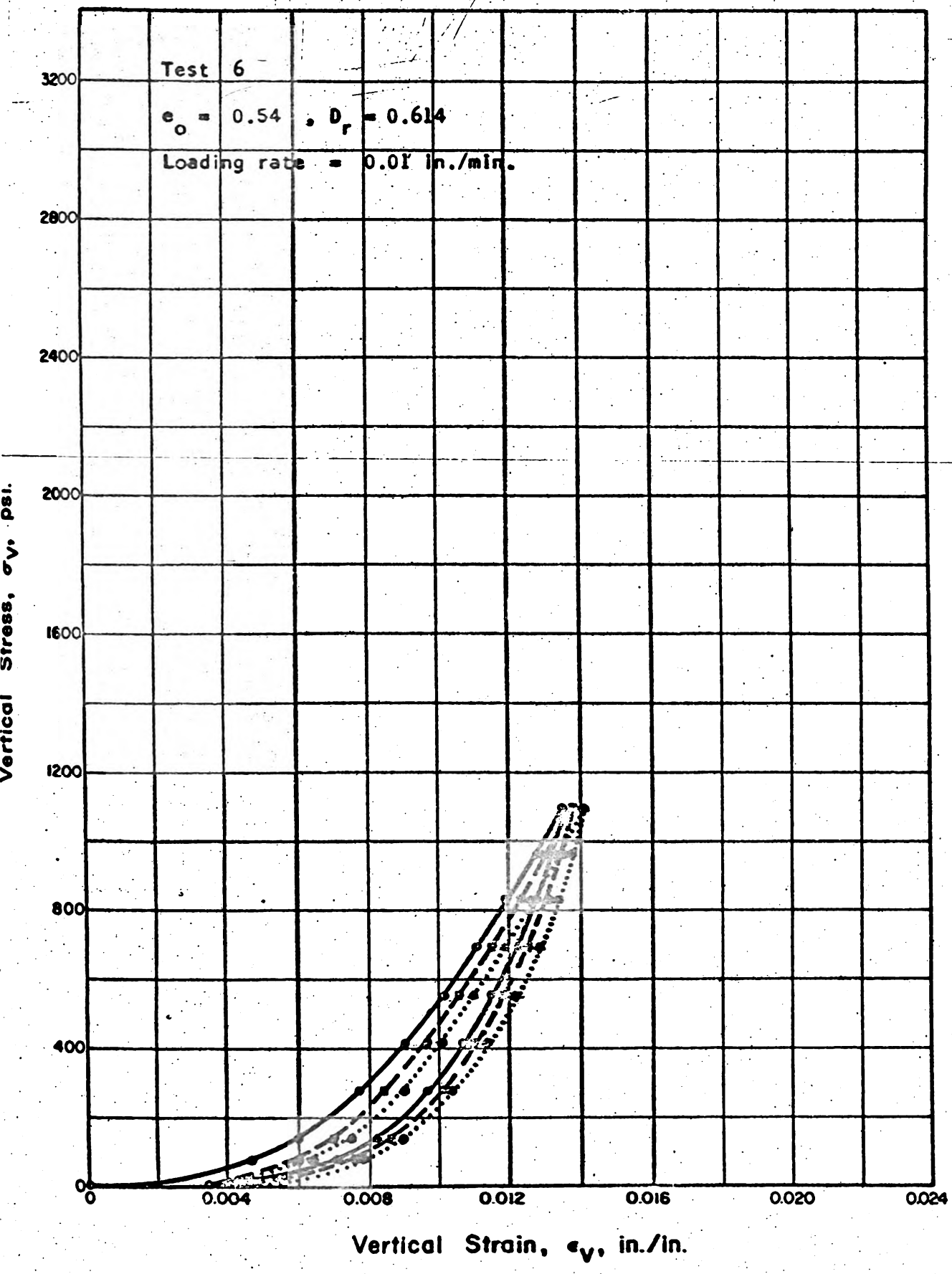

Fig. 5.6 STRESS STRAIN CURVE FOR MINNESOTA SAND IN ONE-DIMENSIONAL COMPRESSION

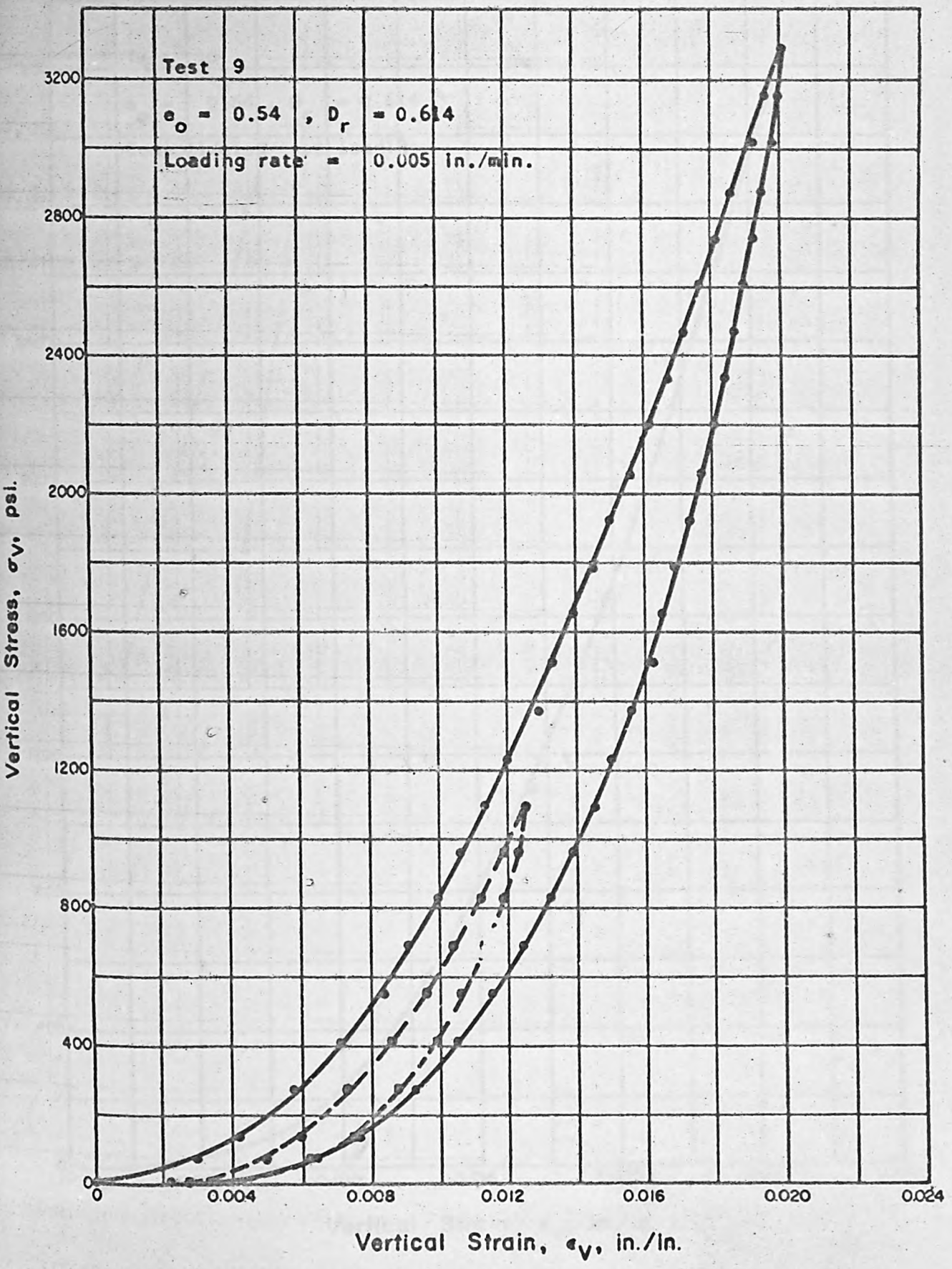

Fig. 5.9 STRESS STRAIN CURVE FOR MINNESOTA SAND IN ONE-DIMENSIONAL COMPRESSION

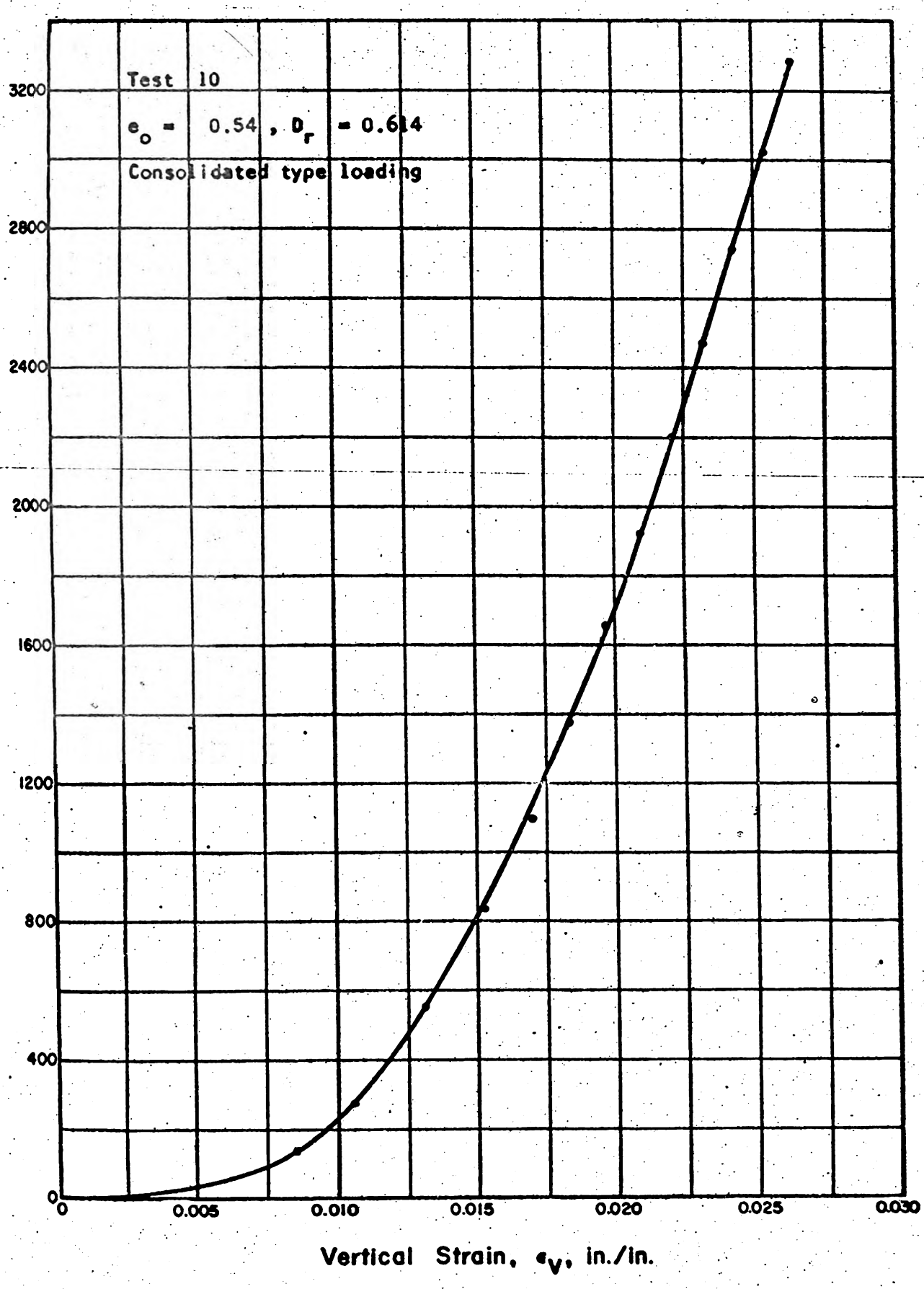

Fig. 5.10 STRESS STRAIN CURVE FOR MINNESOTA SAND IN ONE-DIMENSIONAL COMPRESSION

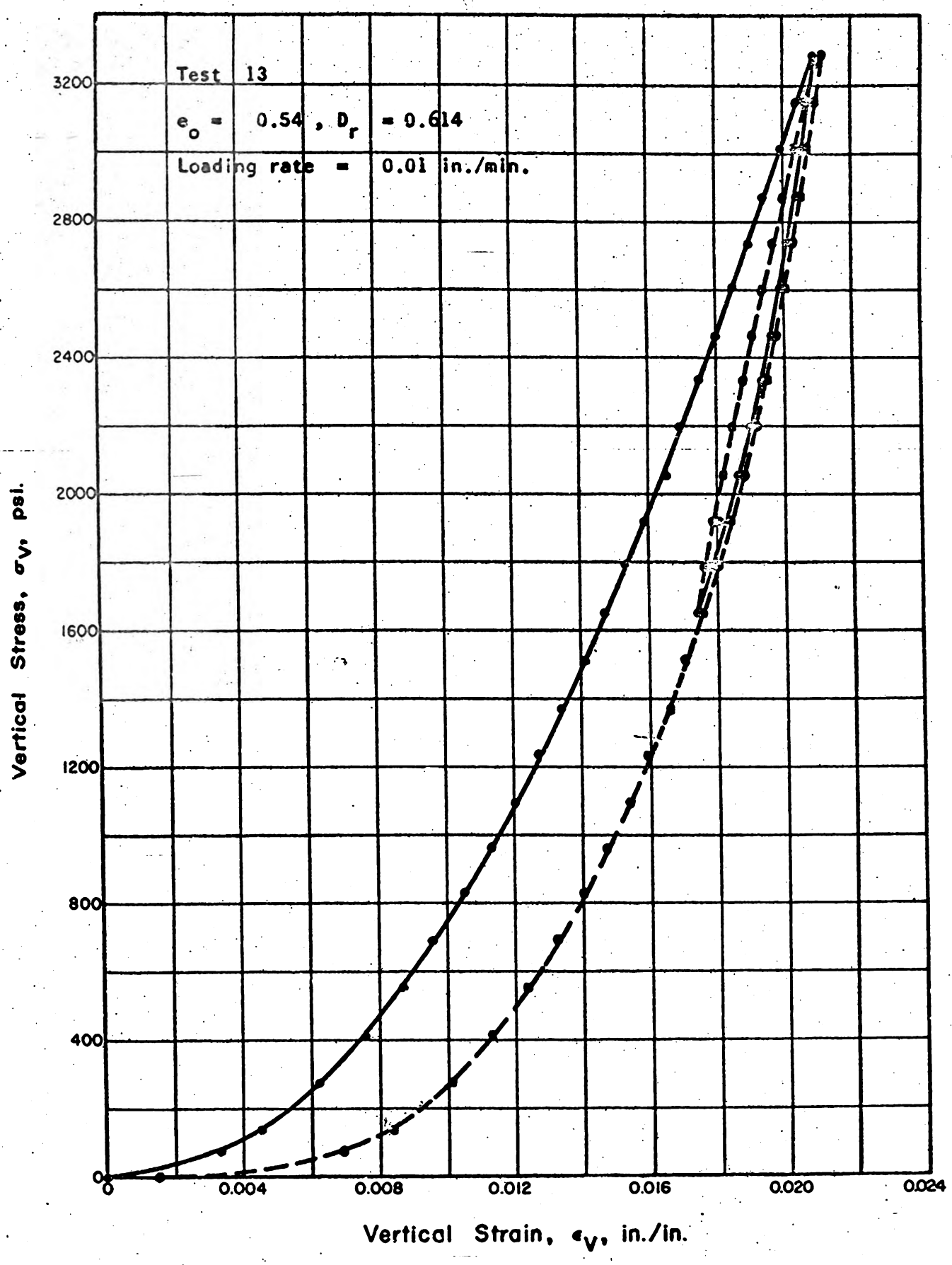

Fig. 5.13 STRESS STRAIN CURVE FOR MINNESOTA SAND IN ONE-DIMENSIONAL COMPRESSION

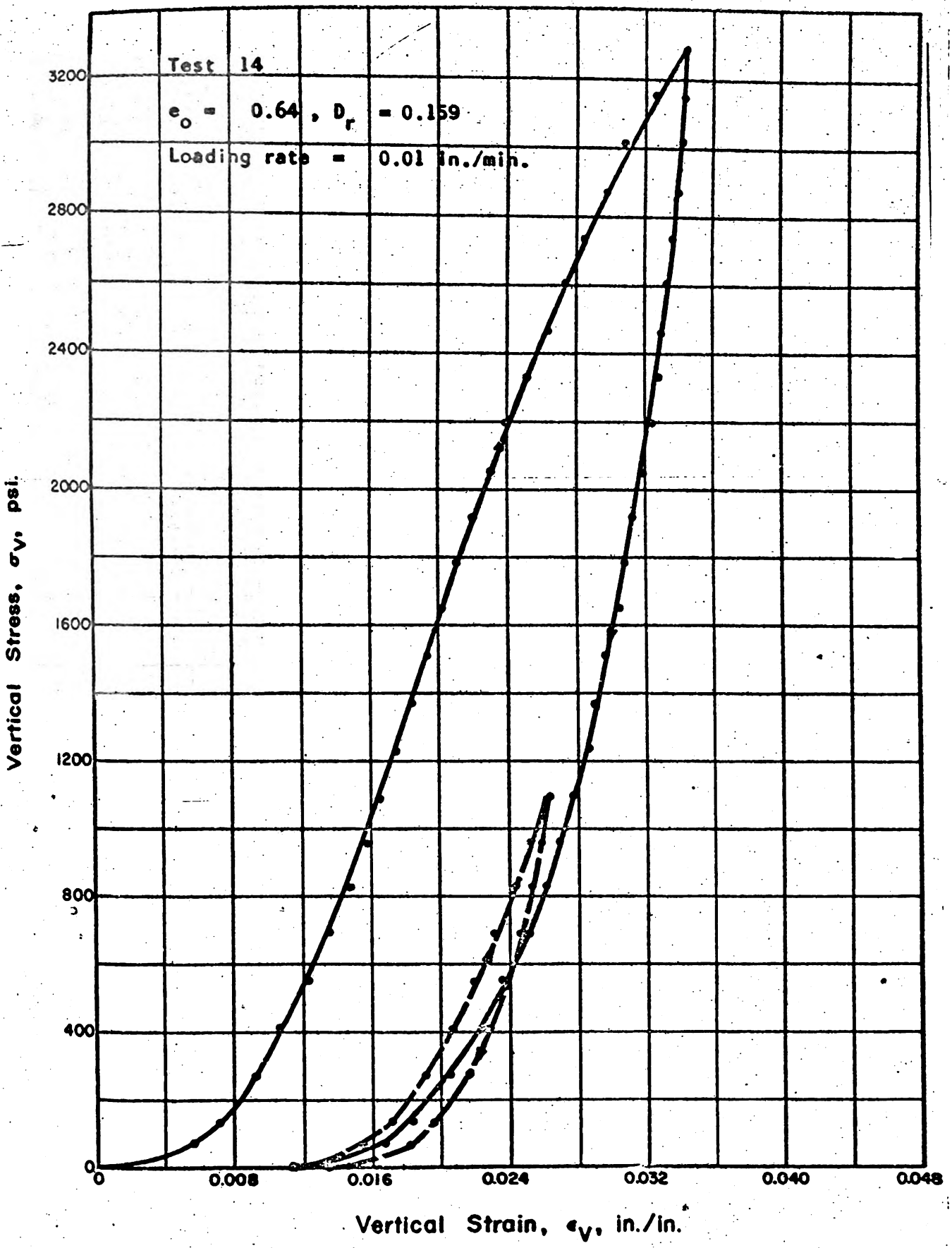

Fig. 5.14 STRESS STRAIN CURVE FOR MINNESOTA SAND IN ONE-DIMENSIONAL COMPRESSION

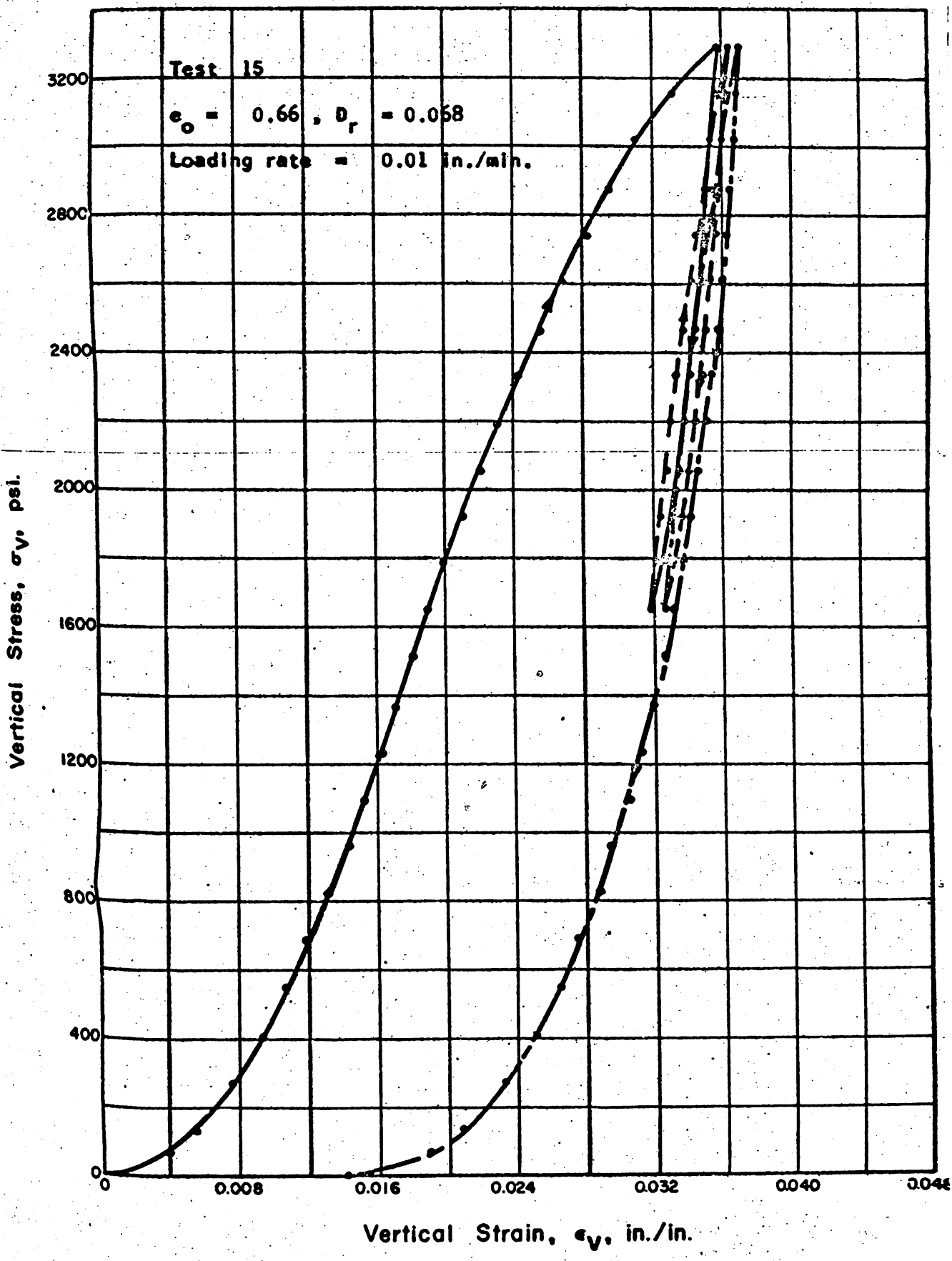

Fig. 5.15 STRESS STRAIN CURVE FOR MINNESOTA SAND IN ONE-DIMENSIONAL COMPRESSION

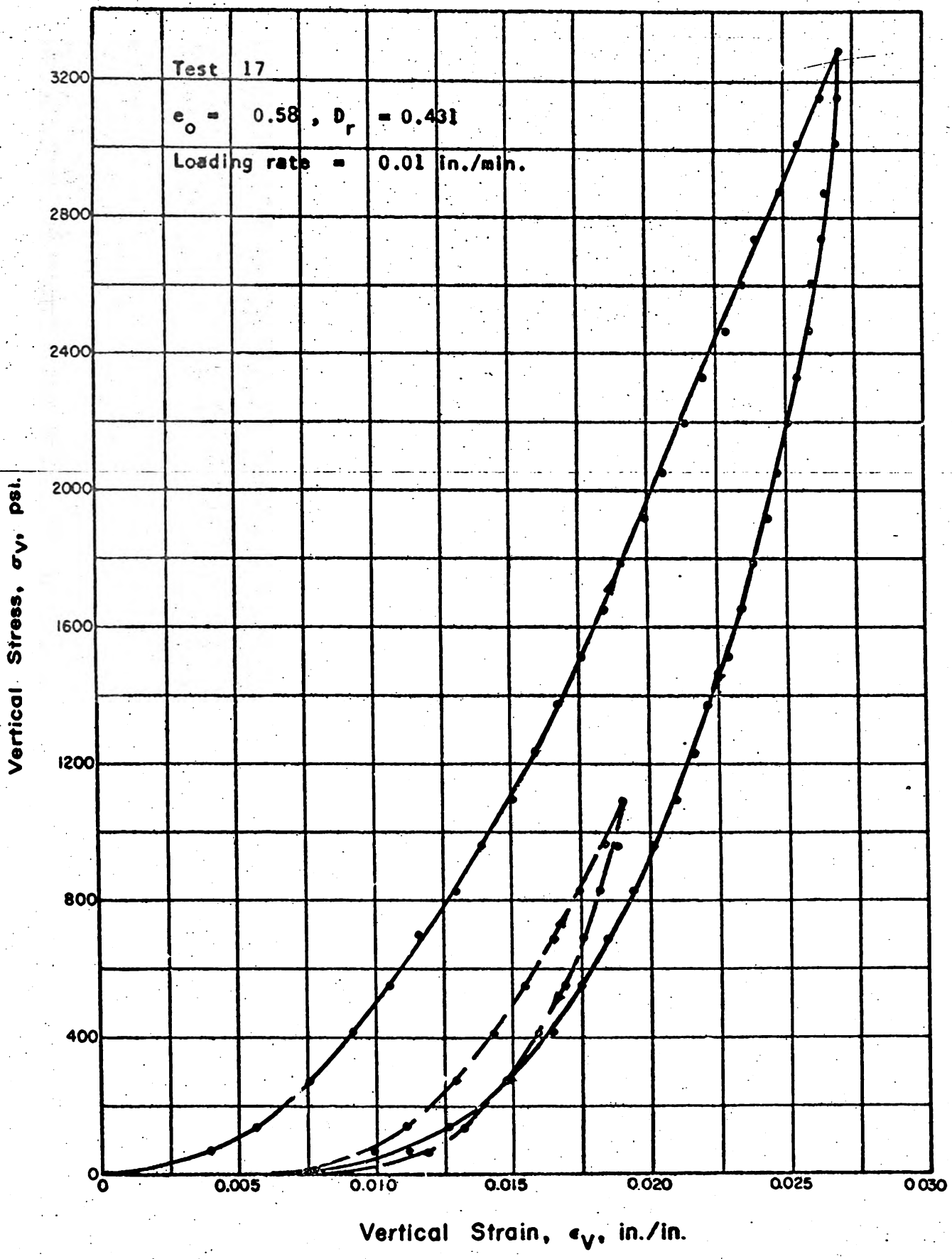

Fig. 5.17 STRESS STRAIN CURVE FOR MINNESOTA SAND IN ONE-DIMENSIONAL COMPRESSION

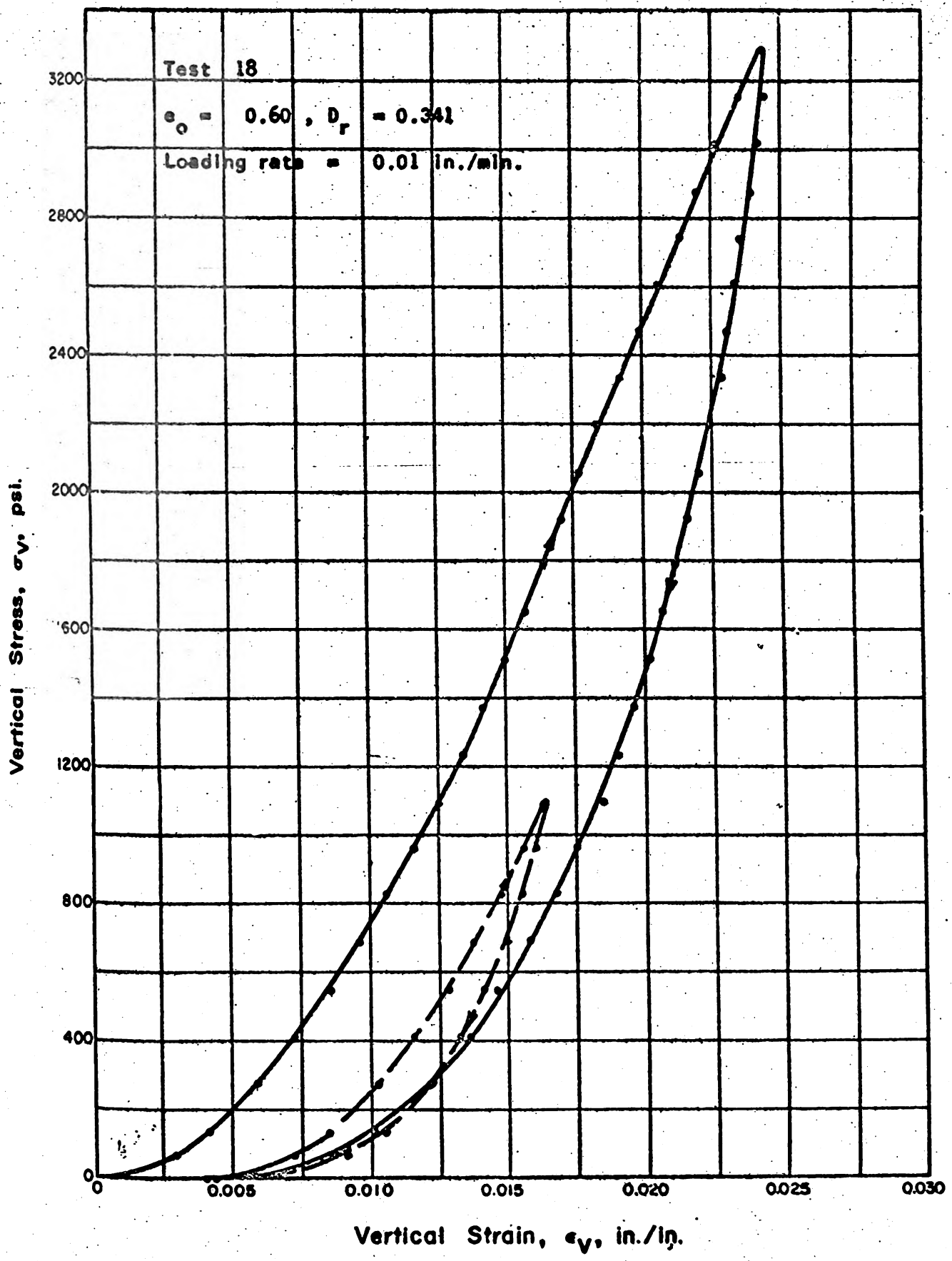

Fig. 5.18 STRESS STRAIN CURVE FOR MINNESOTA SAND IN ONE-DIMENSIONAL COMPRESSION

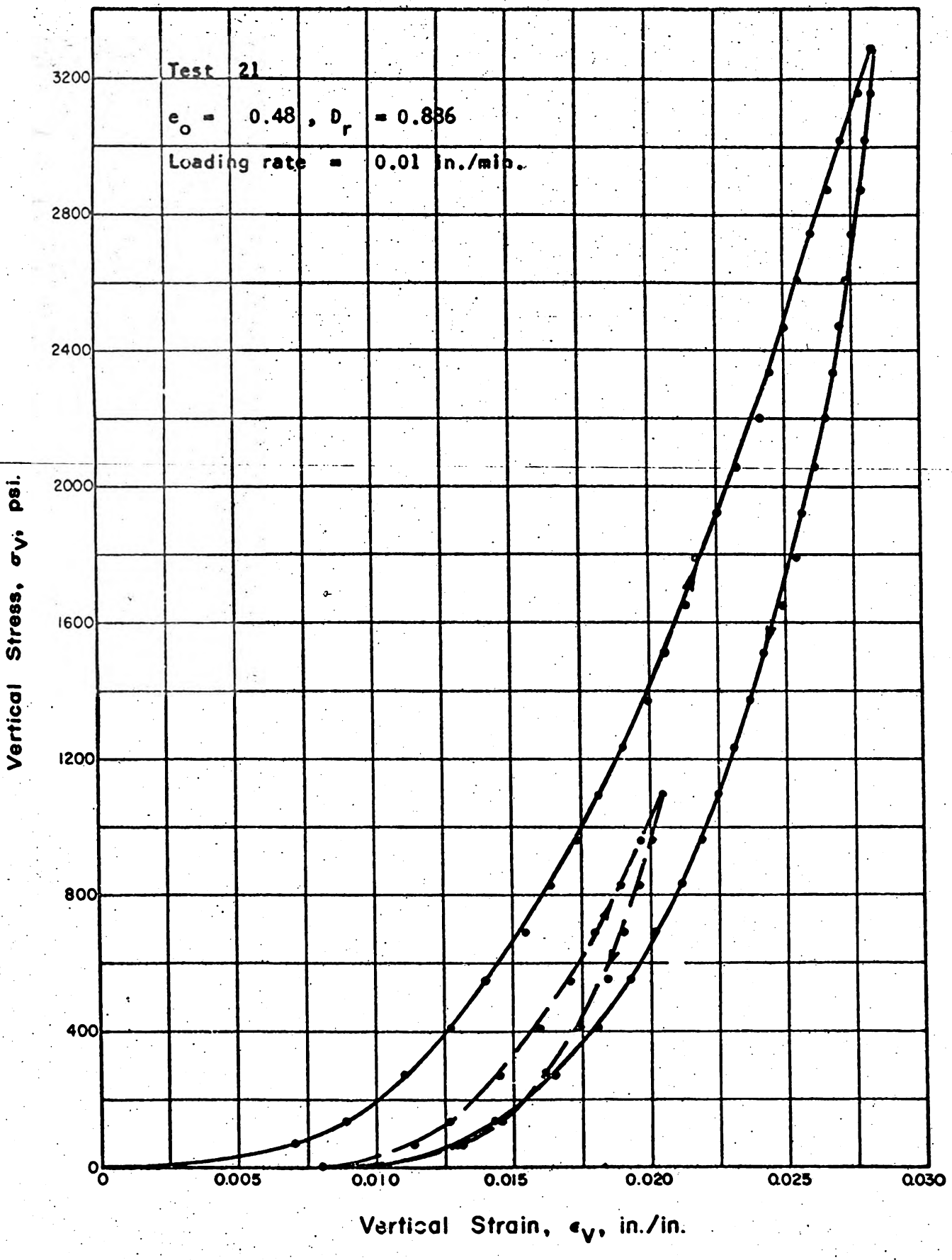

Fig. 5.21 STRESS STRAIN CURVE FOR MINNESOTA SAND IN ONE-DIMENSIONAL COMPRESSION

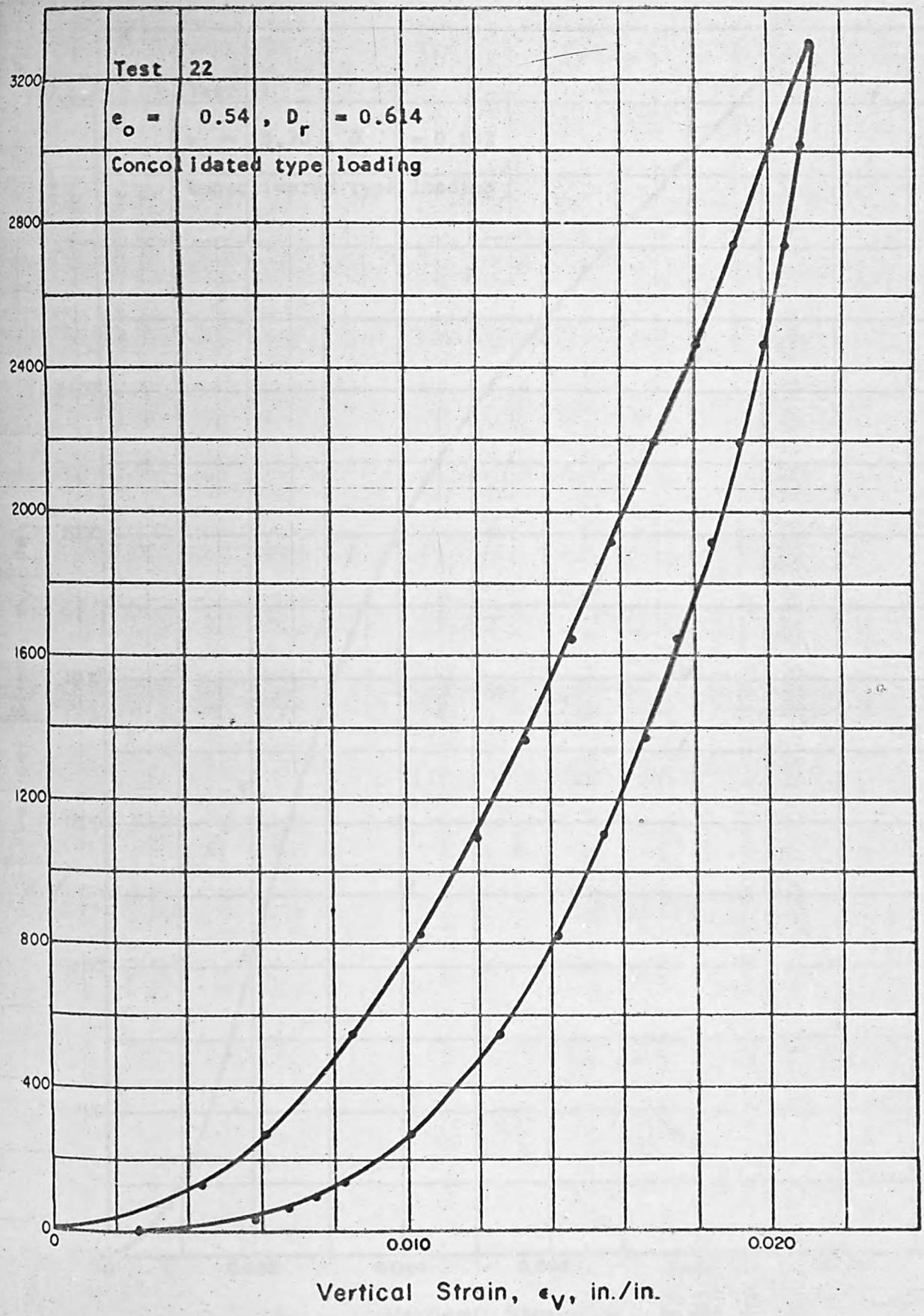

Fig. 5.22 STRESS STRAIN CURVE FOR MINNESOTA SAND IN ONE-DIMENSIONAL COMPRESSION

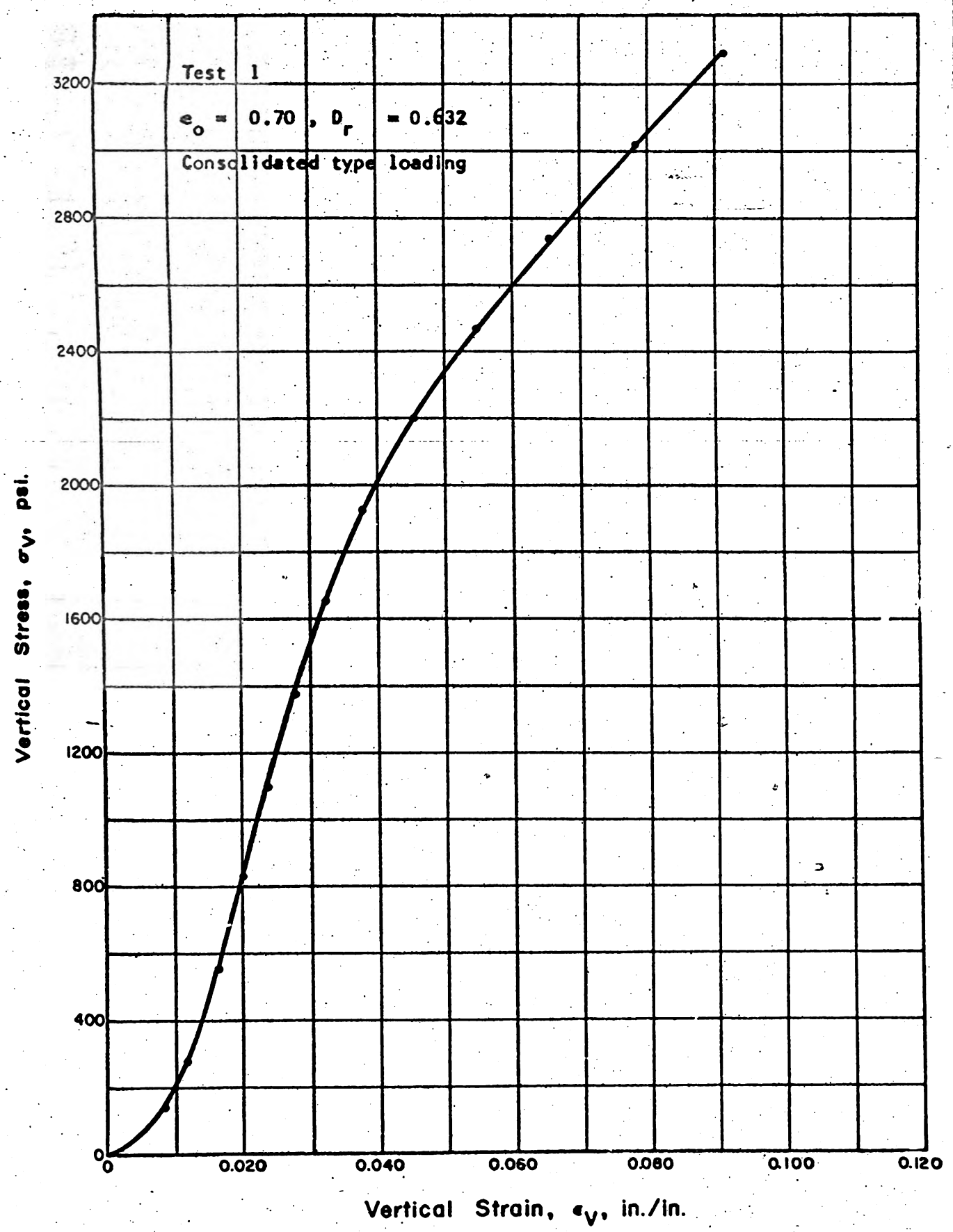

Fig. 5.23 STRESS STRAIN CURVE FOR PENNSYLVANIA SAND IN ONE-DIMENSIONAL COMPRESSION

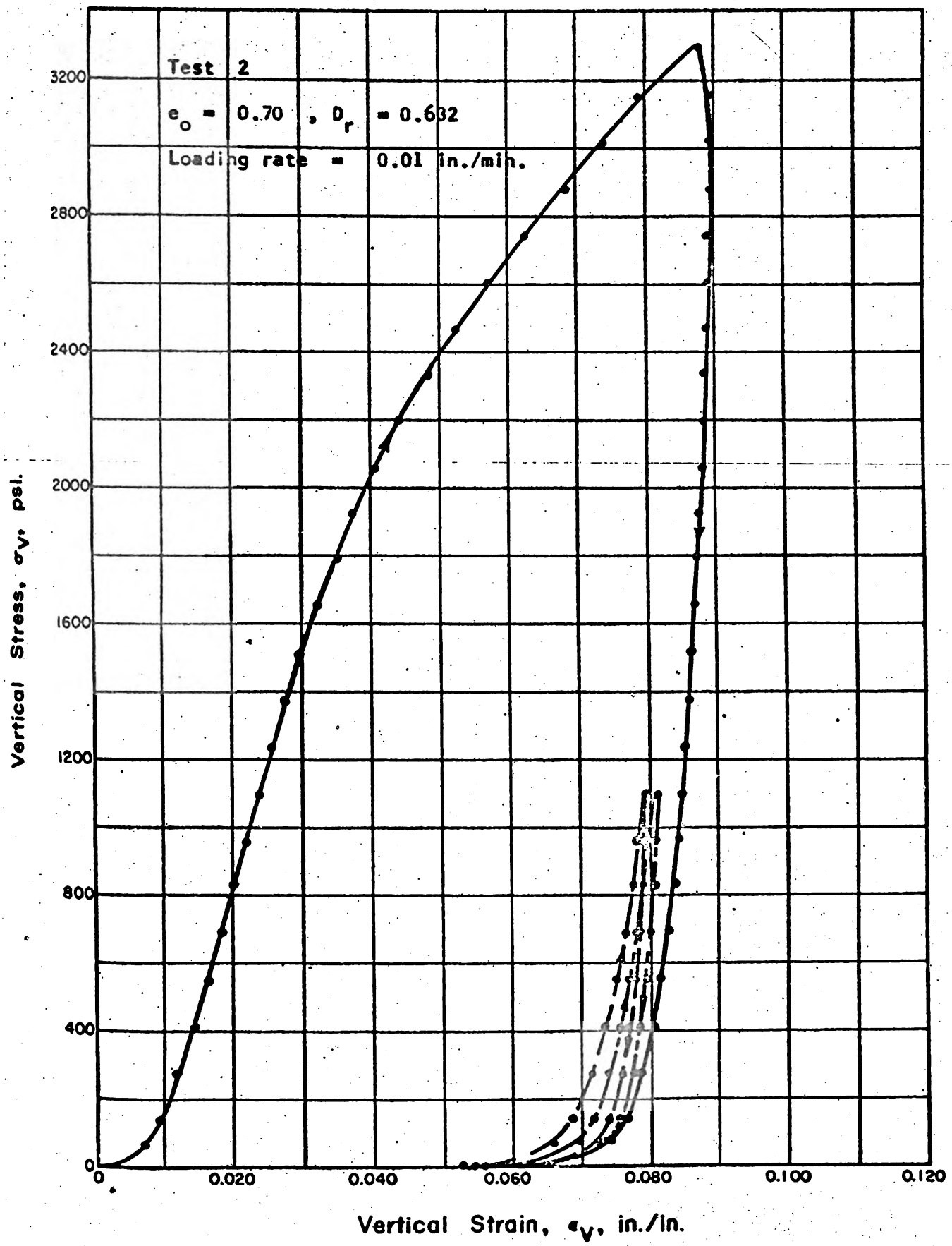

Fig. 5.24 STRESS STRAIN CURVE FOR PENNSYLVANIA SAND IN ONE-DIMENSIONAL COMPRESSION

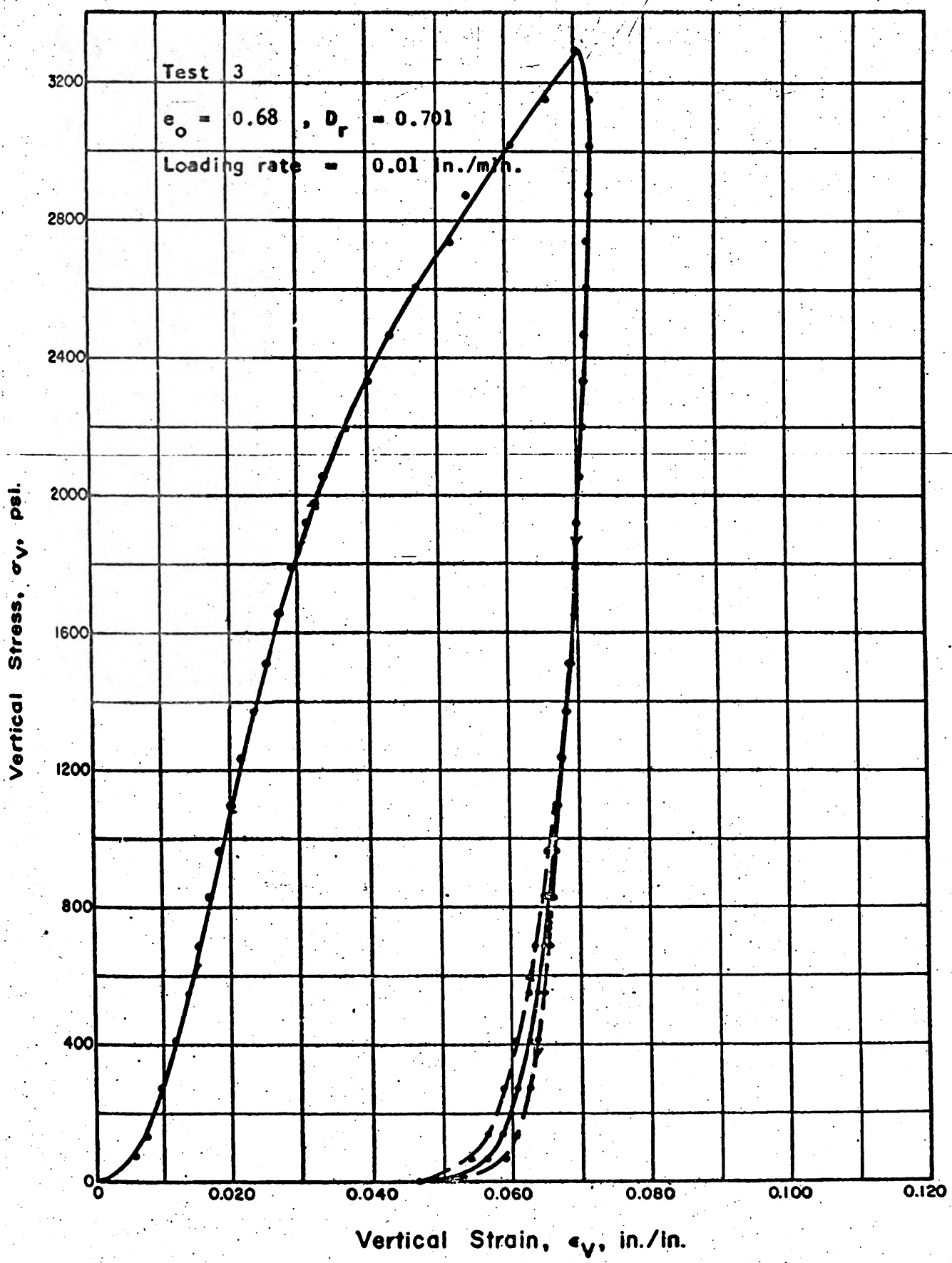

Fig. 5.25 STRESS STRAIN CURVE FOR PENNSYLVANIA SAND IN ONE-DIMENSIONAL COMPRESSION

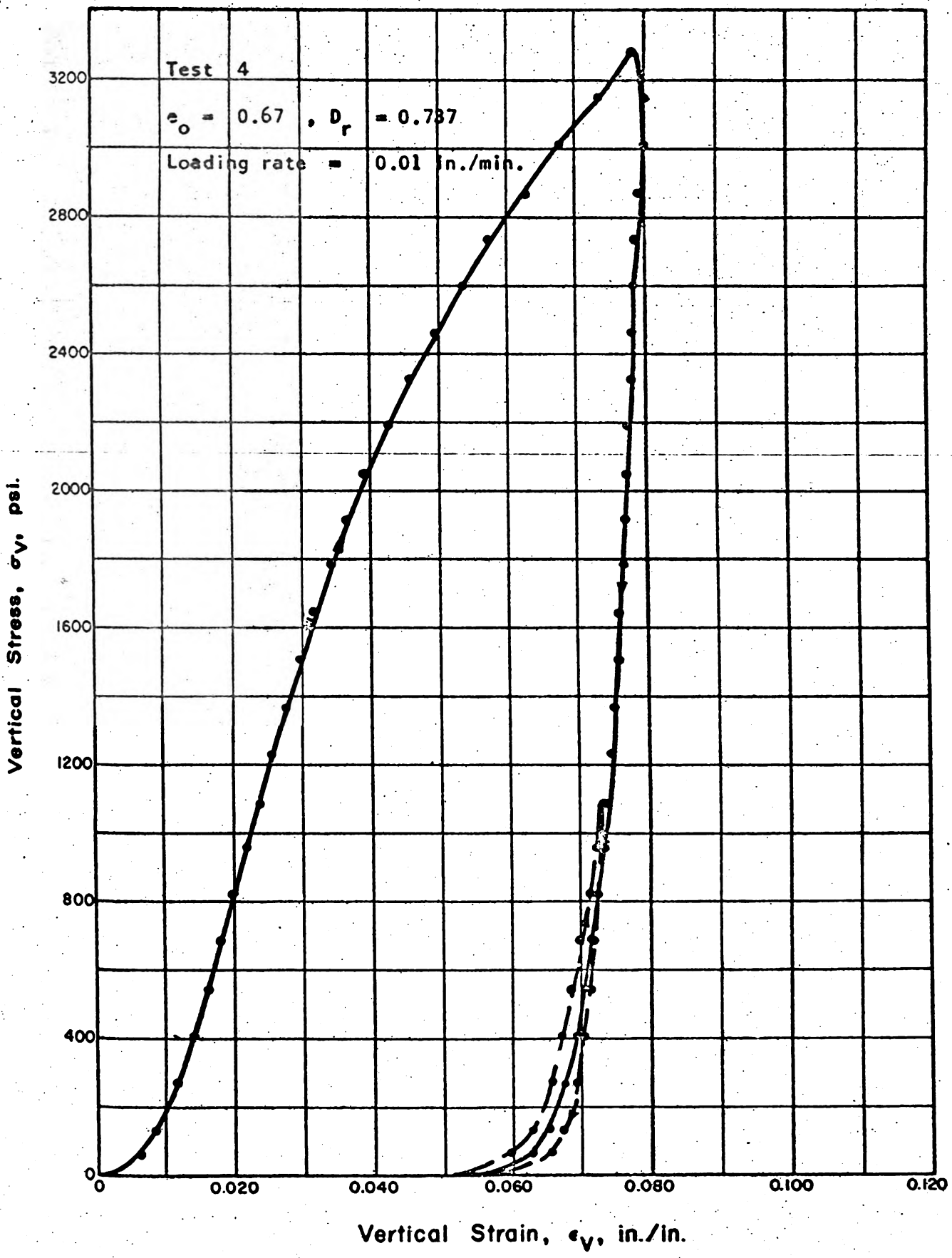

Fig. 5.26 STRESS STRAIN CURVE FOR PENNSYLVANIA SAND IN ONE-DIMENSIONAL COMPRESSION

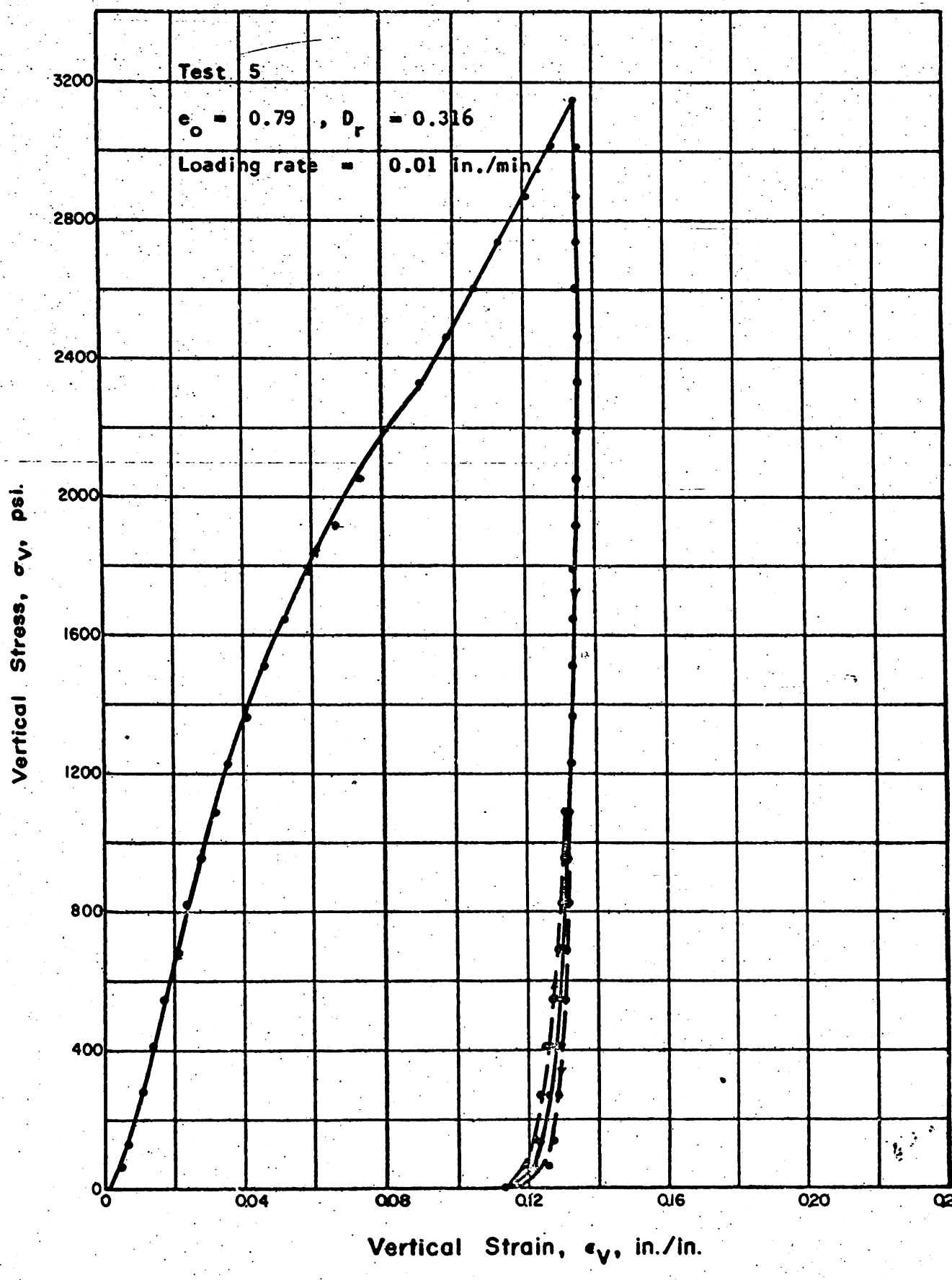

Fig. 5.27 STRESS STRAIN CURVE FOR PENNSYLVANIA SAND IN ONE-DIMENSIONAL COMPRESSION

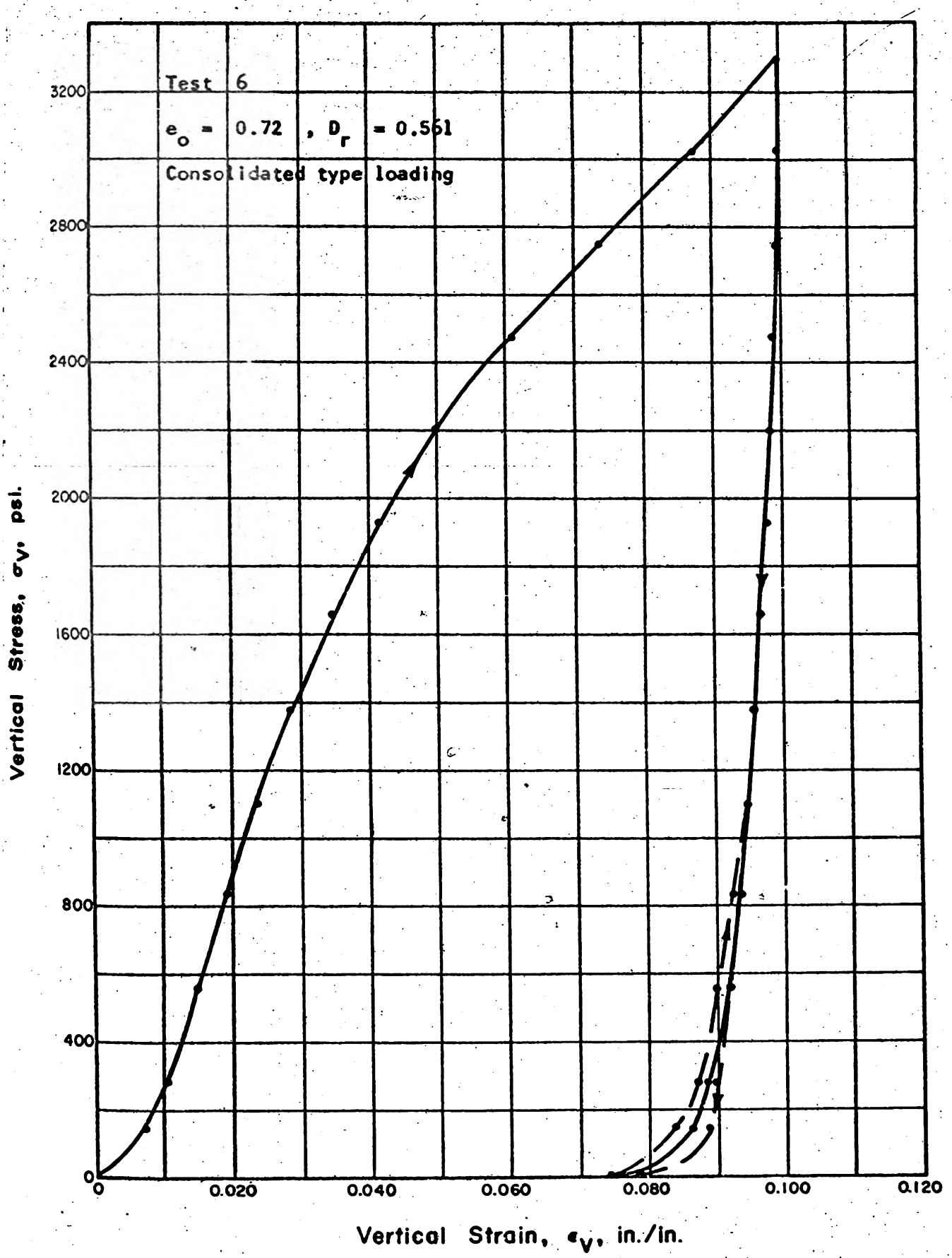

Fig. 5.28 STRESS STRAIN CURVE FOR PENNSYLVANIA SAND IN ONE-DIMENSIONAL COMPRESSION

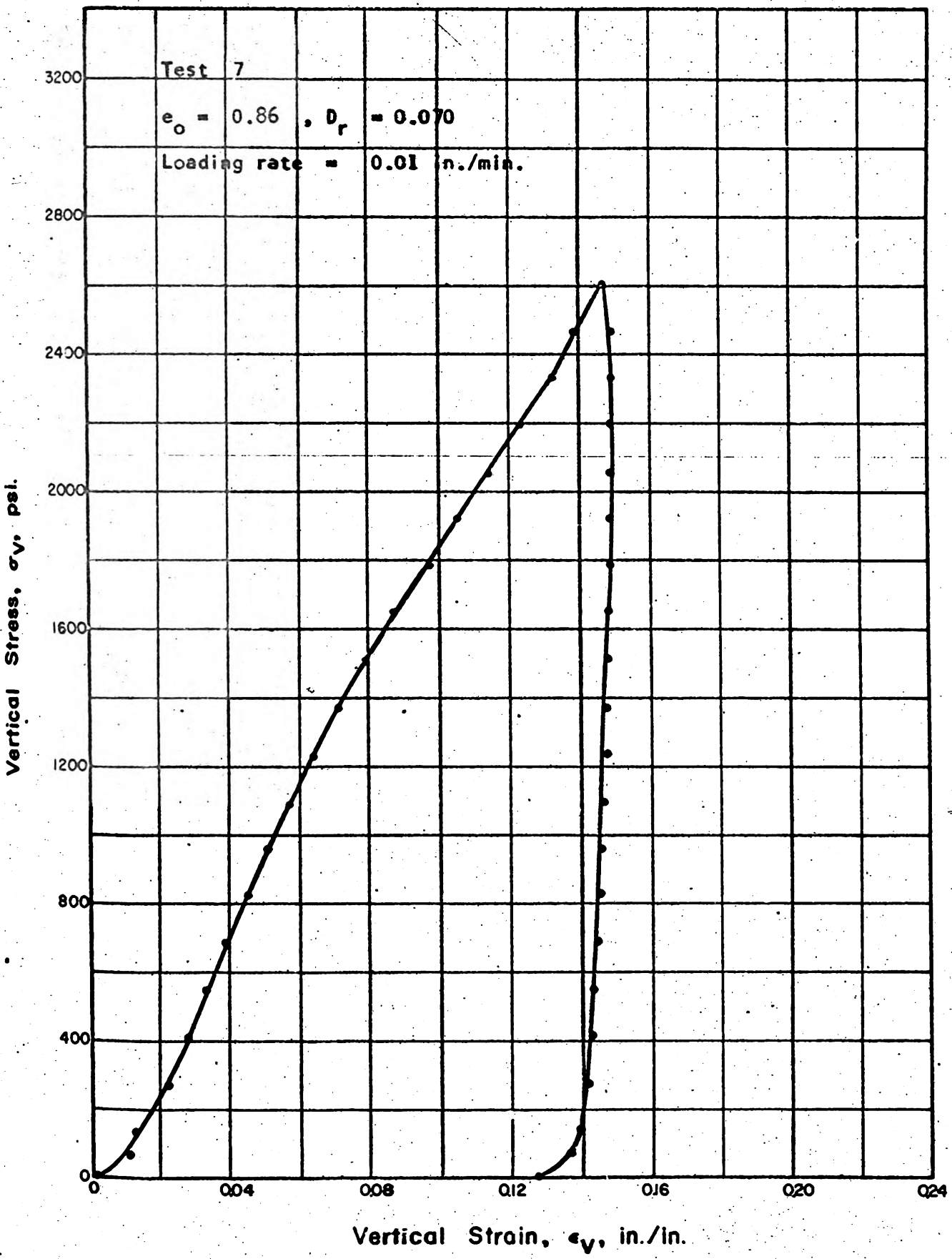

Fig. 5.29 STRESS STRAIN CURVE FOR PENNSYLVANIA SAND IN ONE-DIMENSIONAL COMPRESSION

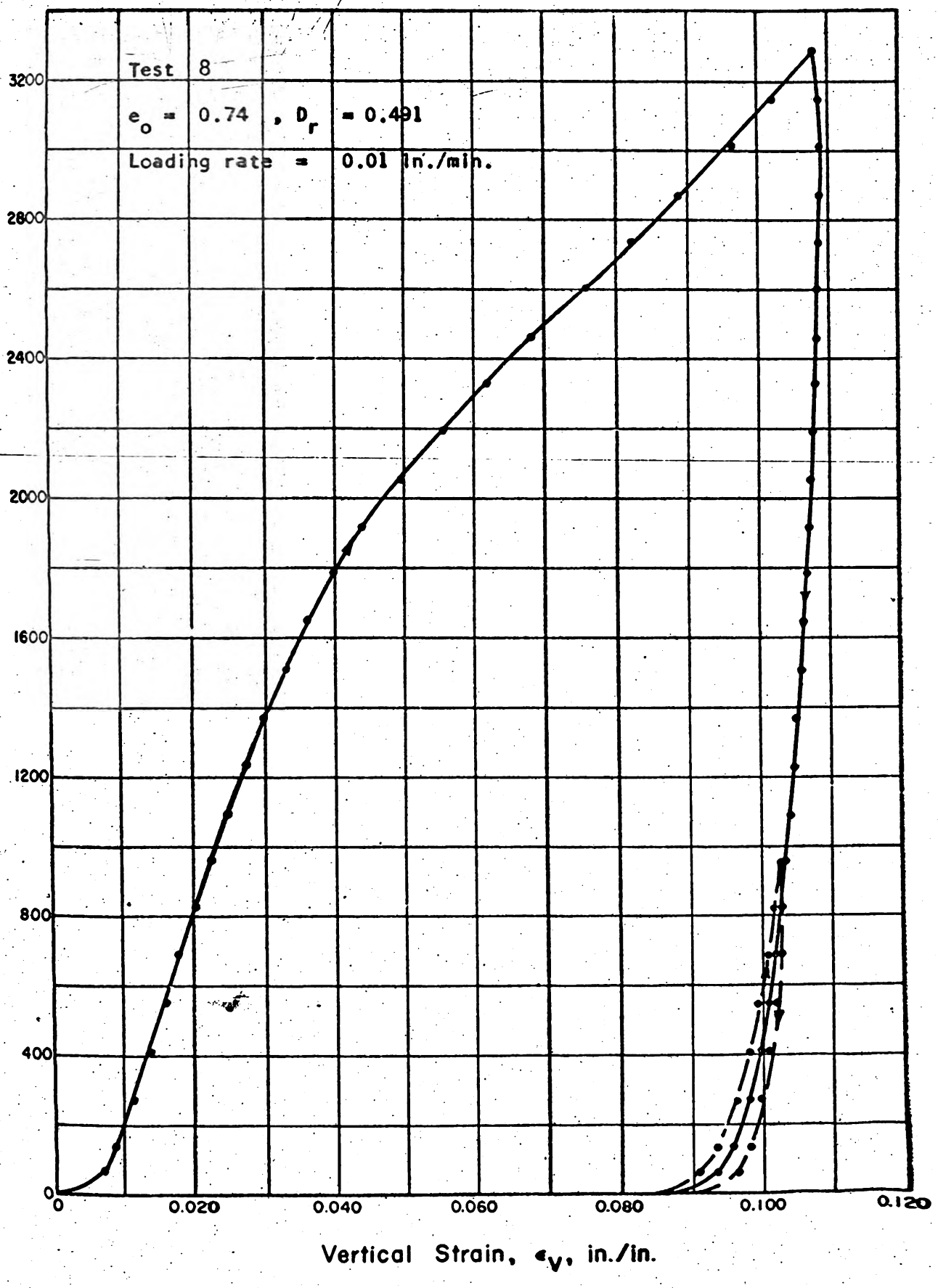

Fig. 5.30 STRESS STRAIN CURVE FOR PENNSYLVANIA SAND IN ONE-DIMENSIONAL COMPRESSION

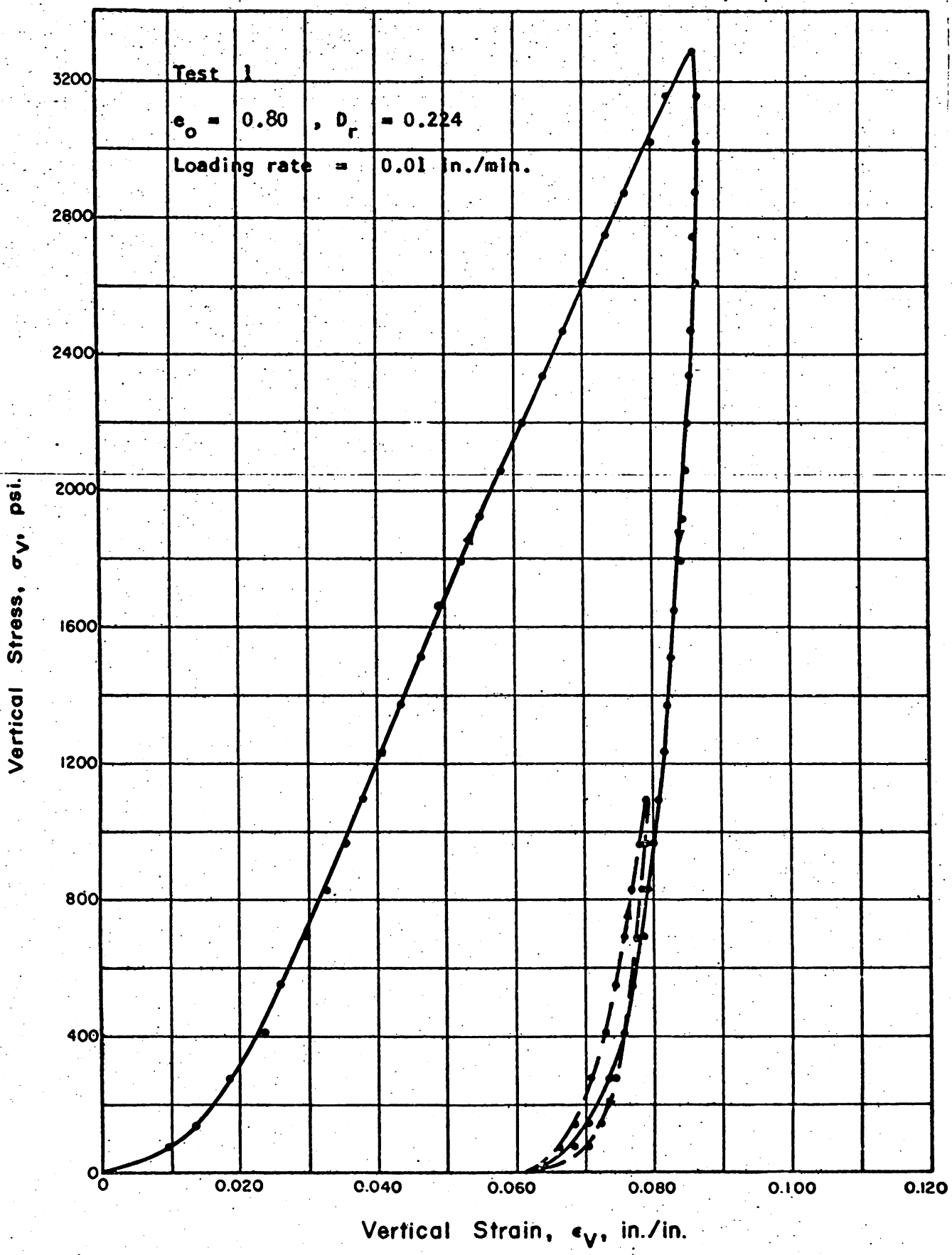

Fig. 5.31 STRESS STRAIN CURVE FOR SANGAMON RIVER SAND IN ONE-DIMENSIONAL COMPRESSION

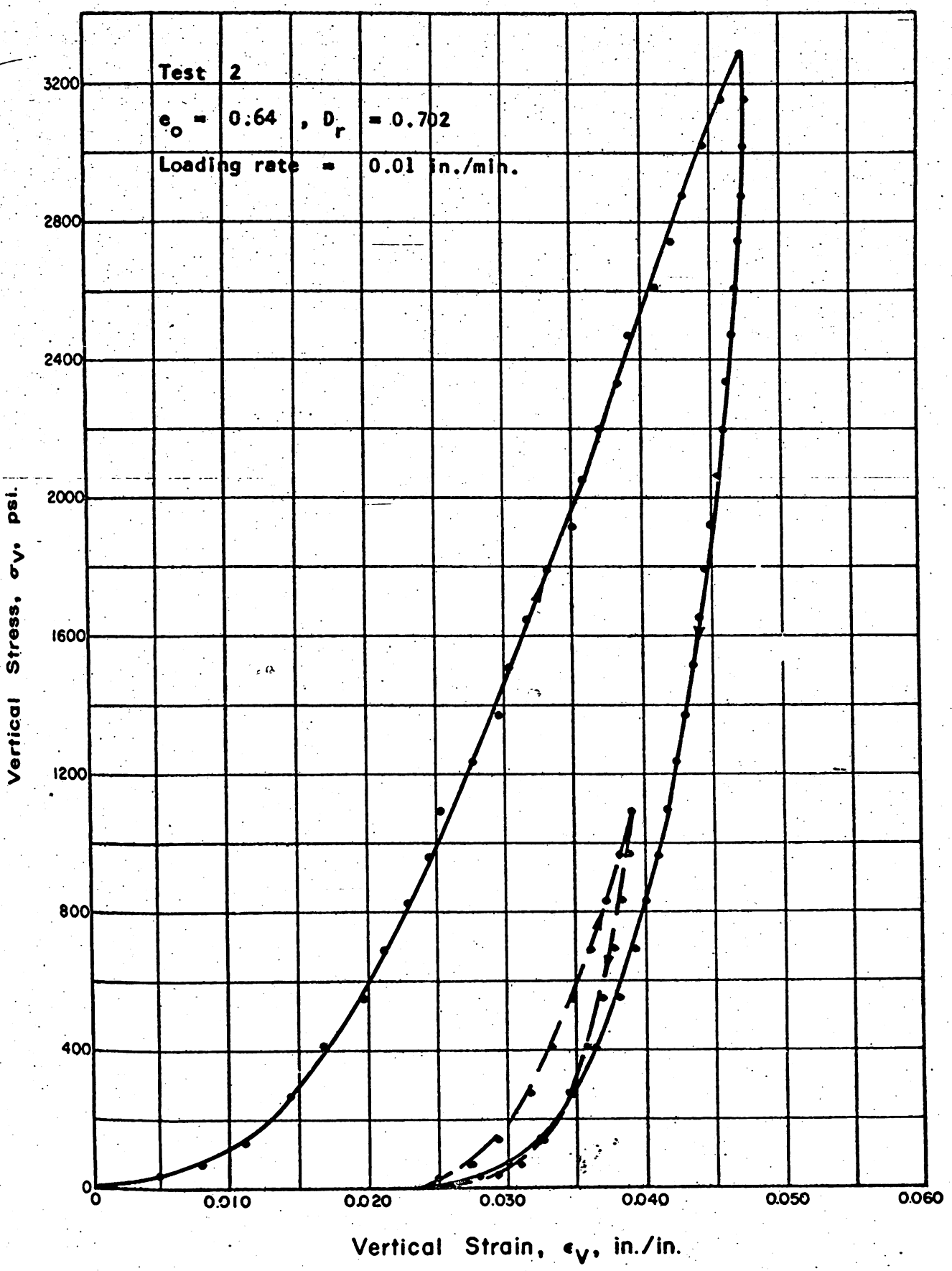

Fig. 5.32 STRESS STRAIN CURVE FOR SANGAMON RIVER SAND IN ONE-DIMENSIONAL COMPRESSION

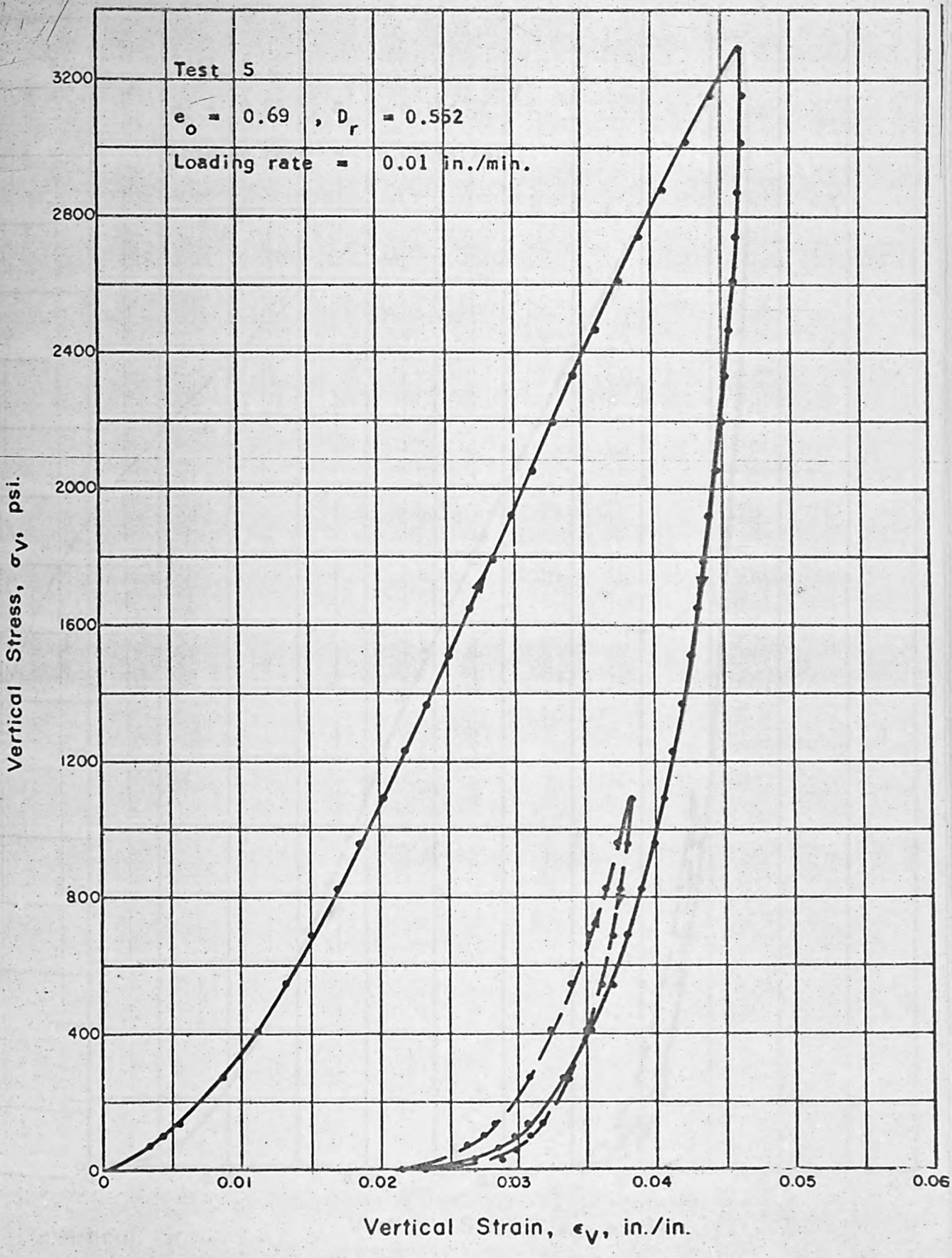

Fig. 5.35 STRESS STRAIN CURVE FOR SANGAMON RIVER SAND IN ONE-DIMENSIONAL COMPRESSION

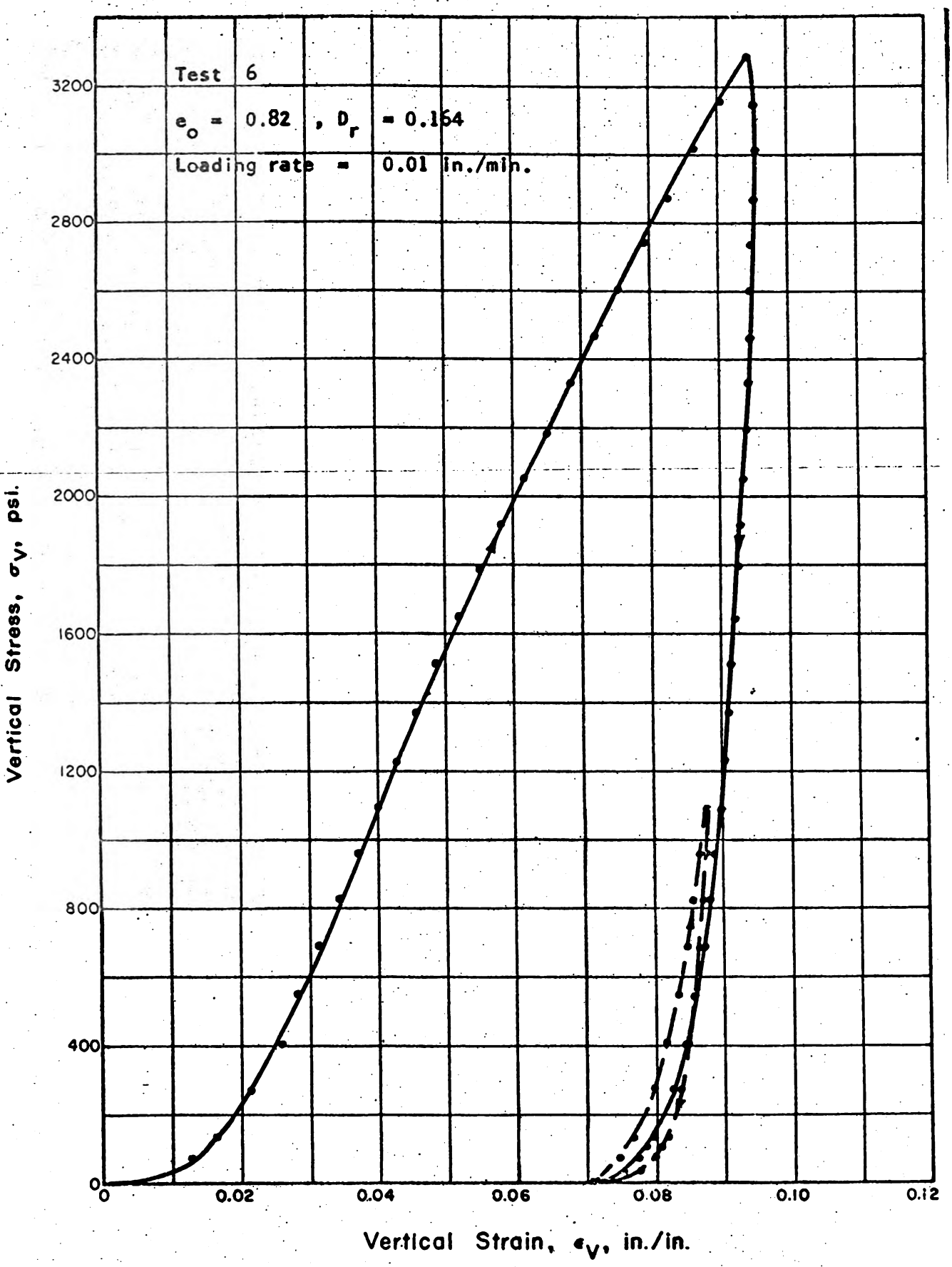

Fig. 5.36 STRESS STRAIN CURVE FOR SANGAMON RIVER SAND IN ONE-DIMENSIONAL COMPRESSION

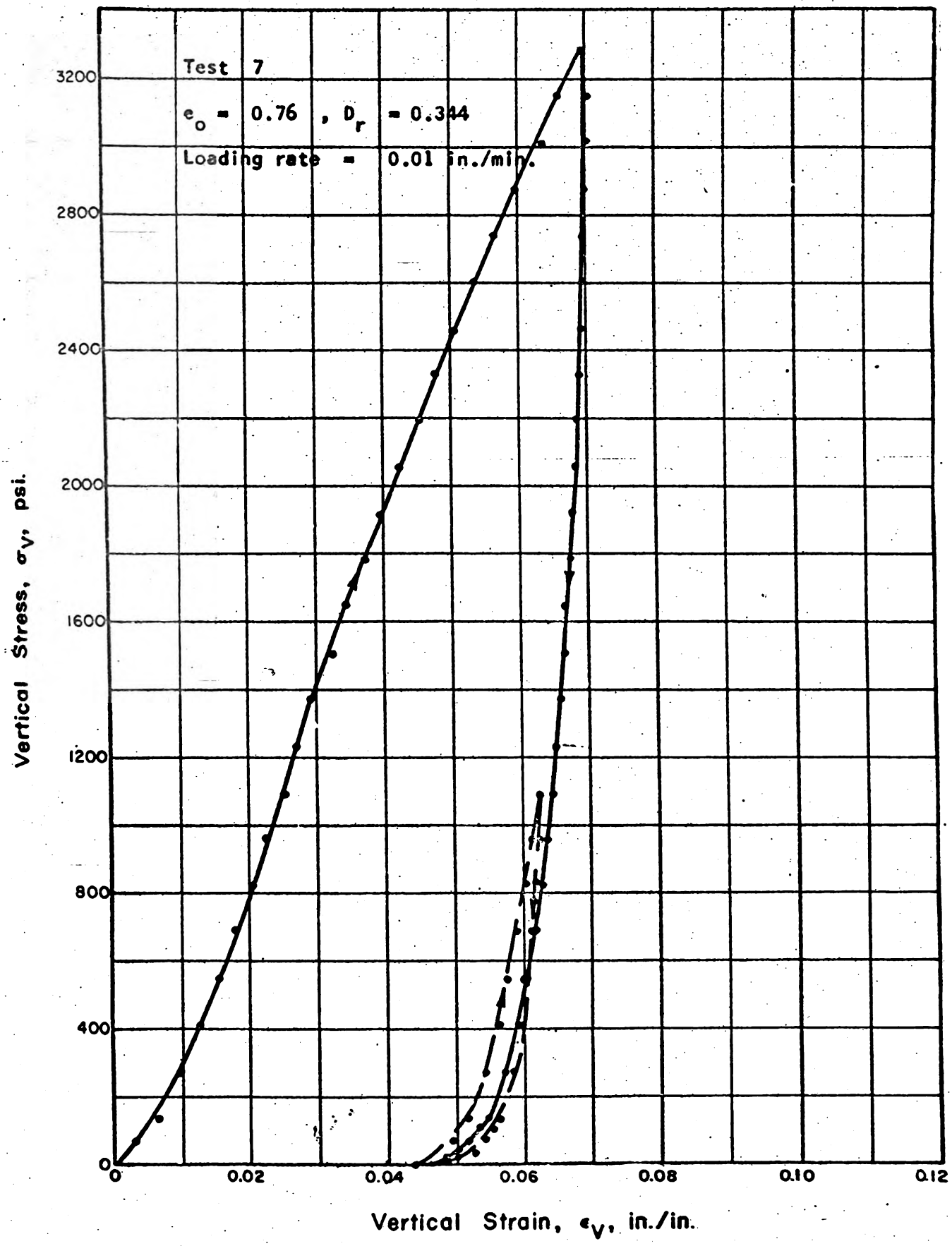

Fig. 5.37 STRESS STRAIN CURVE FOR SANGAMON RIVER SAND IN ONE-DIMENSIONAL COMPRESSION

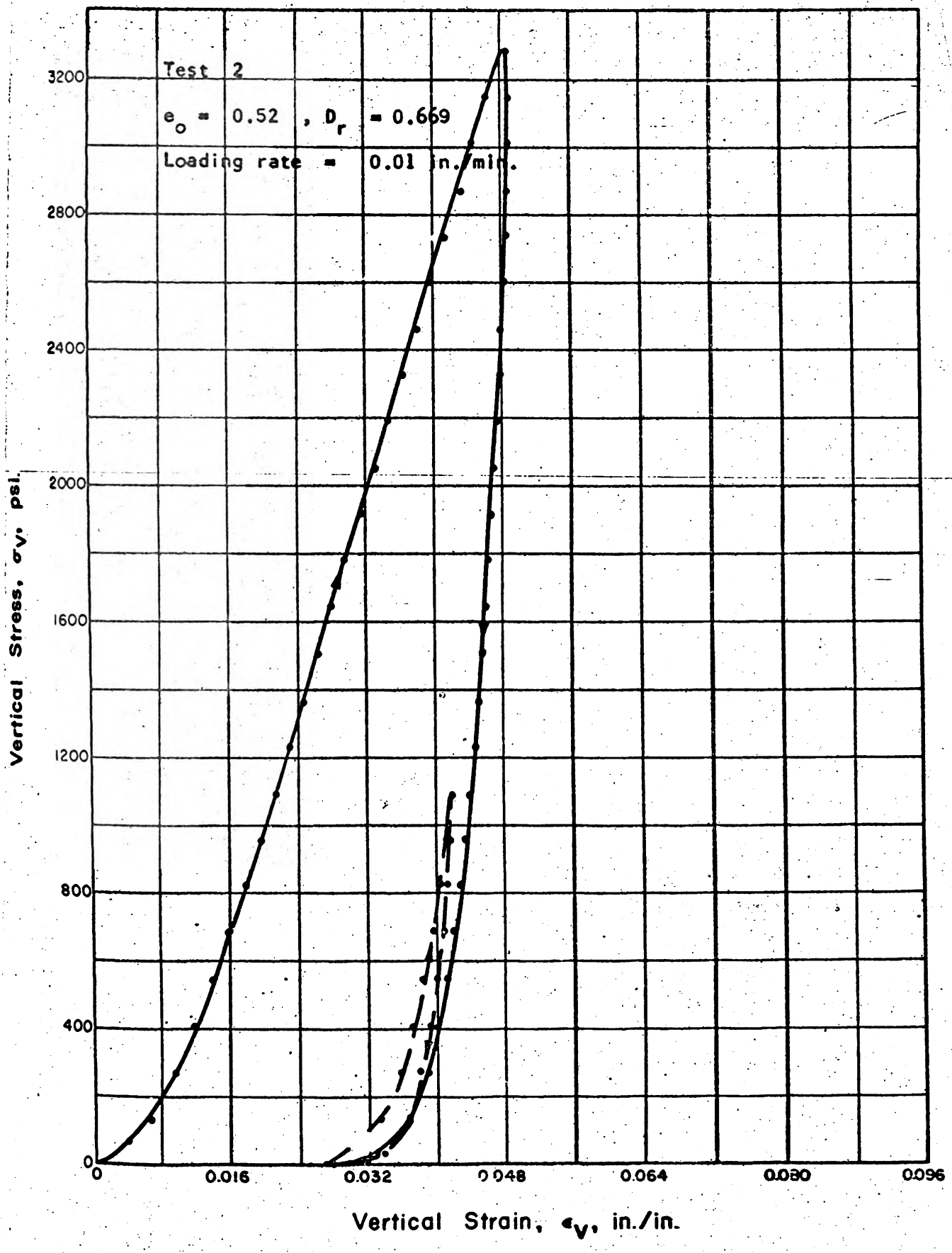

Fig. 5.39 STRESS STRAIN CURVE FOR WABASH RIVER SAND IN ONE-DIMENSIONAL COMPRESSION

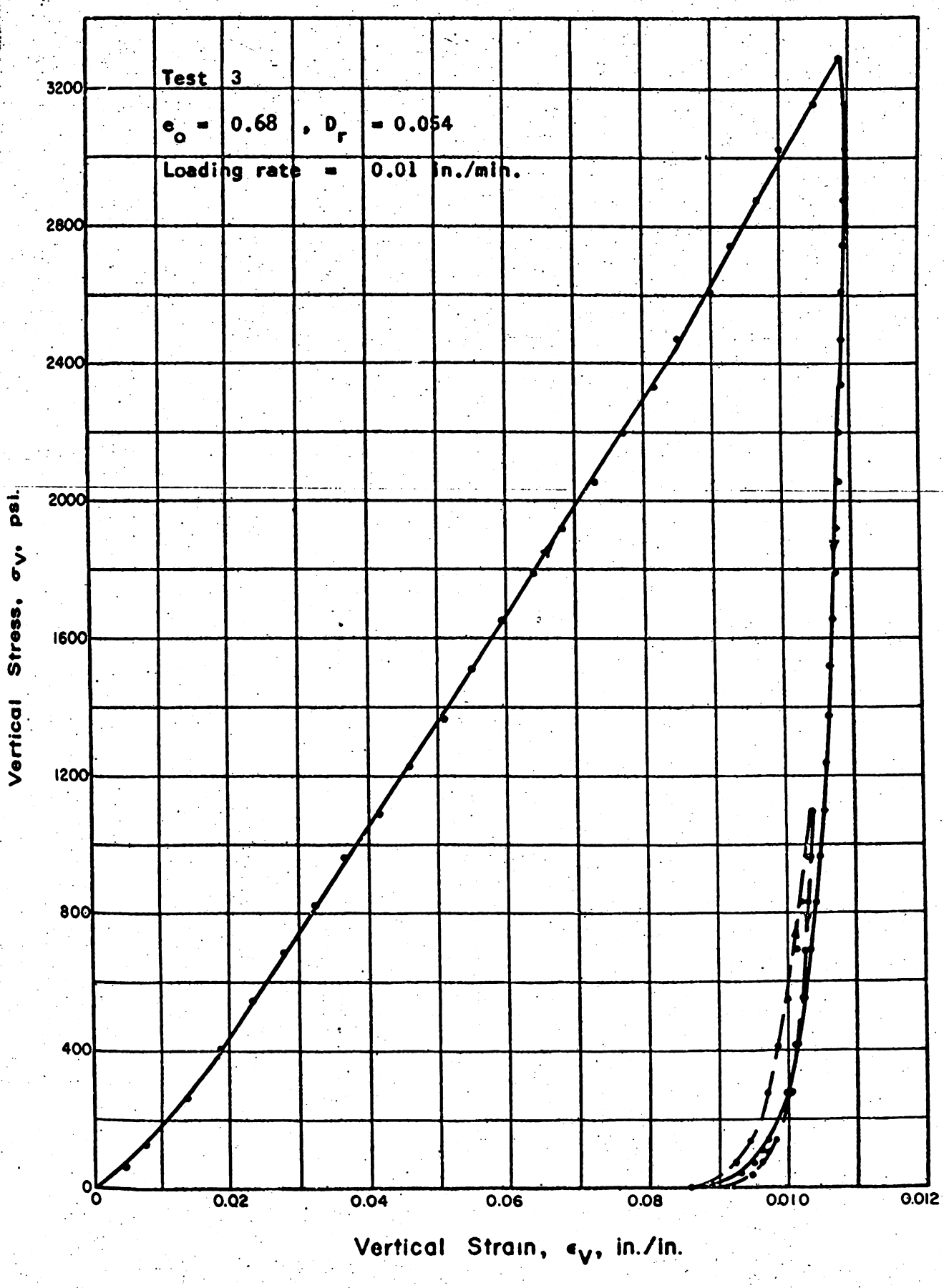

Fig. 5.40 STRESS STRAIN CURVE FOR WABASH RIVER SAND IN ONE-DIMENSIONAL COMPRESSION

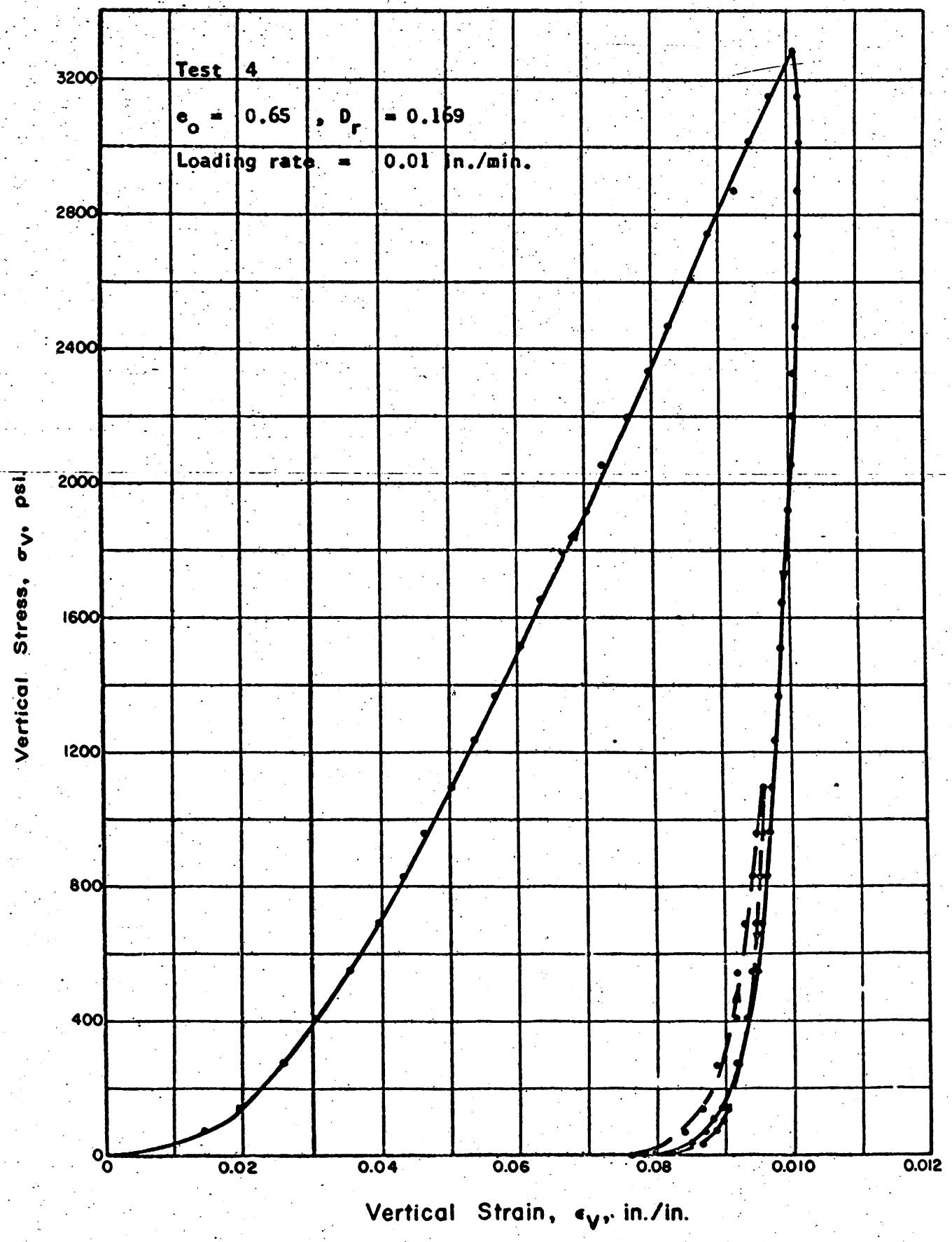

Fig. 5.41 STRESS STRAIN CURVE FOR WABASH RIVER SAND IN ONE-DIMENSIONAL COMPRESSION

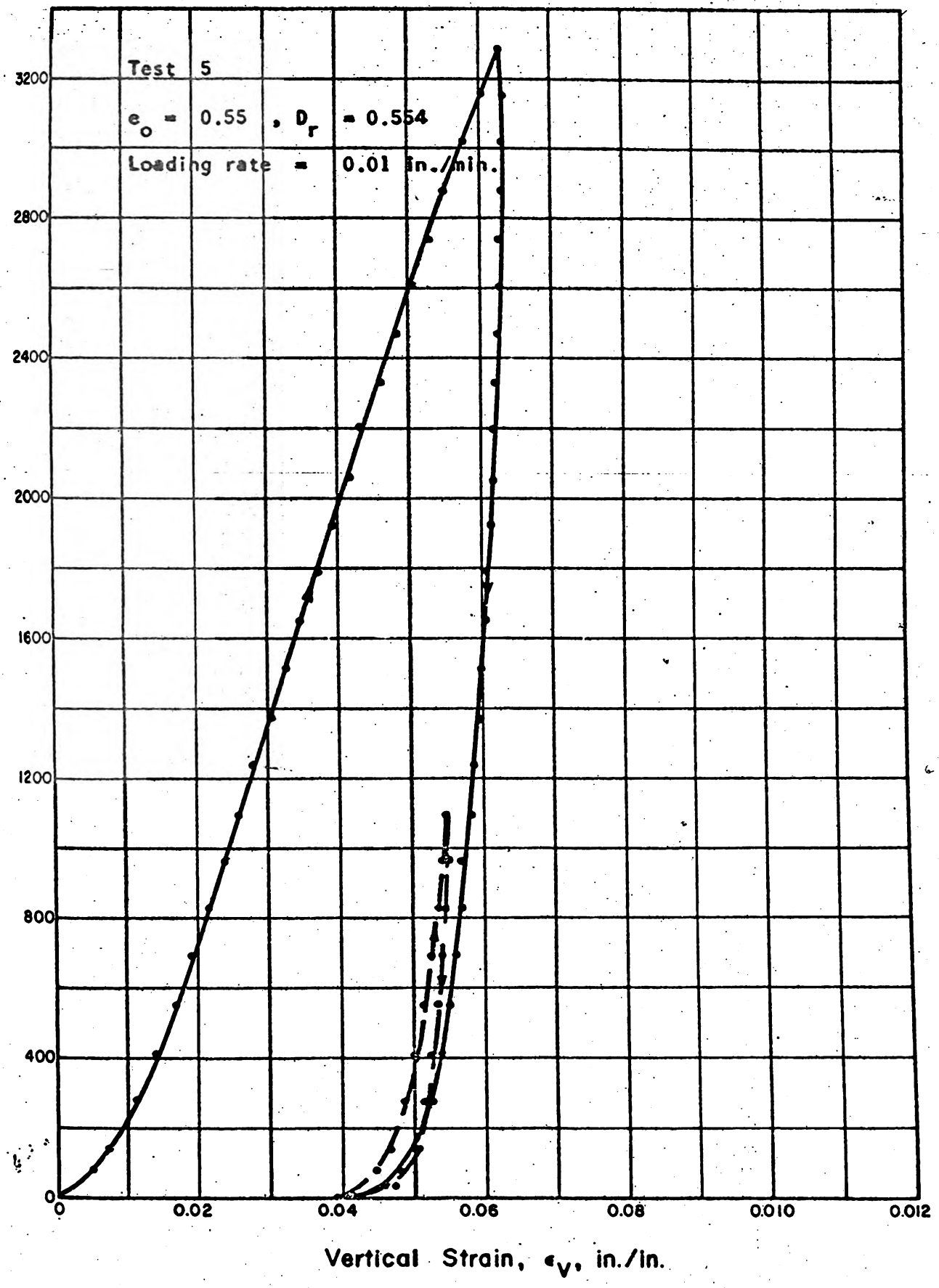

Fig. 5.42 STRESS STRAIN CURVE FOR WABASH RIVER SAND IN ONE-DIMENSIONAL COMPRESSION

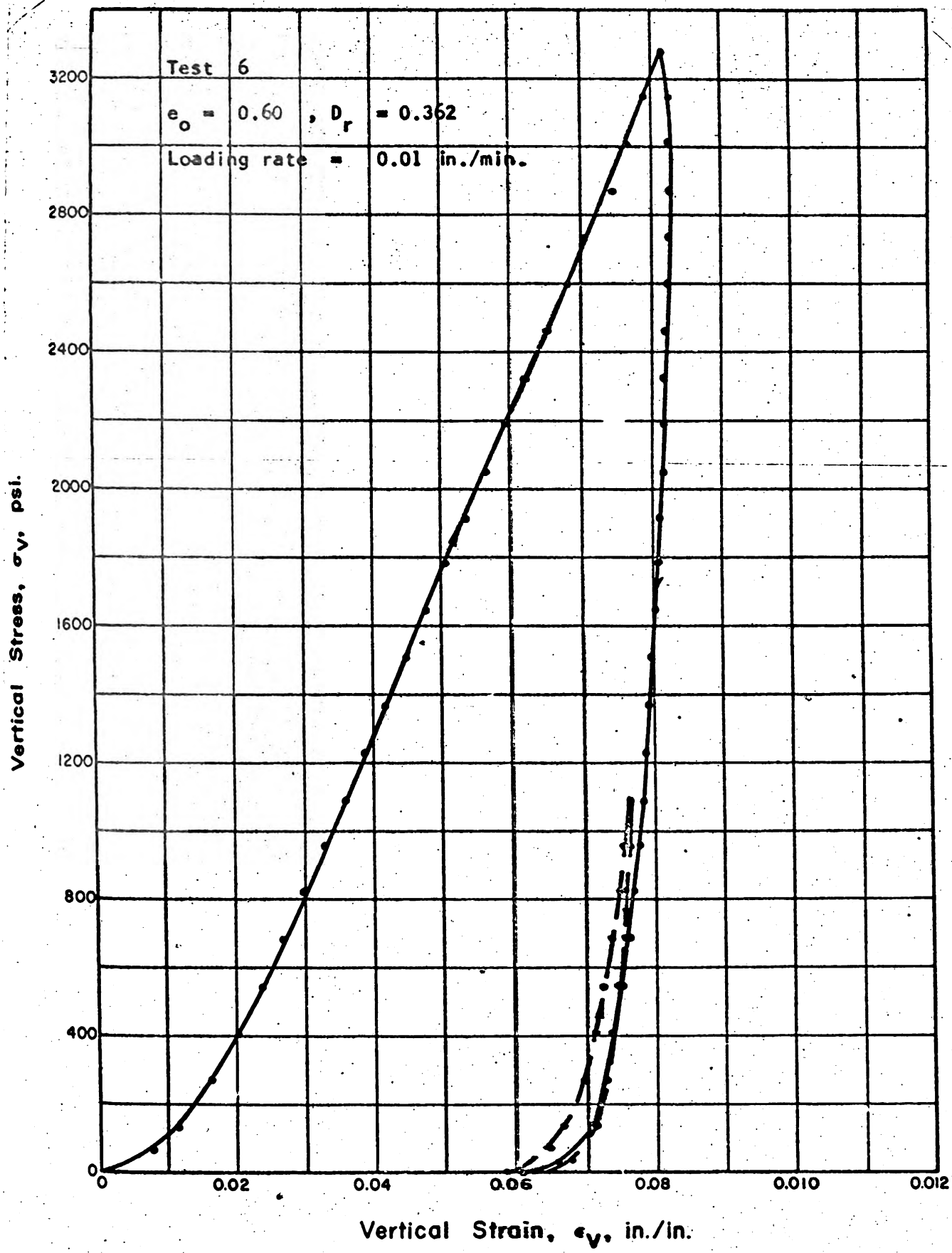

Fig. 5.43 STRESS STRAIN CURVE FOR WABASH RIVER SAND IN ONE-DIMENSIONAL COMPRESSION

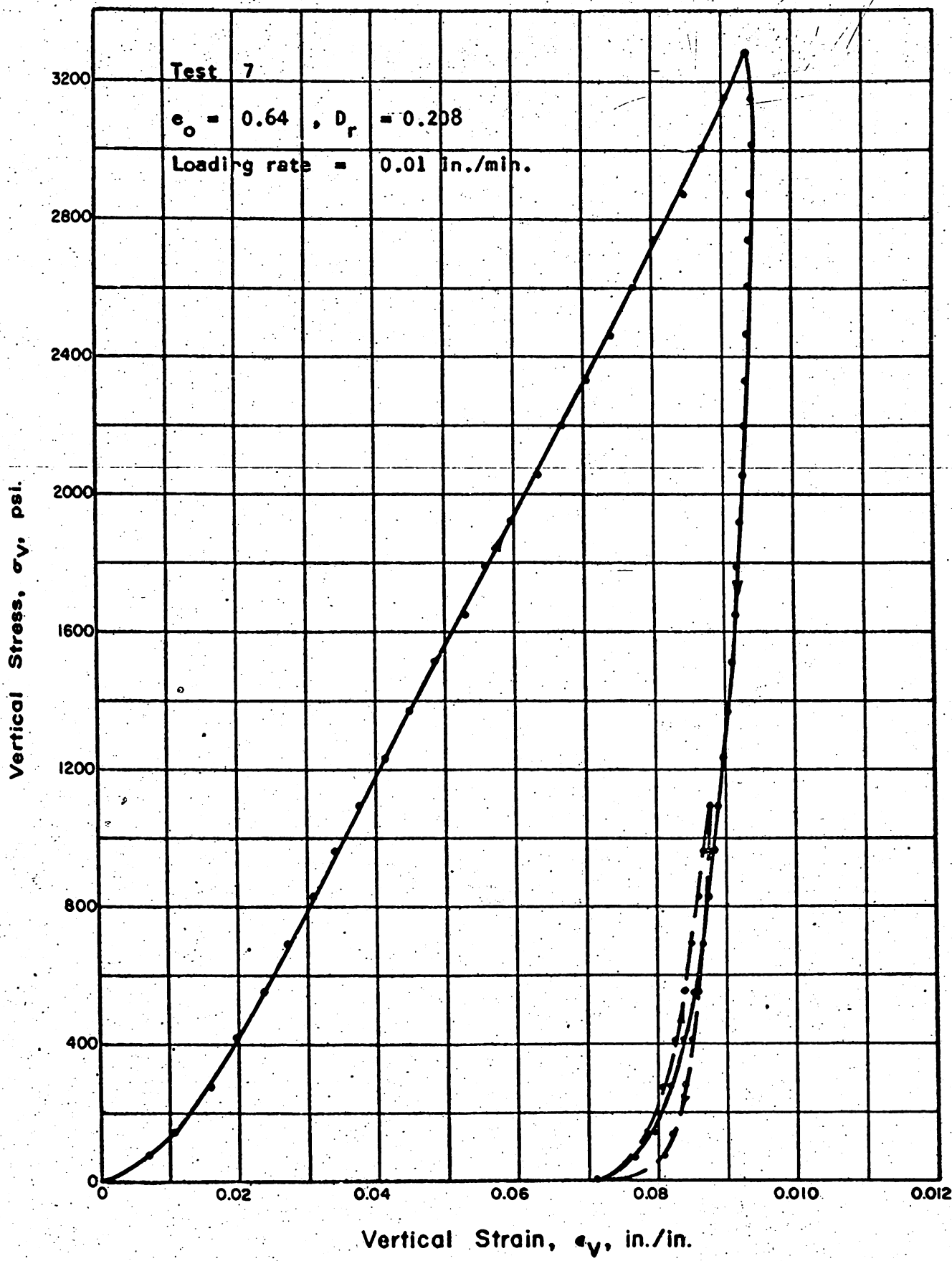

Fig. 5.44 STRESS STRAIN CURVE FOR WABASH RIVER SAND IN ONE-DIMENSIONAL COMPRESSION

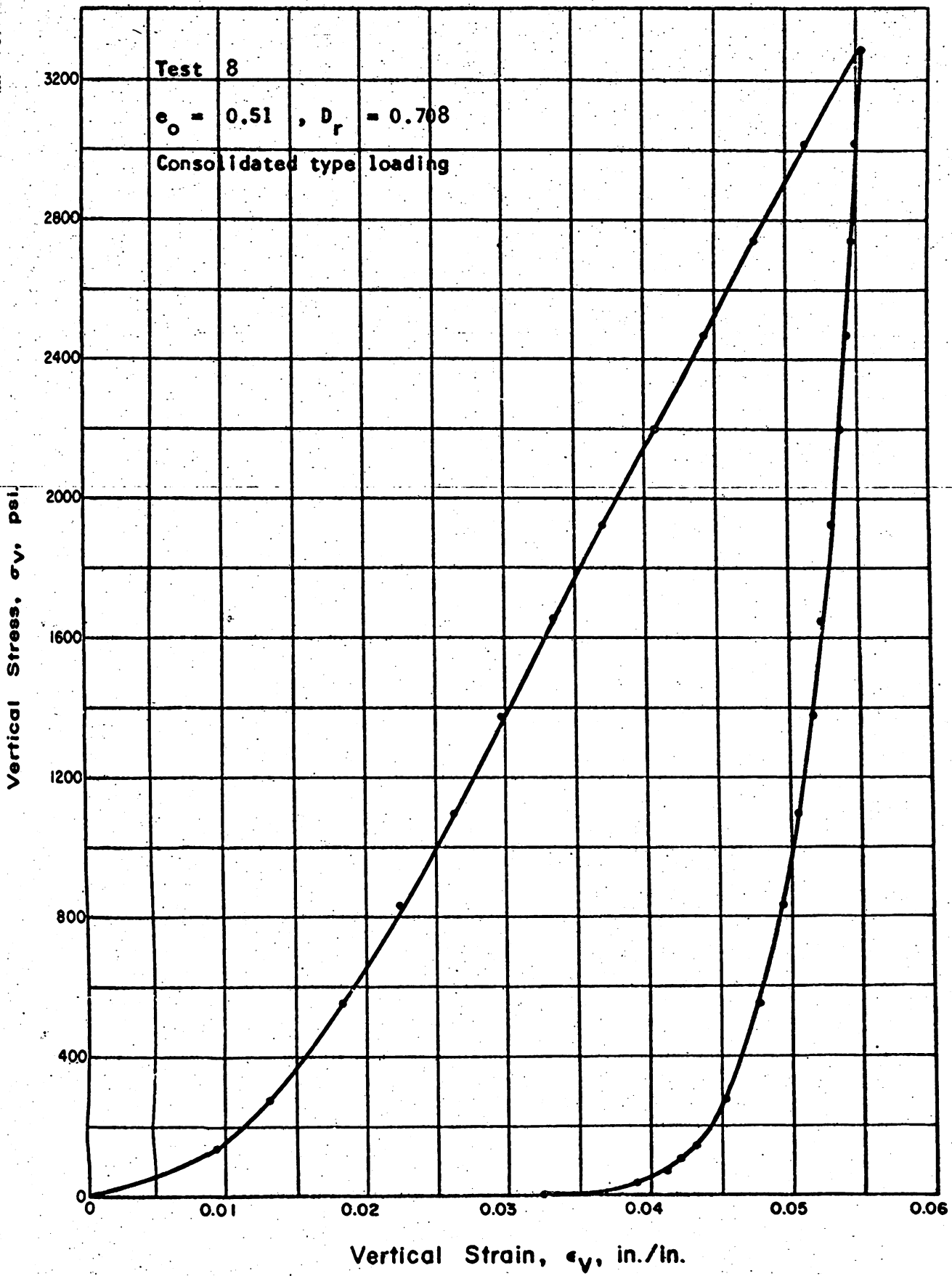

Fig. 5.45 STRESS STRAIN CURVE FOR WABASH RIVER SAND IN ONE-DIMENSIONAL COMPRESSION

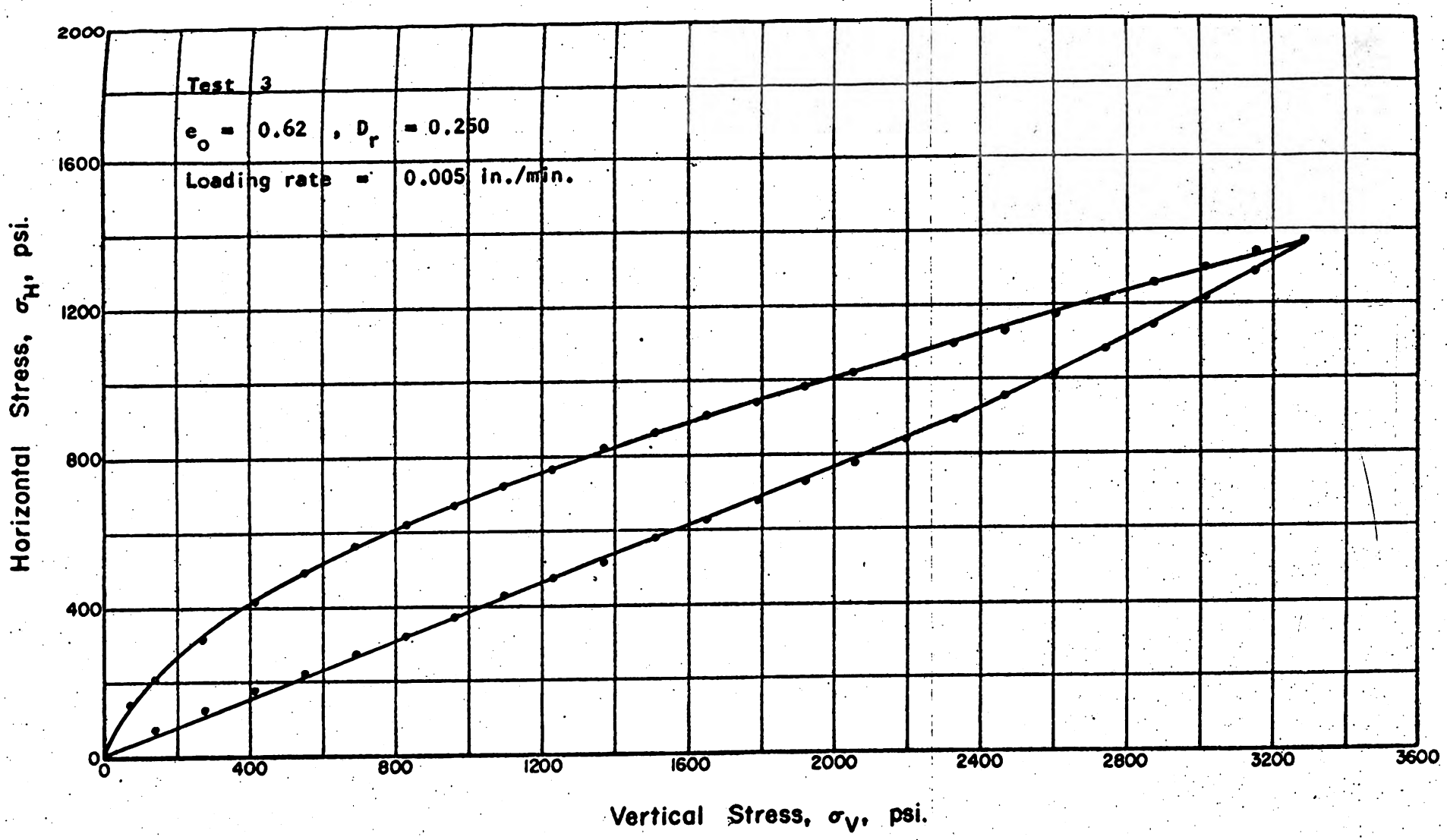

Fig. 5.46 HORIZONTAL STRESS VS. VERTICAL STRESS FOR THE FIRST CYCLE OF LOADING OF MINNESOTA SAND IN ONE-DIMENSIONAL COMPRESSION

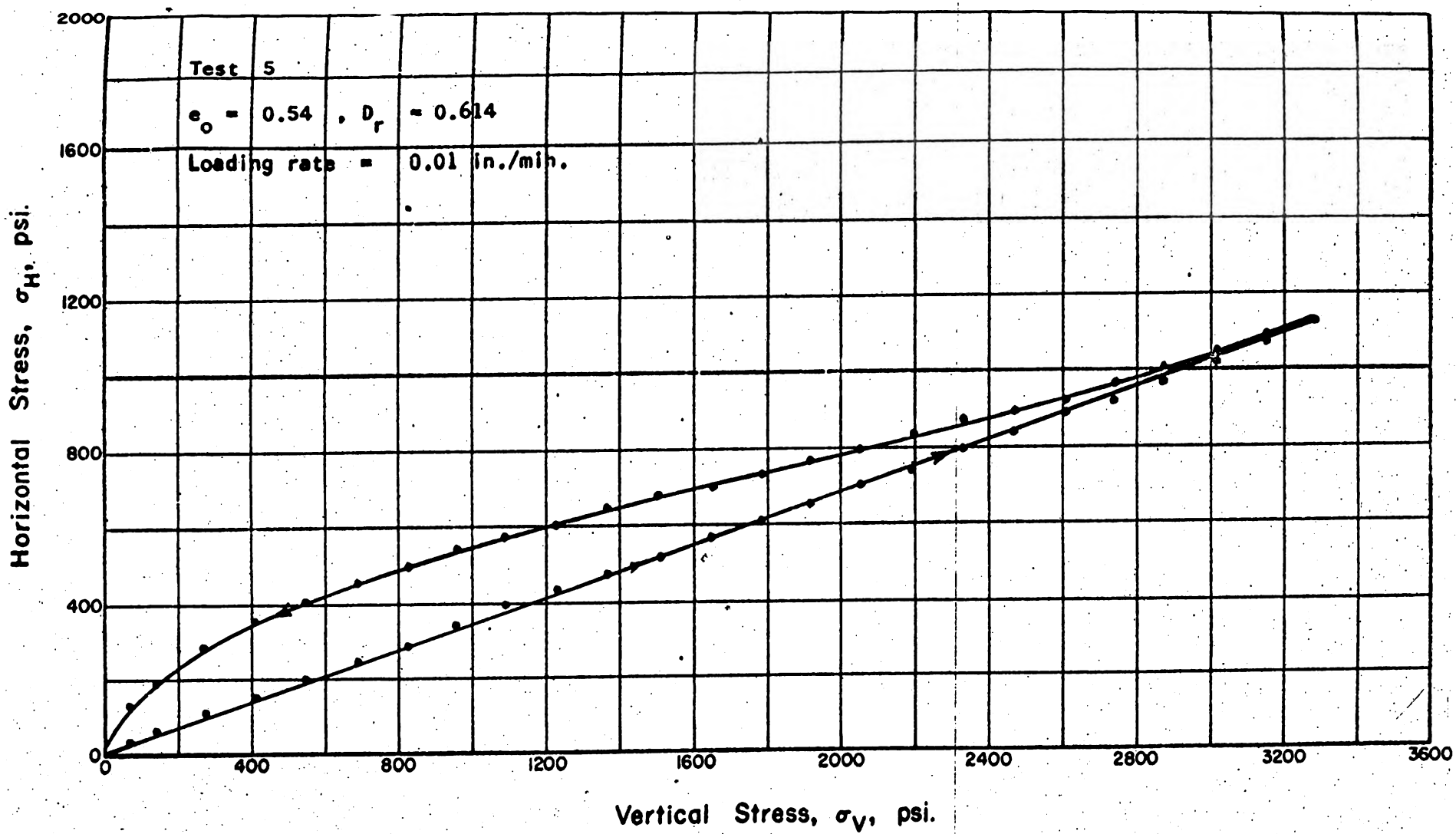

Fig. 5.48 HORIZONTAL STRESS VS. VERTICAL STRESS FOR THE FIRST CYCLE OF LOADING OF MINNESOTA SAND IN ONE-DIMENSIONAL COMPRESSION

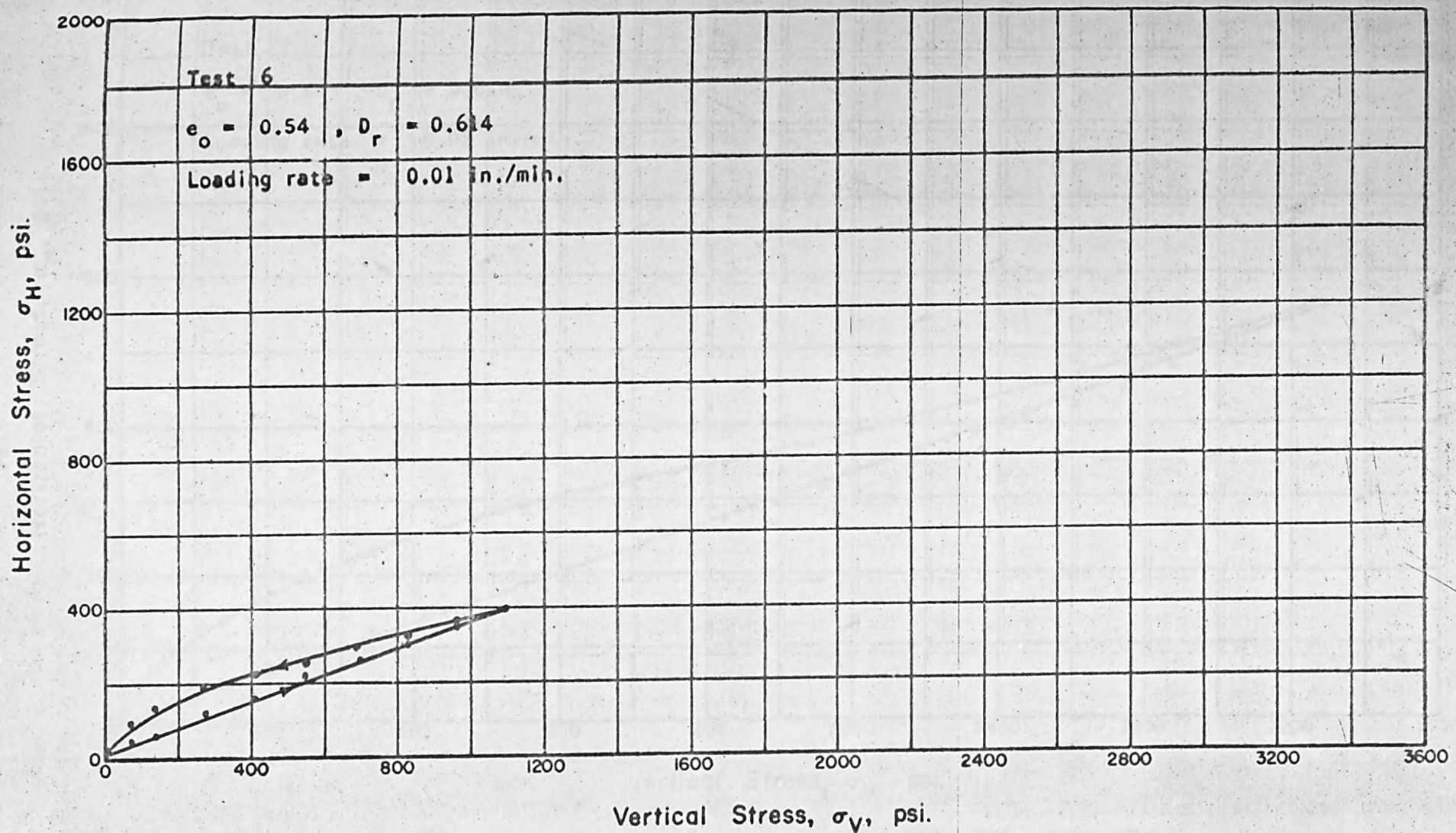

Fig. 5.49 HORIZONTAL STRESS VS. VERTICAL STRESS FOR THE FIRST CYCLE OF LOADING OF MINNESOTA SAND IN ONE-DIMENSIONAL COMPRESSION

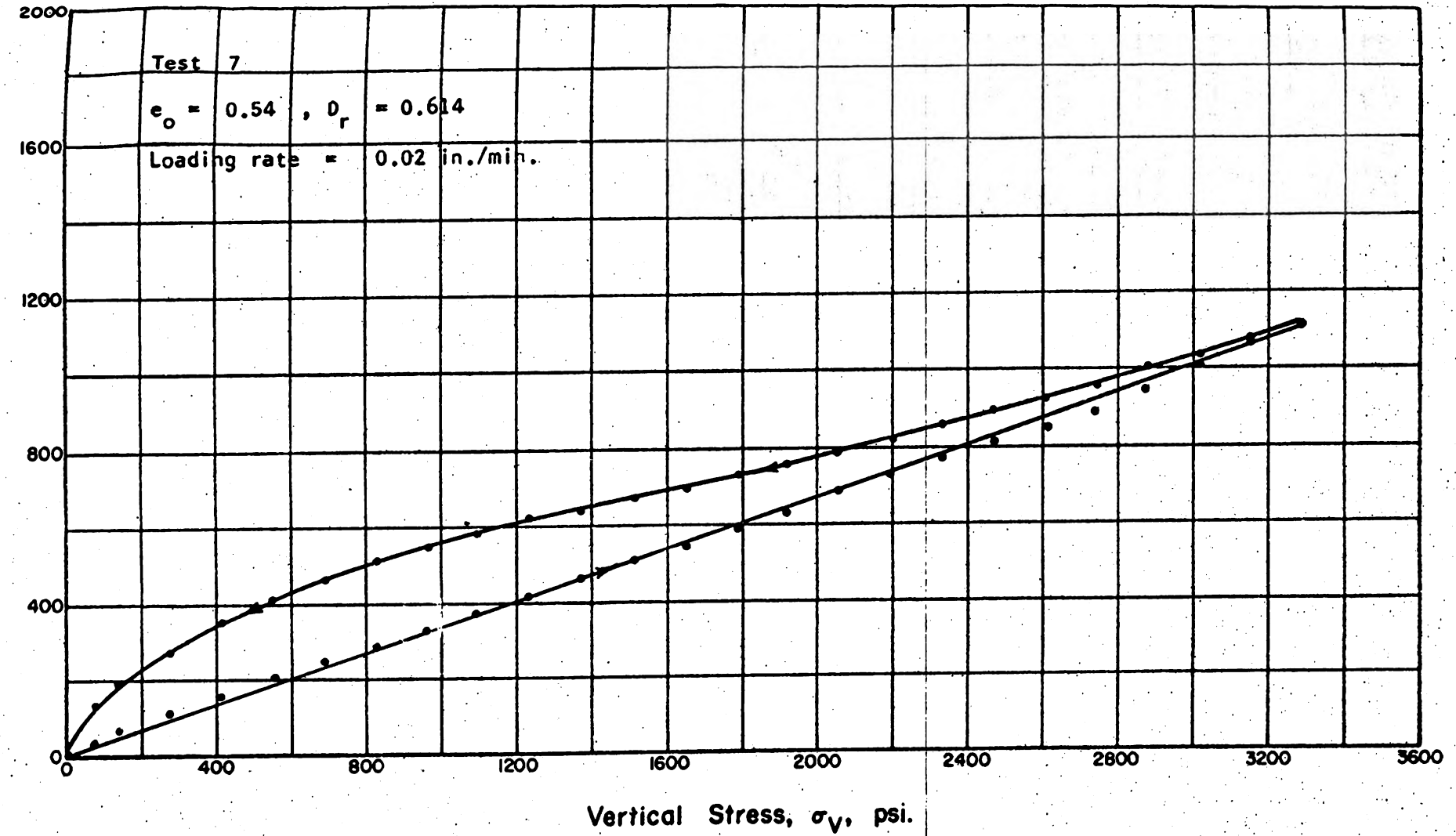

Fig. 5.50 HORIZONTAL STRESS VS. VERTICAL STRESS FOR THE FIRST CYCLE OF LOADING OF MINNESOTA SAND IN ONE-DIMENSIONAL COMPRESSION

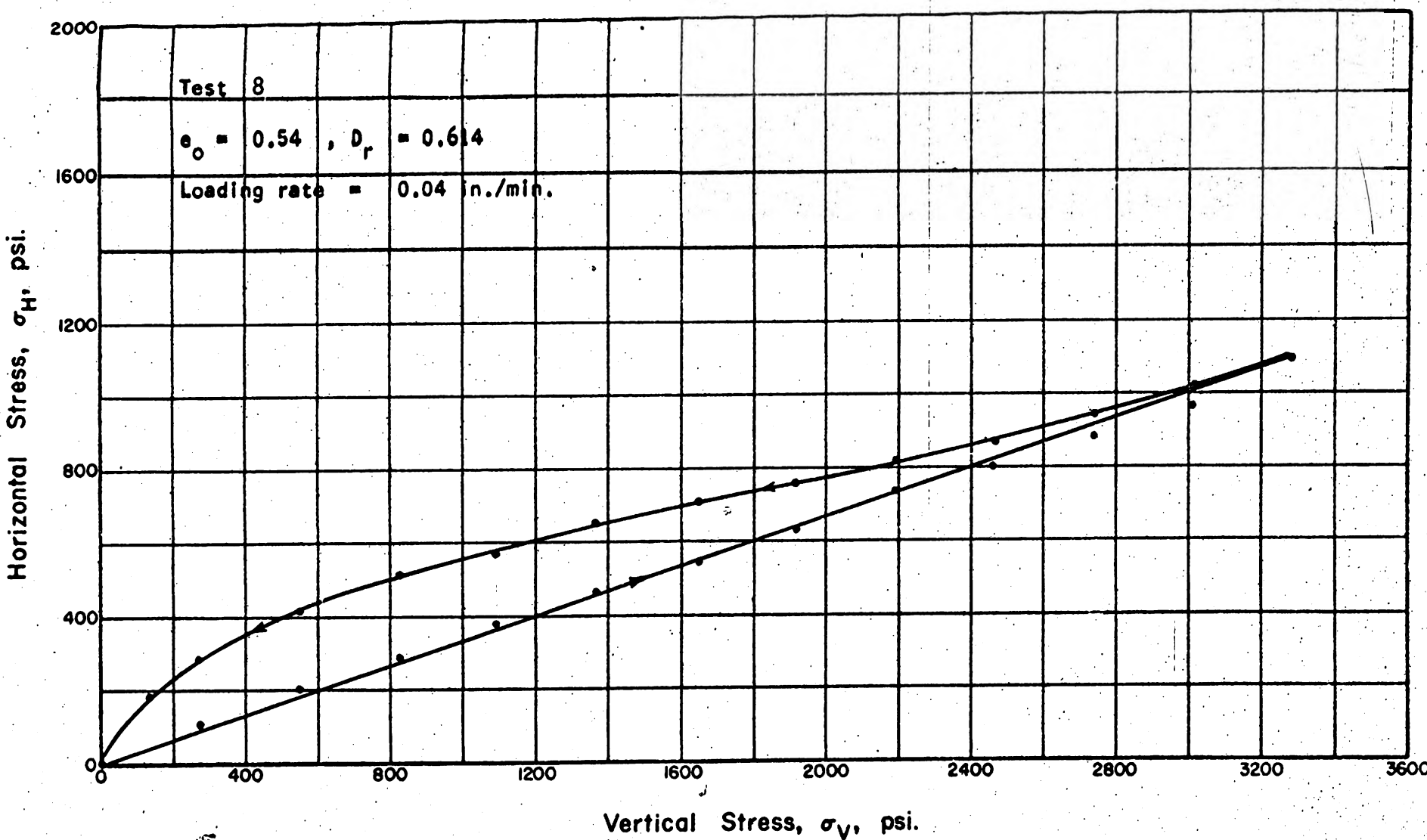

Fig. 5.51 HORIZONTAL STRESS VS. VERTICAL STRESS FOR THE FIRST CYCLE OF LOADING OF MINNESOTA SAND IN ONE-DIMENSIONAL COMPRESSION

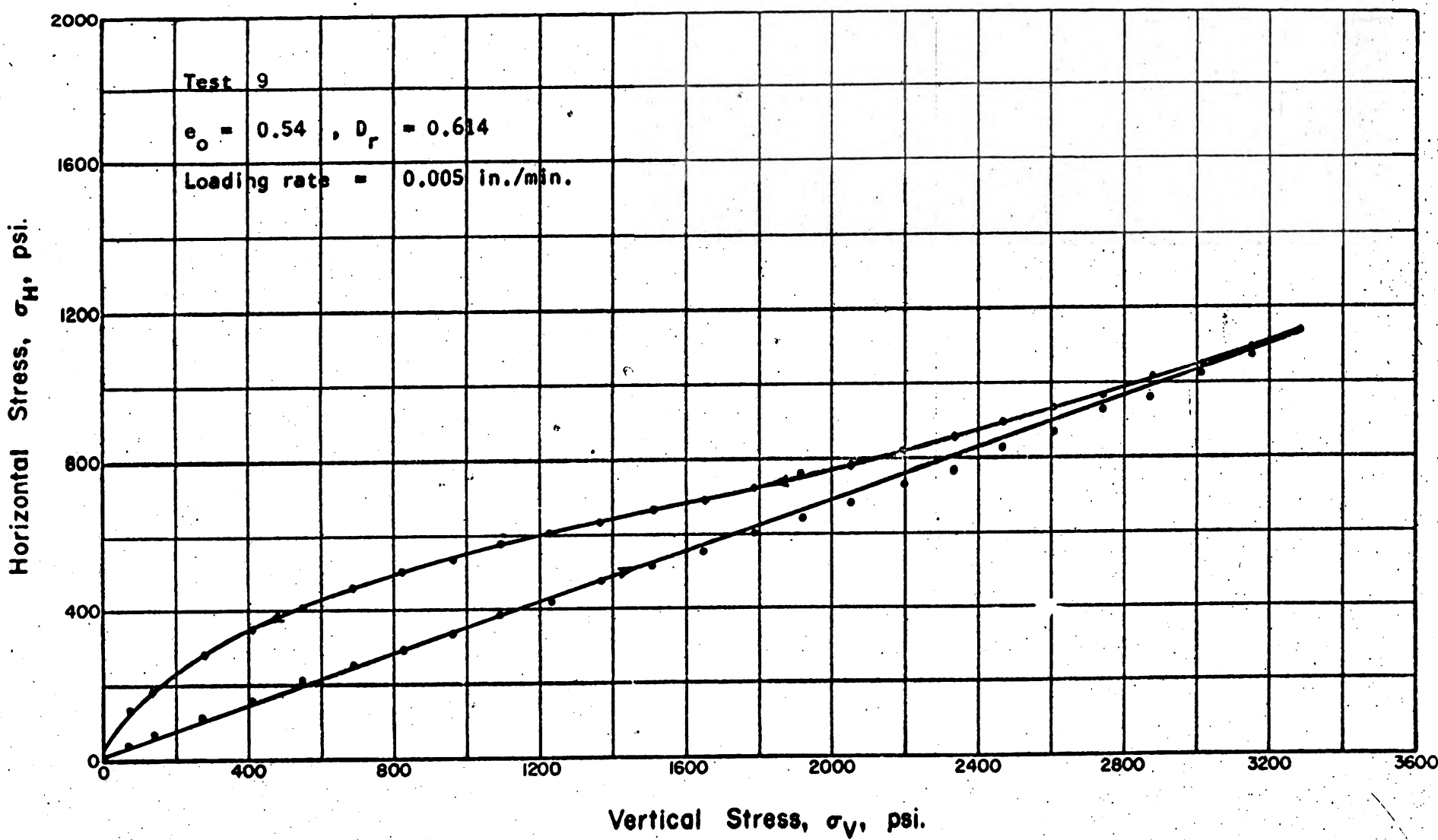

Fig. 5.52 HORIZONTAL STRESS VS. VERTICAL STRESS FOR THE FIRST CYCLE OF LOADING OF MINNESOTA SAND IN ONE-DIMENSIONAL COMPRESSION

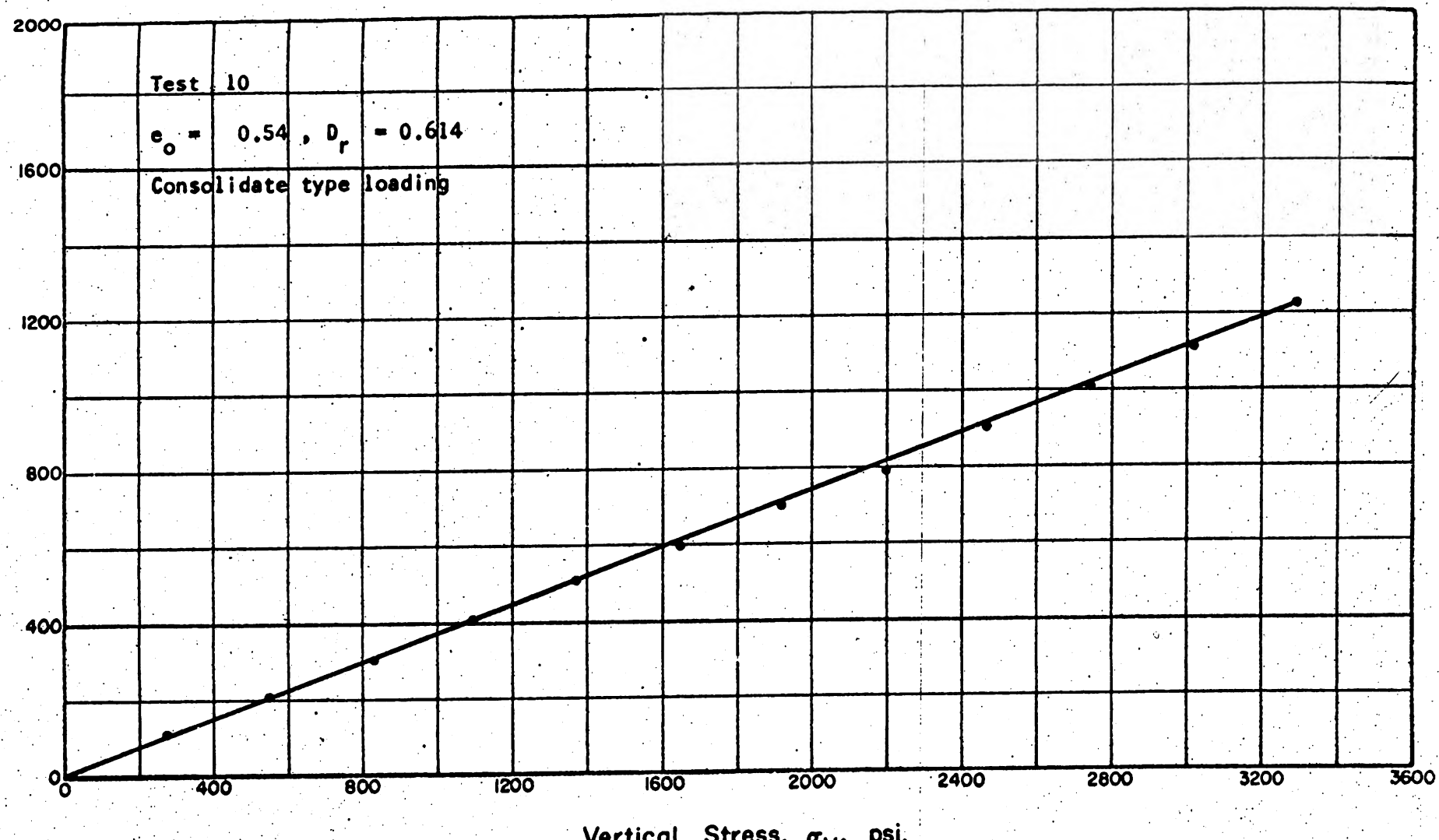

Fig. 5.53 HORIZONTAL STRESS VS. VERTICAL STRESS FOR THE FIRST CYCLE OF LOADING OF MINNESOTA SAND IN ONE-DIMENSIONAL COMPRESSION

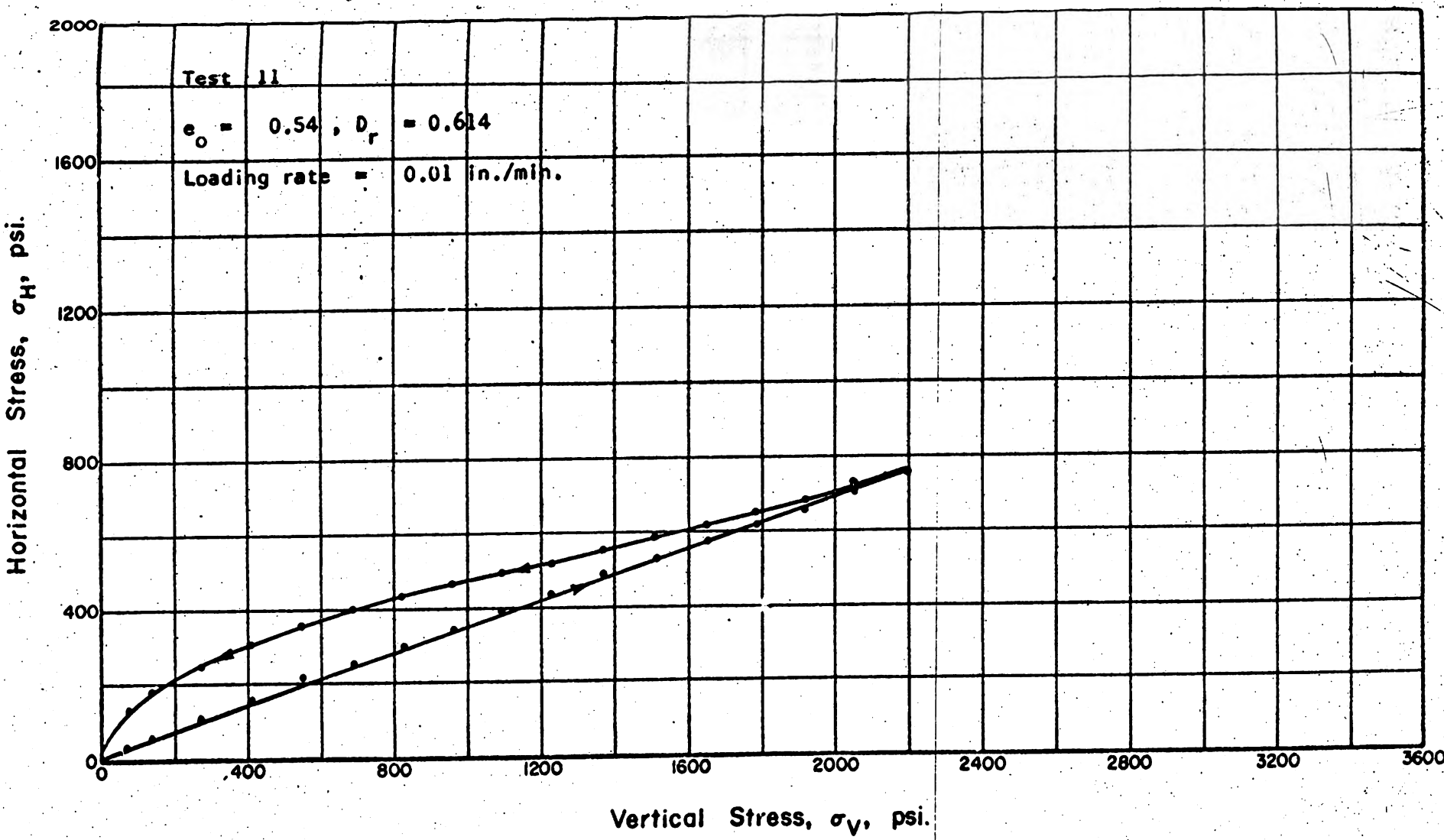

Fig. 5.54 HORIZONTAL STRESS VS. VERTICAL STRESS FOR THE FIRST CYCLE OF LOADING OF MINNESOTA SAND IN ONE-DIMENSIONAL COMPRESSION

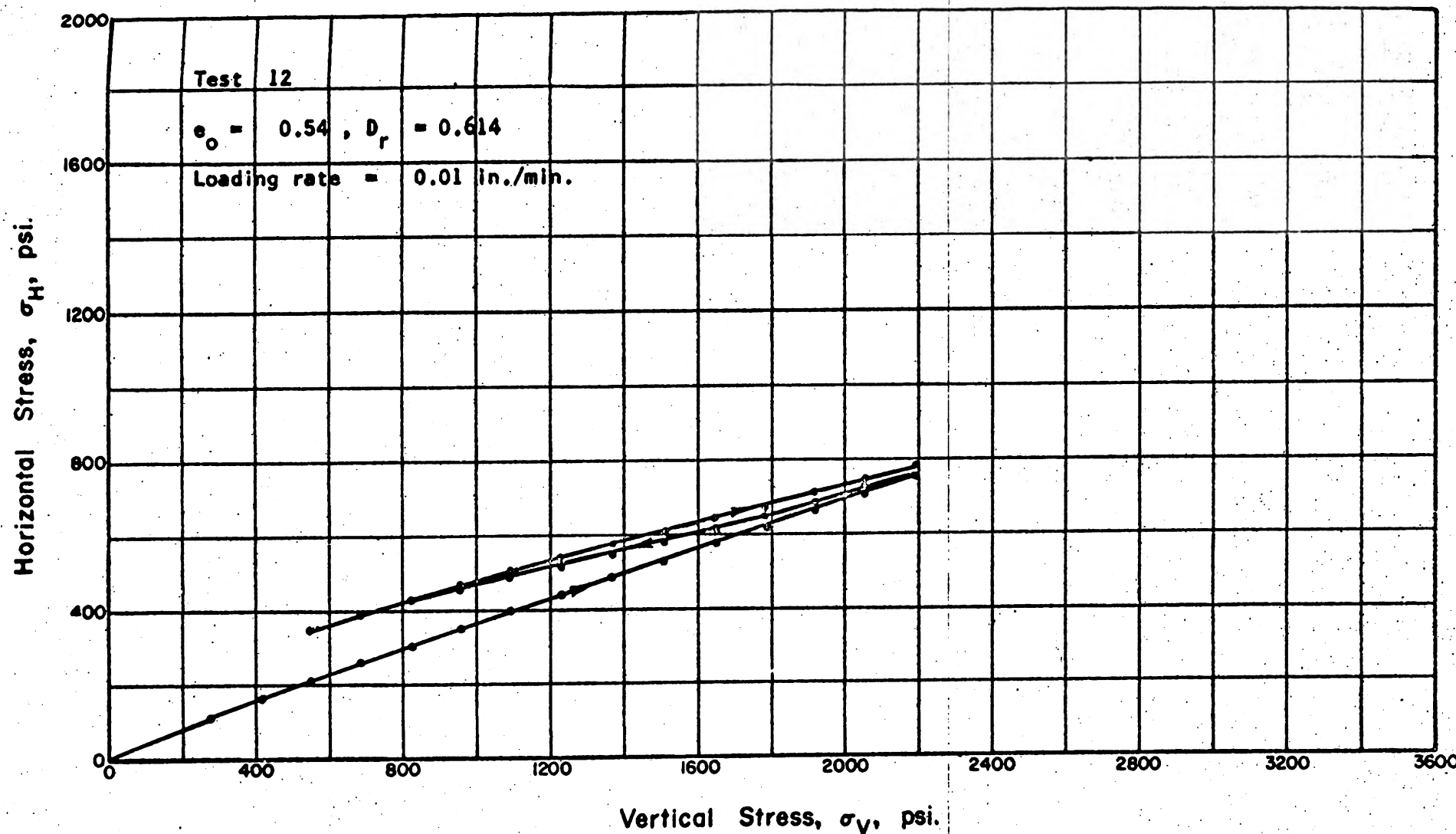

Fig. 5.55 HORIZONTAL STRESS VS. VERTICAL STRESS FOR ONE AND ONE-HALF CYCLES OF LOADING OF MINNESOTA SAND IN ONE-DIMENSIONAL COMPRESSION

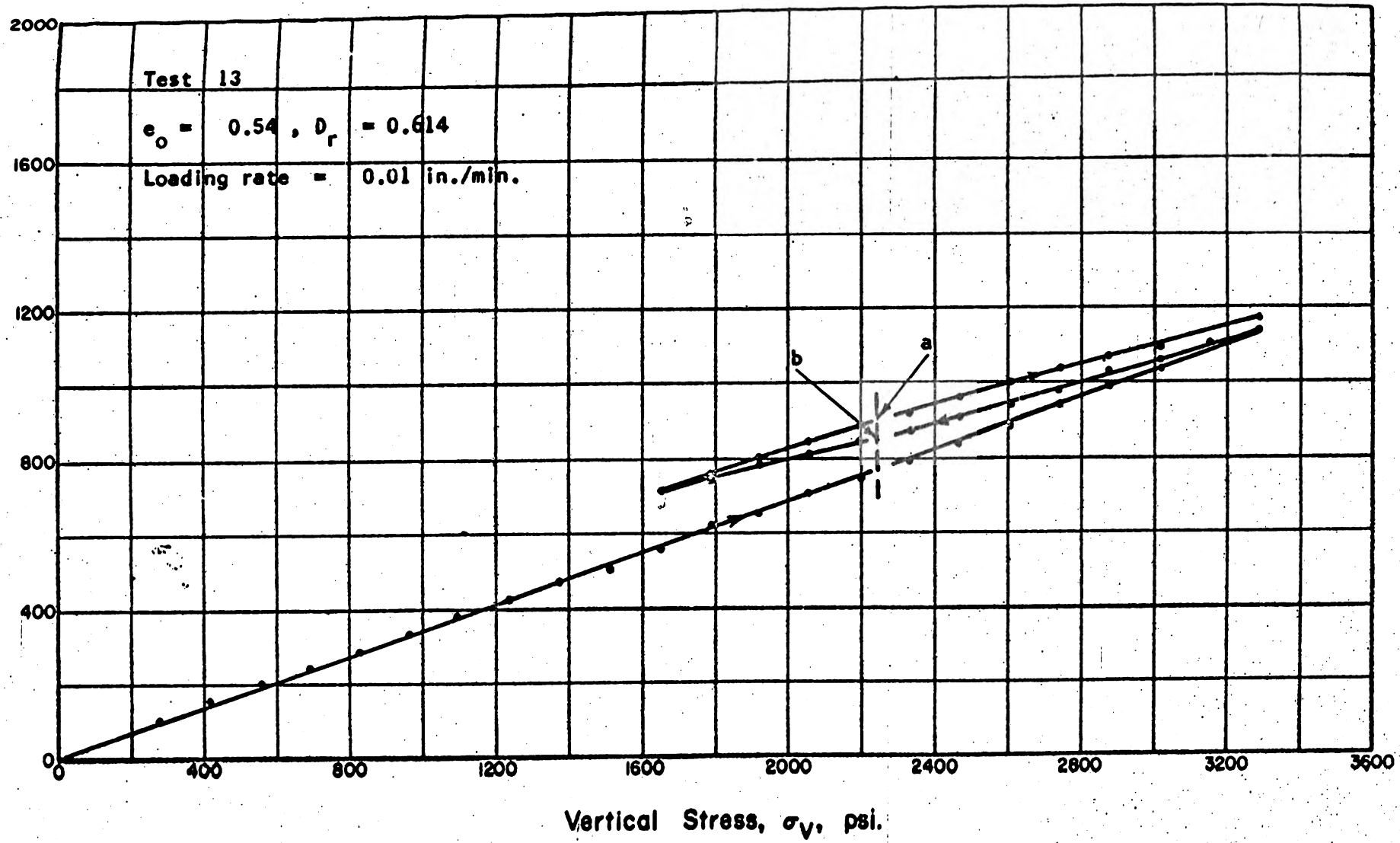

Fig. 5.56 HORIZONTAL STRESS VS. VERTICAL STRESS FOR ONE AND ONE-HALF CYCLES OF LOADING OF MINNESOTA SAND IN ONE-DIMENSIONAL COMPRESSION

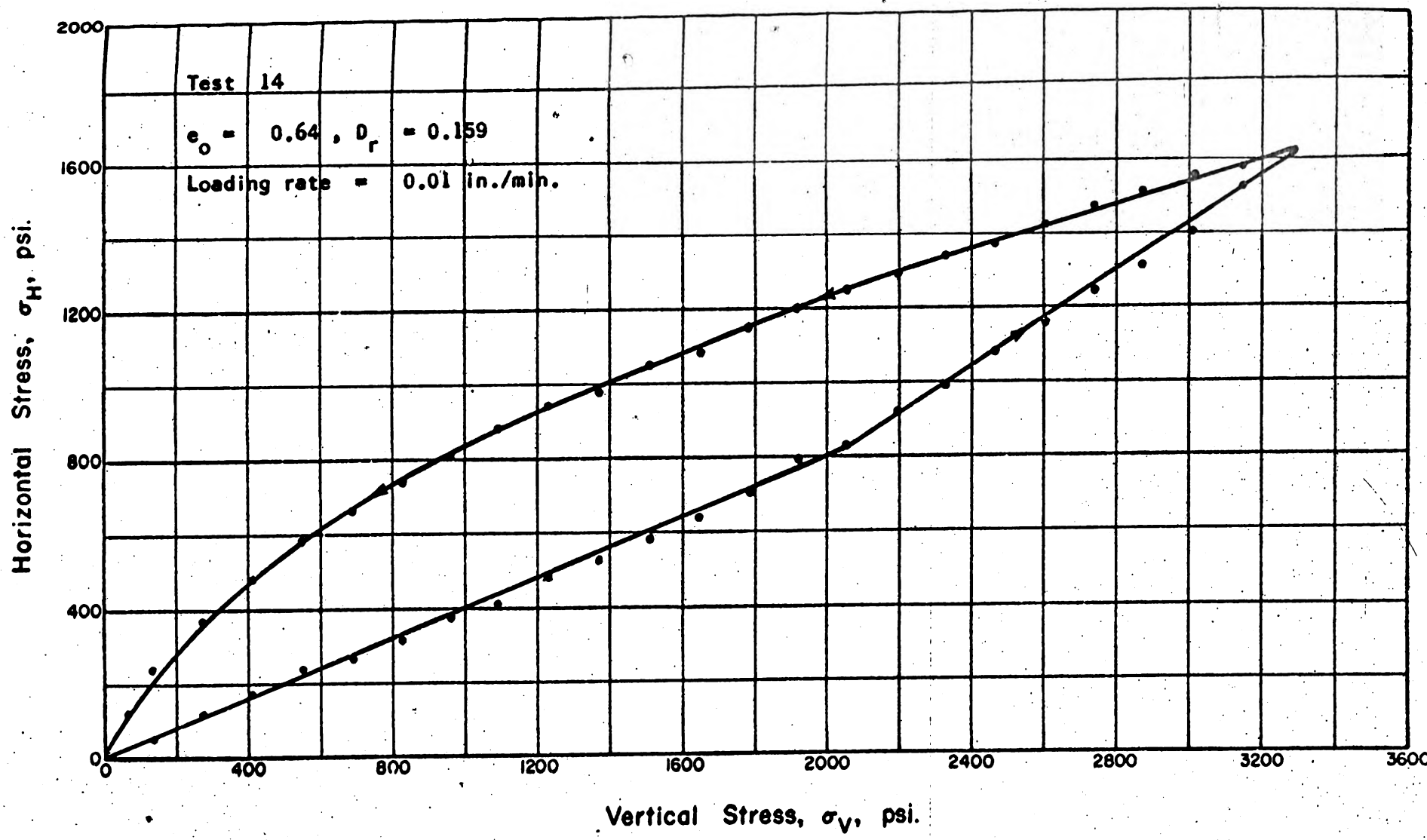

Fig. 5.57 HORIZONTAL STRESS VS. VERTICAL STRESS FOR THE FIRST CYCLE OF LOADING OF MINNESOTA SAND IN ONE-DIMENSIONAL COMPRESSION

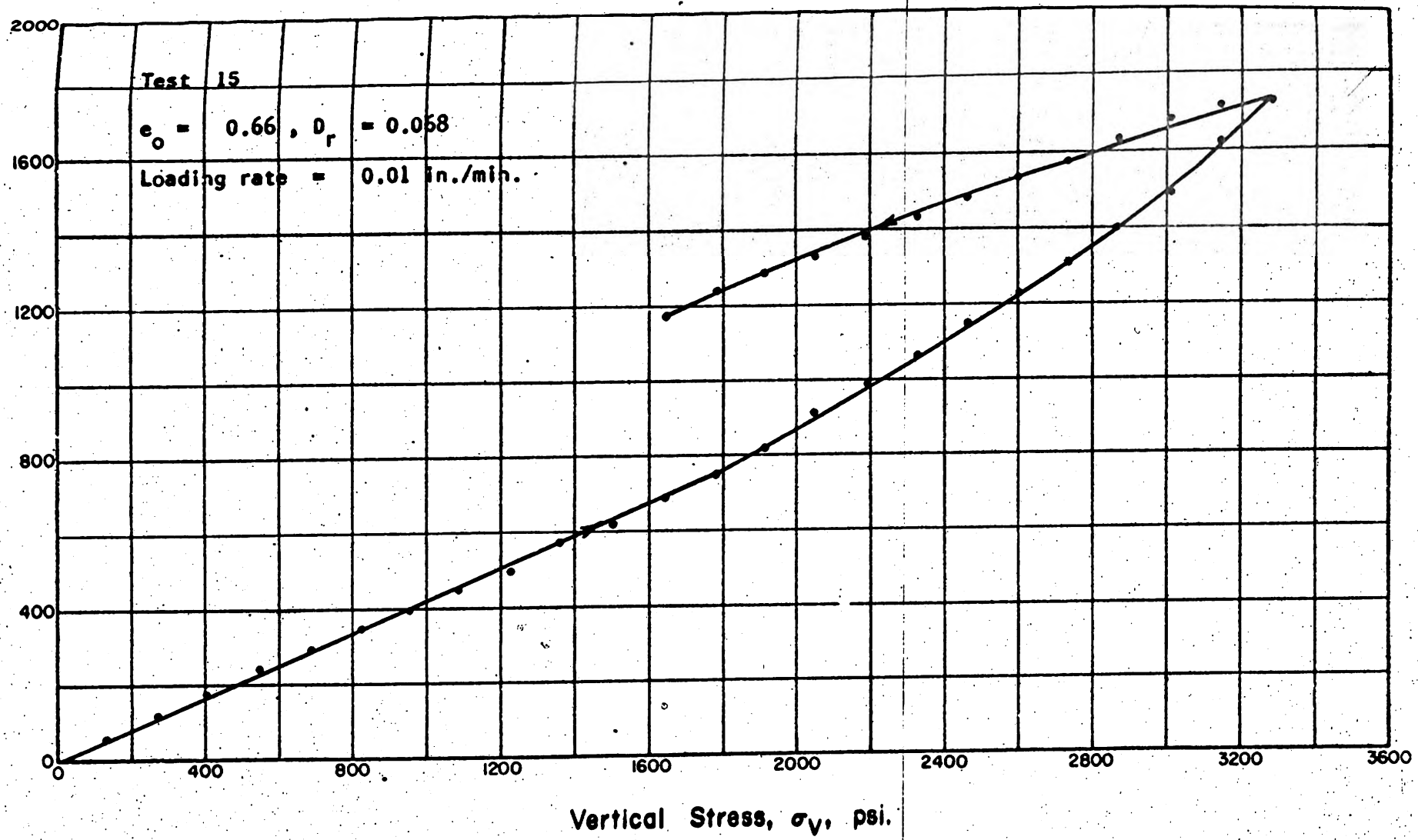

Fig. 5.58 HORIZONTAL STRESS VS. VERTICAL STRESS FOR THE FIRST CYCLE OF LOADING OF MINNESOTA SAND IN ONE-DIMENSIONAL COMPRESSION

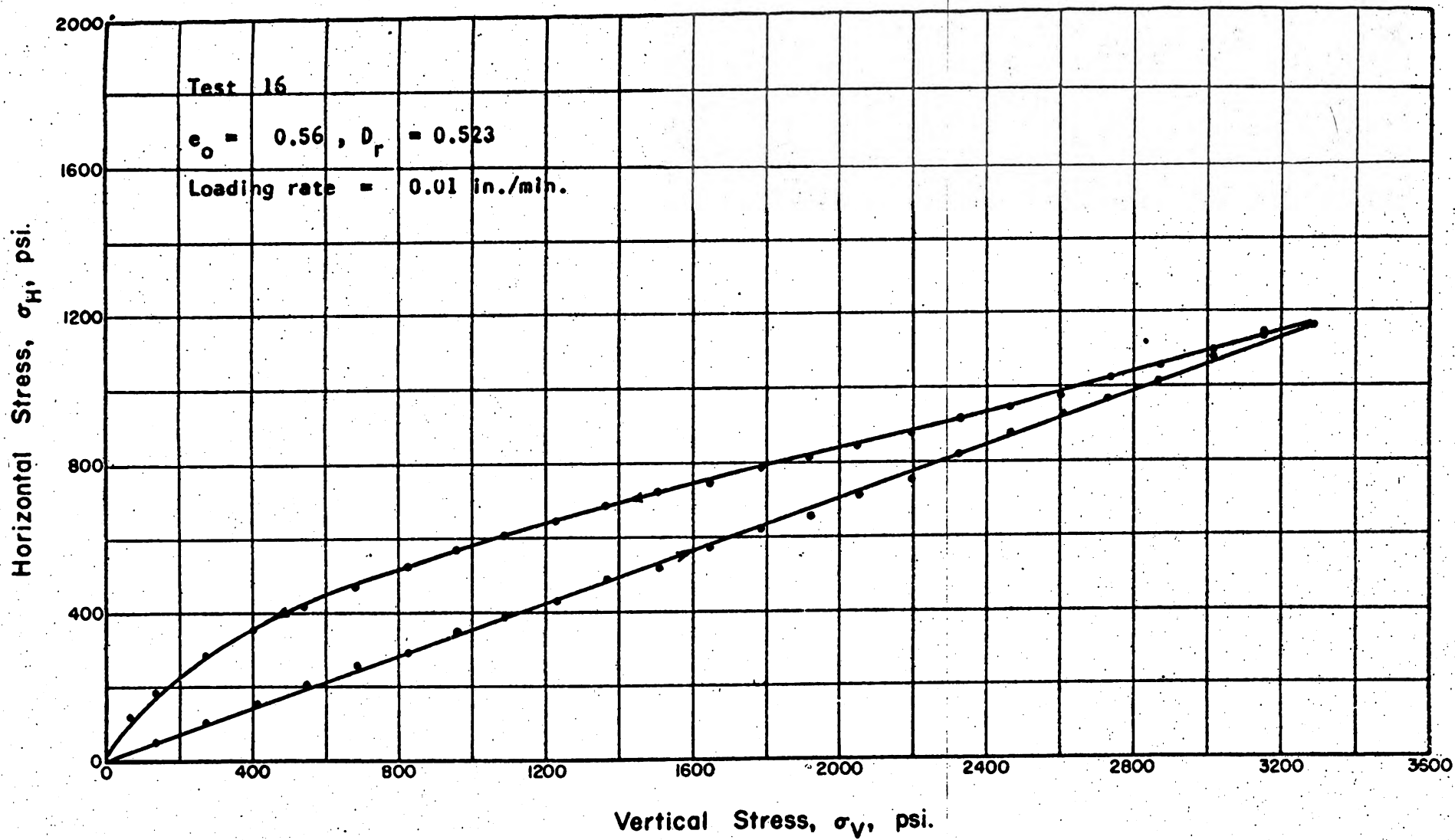

Fig. 5.59 HORIZONTAL STRESS VS. VERTICAL STRESS FOR THE FIRST CYCLE OF LOADING OF MINNESOTA SAND IN ONE-DIMENSIONAL COMPRESSION

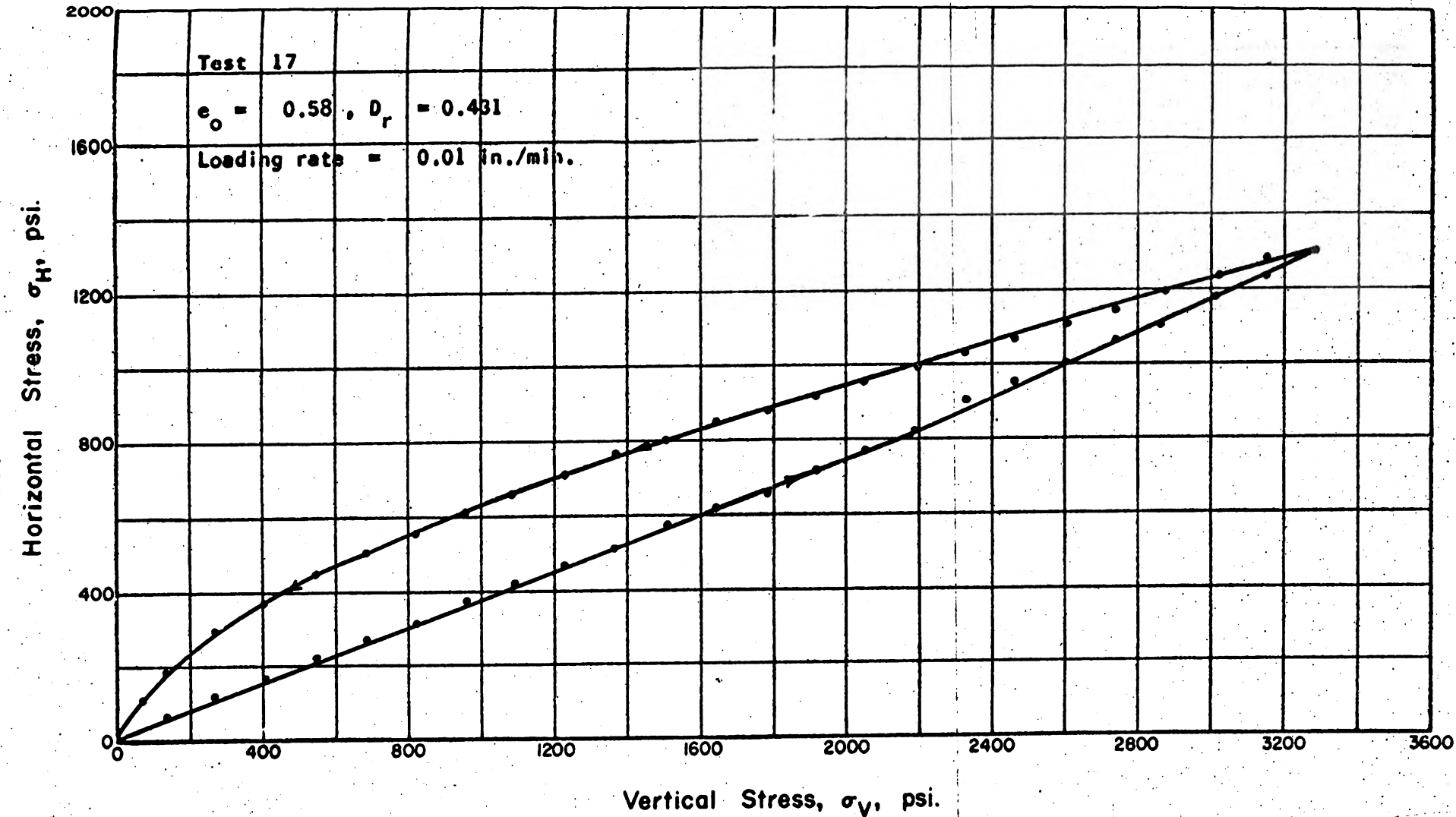

Fig. 5.60 HORIZONTAL STRESS VS. VERTICAL STRESS FOR THE FIRST CYCLE OF LOADING OF MINNESOTA SAND IN ONE-DIMENSIONAL COMPRESSION

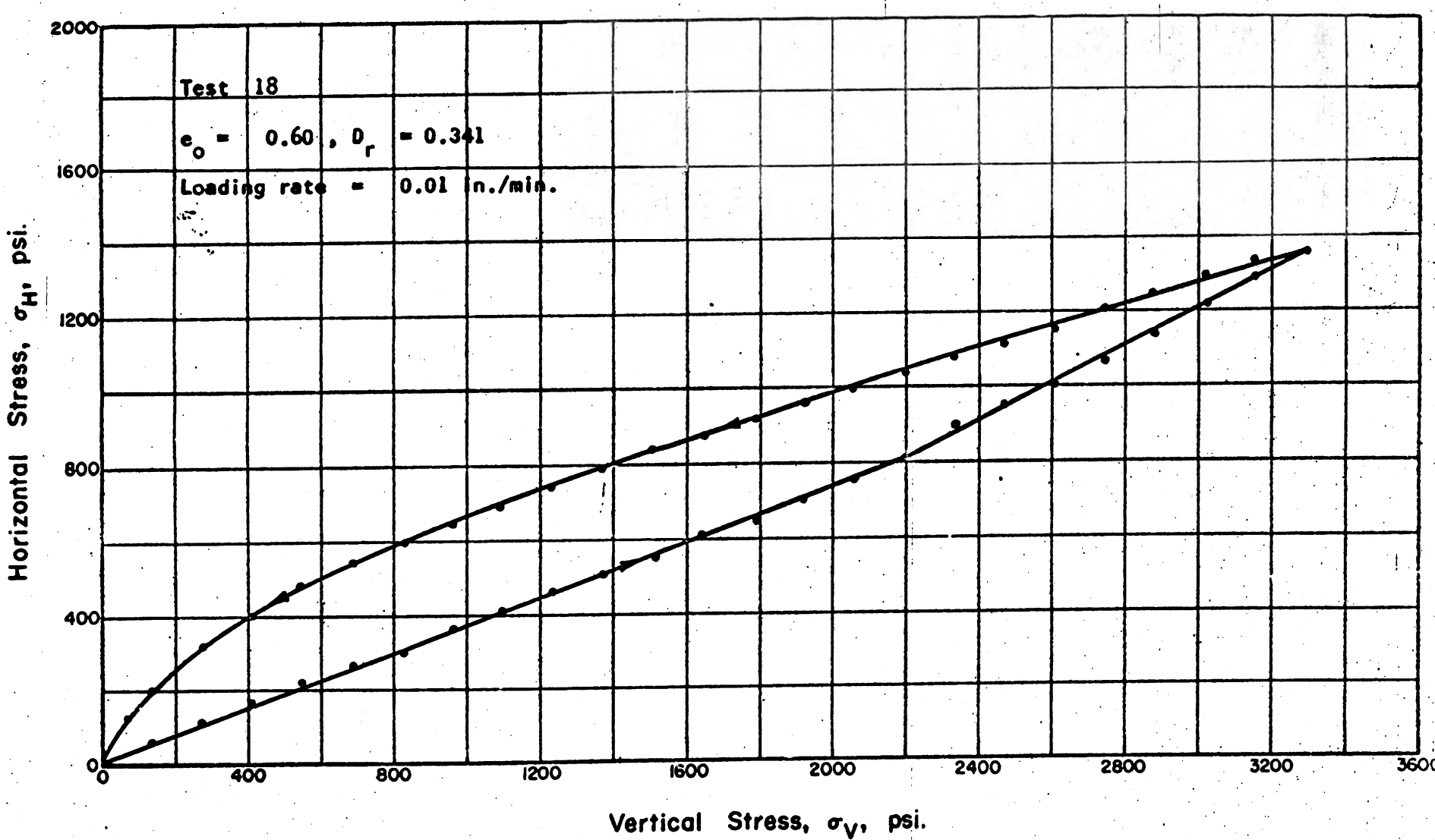

Fig. 5.61 HORIZONTAL STRESS VS. VERTICAL STRESS FOR THE FIRST CYCLE OF LOADING OF MINNESOTA SAND IN ONE-DIMENSIONAL COMPRESSION

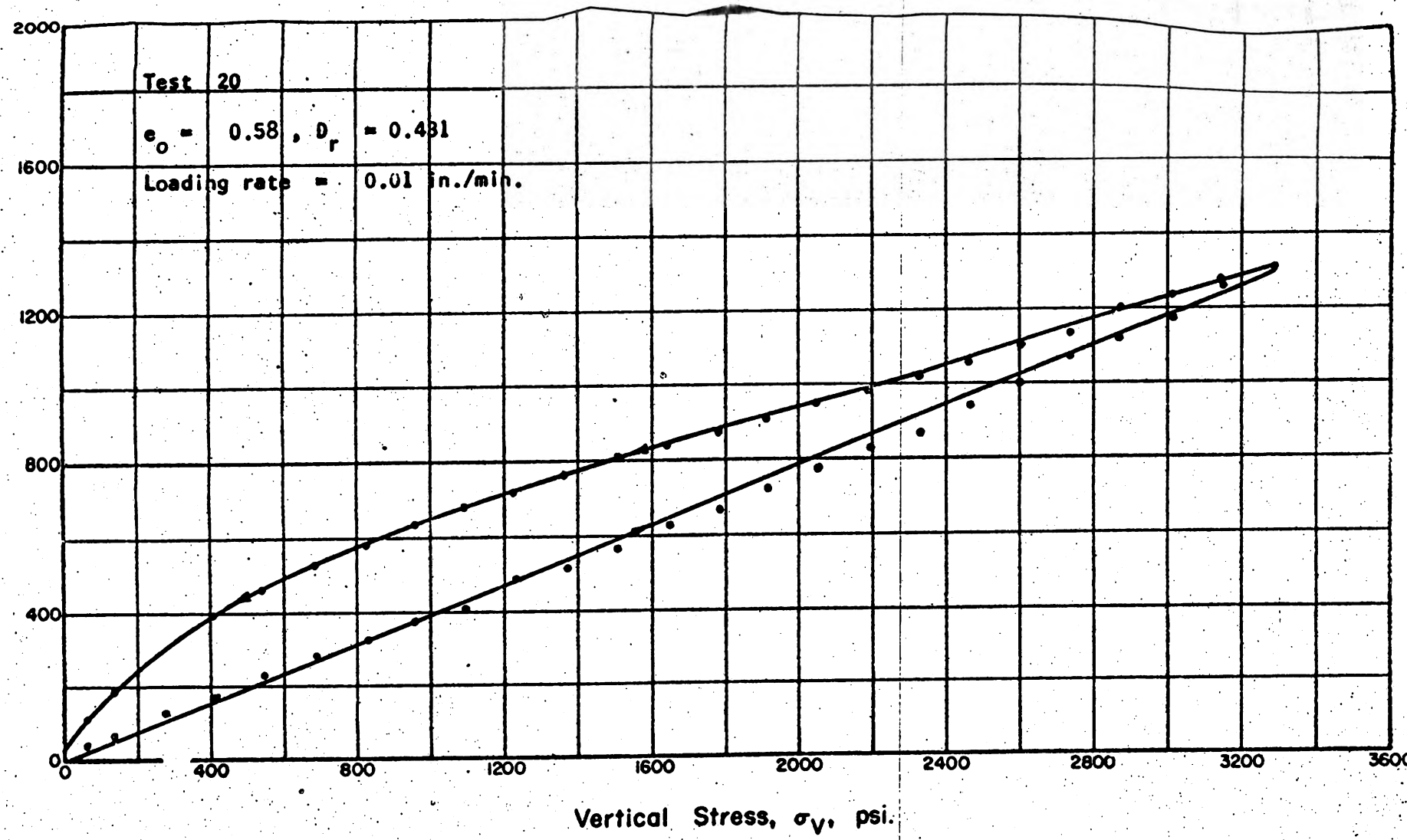

Fig. 5.63 HORIZONTAL STRESS VS. VERTICAL STRESS FOR THE FIRST CYCLE OF LOADING OF MINNESOTA SAND IN ONE-DIMENSIONAL COMPRESSION

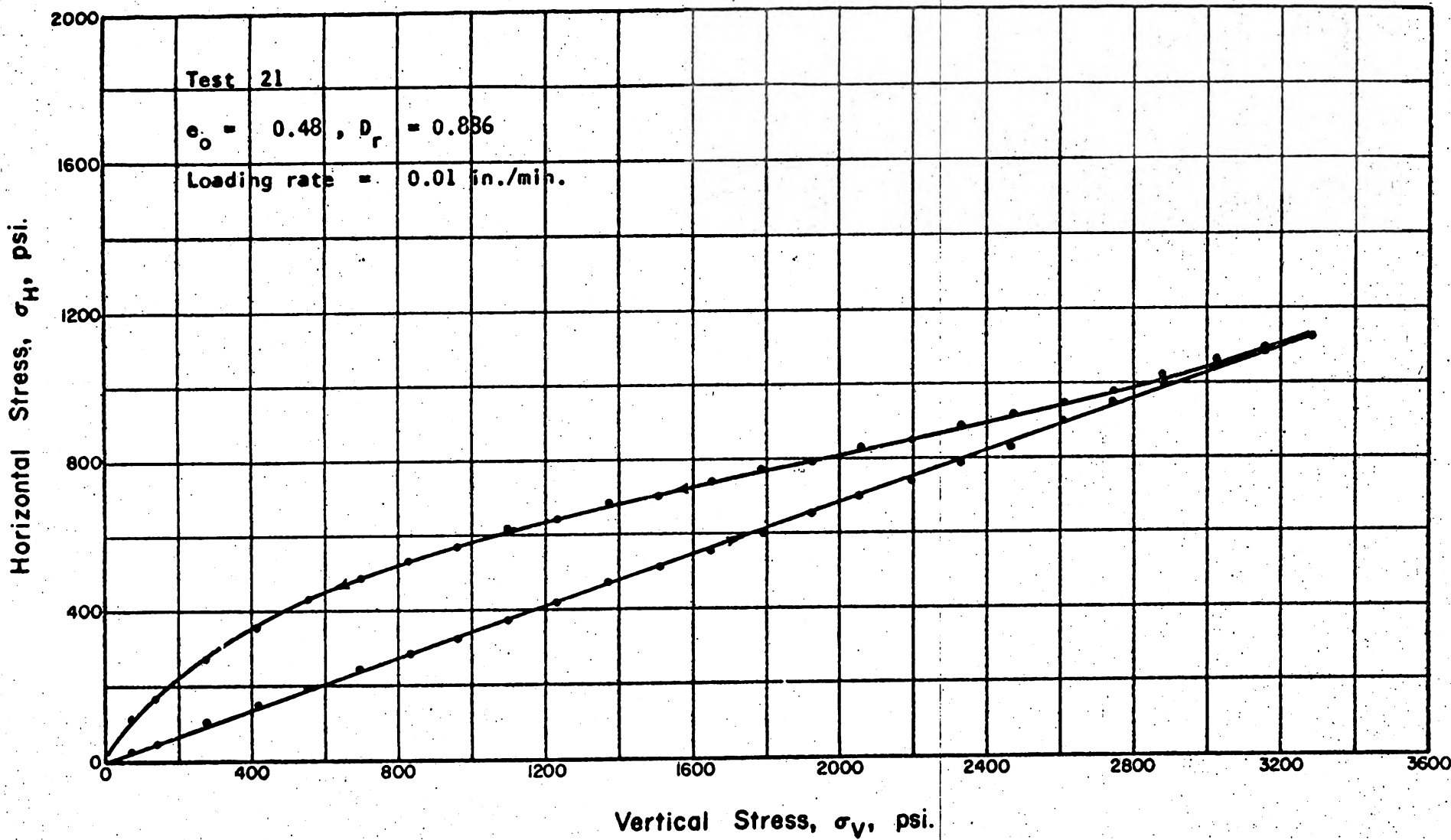

Fig. 5.64 HORIZONTAL STRESS VS. VERTICAL STRESS FOR THE FIRST CYCLE OF LOADING OF MINNESOTA SAND IN ONE-DIMENSIONAL COMPRESSION

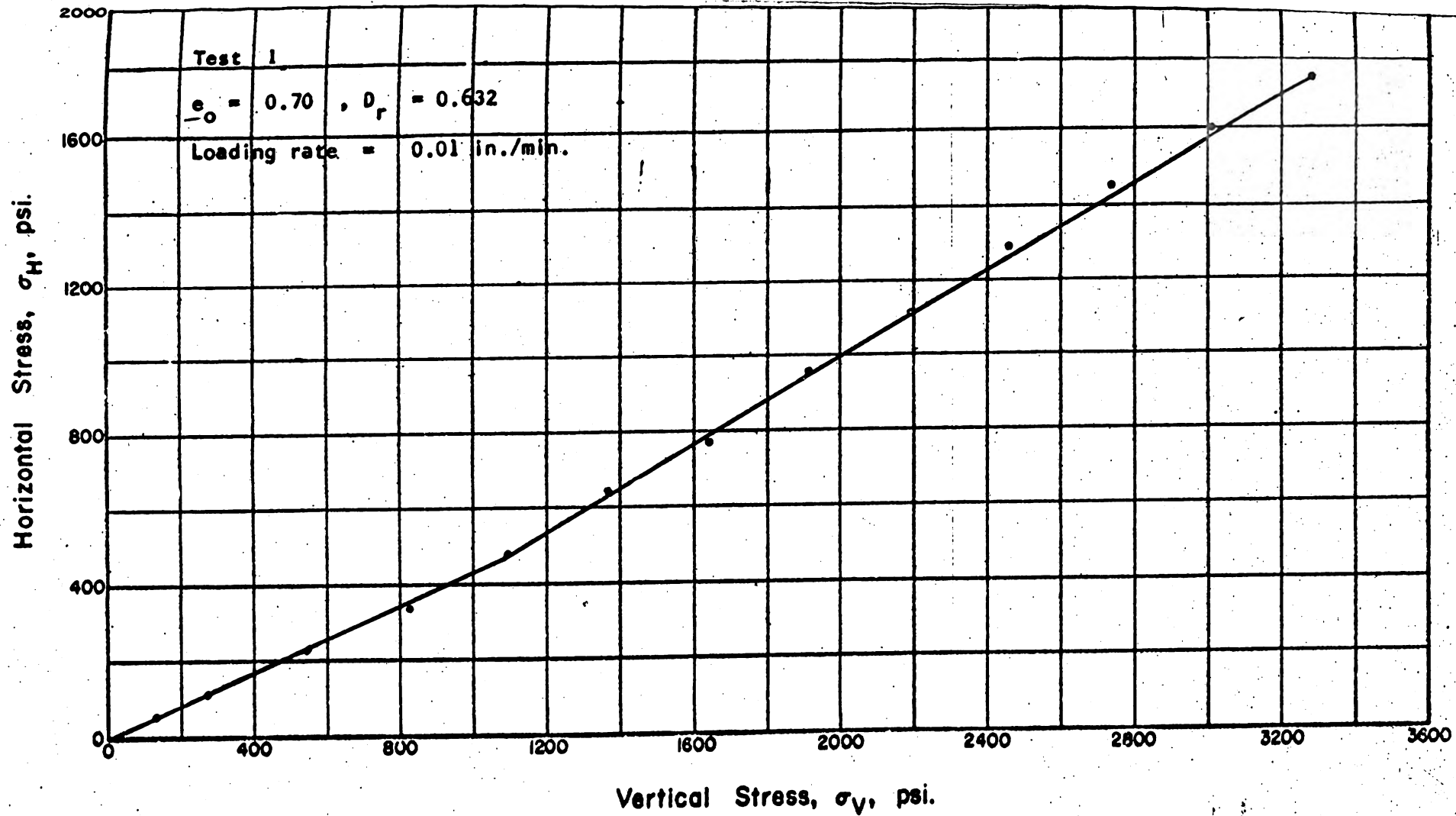

Fig. 5.66 HORIZONTAL STRESS VS. VERTICAL STRESS FOR THE FIRST CYCLE OF LOADING OF PENNSYLVANIA SAND IN ONE-DIMENSIONAL COMPRESSION

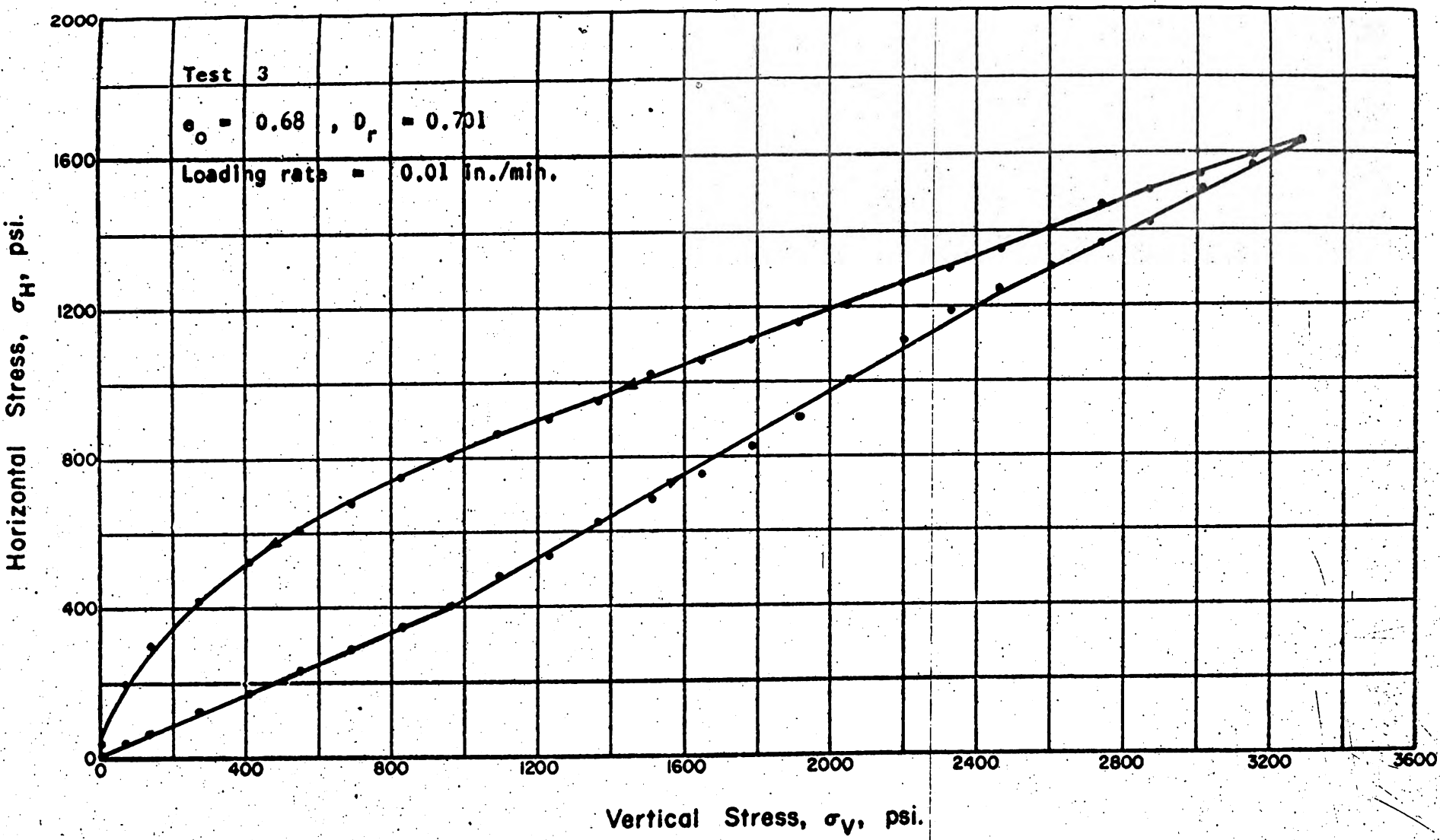

Fig. 5:68 HORIZONTAL STRESS VS. VERTICAL STRESS FOR THE FIRST CYCLE OF LOADING OF PENNSYLVANIA SAND IN ONE-DIMENSIONAL COMPRESSION

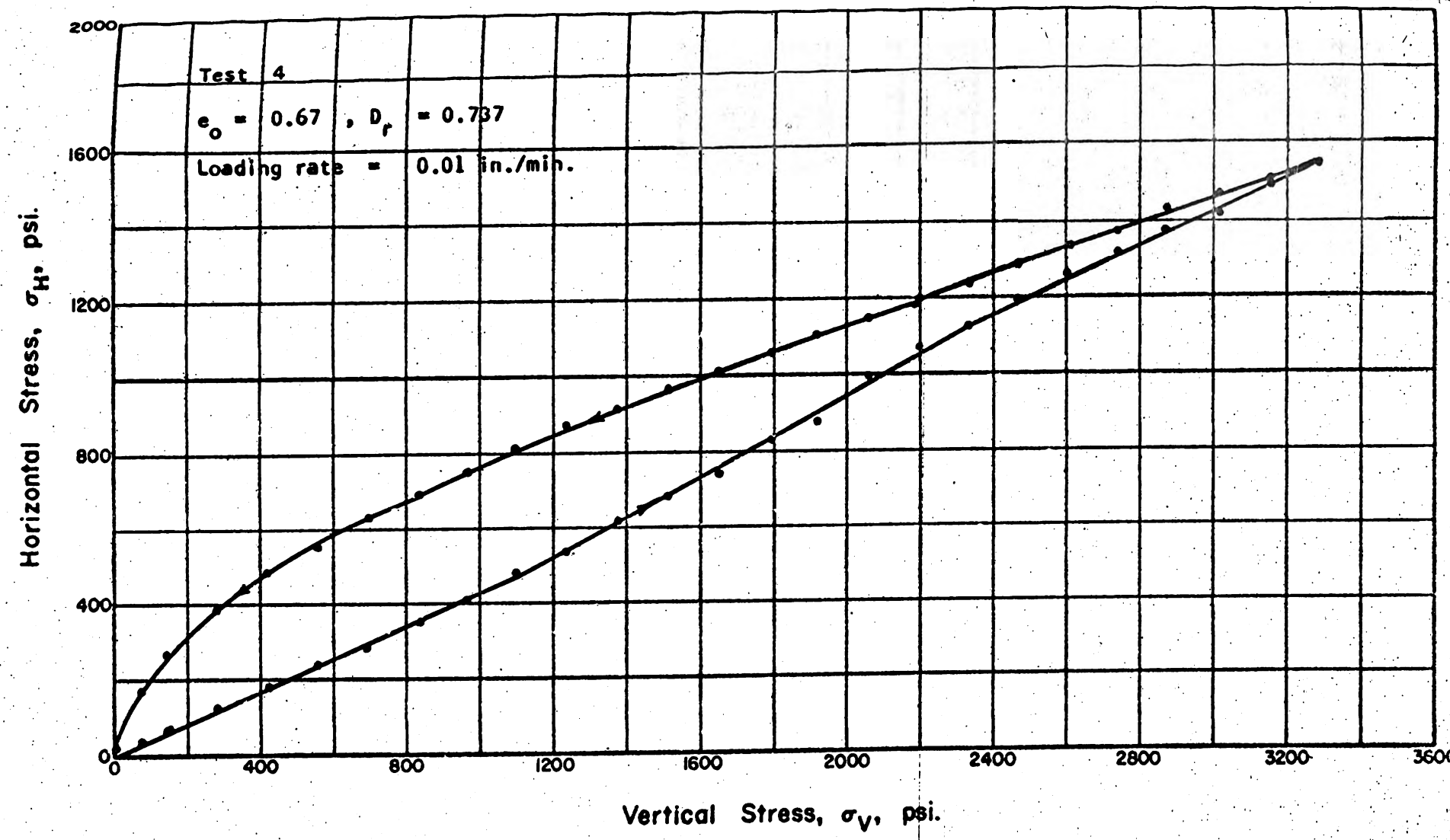

Fig. 5.69 HORIZONTAL STRESS VS. VERTICAL STRESS FOR THE FIRST CYCLE OF LOADING OF PENNSYLVANIA SAND IN ONE-DIMENSIONAL COMPRESSION

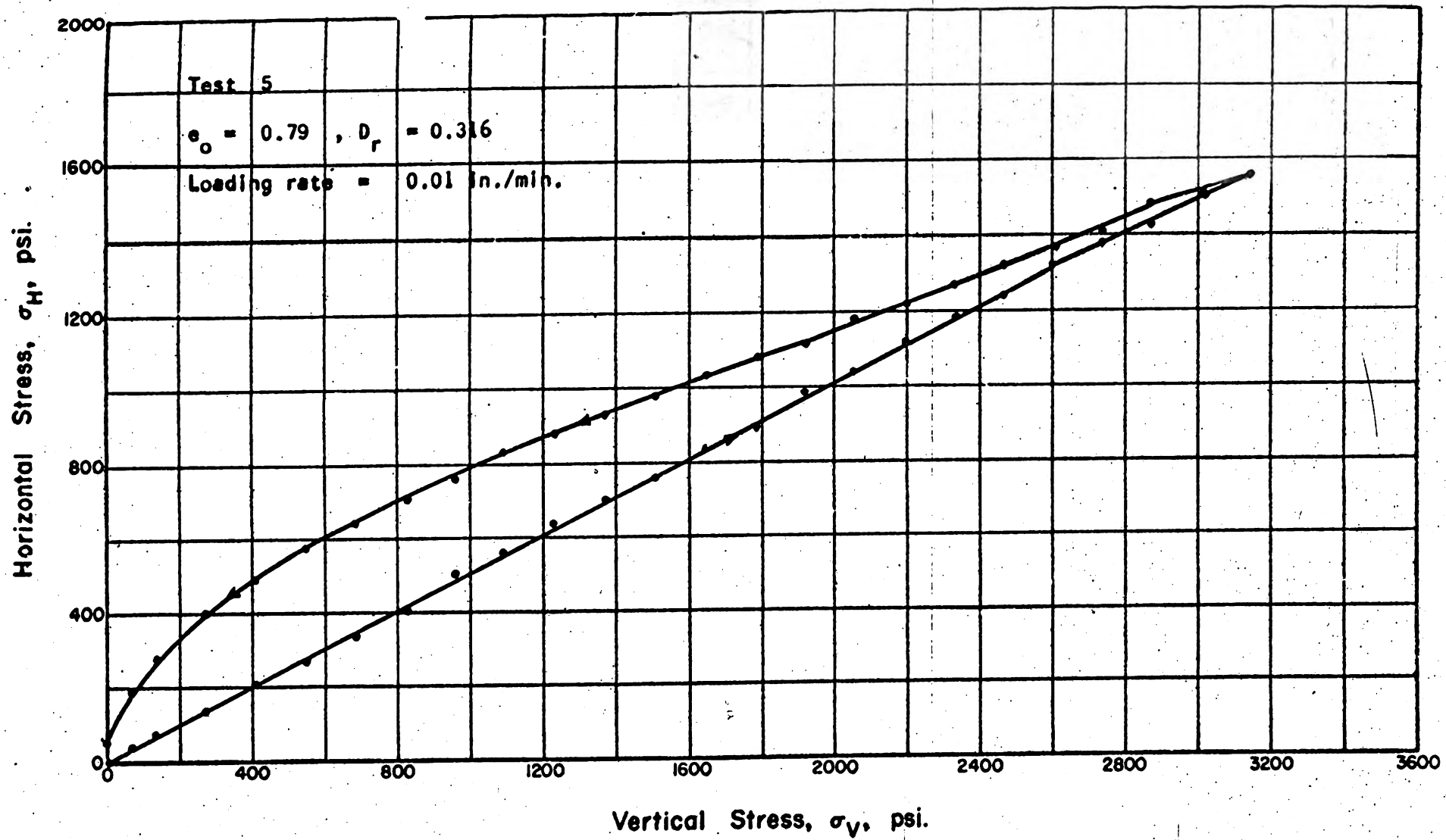

Fig. 5.70 HORIZONTAL STRESS VS. VERTICAL STRESS FOR THE FIRST CYCLE OF LOADING OF PENNSYLVANIA SAND IN ONE-DIMENSIONAL COMPRESSION

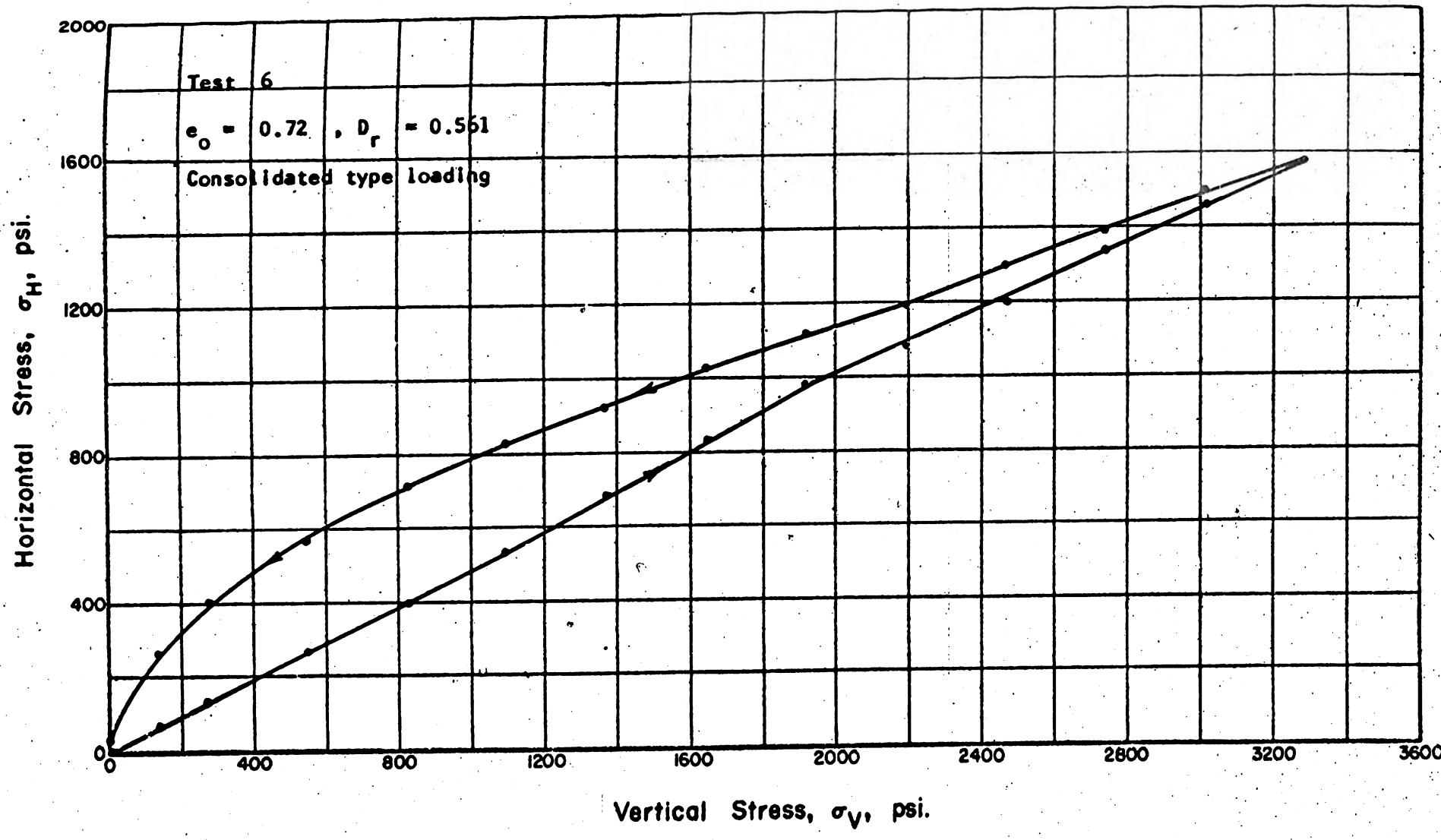

Fig. 5.71 HORIZONTAL STRESS VS. VERTICAL STRESS FOR THE FIRST CYCLE OF LOADING OF PENNSYLVANIA SAND IN ONE-DIMENSIONAL COMPRESSION

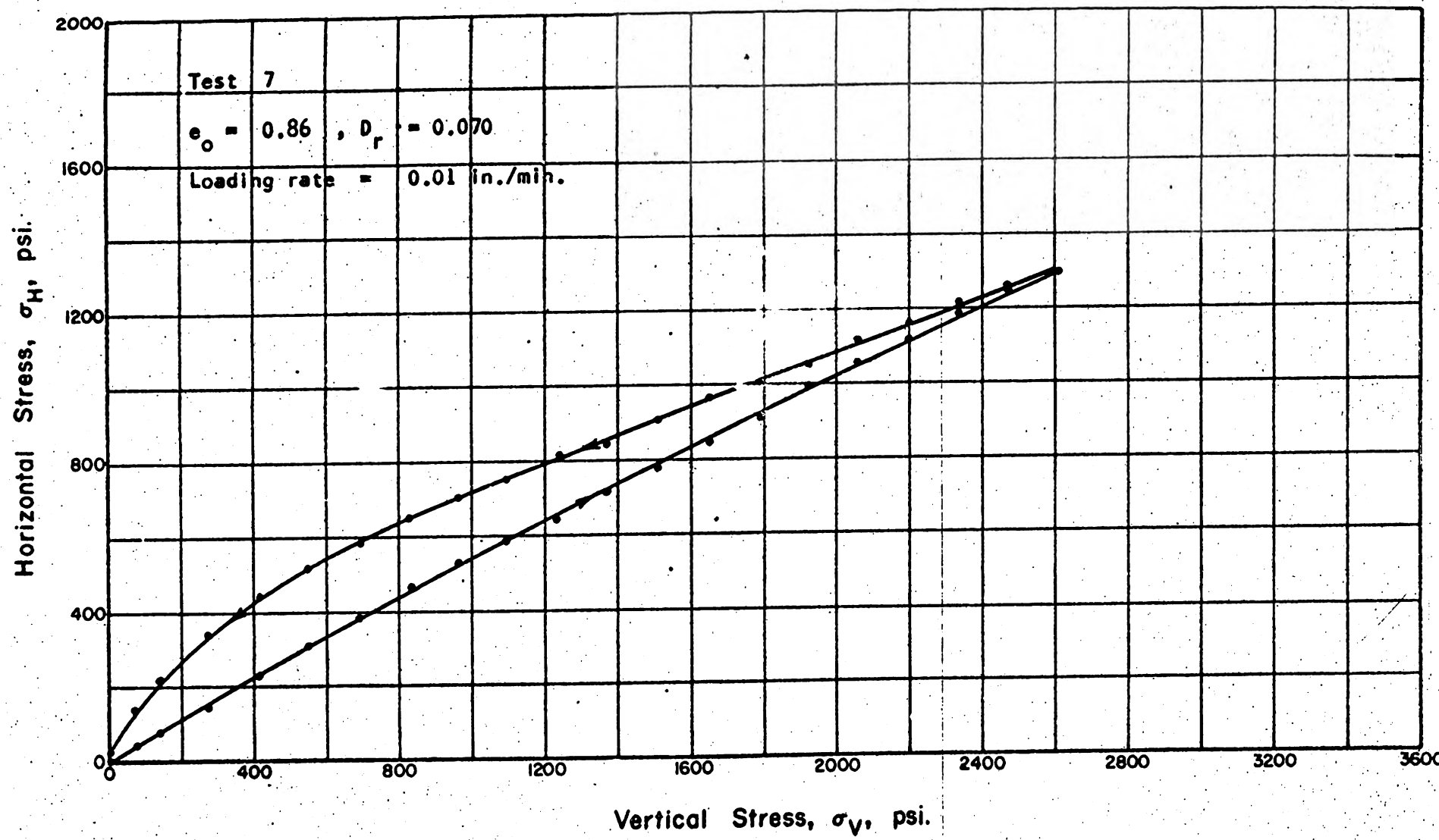

Fig. 5.72 HORIZONTAL STRESS VS. VERTICAL STRESS FOR THE FIRST CYCLE OF LOADING OF PENNSYLVANIA SAND IN ONE-DIMENSIONAL COMPRESSION

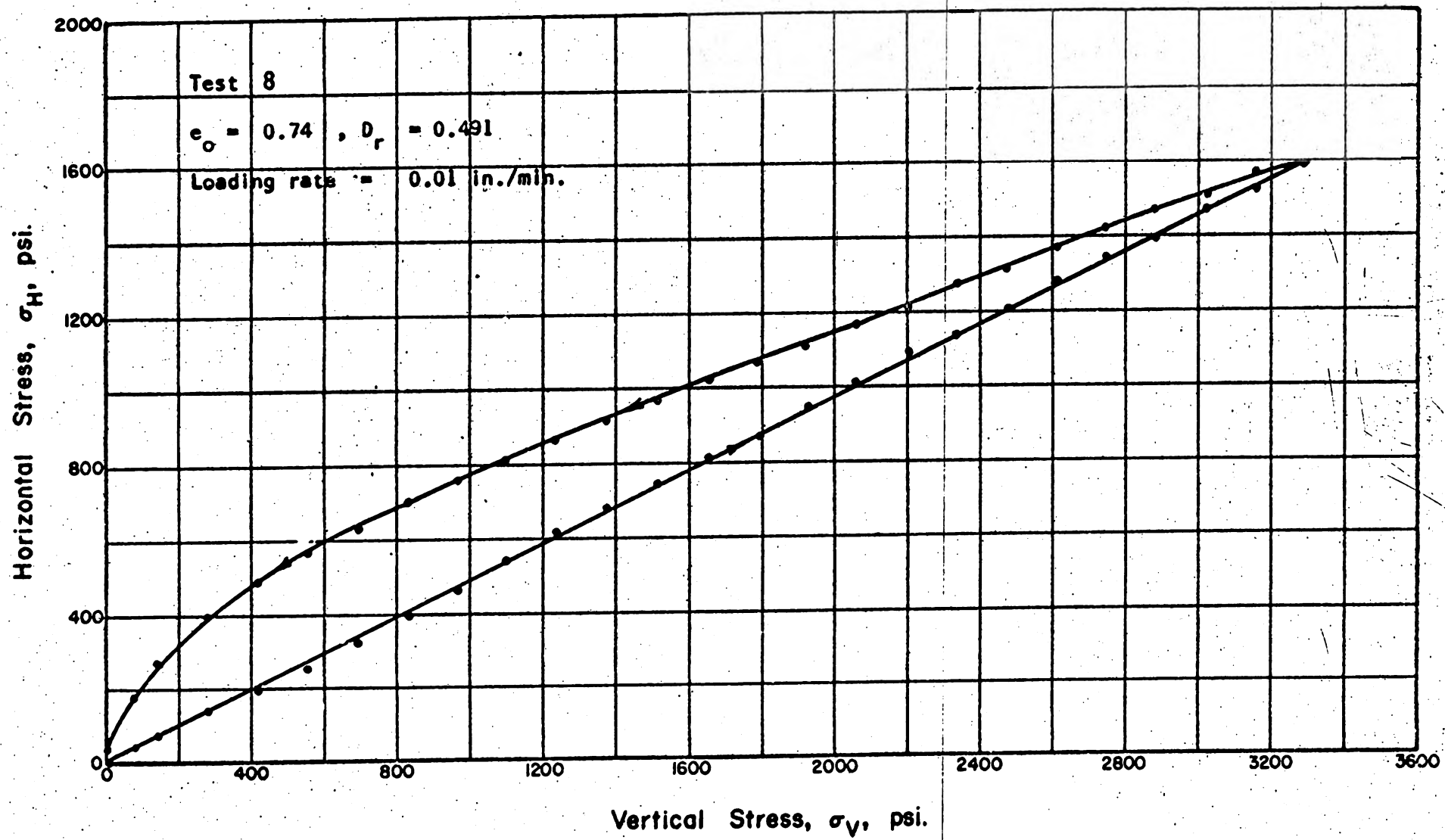

Fig. 5.73 HORIZONTAL STRESS VS. VERTICAL STRESS FOR THE FIRST CYCLE OF LOADING OF PENNSYLVANIA SAND IN ONE-DIMENSIONAL COMPRESSION

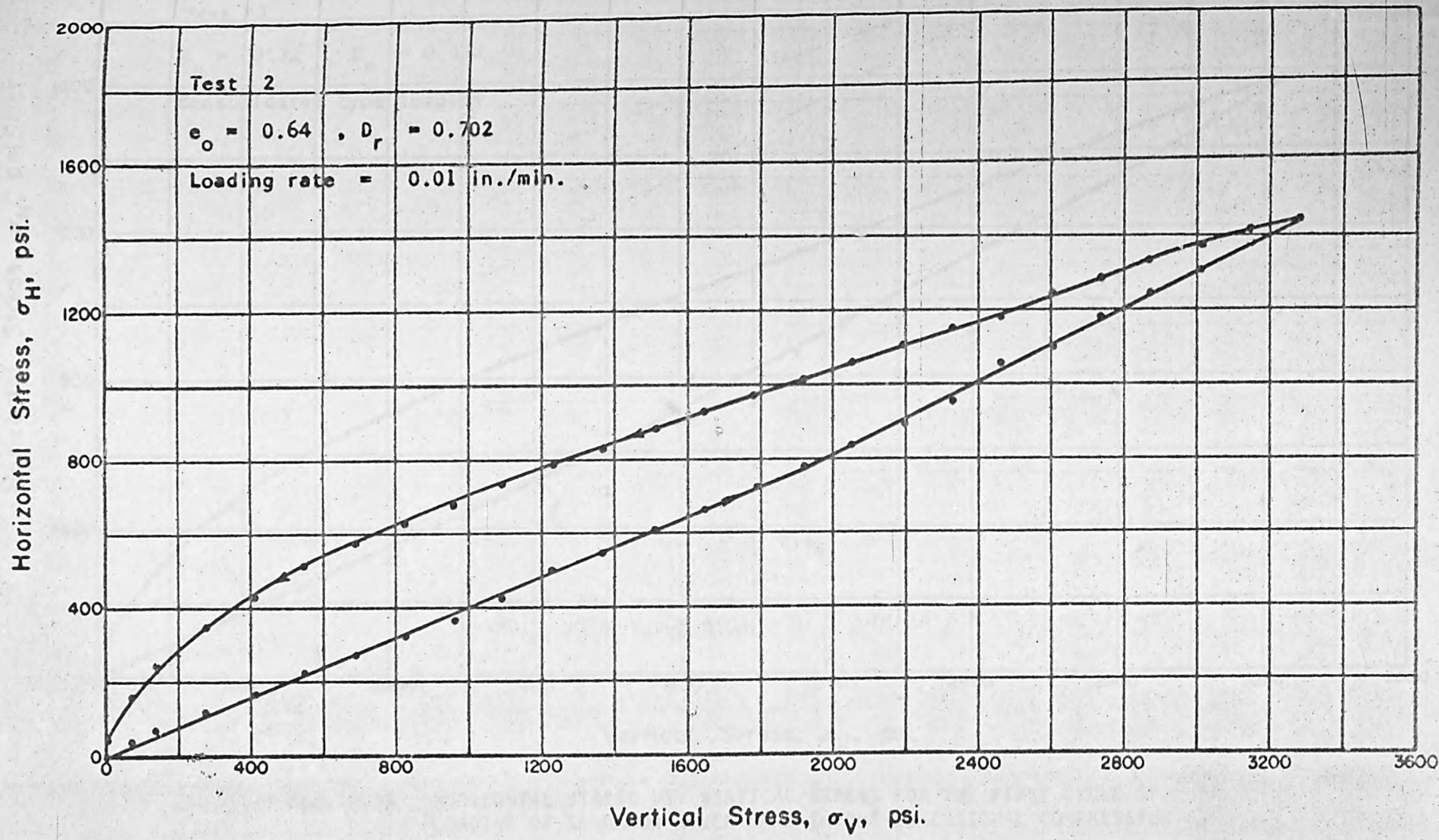

Fig. 5.75 HORIZONTAL STRESS VS. VERTICAL STRESS FOR THE FIRST CYCLE OF LOADING OF SANGAMON RIVER SAND IN ONE-DIMENSIONAL COMPRESSION

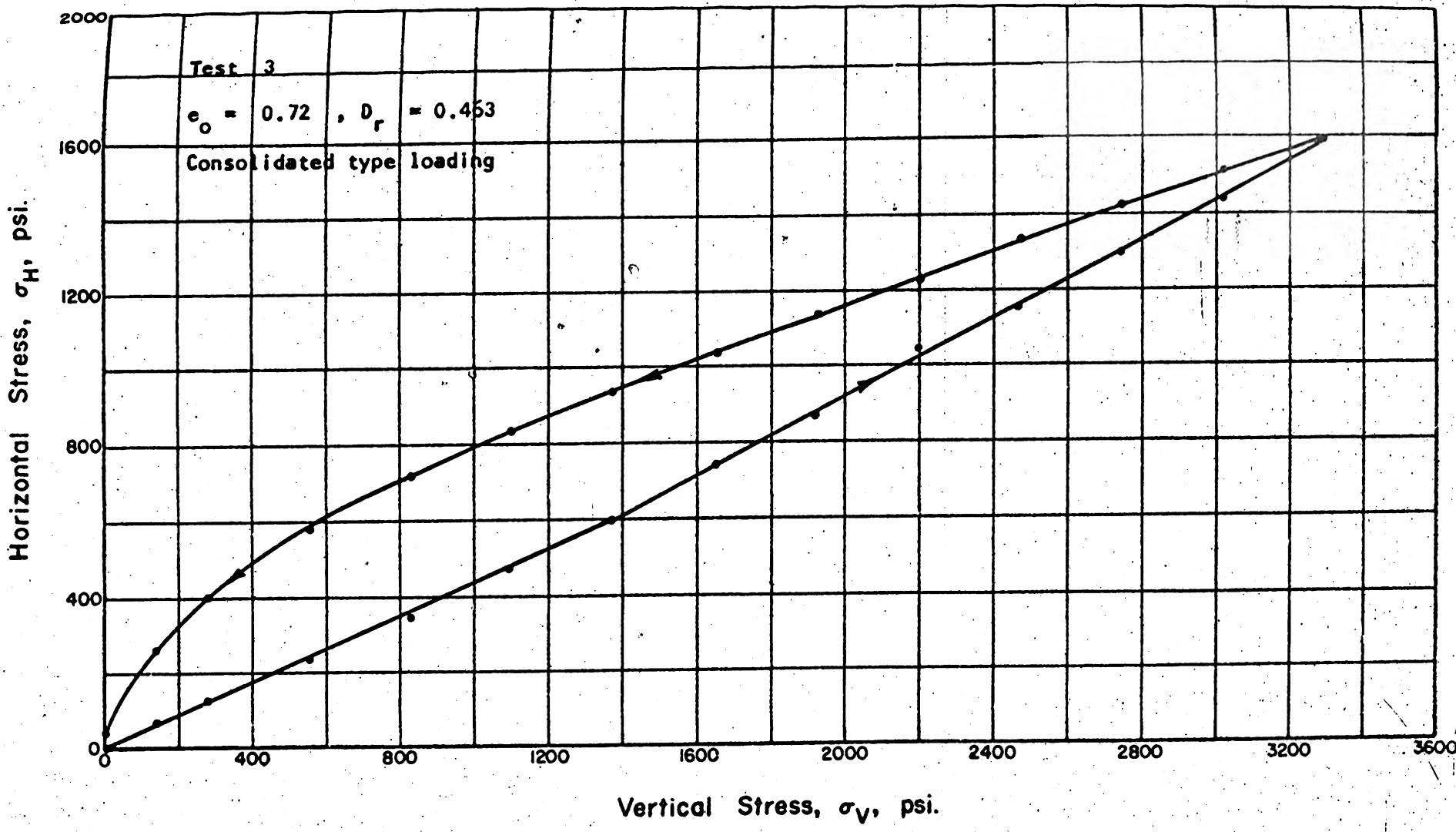

Fig. 5.76 HORIZONTAL STRESS VS. VERTICAL STRESS FOR THE FIRST CYCLE OF LOADING OF SANGAMON RIVER SAND IN ONE-DIMENSIONAL COMPRESSION

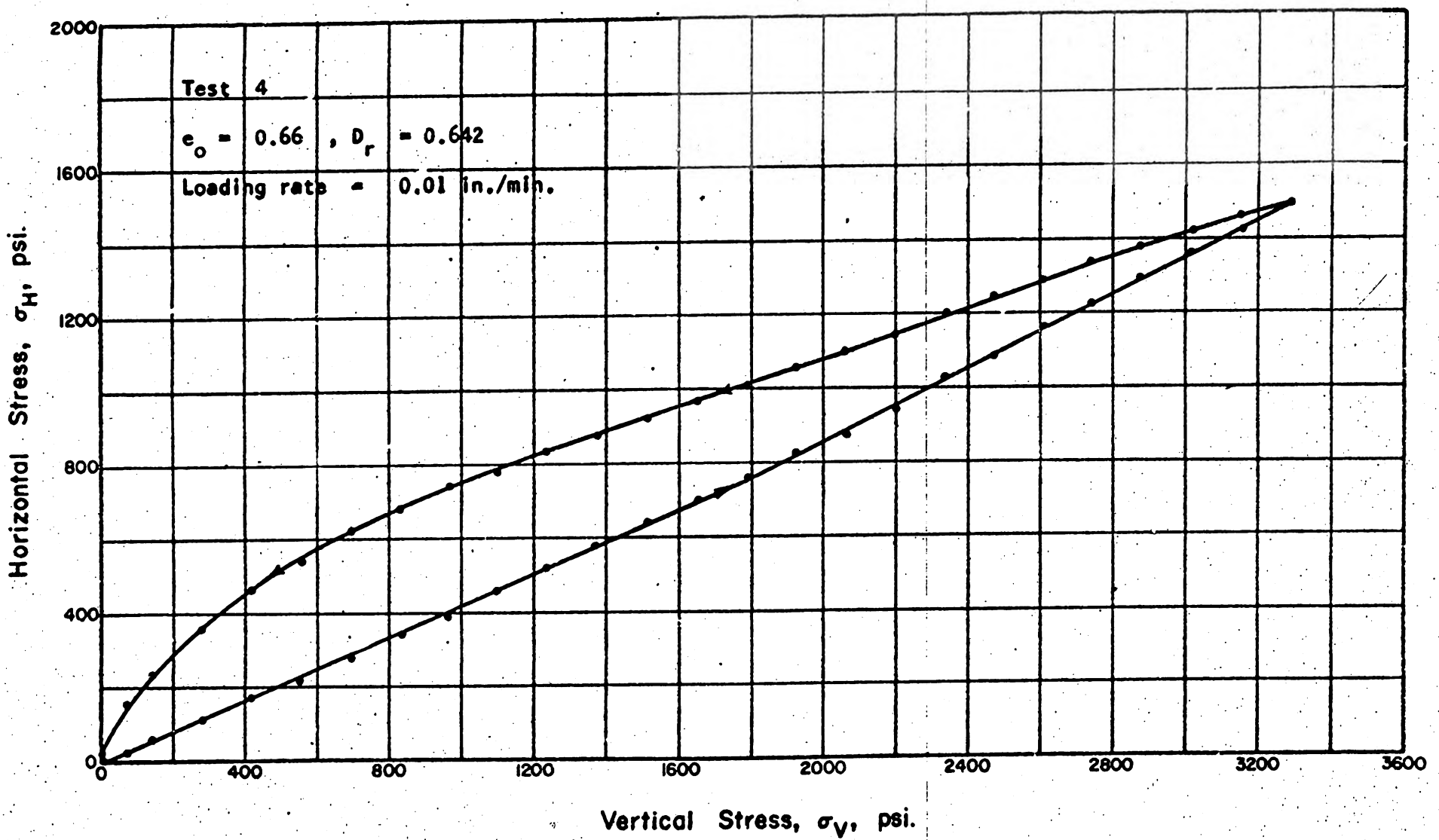

Fig. 5.77 HORIZONTAL STRESS VS. VERTICAL STRESS FOR THE FIRST CYCLE OF LOADING OF SANGAMON RIVER SAND IN ONE-DIMENSIONAL COMPRESSION

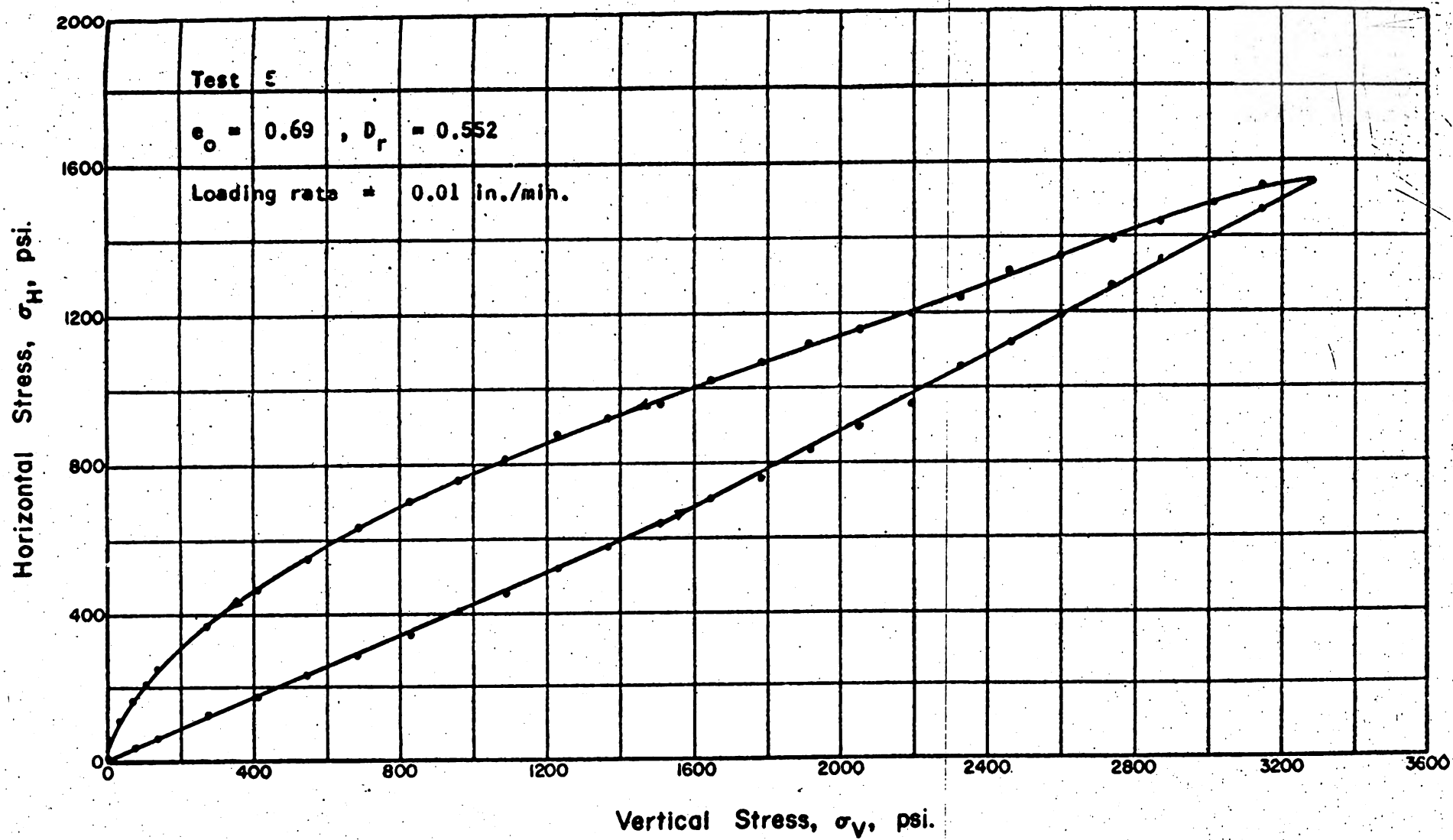

Fig. 5.78 HORIZONTAL STRESS VS. VERTICAL STRESS FOR THE FIRST CYCLE OF LOADING OF SANGAMON RIVER SAND IN ONE-DIMENSIONAL COMPRESSION

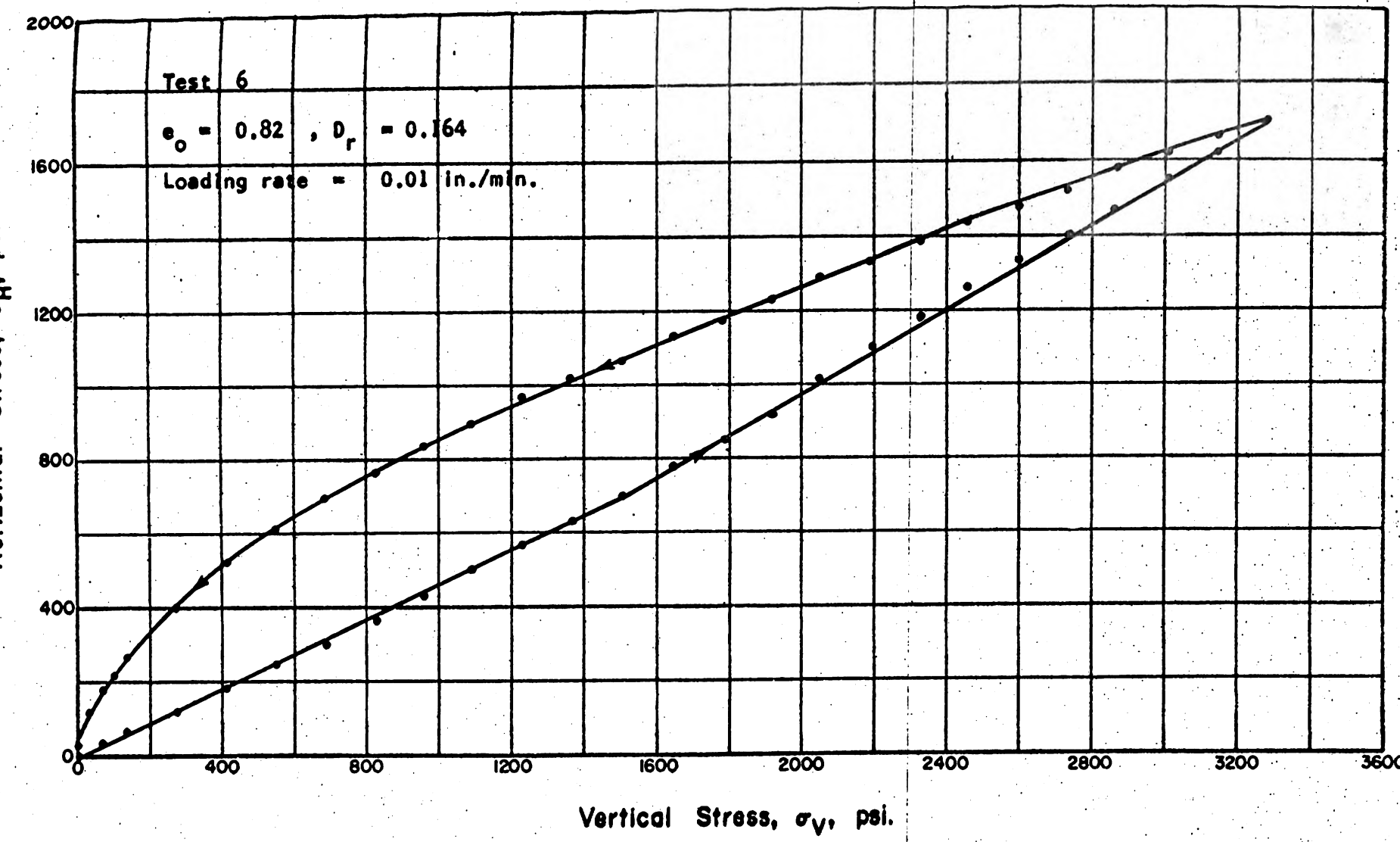

Fig. 5.79 HORIZONTAL STRESS VS. VERTICAL STRESS FOR THE FIRST CYCLE OF LOADING OF SANGAMON RIVER SAND IN ONE-DIMENSIONAL COMPRESSION

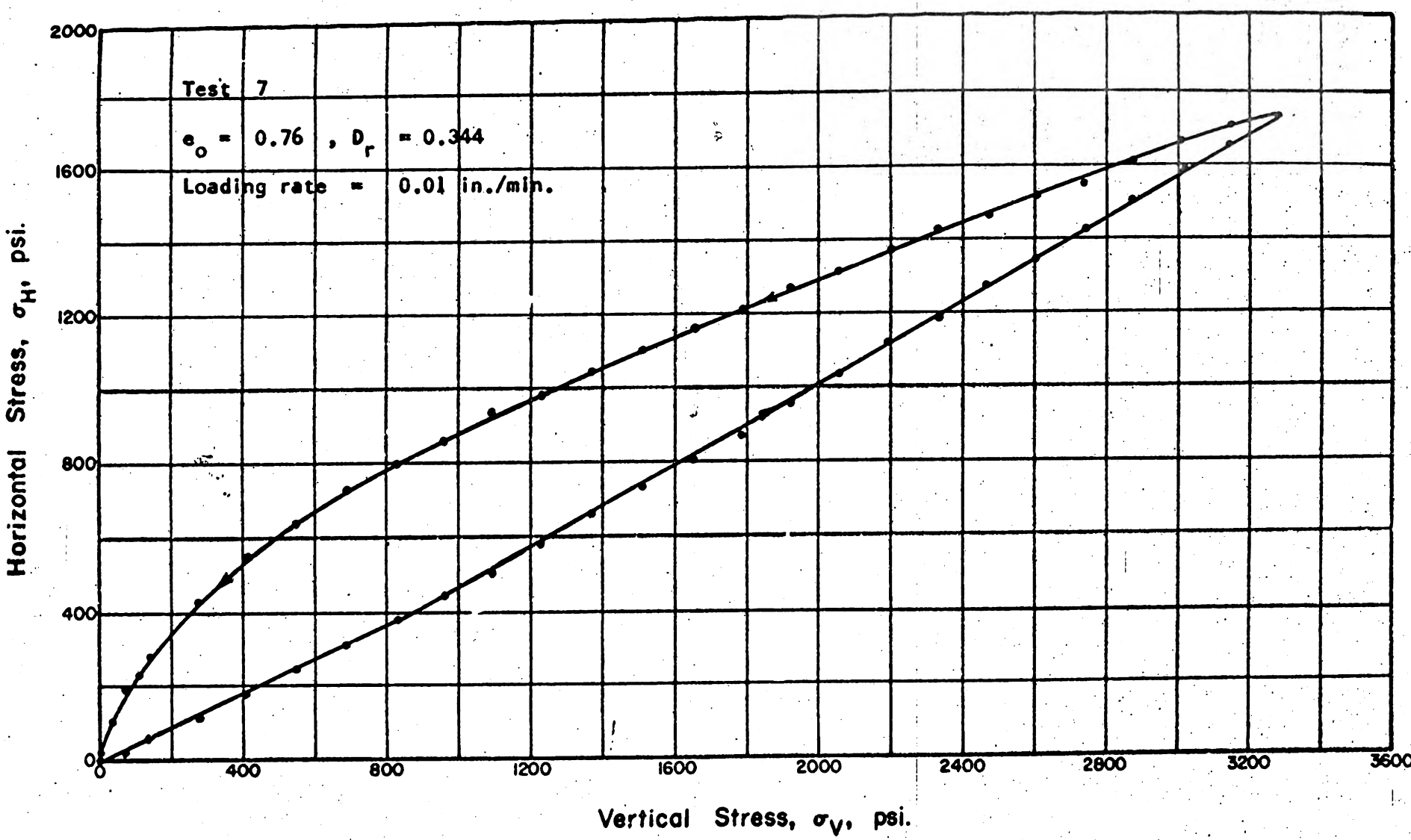

Fig. 5.80 HORIZONTAL STRESS VS. VERTICAL STRESS FOR THE FIRST CYCLE OF LOADING OF SANGAMON RIVER SAND IN ONE-DIMENSIONAL COMPRESSION

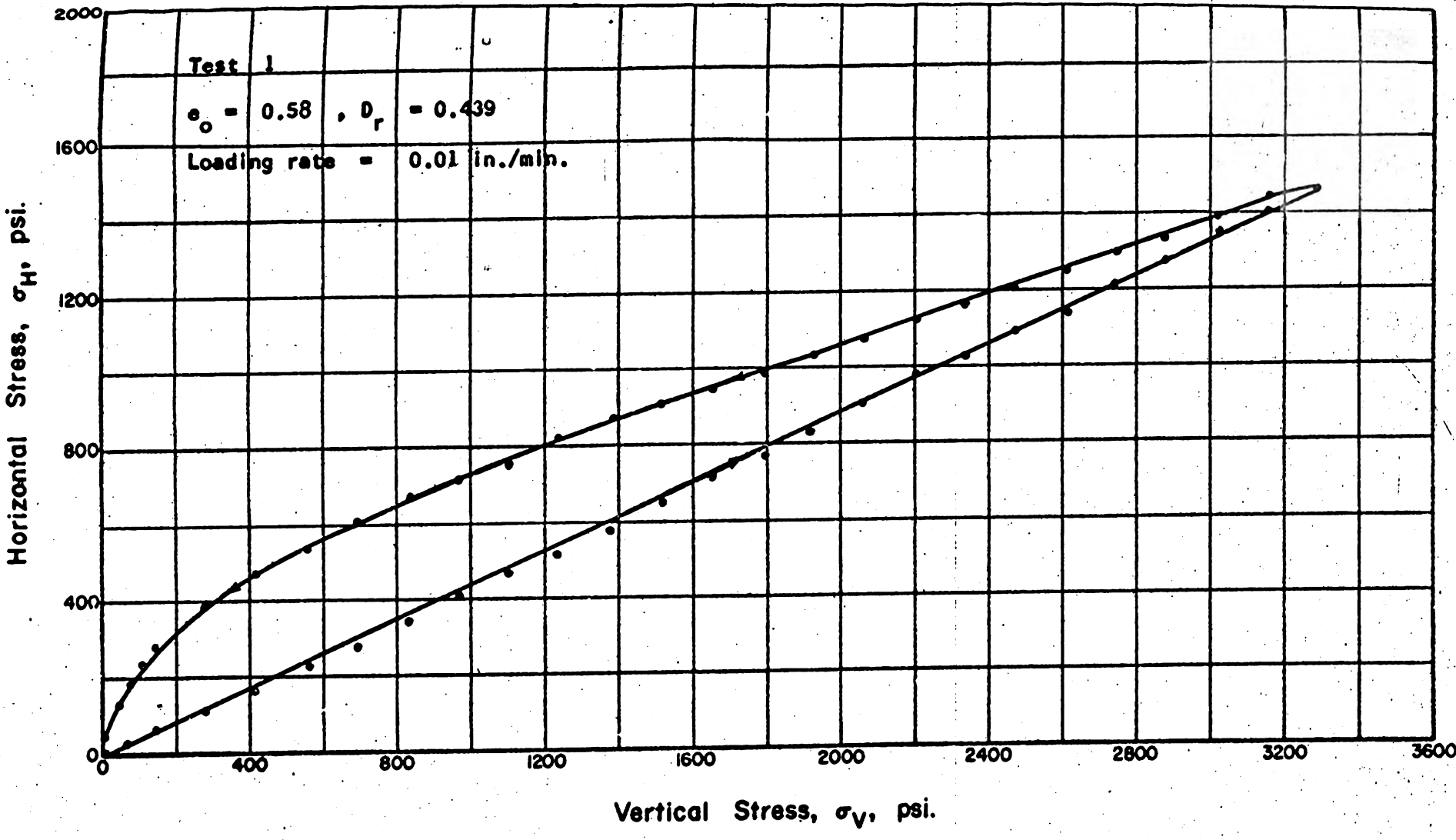

Fig. 5.81 HORIZONTAL STRESS VS. VERTICAL STRESS FOR THE FIRST CYCLE OF LOADING OF WABASH RIVER SAND IN ONE-DIMENSIONAL COMPRESSION

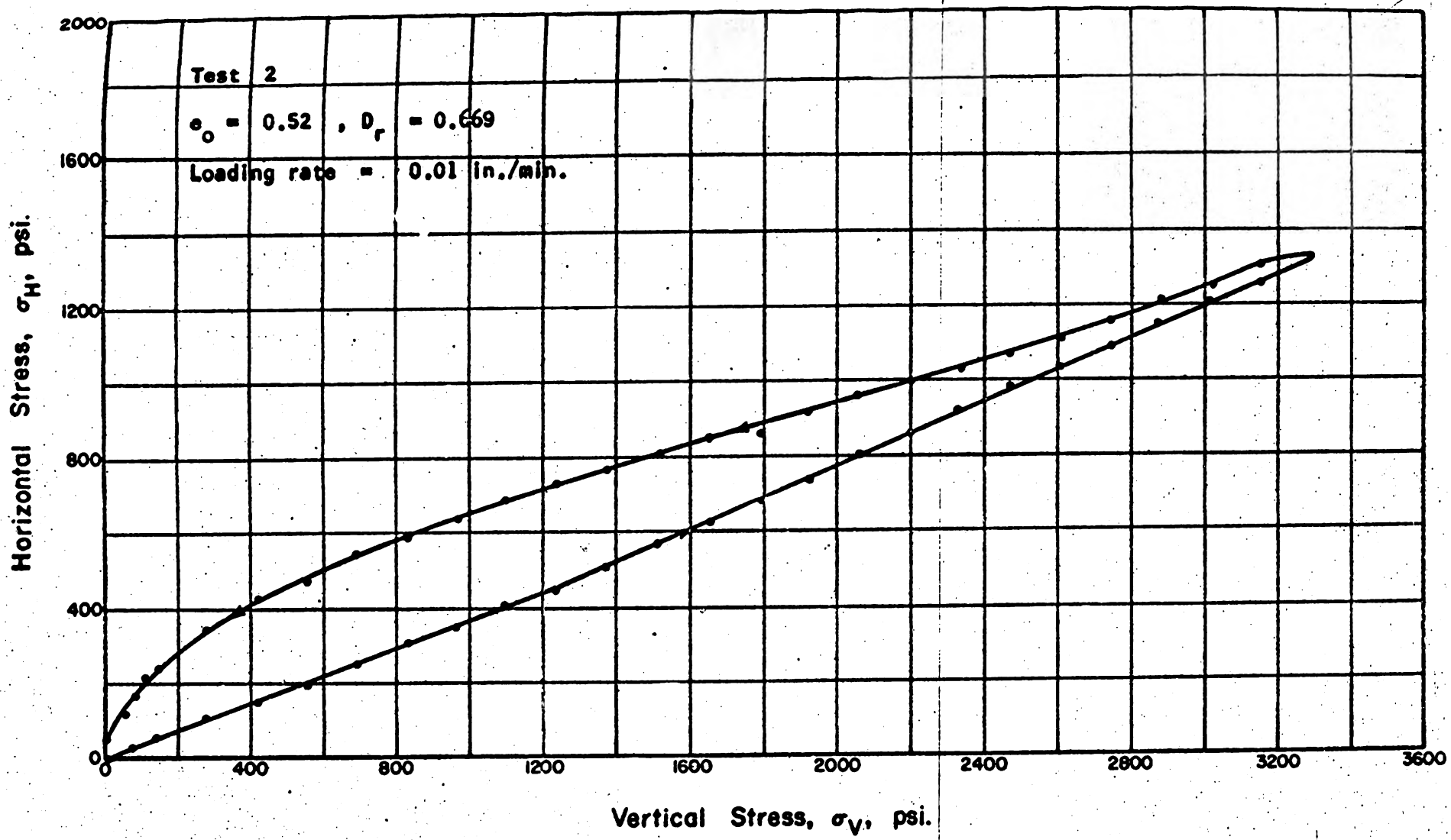

Fig. 5.82 HORIZONTAL STRESS VS. VERTICAL STRESS FOR THE FIRST CYCLE OF LOADING OF WABASH RIVER SAND IN ONE-DIMENSIONAL COMPRESSION

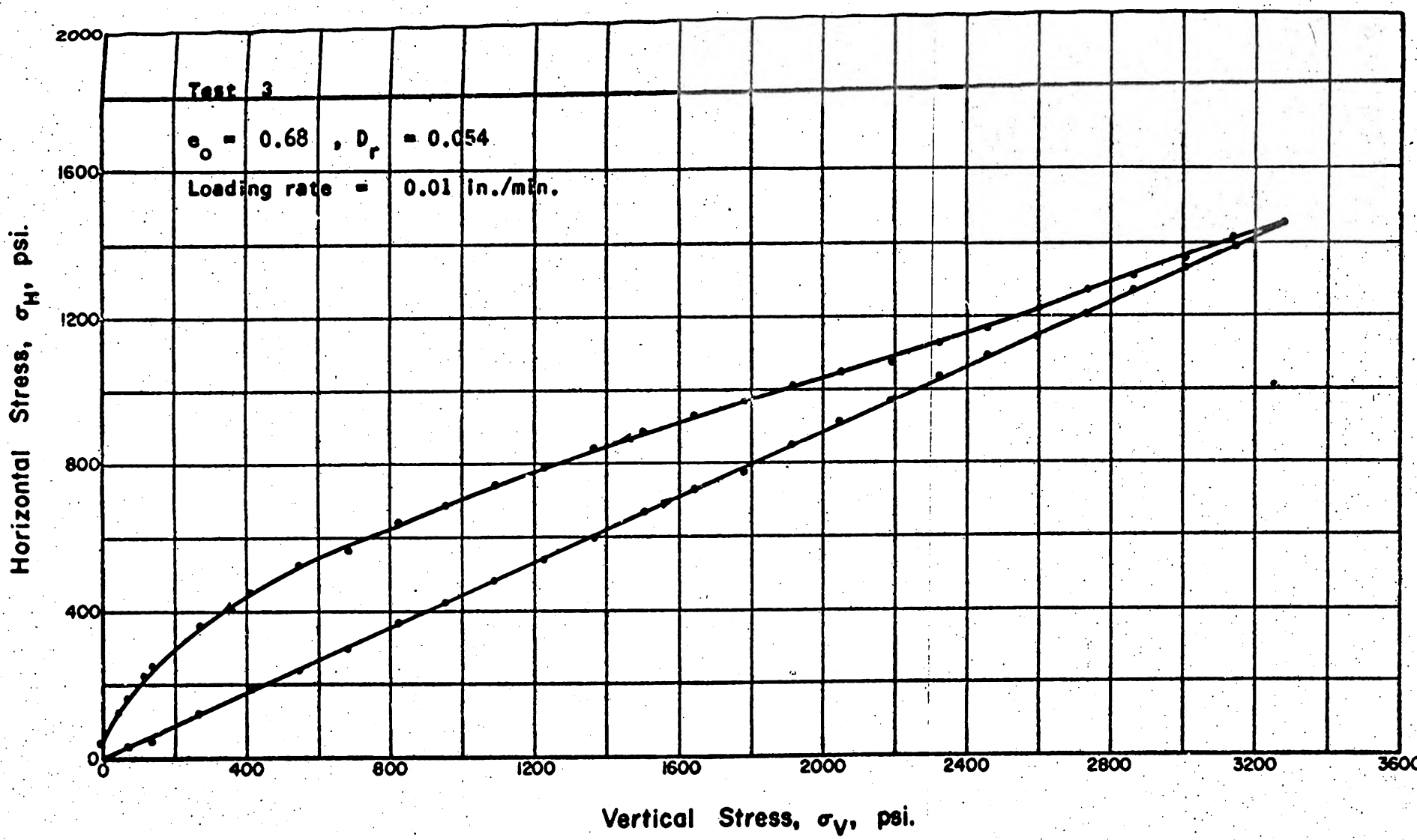

Fig. 5.83 HORIZONTAL STRESS VS. VERTICAL STRESS FOR THE FIRST CYCLE OF LOADING OF WABASH RIVER SAND IN ONE-DIMENSIONAL COMPRESSION

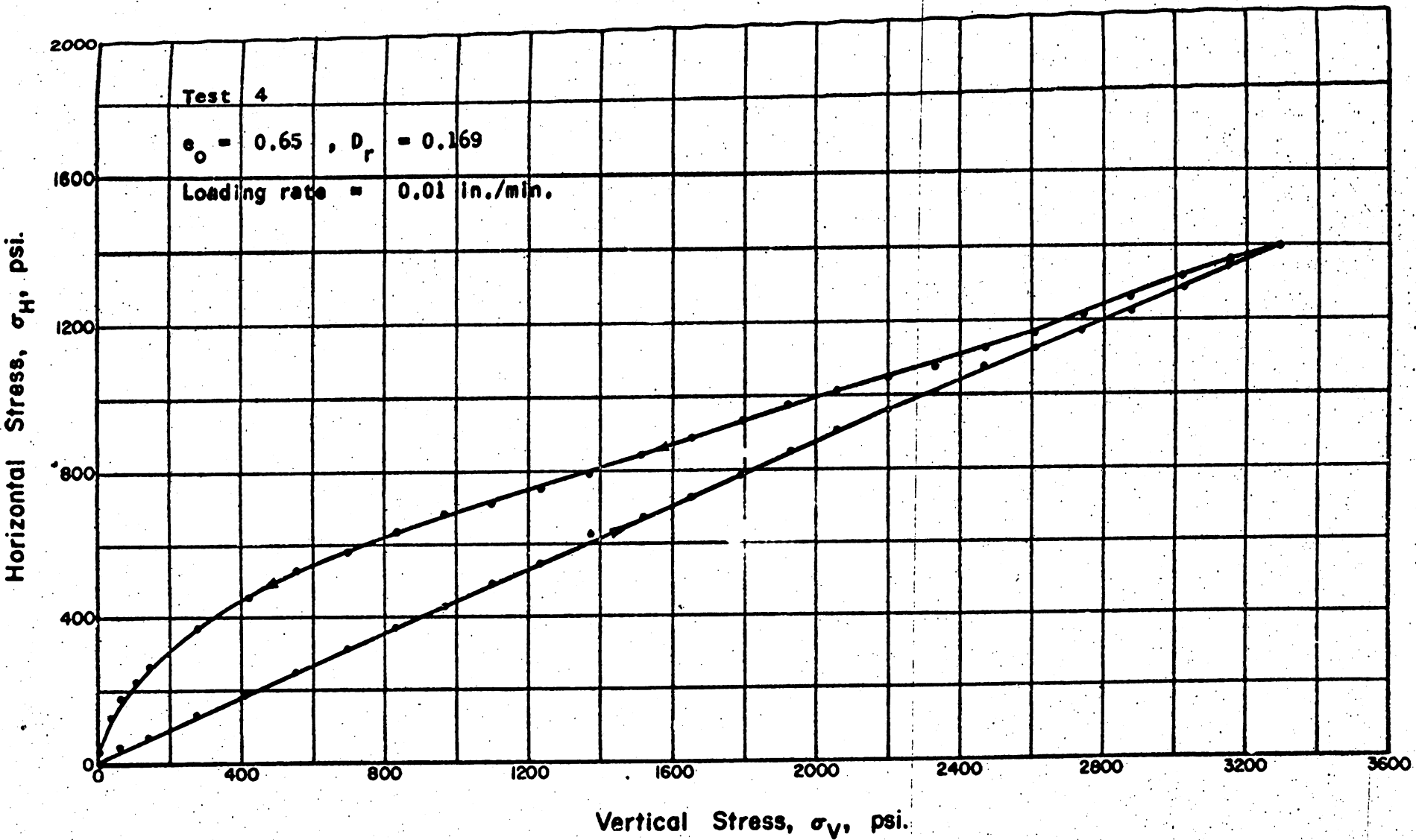

Fig. 5.84 HORIZONTAL STRESS VS. VERTICAL STRESS FOR THE FIRST CYCLE OF LOADING OF WABASH RIVER SAND IN ONE-DIMENSIONAL COMPRESSION

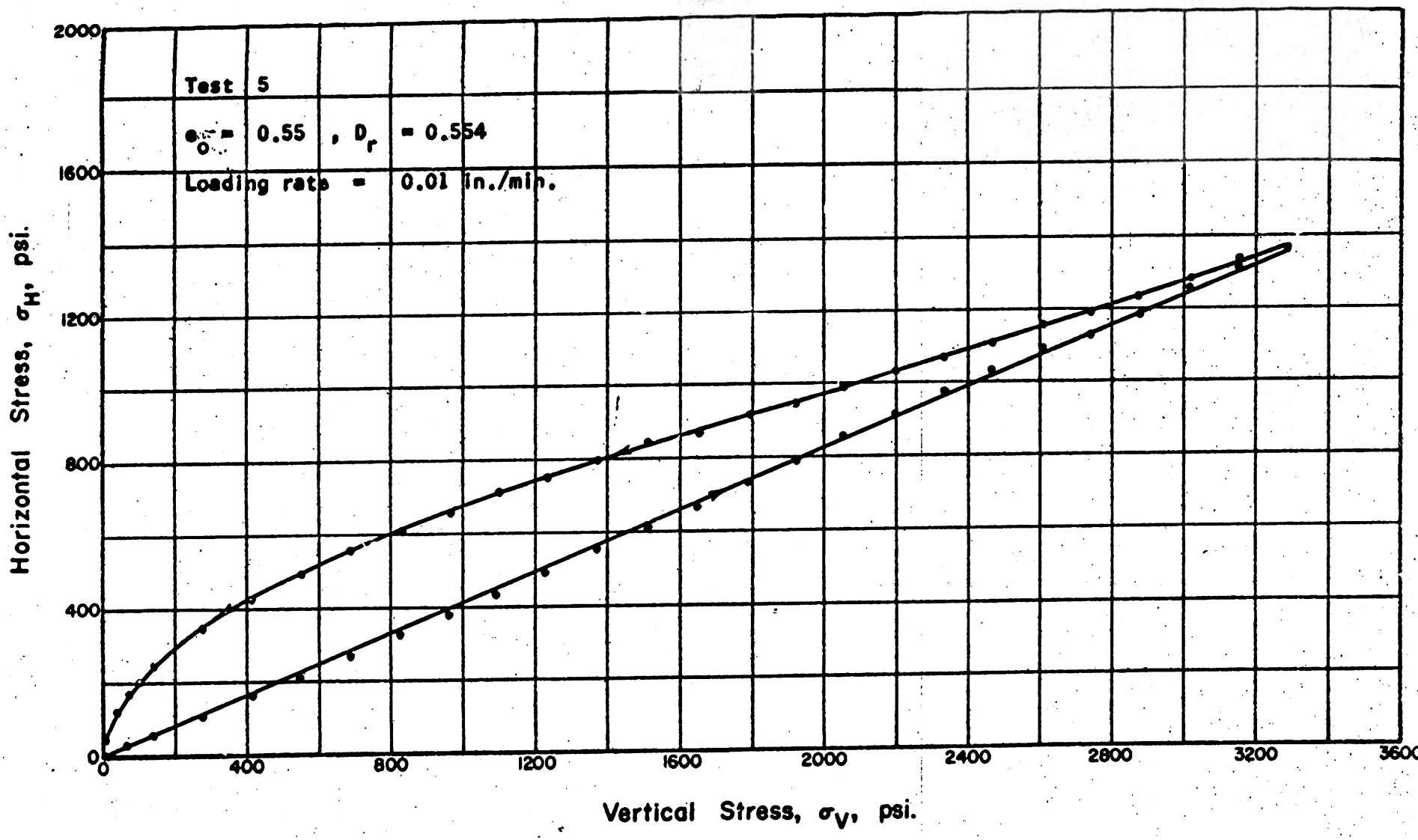

Fig. 5.85 HORIZONTAL STRESS VS. VERTICAL STRESS FOR THE FIRST CYCLE OF LOADING OF WABASH RIVER SAND IN ONE-DIMENSIONAL COMPRESSION

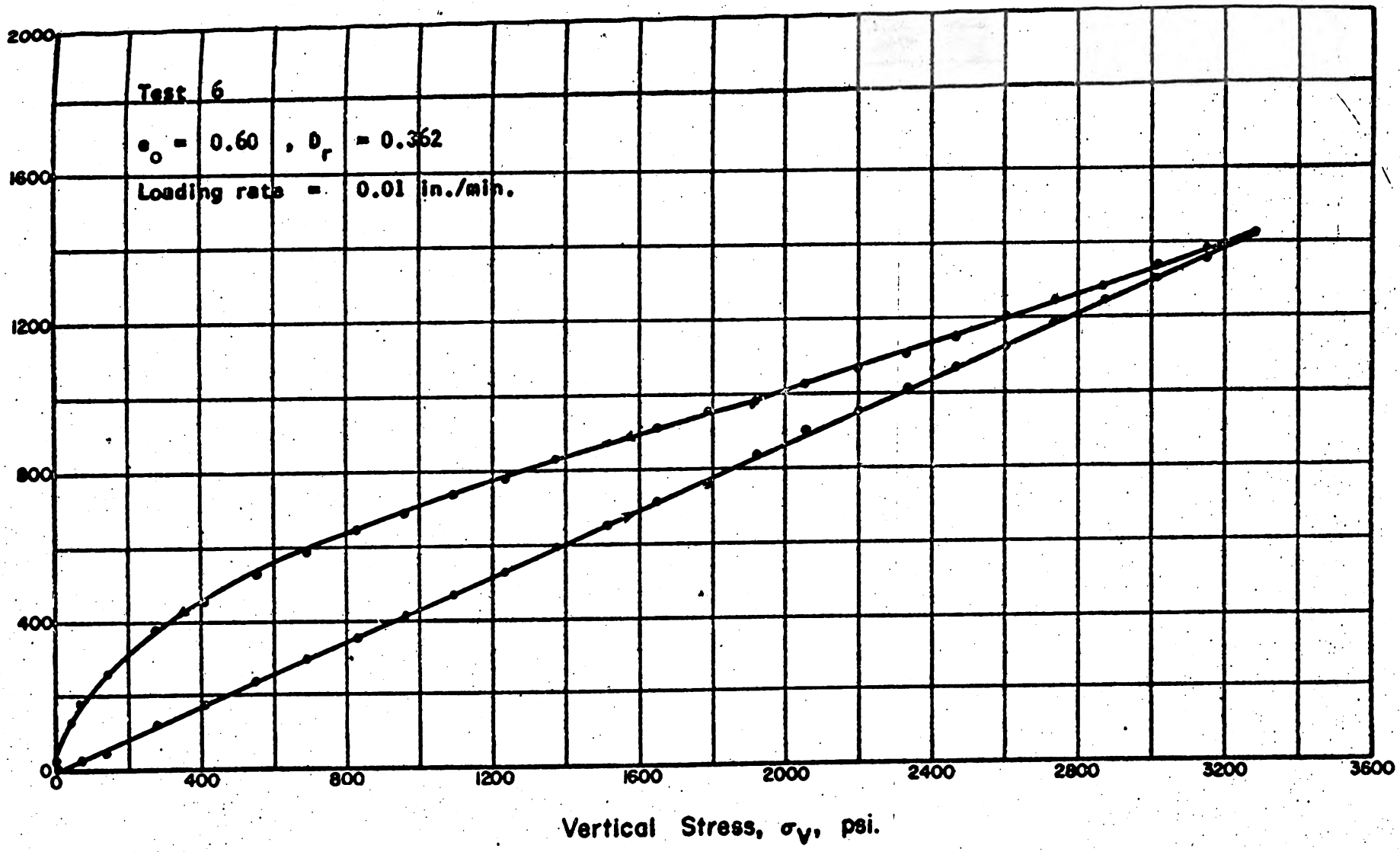

Fig. 5.86 HORIZONTAL STRESS VS. VERTICAL STRESS FOR THE FIRST CYCLE OF LOADING OF WABASH RIVER SAND IN ONE-DIMENSIONAL COMPRESSION

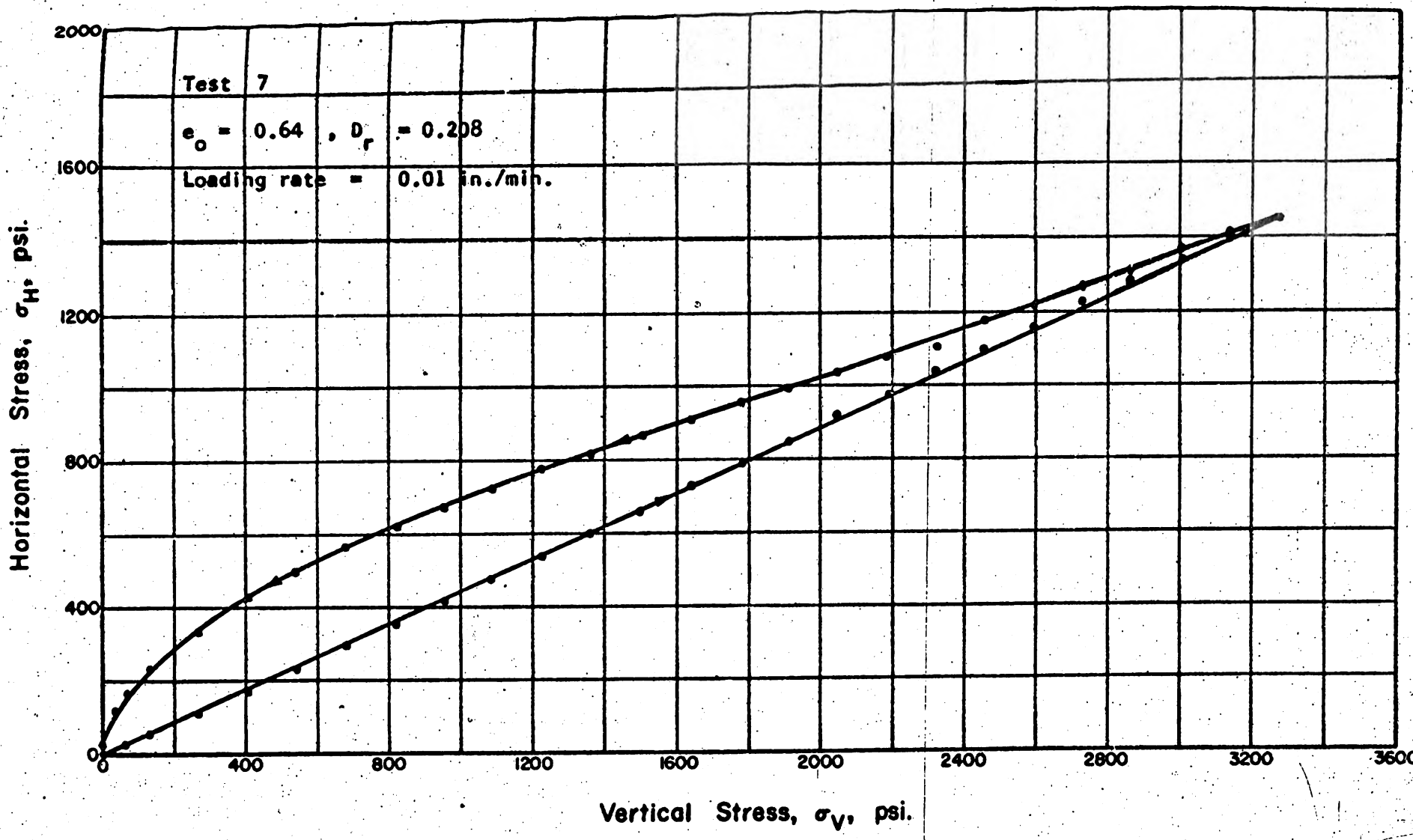

Fig. 5.87 HORIZONTAL STRESS VS. VERTICAL STRESS FOR THE FIRST CYCLE OF LOADING OF WABASH RIVER SAND IN ONE-DIMENSIONAL COMPRESSION

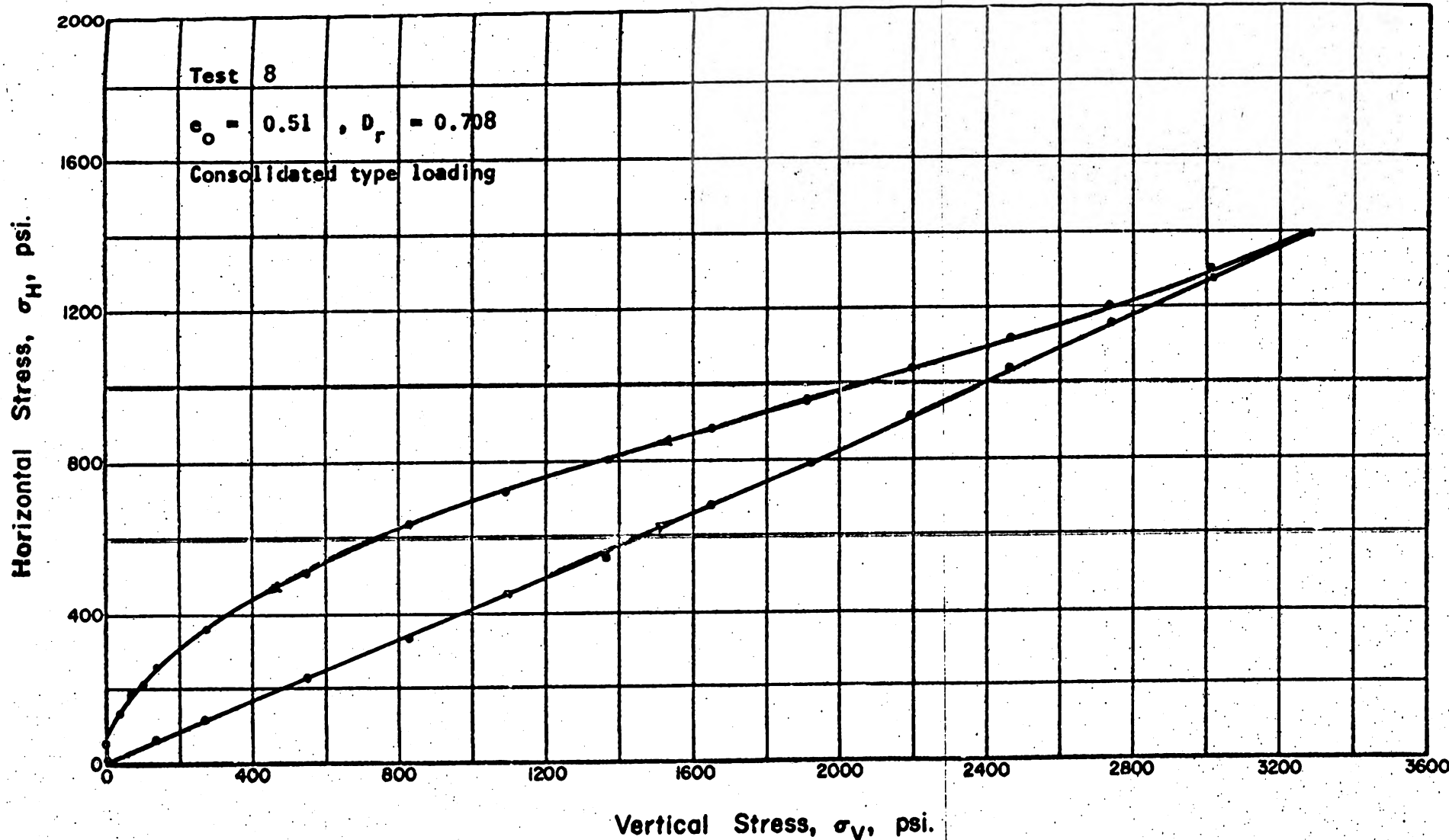

Fig. 5.88 HORIZONTAL STRESS VS. VERTICAL STRESS FOR THE FIRST CYCLE OF LOADING OF WABASH RIVER SAND IN ONE-DIMENSIONAL COMPRESSION

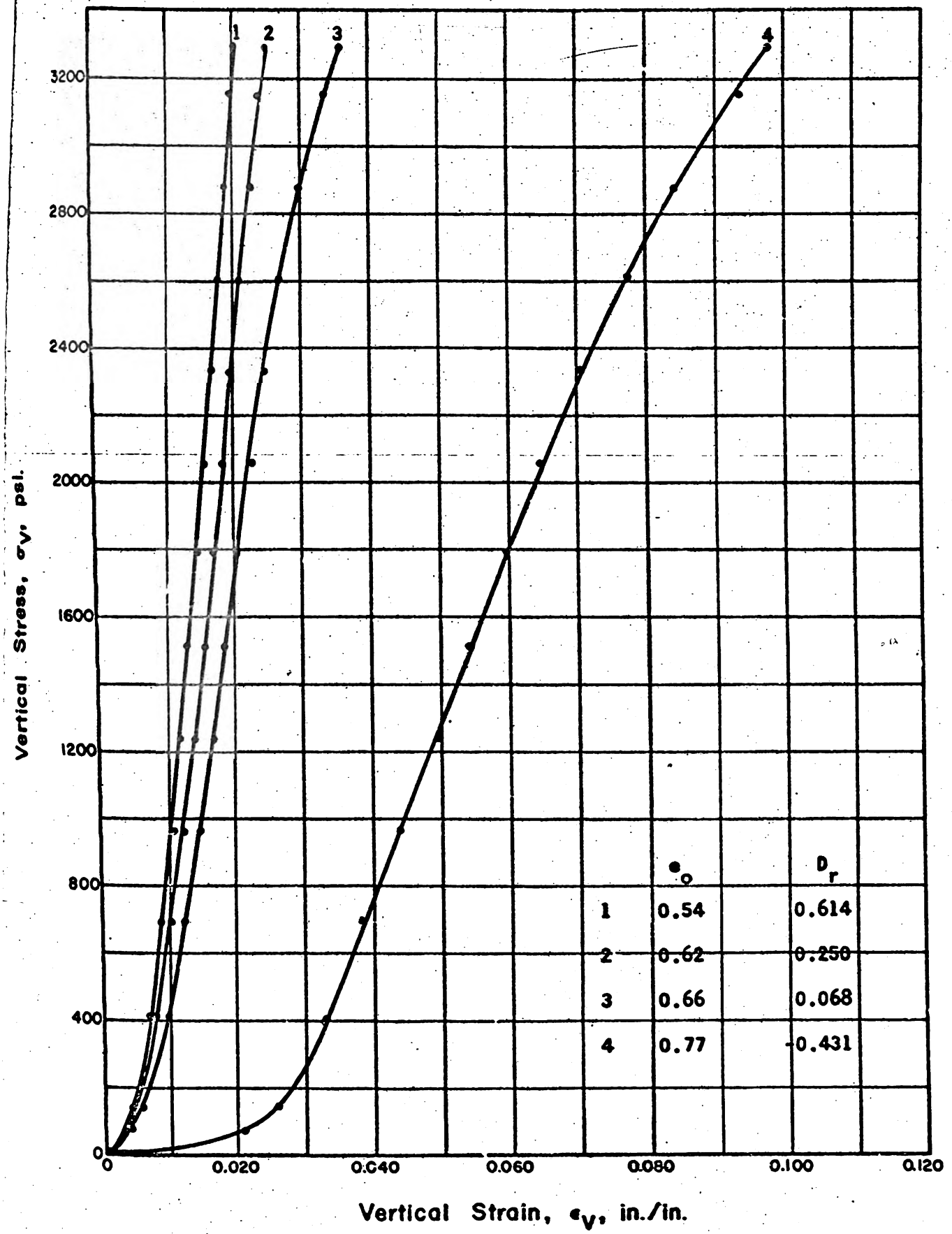

Fig. 6.1 STRESS STRAIN CURVES FOR MINNESOTA SAND IN ONE-DIMENSIONAL COMPRESSION

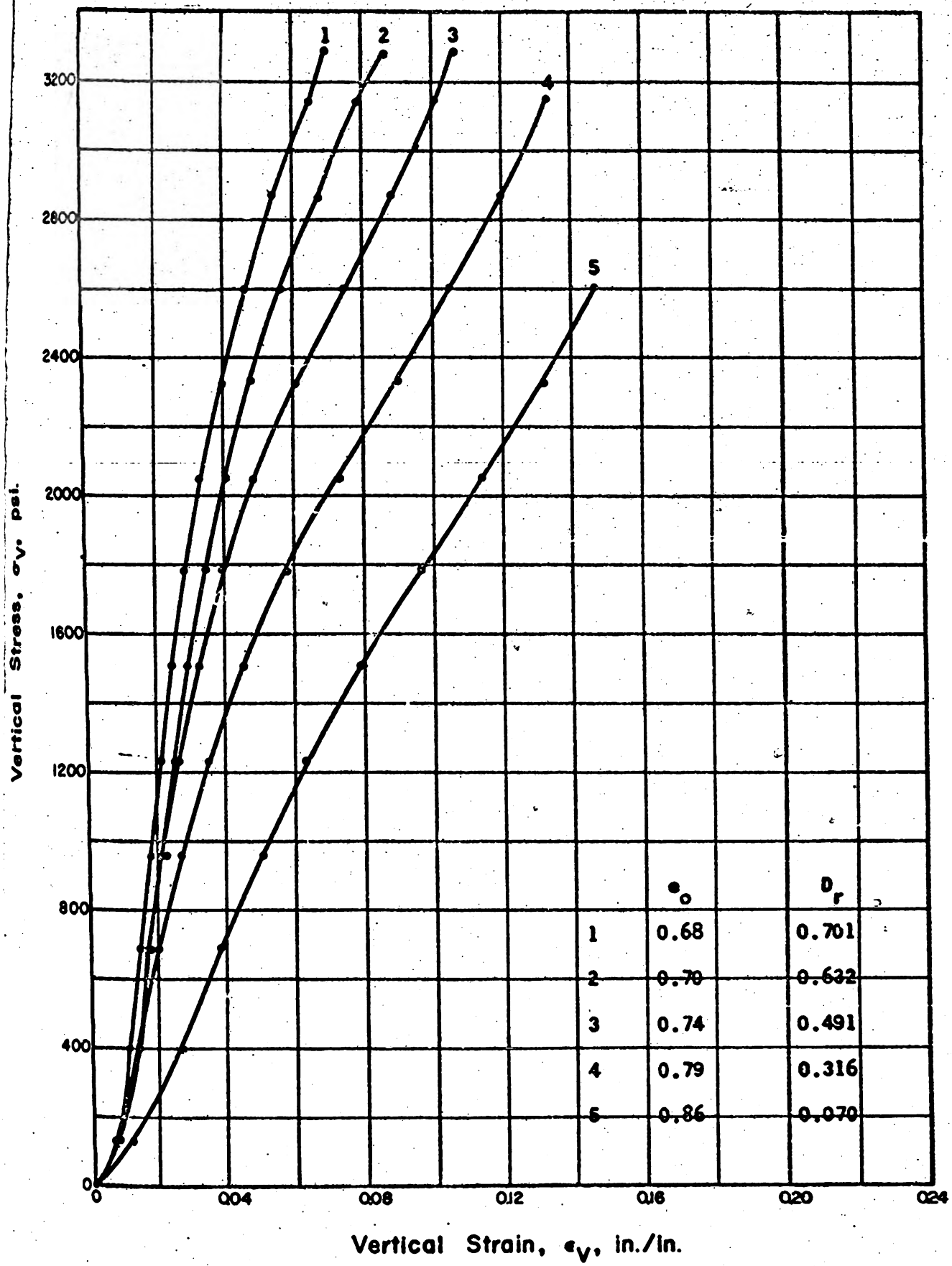

Fig. 6.2 STRESS STRAIN CURVES FOR PENNSYLVANIA SAND IN ONE-DIMENSIONAL COMPRESSION

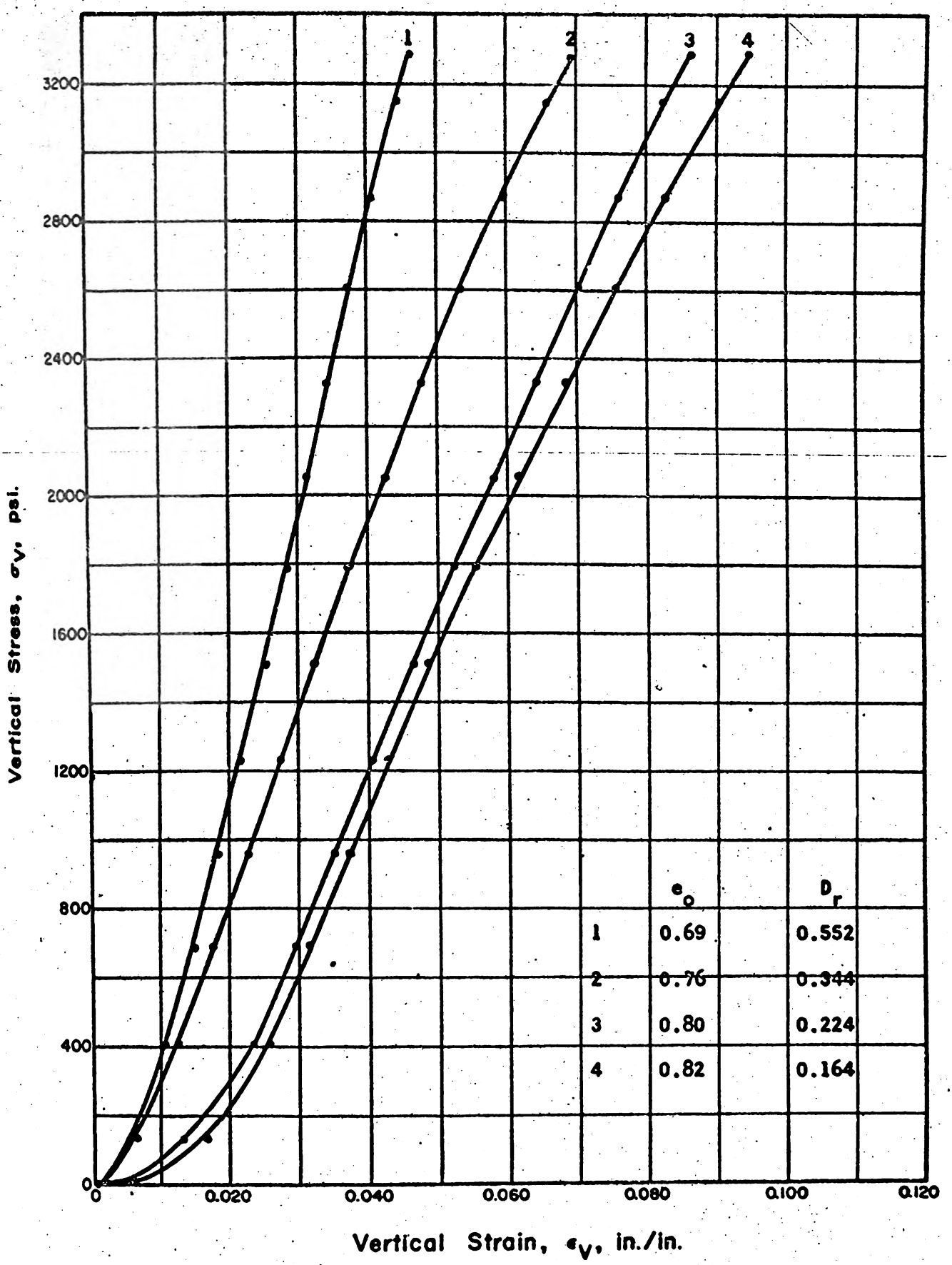

Fig. 6.3 STRESS STRAIN CURVES FOR SANGAMON RIVER SAND IN ONE-DIMENSIONAL COMPRESSION

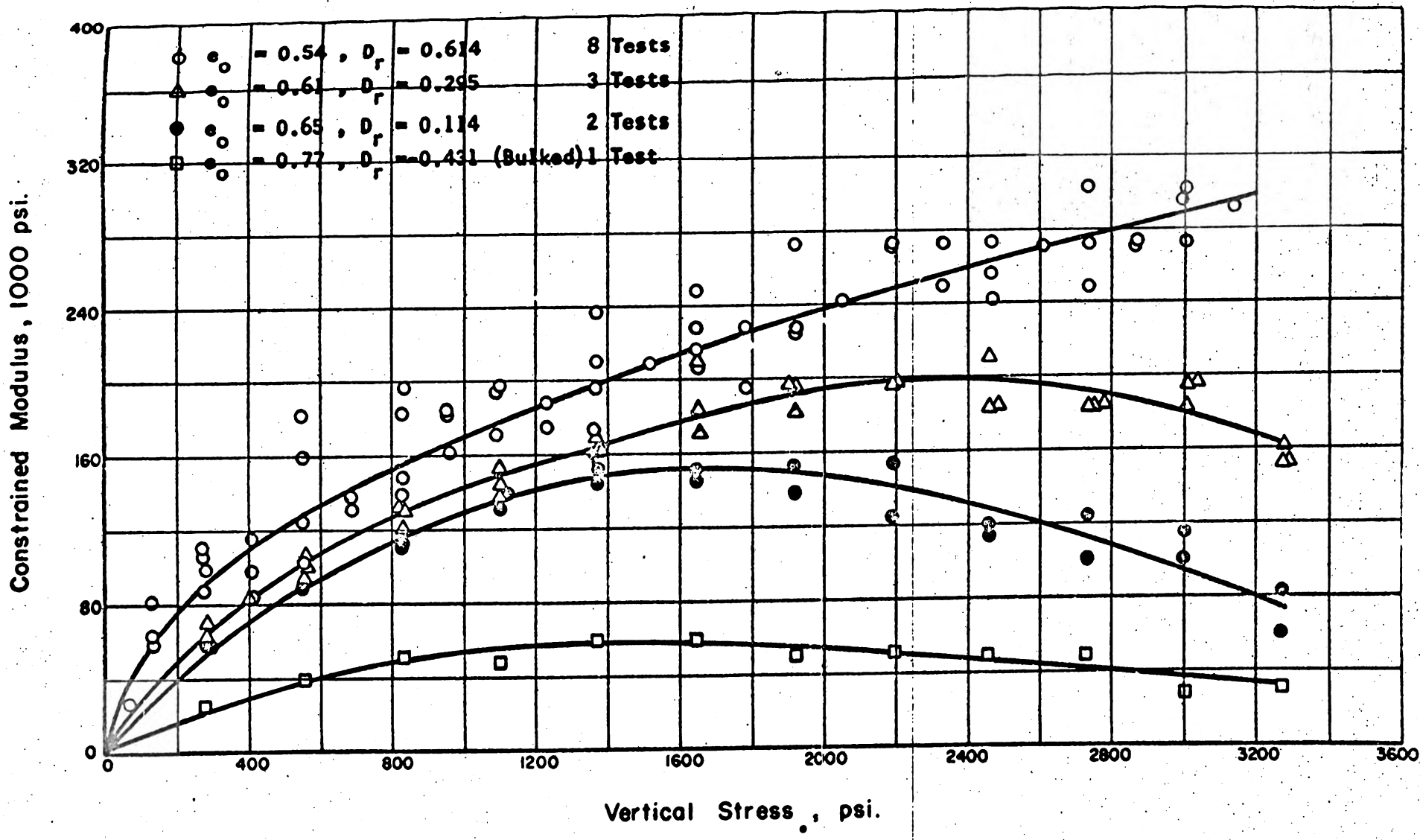

Fig. 6.5 RELATIONSHIP BETWEEN CONSTRAINED MODULUS AND VERTICAL STRESS FOR MINNESOTA SAND IN ONE-DIMENSIONAL COMPRESSION

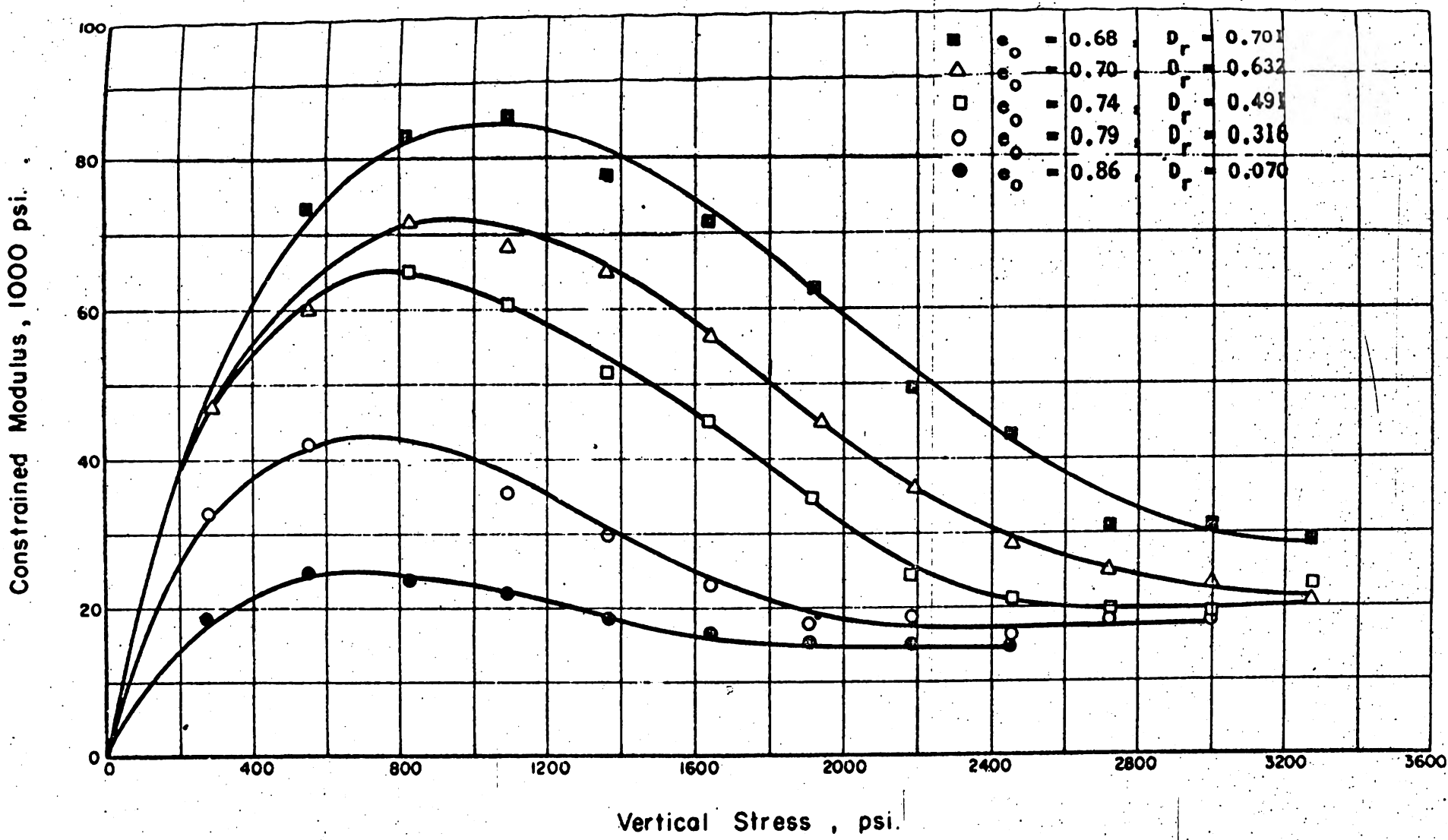

Fig. 6.6 RELATIONSHIP BETWEEN CONSTRAINED MODULUS AND VERTICAL STRESS FOR PENNSYLVANIA SAND IN ONE-DIMENSIONAL COMPRESSION

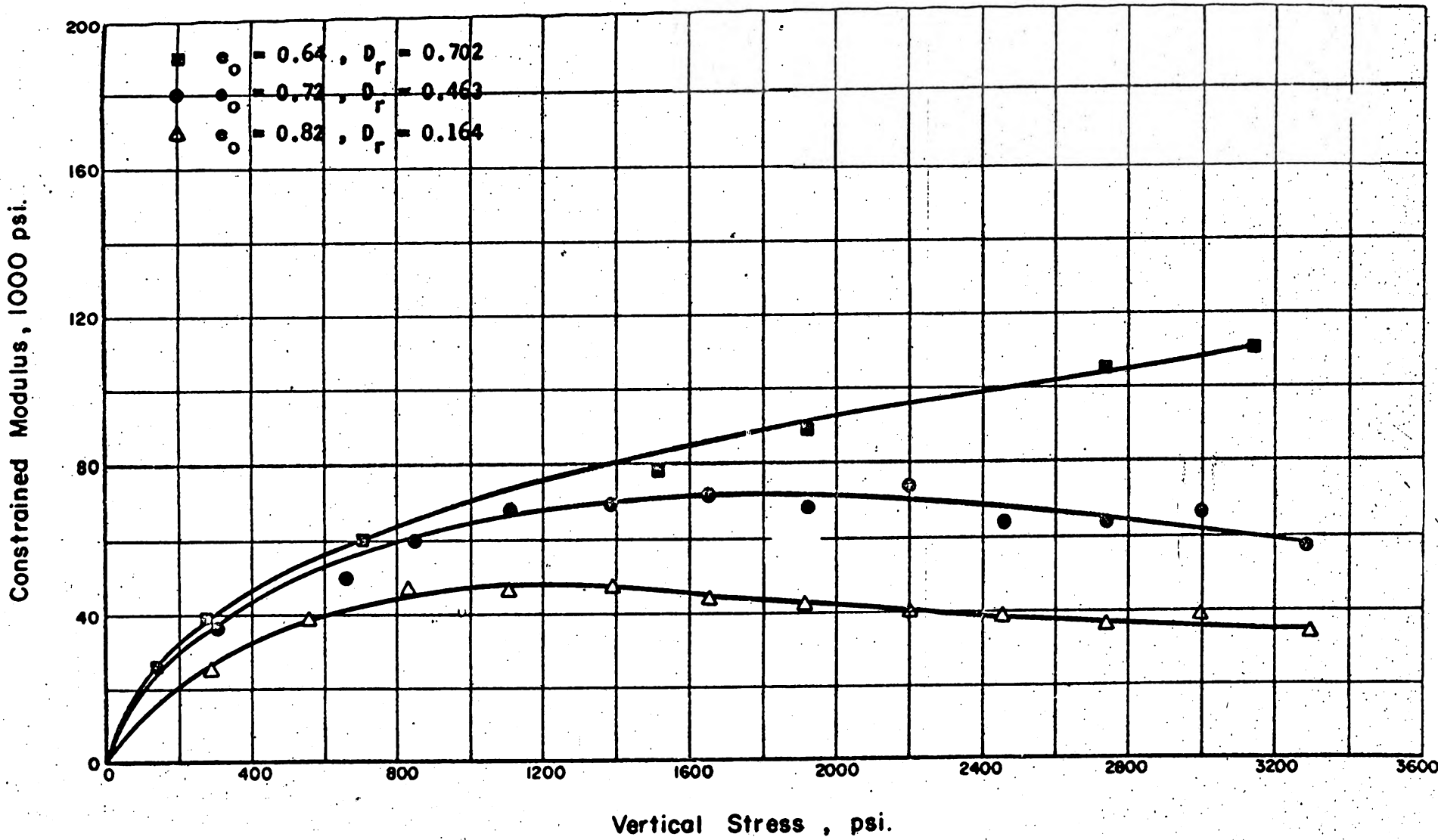

Fig. 6.7 RELATIONSHIP BETWEEN CONSTRAINED MODULUS AND VERTICAL STRESS FOR SANGAMON RIVER SAND IN ONE-DIMENSIONAL COMPRESSION

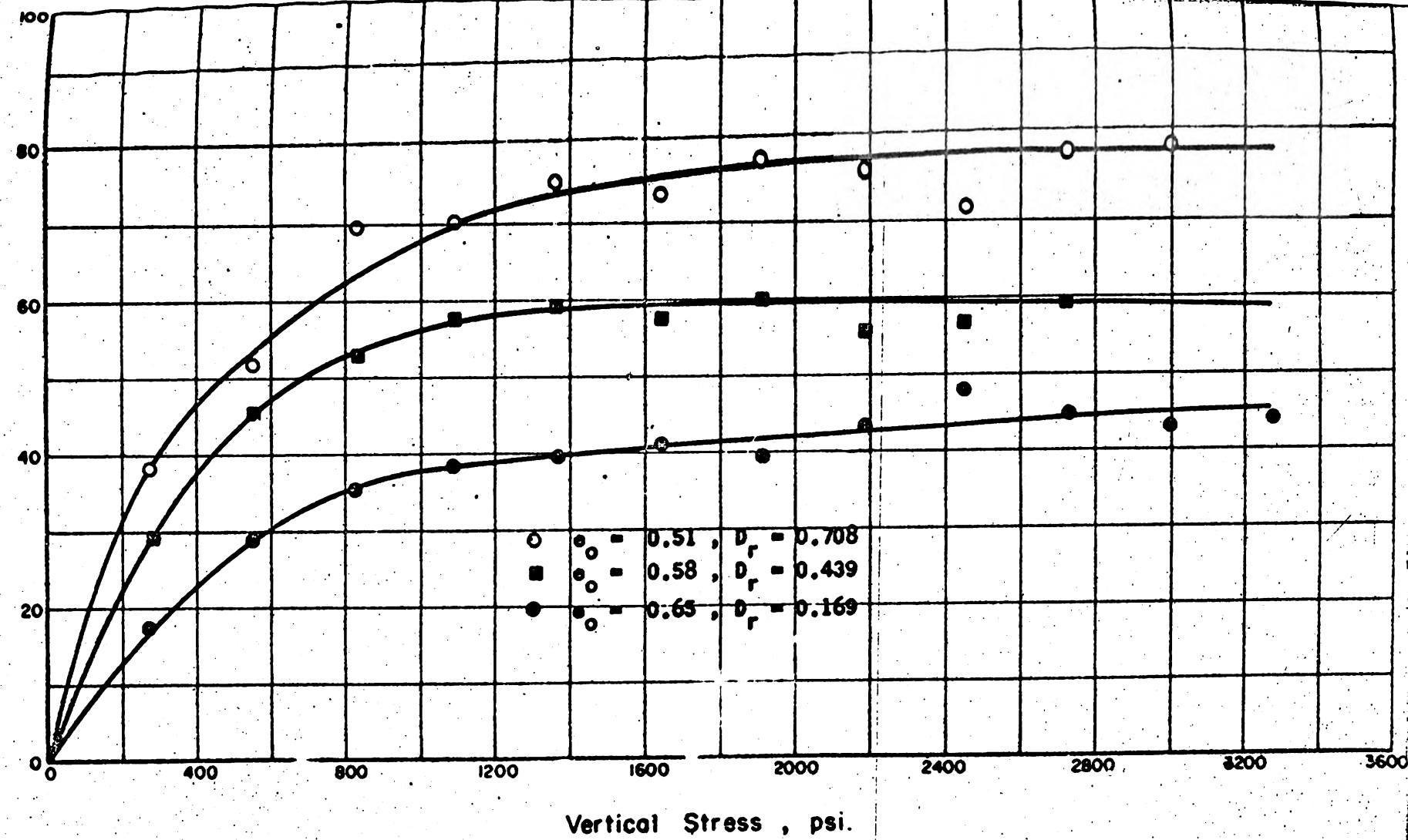

Fig. 6.8 RELATIONSHIP BETWEEN CONSTRAINED MODULUS AND VERTICAL STRESS FOR WABASH RIVER SAND IN ONE-DIMENSIONAL COMPRESSION

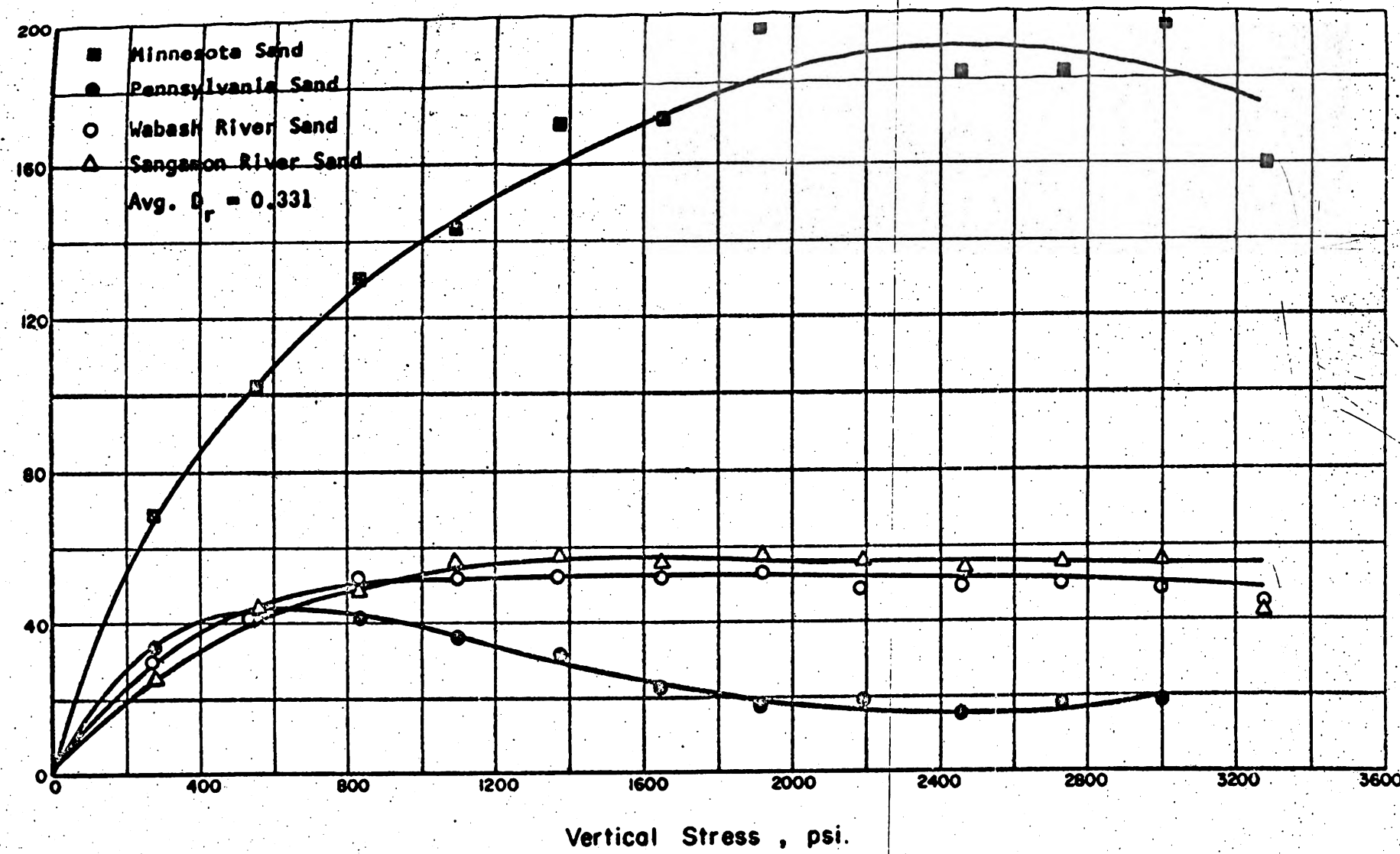

Fig. 6.9 RELATIONSHIP BETWEEN CONSTRAINED MODULUS AND VERTICAL STRESS AT CONSTANT RELATIVE DENSITY FOR THE FOUR SANDS TESTED IN ONE-DIMENSIONAL COMPRESSION

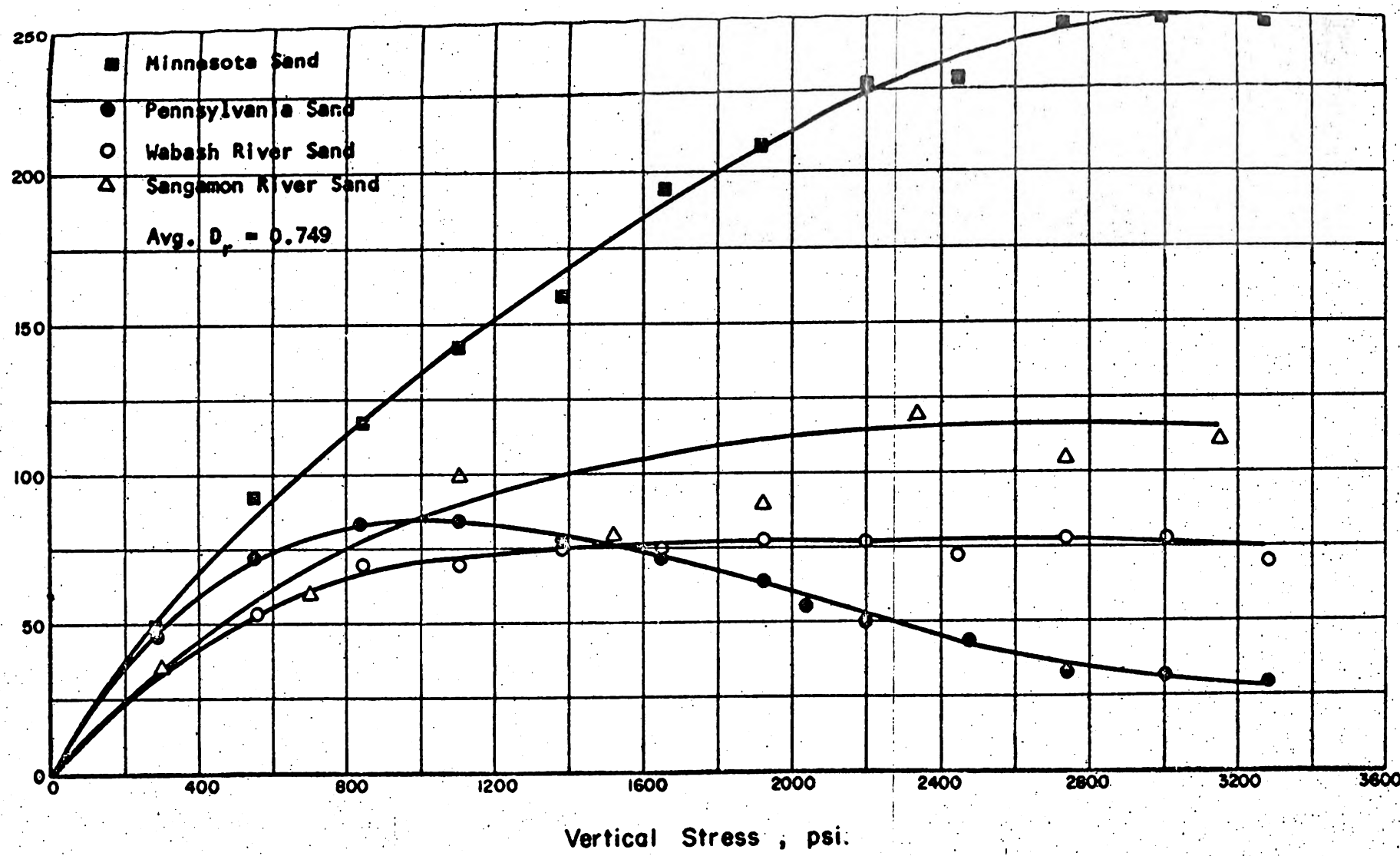

Fig. 6.10 RELATIONSHIP BETWEEN CONSTRAINED MODULUS AND VERTICAL STRESS AT CONSTANT RELATIVE DENSITY FOR THE FOUR SANDS TESTED IN ONE-DIMENSIONAL COMPRESSION

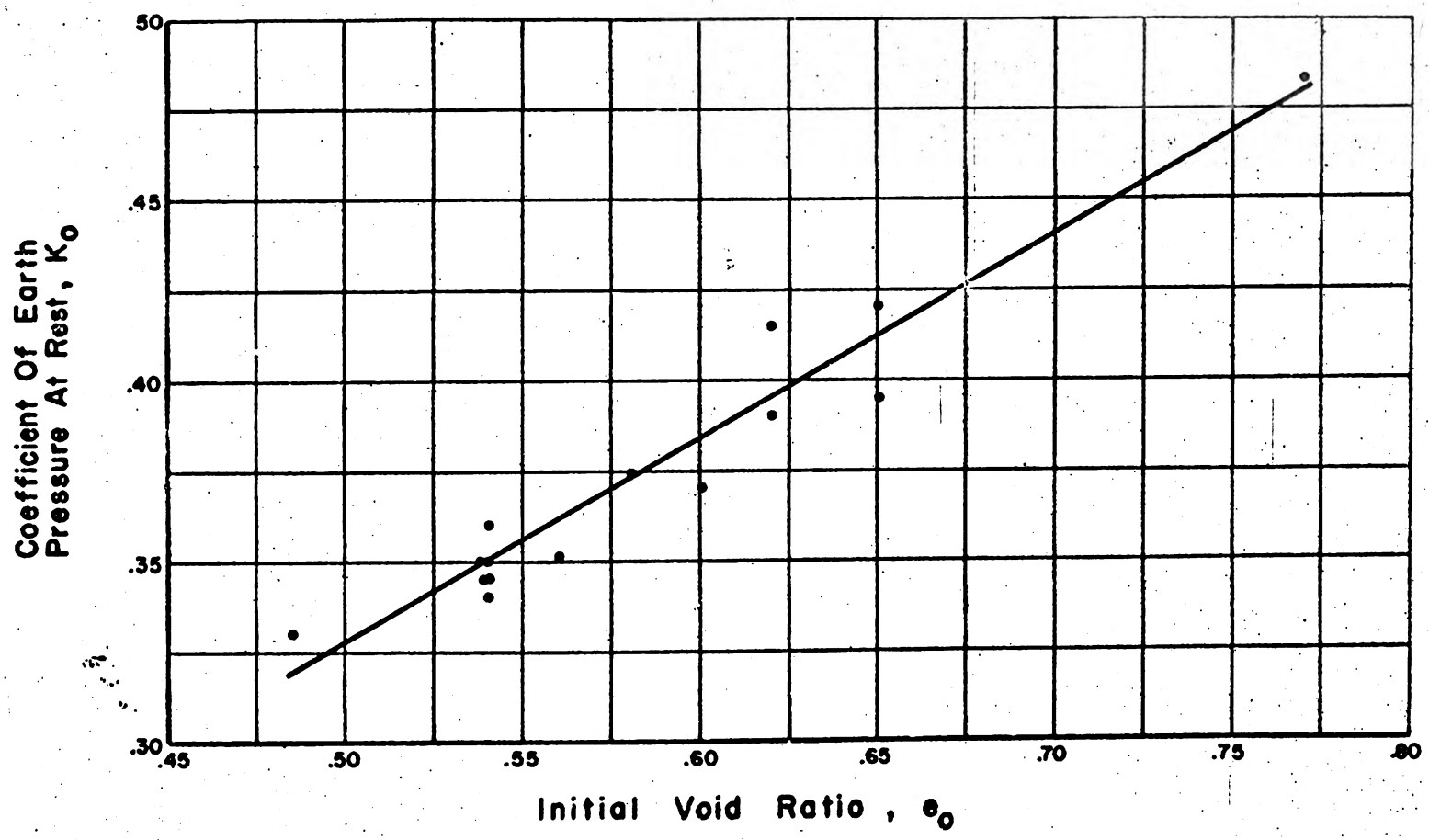

Fig. 6.11 RELATIONSHIP BETWEEN THE COEFFICIENT OF EARTH PRESSURE AT REST AND INITIAL VOID RATIO FOR MINNESOTA SAND

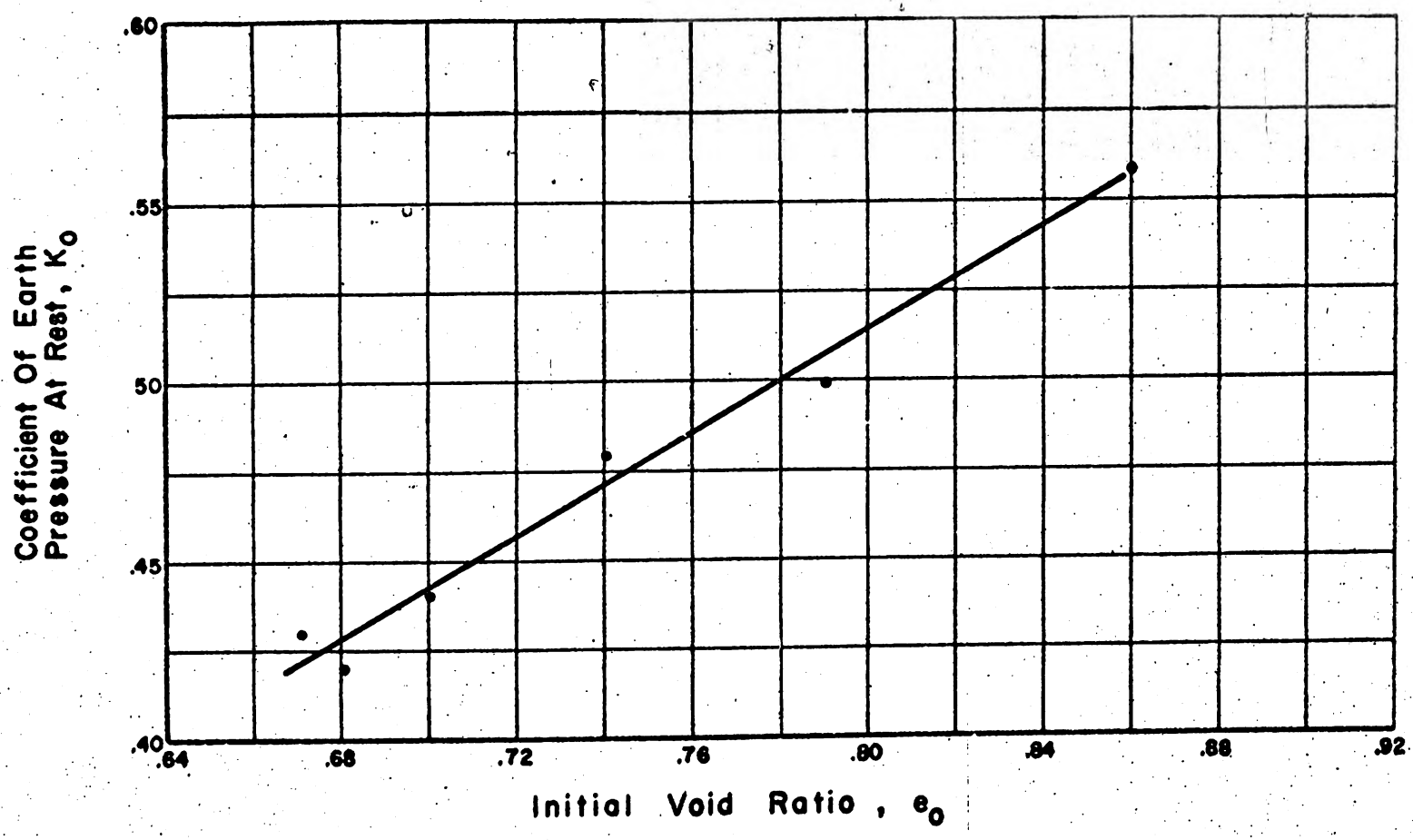

Fig. 6.12 RELATIONSHIP BETWEEN THE COEFFICIENT OF EARTH PRESSURE AT REST AND INITIAL VOID RATIO FOR PENNSYLVANIA SAND

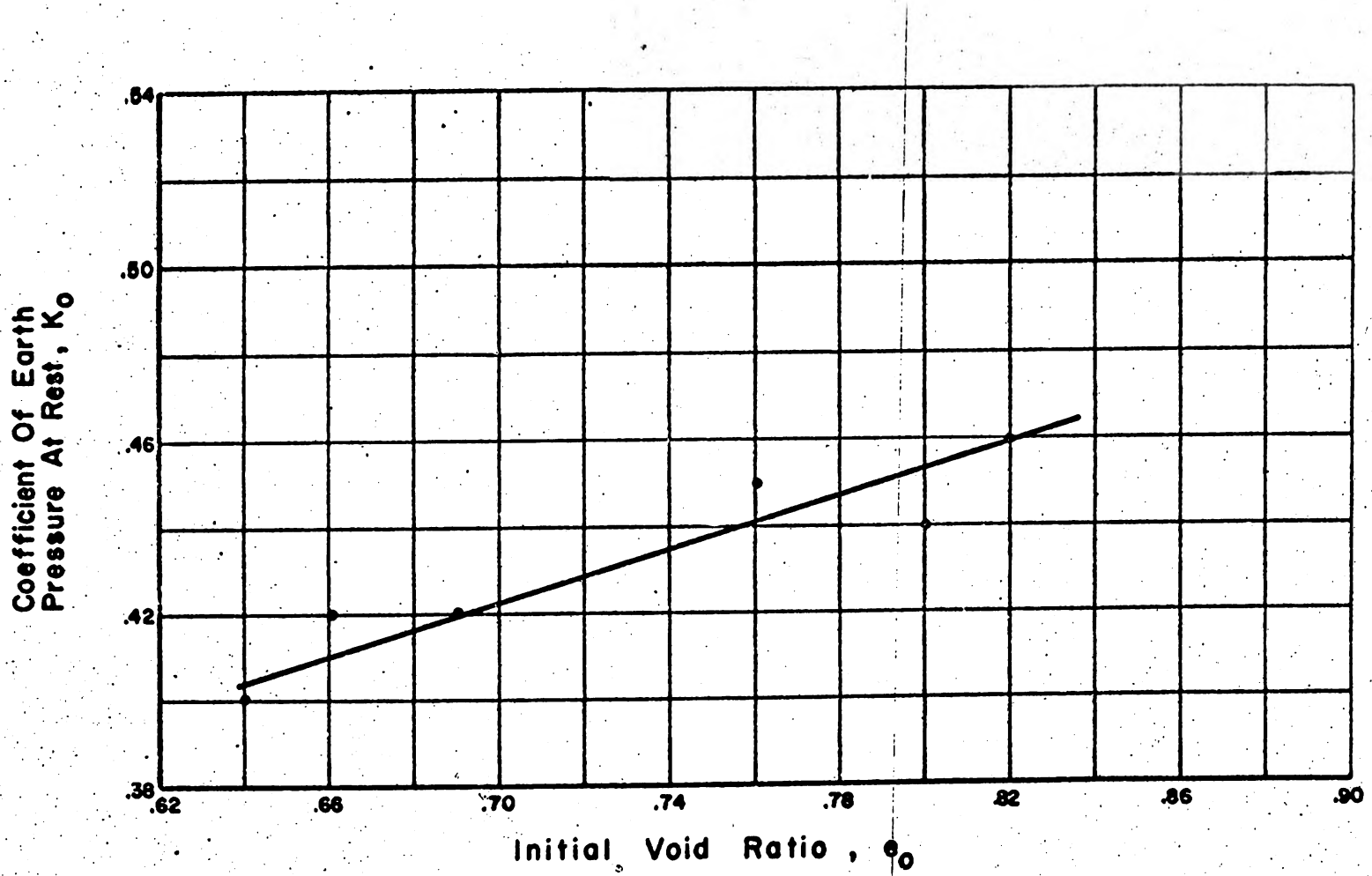

Fig. 6.13 RELATIONSHIP BETWEEN THE COEFFICIENT OF EARTH PRESSURE AT REST AND INITIAL VOID RATIO FOR SANGAMON RIVER SAND

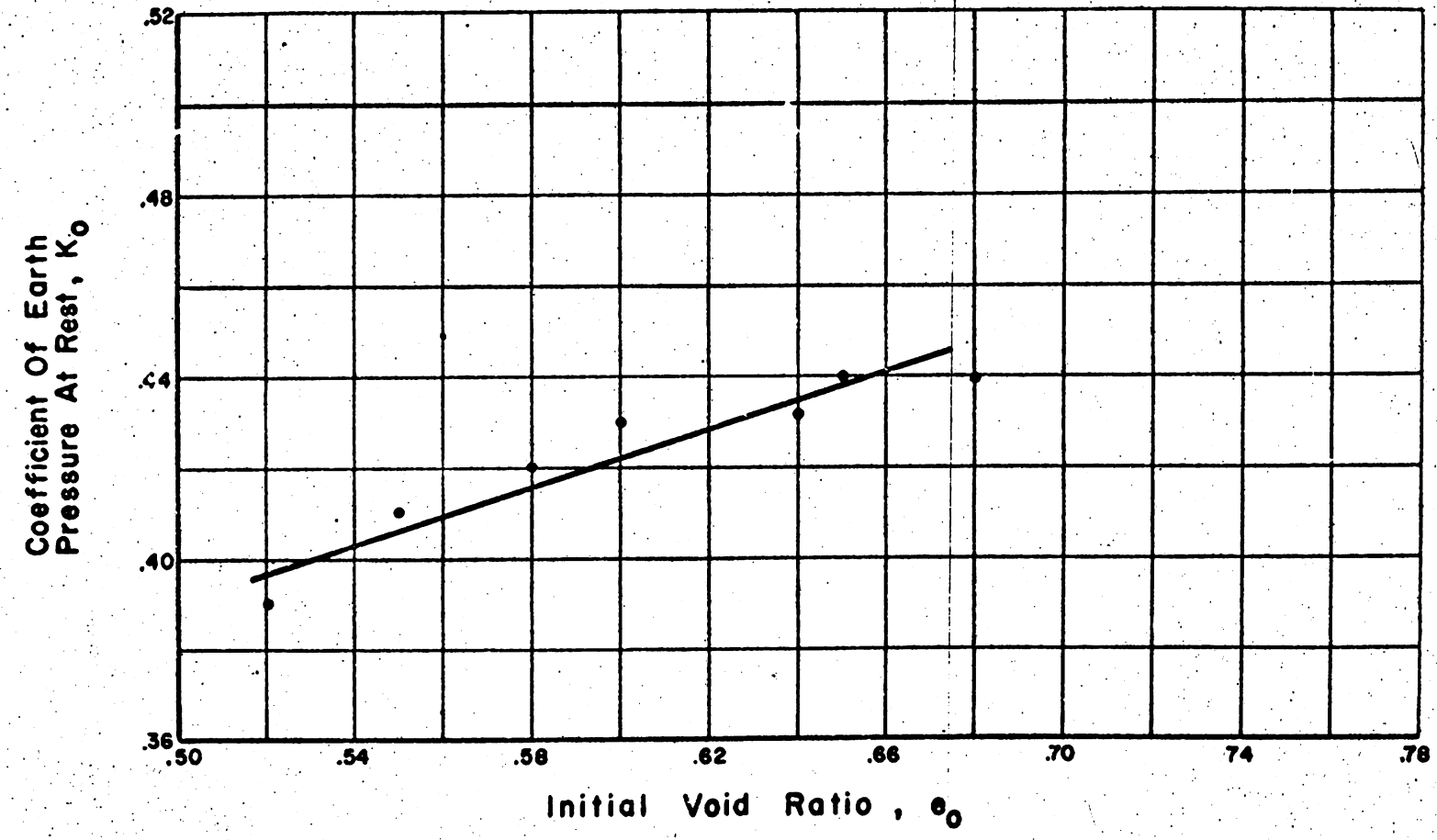

Fig. 6.14 RELATIONSHIP BETWEEN THE COEFFICIENT OF EARTH PRESSURE AT REST AND INITIAL VOID RATIO FOR WABASH RIVER SAND

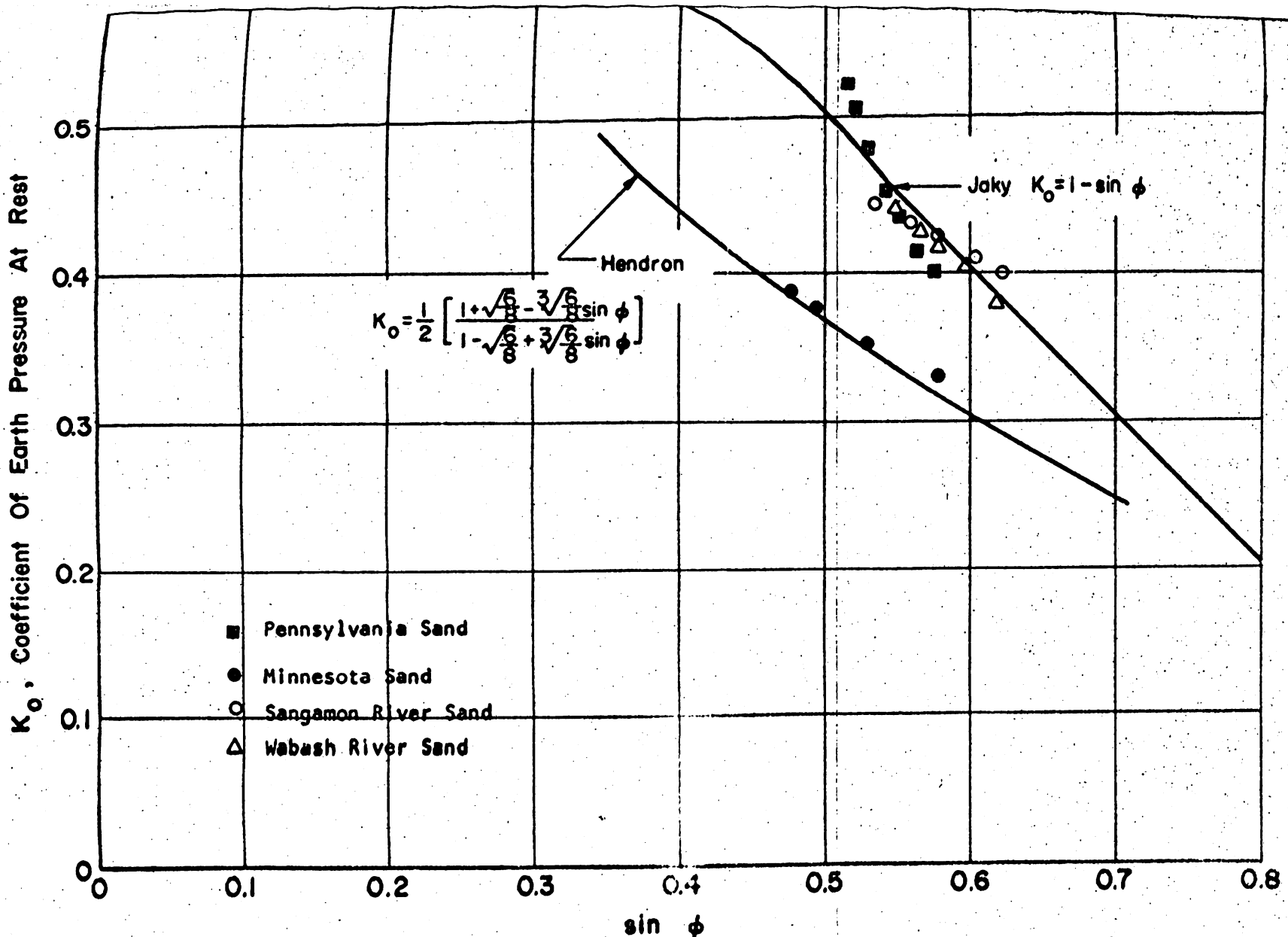

Fig. 6.15 RELATIONSHIP BETWEEN THE COEFFICIENT OF EARTH PRESSURE AT REST AND THE ANGLE OF INTERNAL FRICTION FOR THE FOUR SANDS TESTED

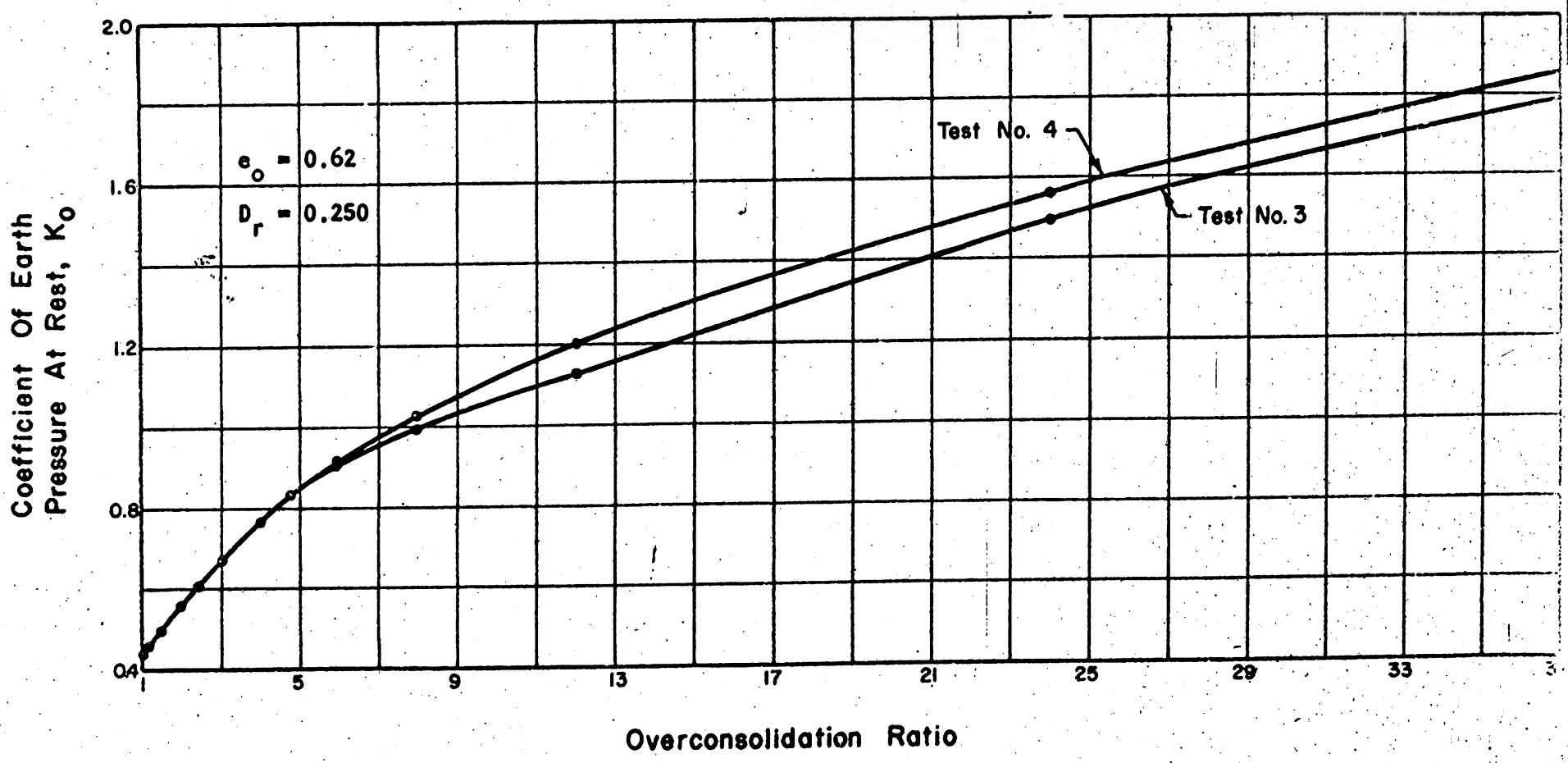

Fig. 6.16 RELATIONSHIP BETWEEN THE COEFFICIENT OF EARTH PRESSURE AT REST AND THE OVERCONSOLIDATION RATIO FOR MINNESOTA SAND

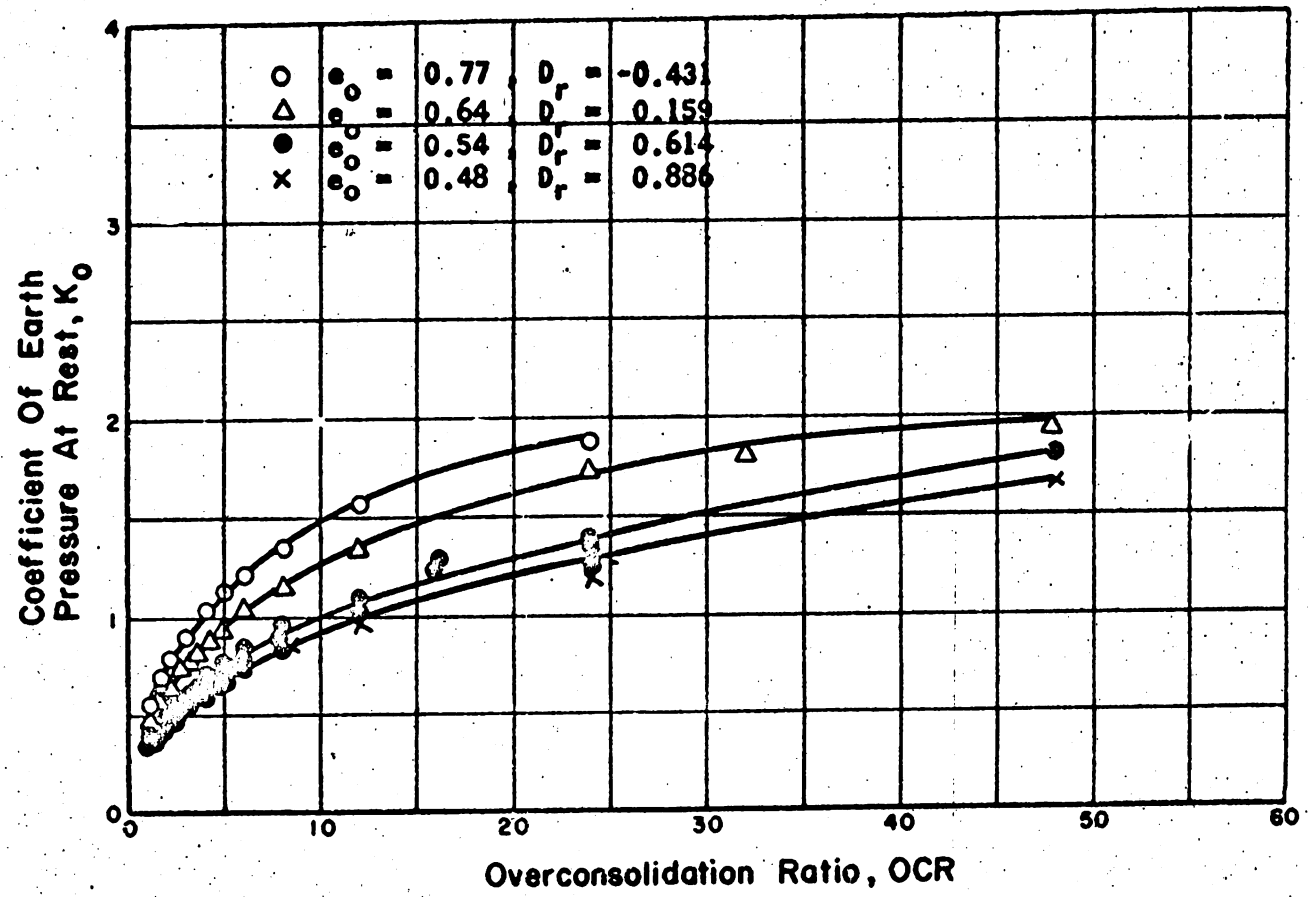

Fig. 6.17 RELATIONSHIP BETWEEN THE COEFFICIENT OF EARTH PRESSURE AT REST AND THE OVERCONSOLIDATION RATIO FOR MINNESOTA SAND

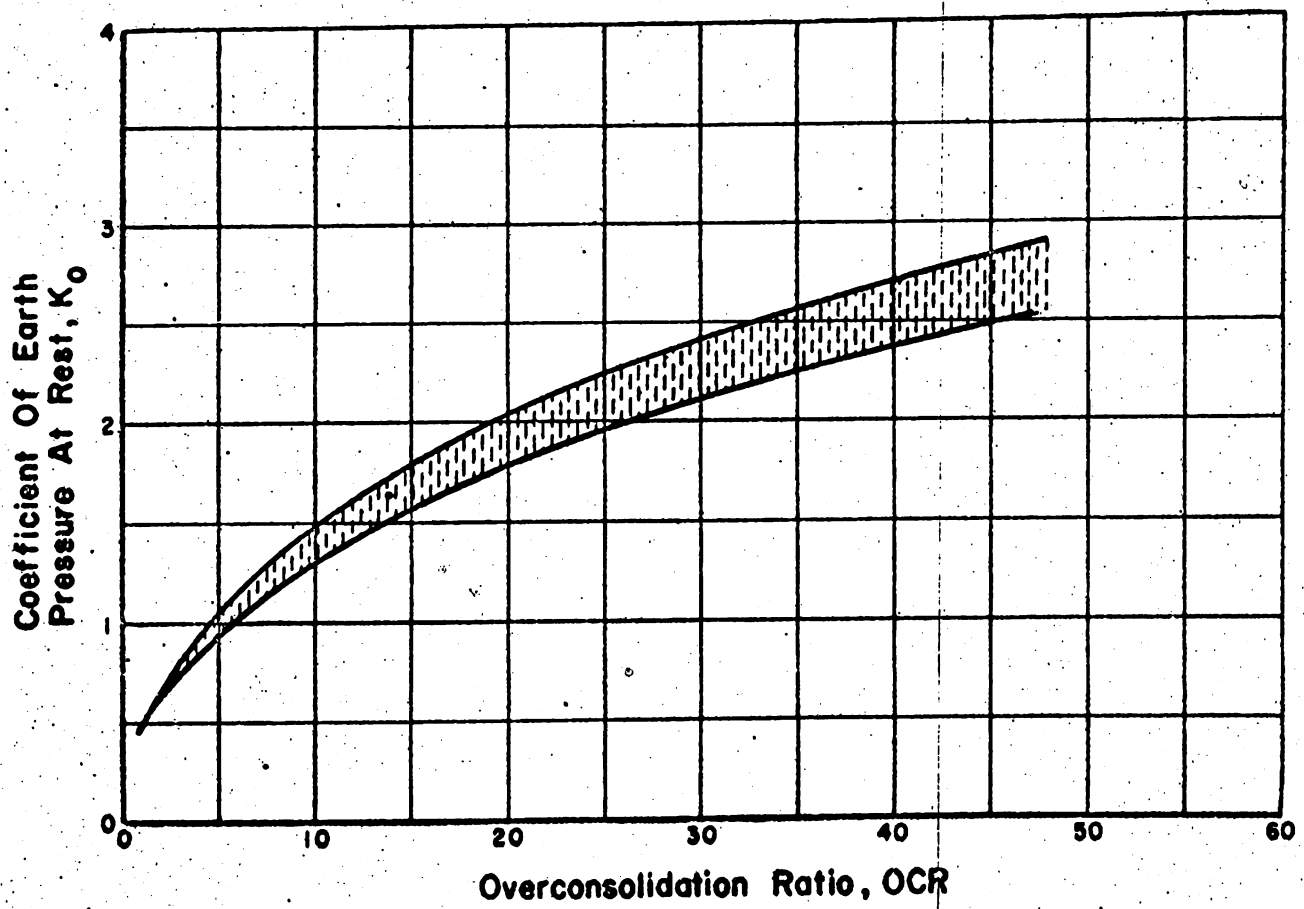

Fig. 6.18 RELATIONSHIP BETWEEN THE COEFFICIENT OF EARTH PRESSURE AT REST AND THE OVERCONSOLIDATION RATIO FOR PENNSYLVANIA SAND

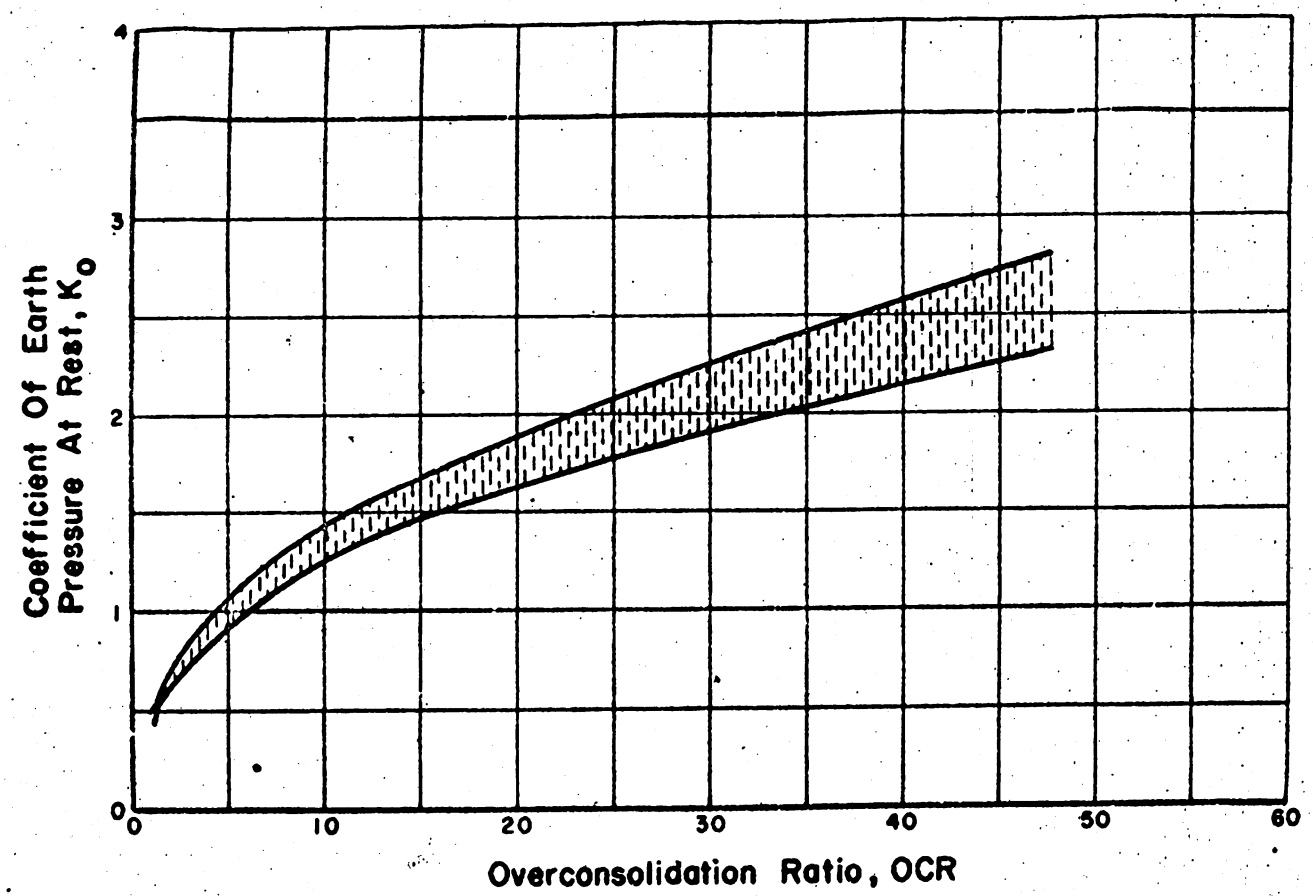

Fig. 6.19 RELATIONSHIP BETWEEN THE COEFFICIENT OF EARTH PRESSURE AT REST AND THE OVERCONSOLIDATION RATIO FOR SANGAMON RIVER SAND

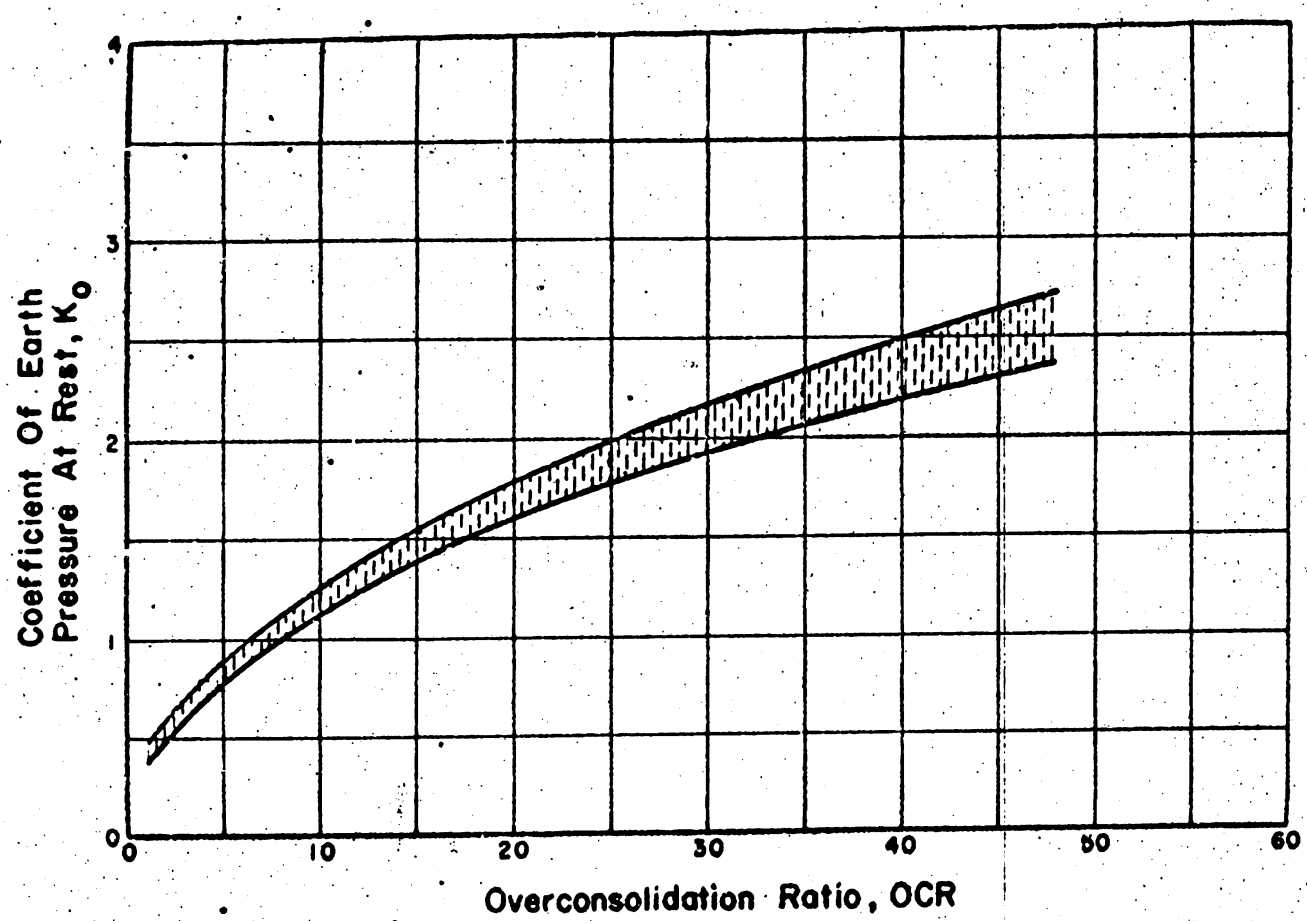

Fig. 6.20 RELATIONSHIP BETWEEN THE COEFFICIENT OF EARTH PRESSURE AT REST AND THE OVERCONSOLIDATION RATIO FOR WABASH RIVER SAND

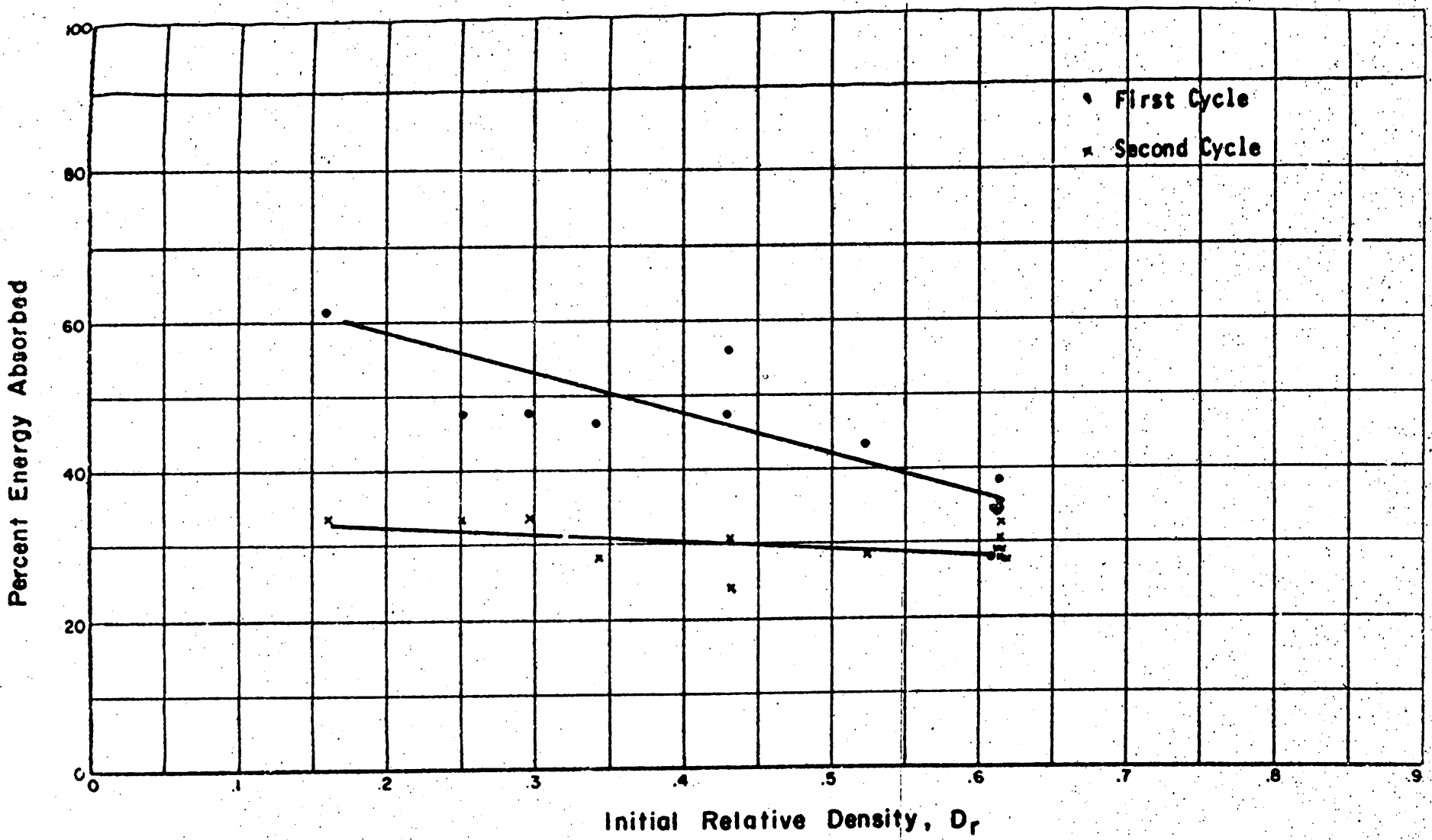

Fig. 6.21 RELATIONSHIP BETWEEN ENERGY ABSORPTION AND INITIAL RELATIVE DENSITY FOR MINNESOTA SAND

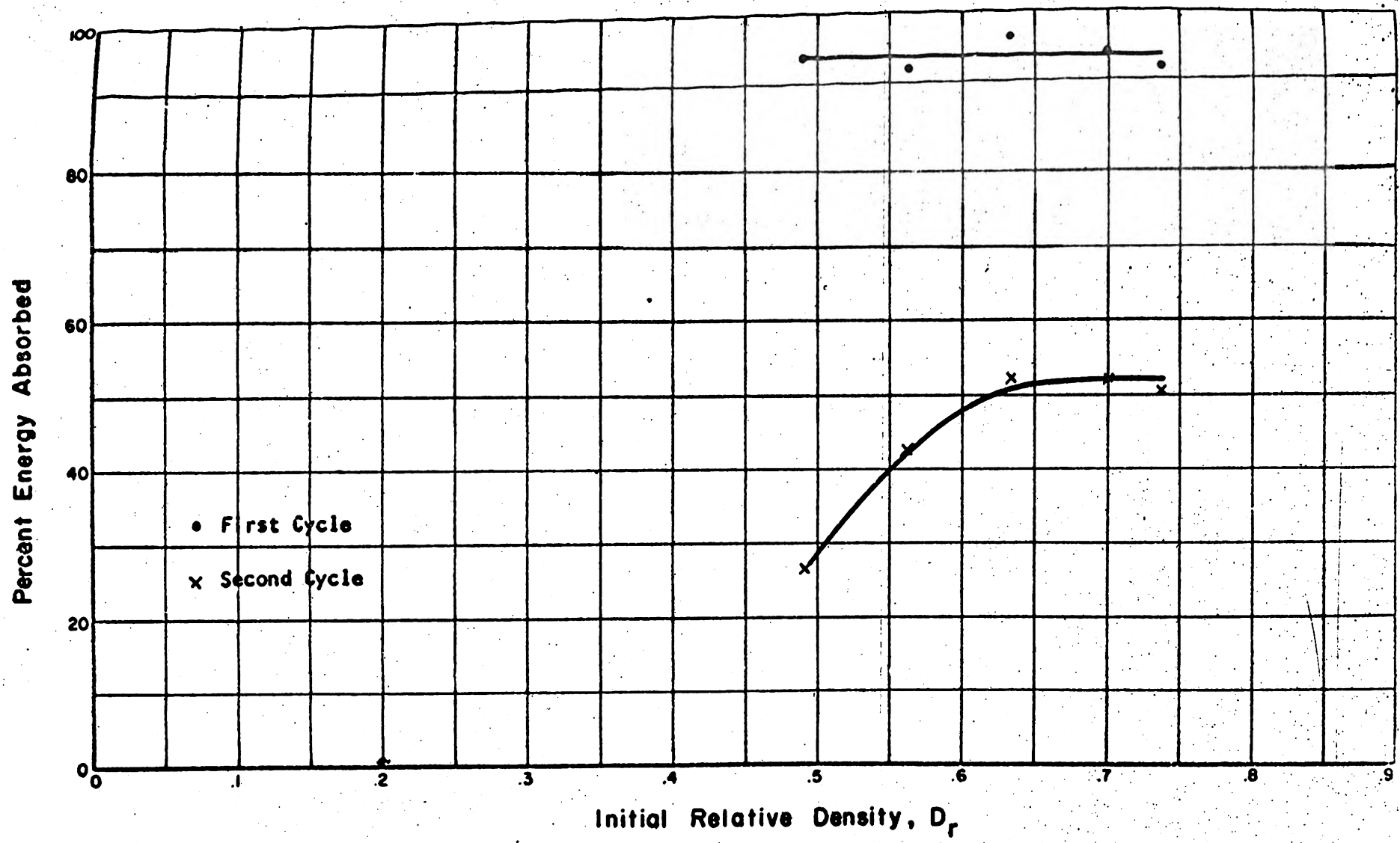

Fig. 6.22 RELATIONSHIP BETWEEN ENERGY ABSORPTION AND INITIAL RELATIVE DENSITY FOR PENNSYLVANIA SAND

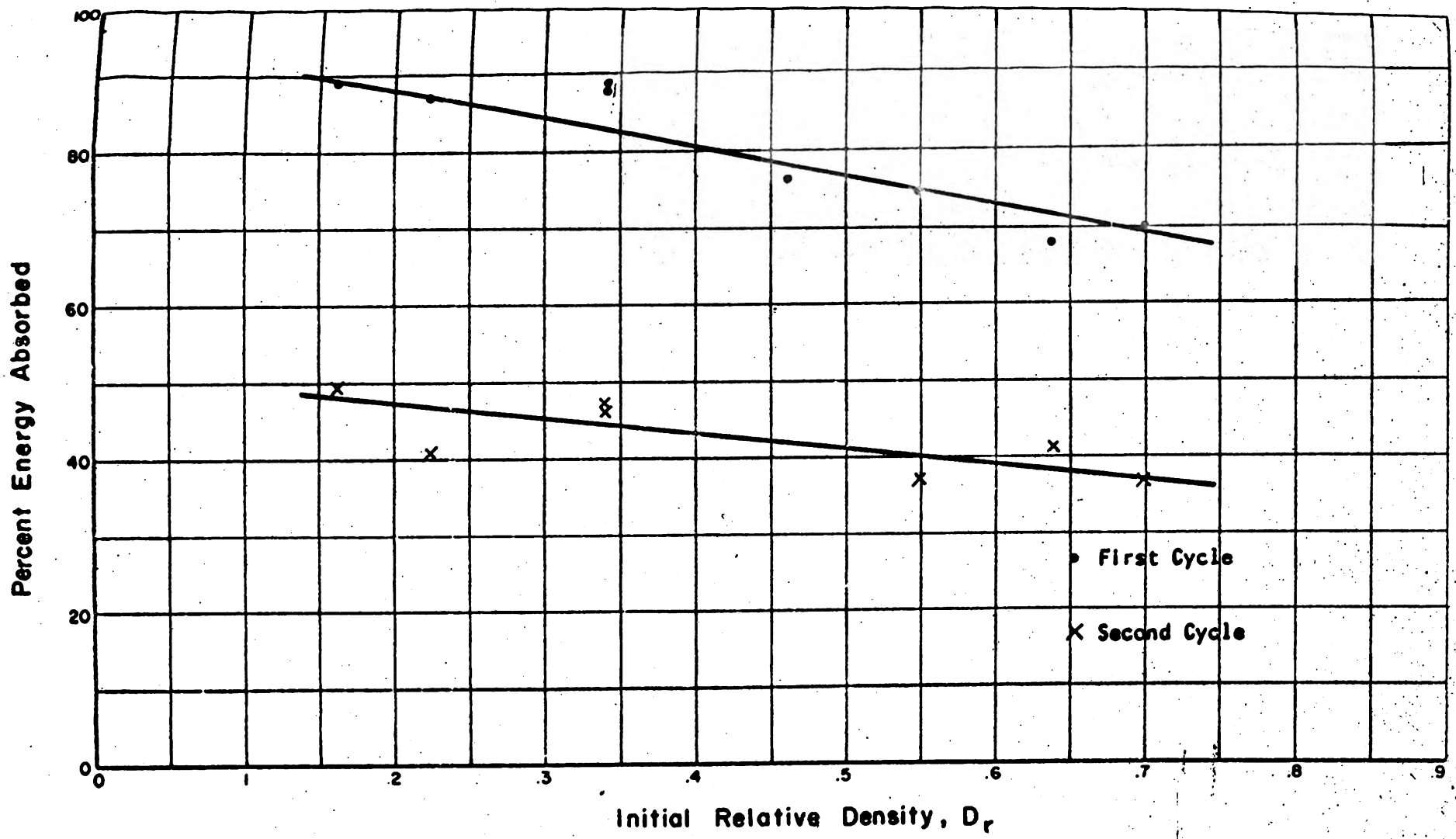

Fig. 6.23 · RELATIONSHIP BETWEEN ENERGY ABSORPTION AND INITIAL RELATIVE DENSITY FOR SANGAMON RIVER SAND

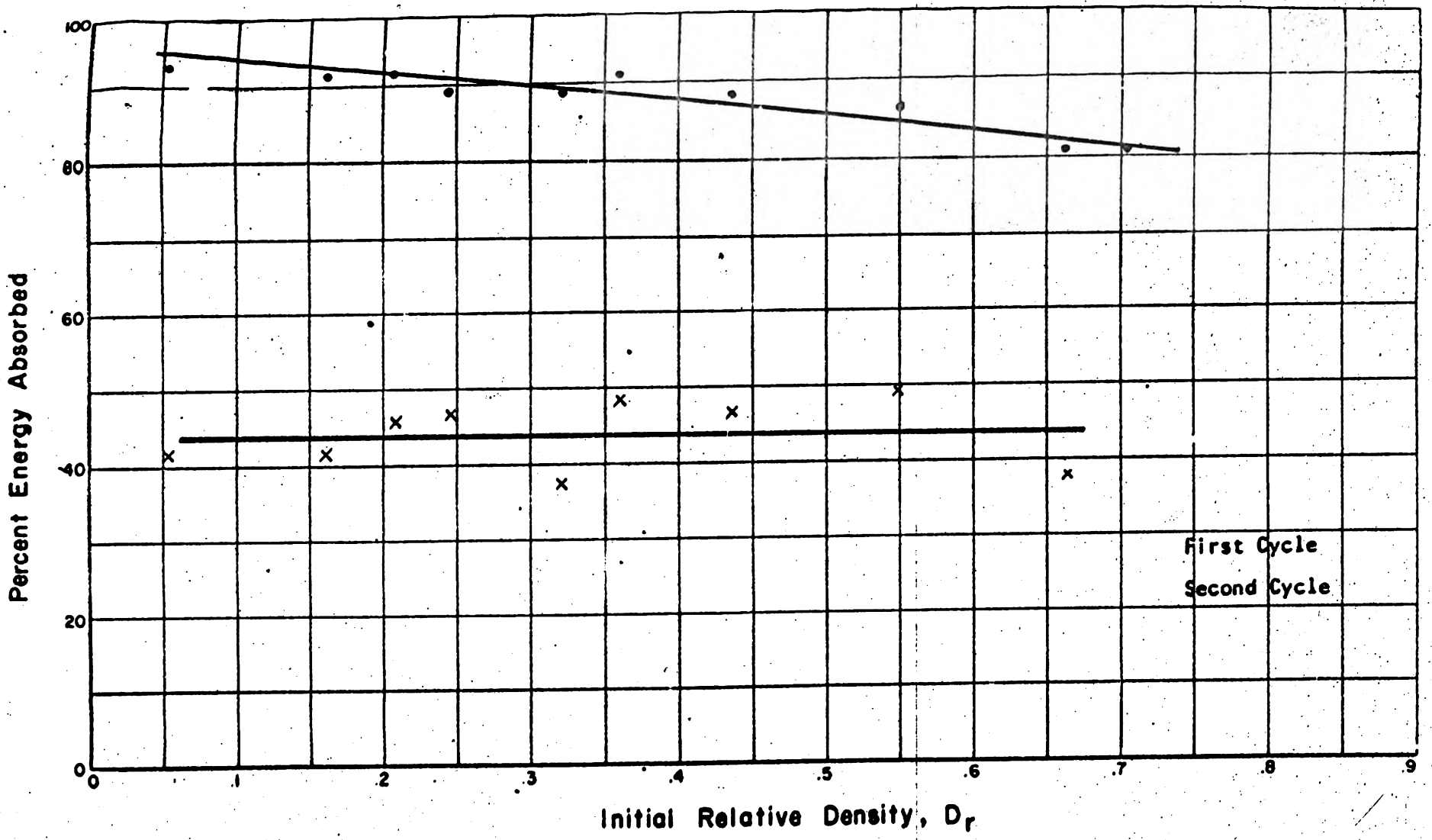

Fig. 6.24 RELATIONSHIP BETWEEN ENERGY ABSORPTION AND INITIAL RELATIVE DENSITY FOR WABASH RIVER SAND

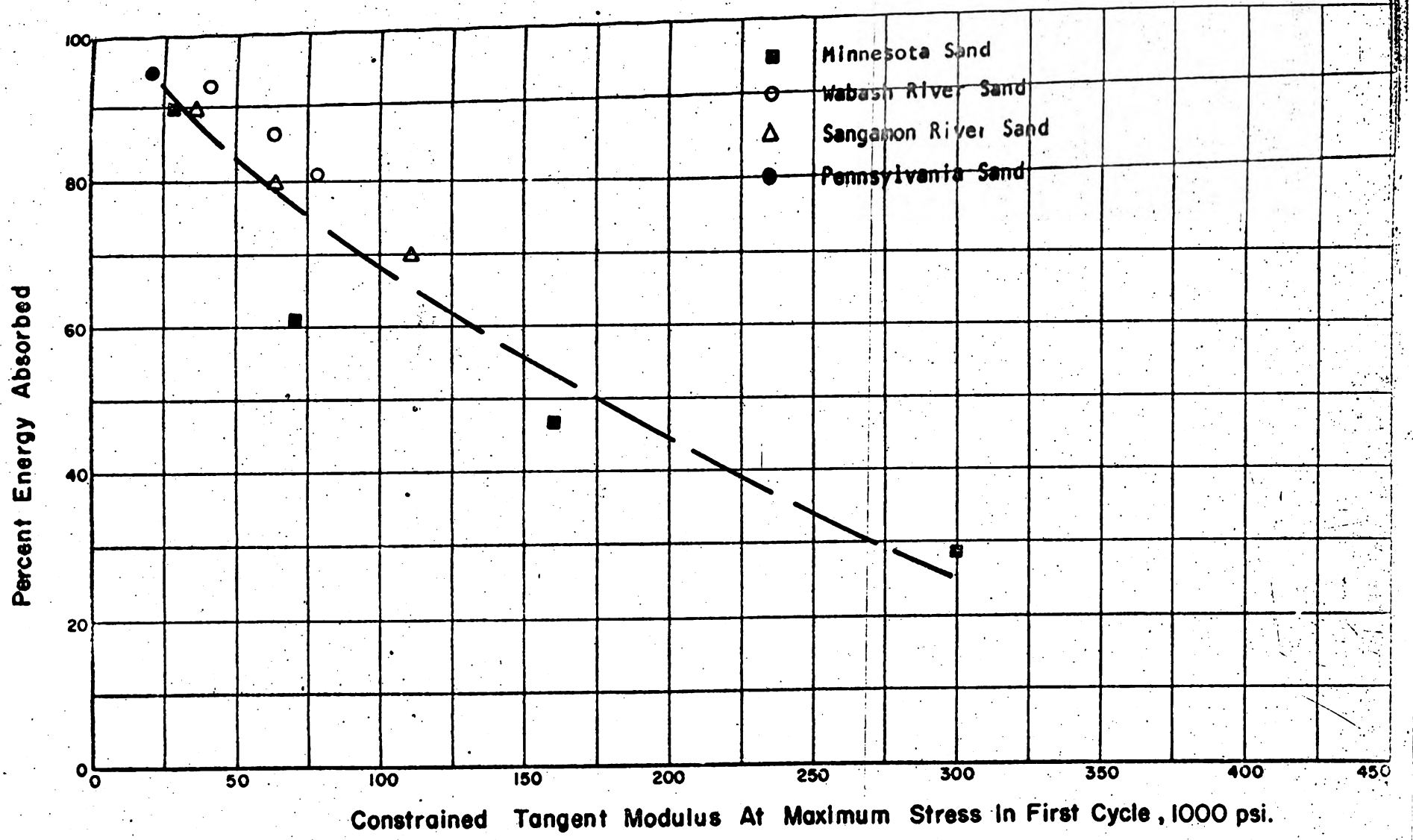

Fig. 6.25 RELATIONSHIP BETWEEN ENERGY ABSORPTION IN THE FIRST CYCLE AND CONSTRAINED MODULUS AT MAXIMUM STRESS IN THE FIRST CYCLE FOR FOUR SANDS TESTED

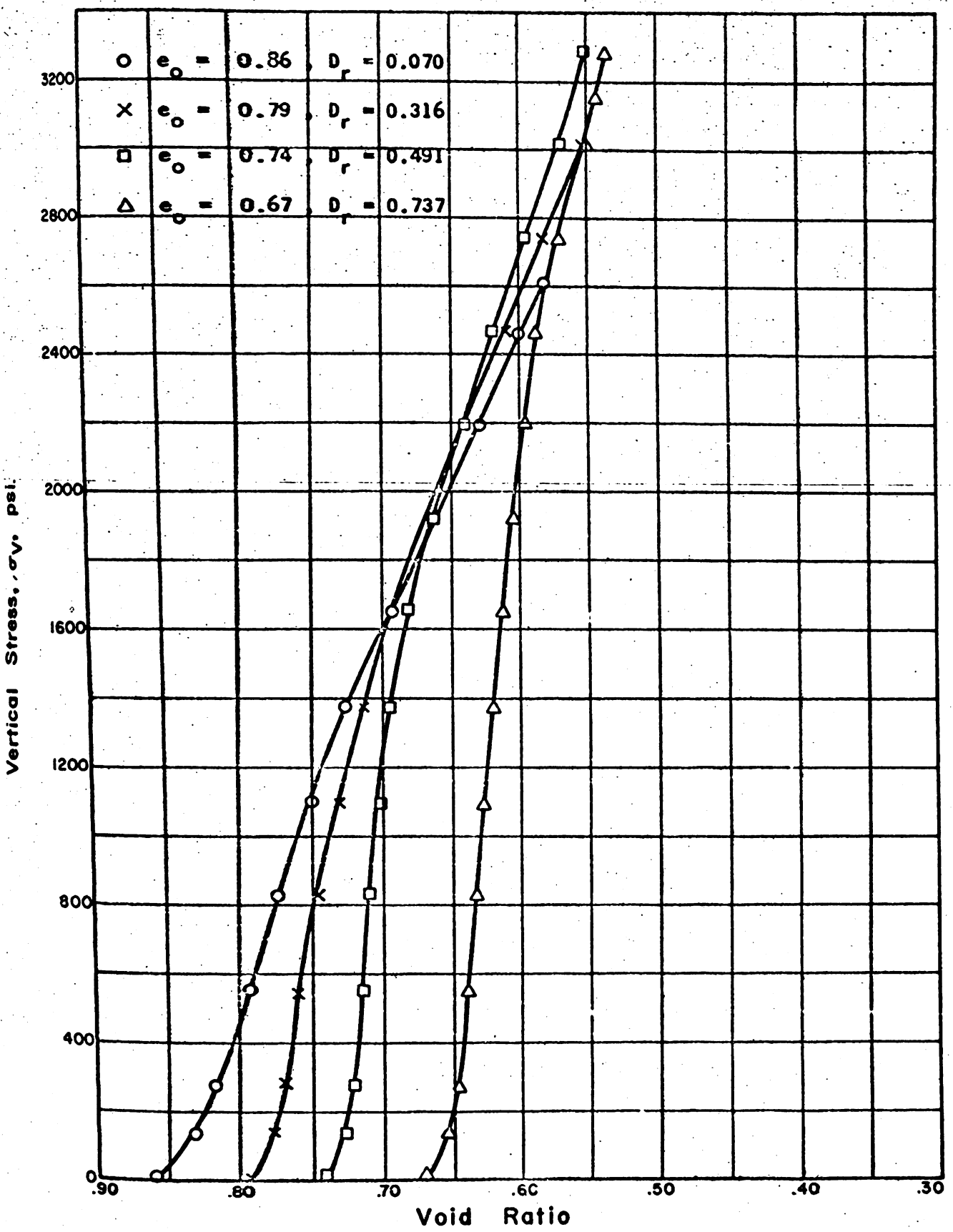

Fig. 6.26 RELATIONSHIP BETWEEN VERTICAL STRESS AND VOID RATIO FOR PENNSYLVANIA SAND IN ONE-DIMENSIONAL COMPRESSION

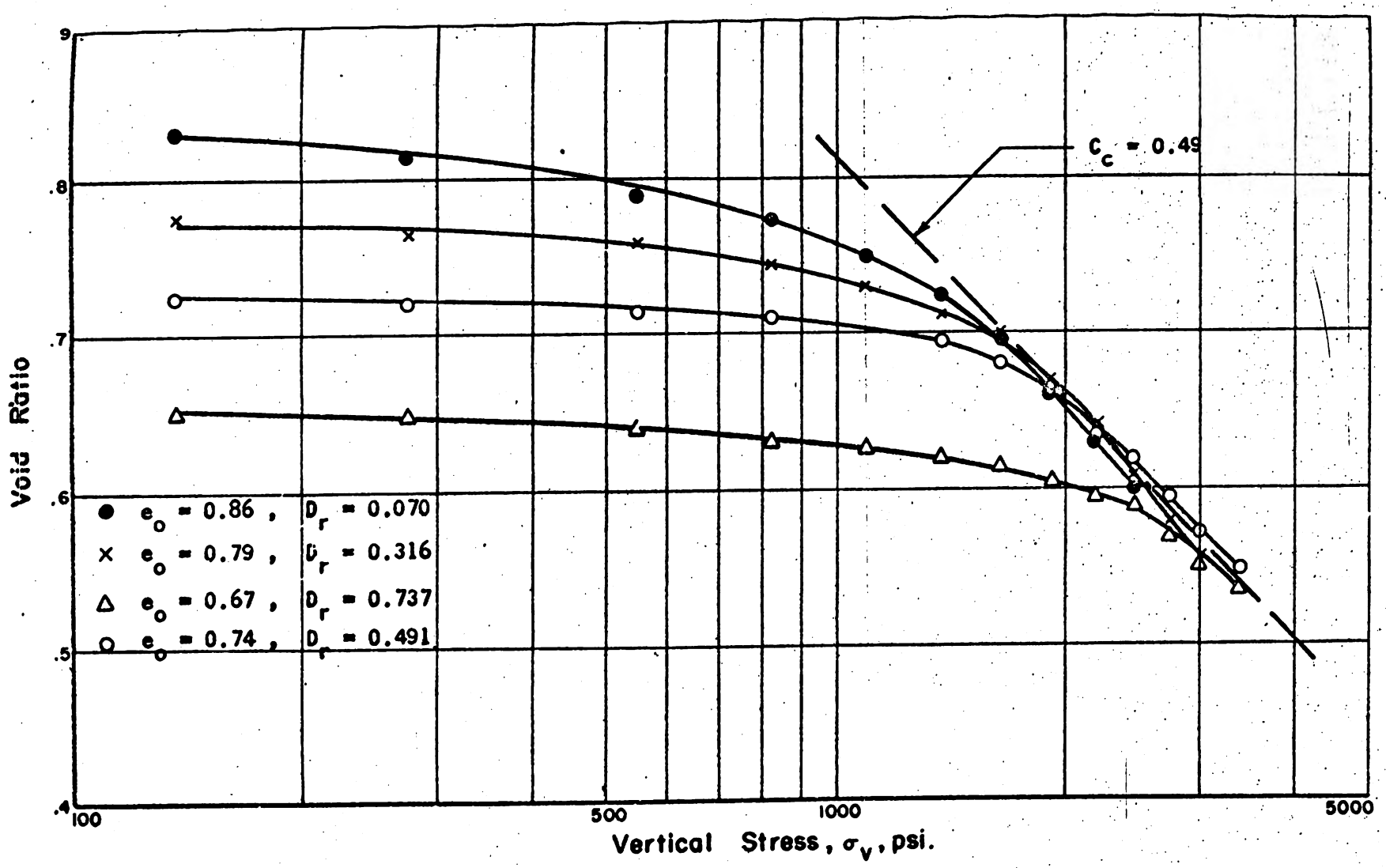

Fig. 6.27 RELATIONSHIP BETWEEN VERTICAL STRESS AND VOID RATIO FOR PENNSYLVANIA SAND IN ONE-DIMENSIONAL COMPRESSION

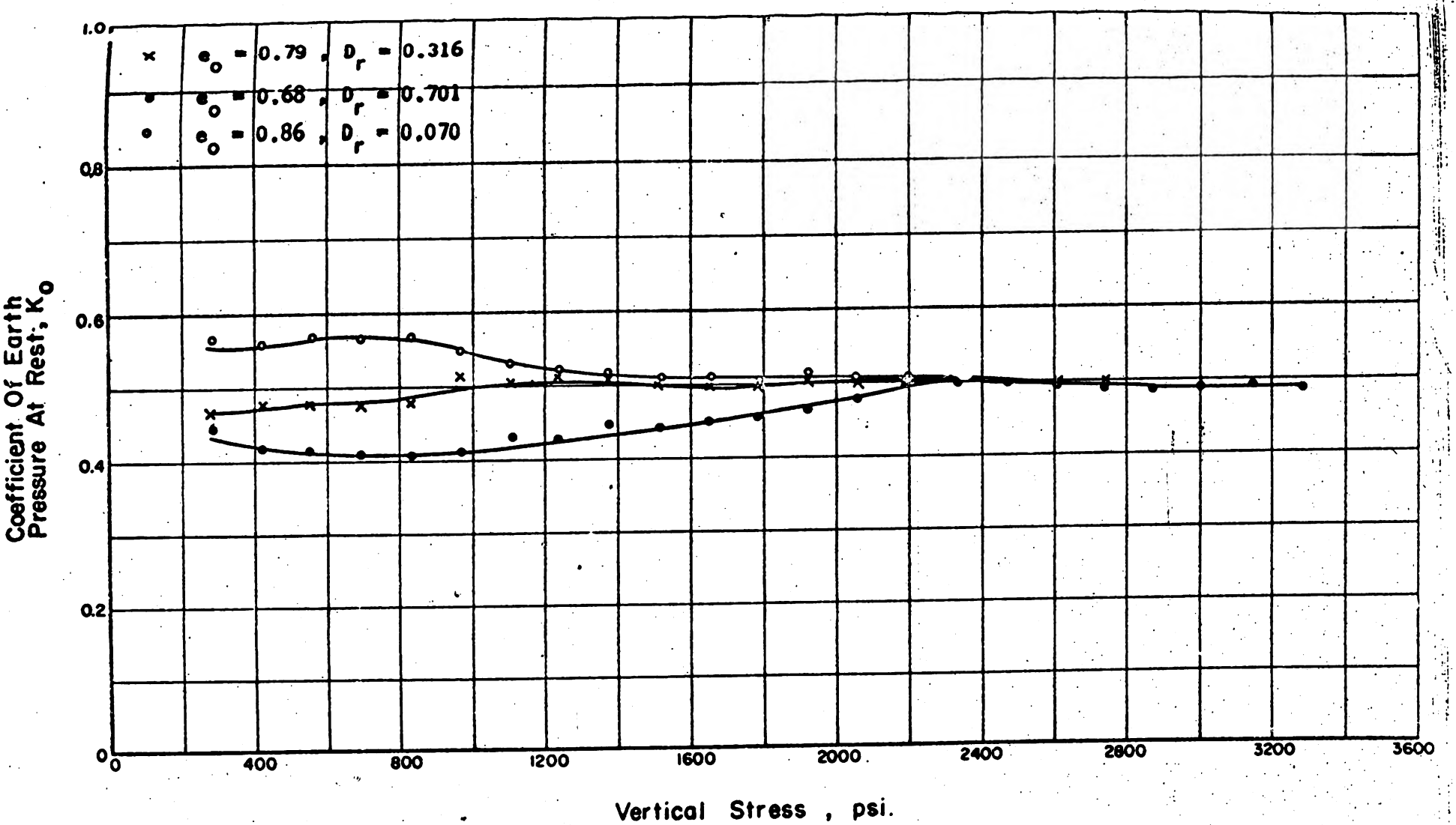

Fig. 6.28 VARIATION OF THE COEFFICIENT OF EARTH PRESSURE AT REST WITH VERTICAL STRESS FOR PENNSYLVANIA SAND

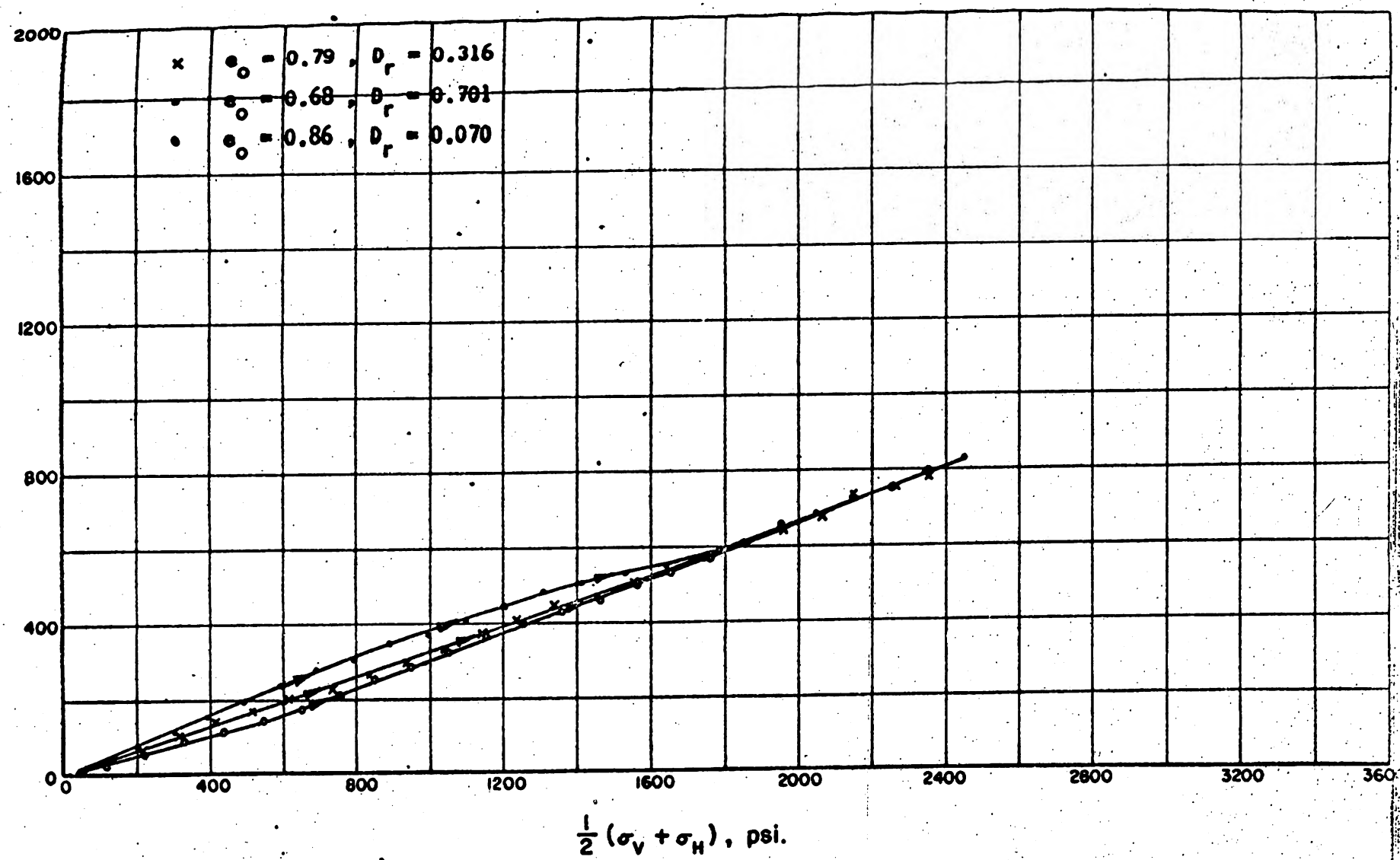

Fig. 6.29 STRESS PATHS FOR LOADING OF PENNSYLVANIA SAND IN ONE-DIMENSIONAL COMPRESSION

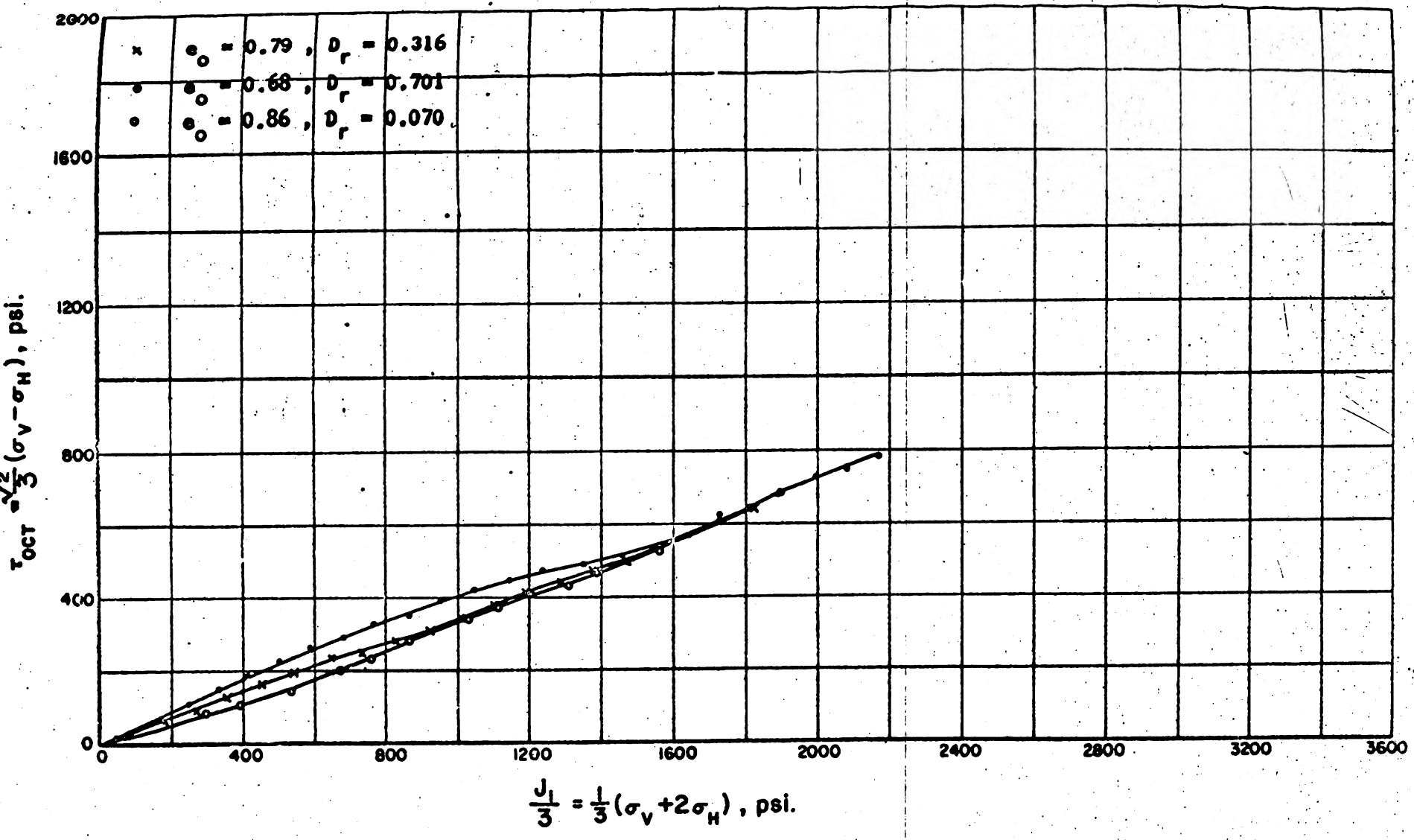

Fig. 6.30 VARIATION OF THE OCTAHEDRAL SHEARING STRESS WITH THE MEAN PRINCIPAL STRESS FOR PENNSYLVANIA SAND IN ONE-DIMENSIONAL COMPRESSION

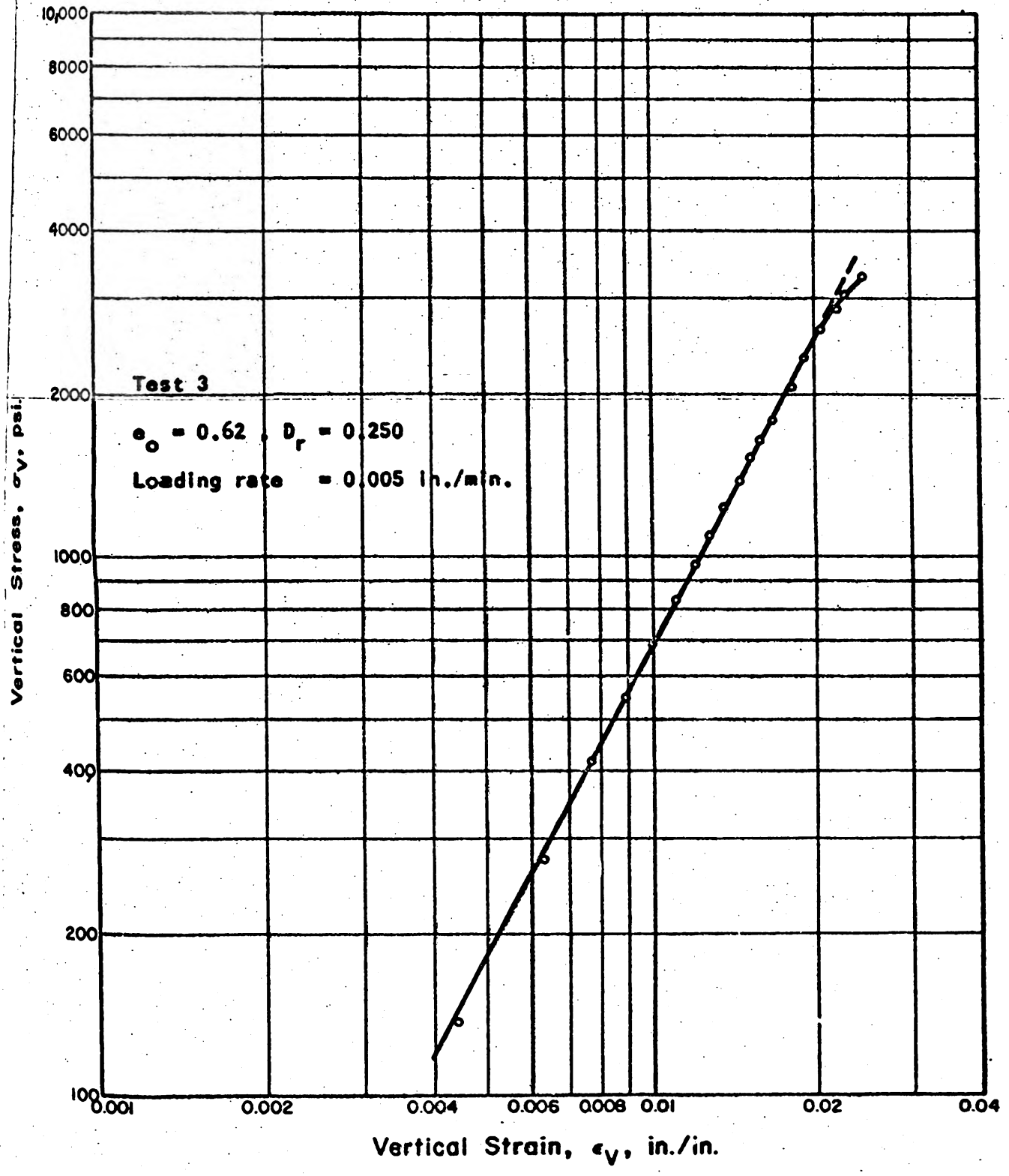

Fig. 6.31 LOGARITHMIC PLOT OF STRESS STRAIN CURVE FOR MINNESOTA SAND IN ONE-DIMENSIONAL COMPRESSION

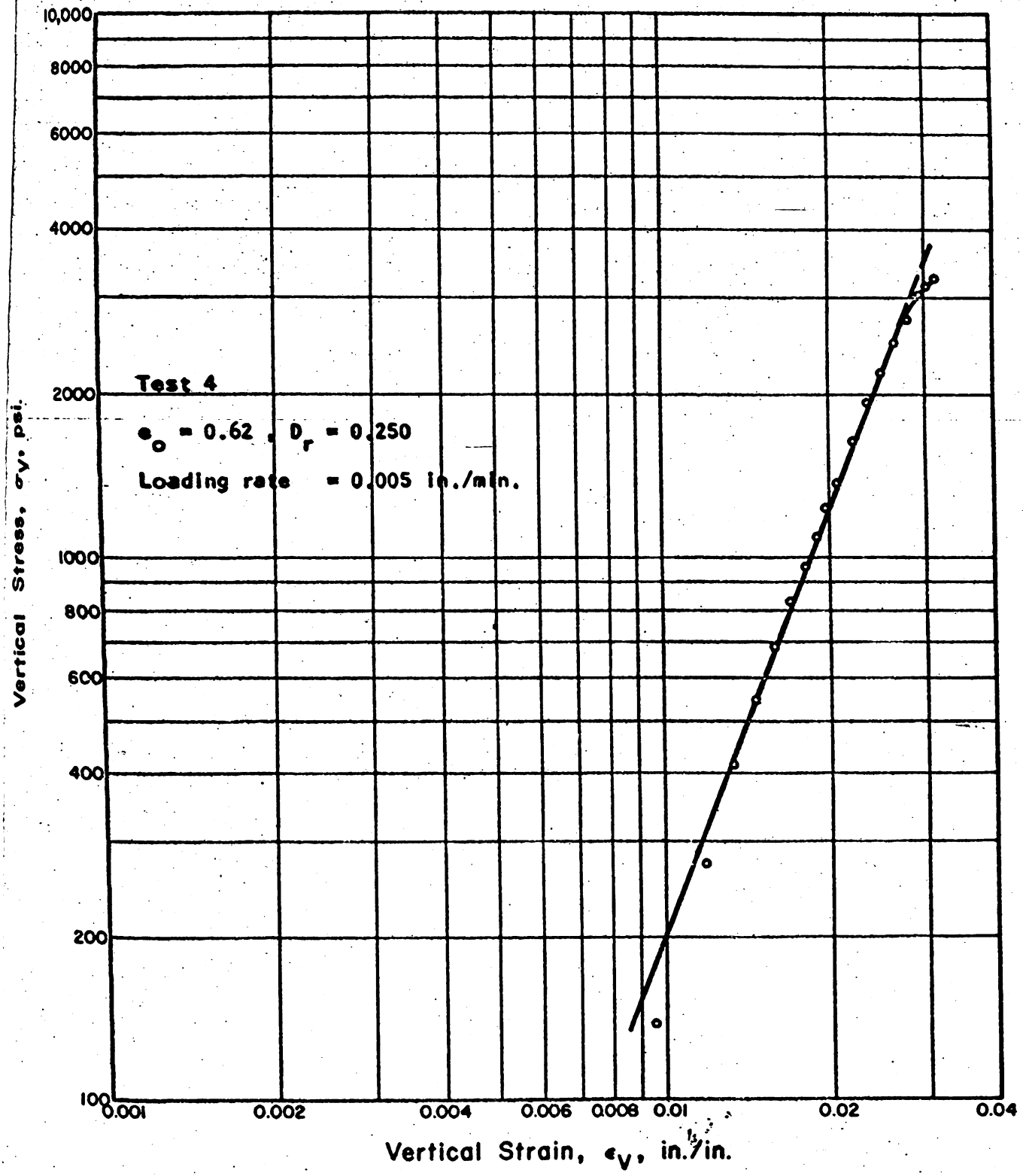

Fig. 6.32 LOGARITHMIC PLOT OF STRESS STRAIN CURVE FOR MINNESOTA SAND IN ONE-DIMENSIONAL COMPRESSION

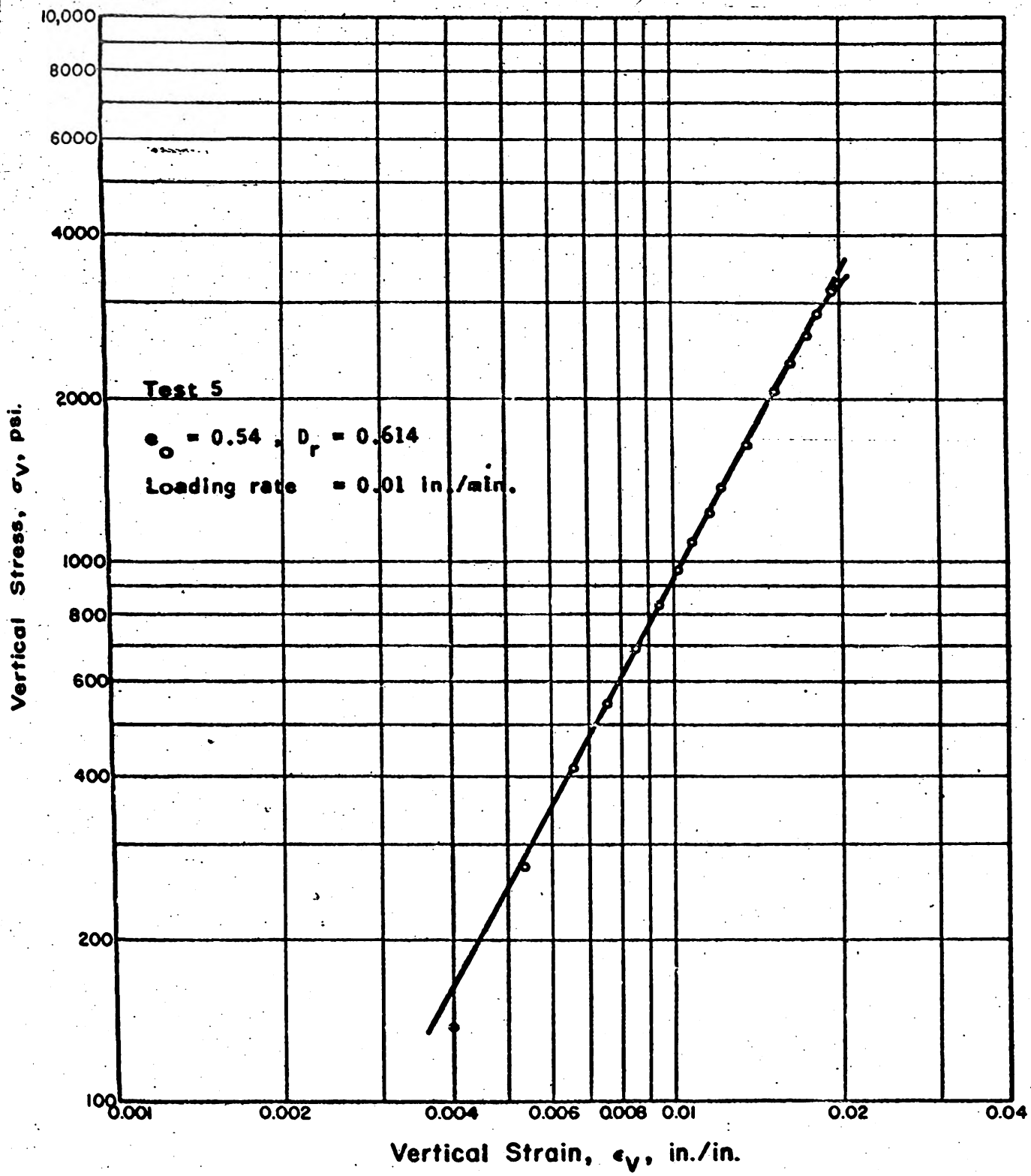

Fig. 6.33 LOGARITHMIC PLOT OF STRESS STRAIN CURVE FOR MINNESOTA SAND IN ONE-DIMENSIONAL COMPRESSION

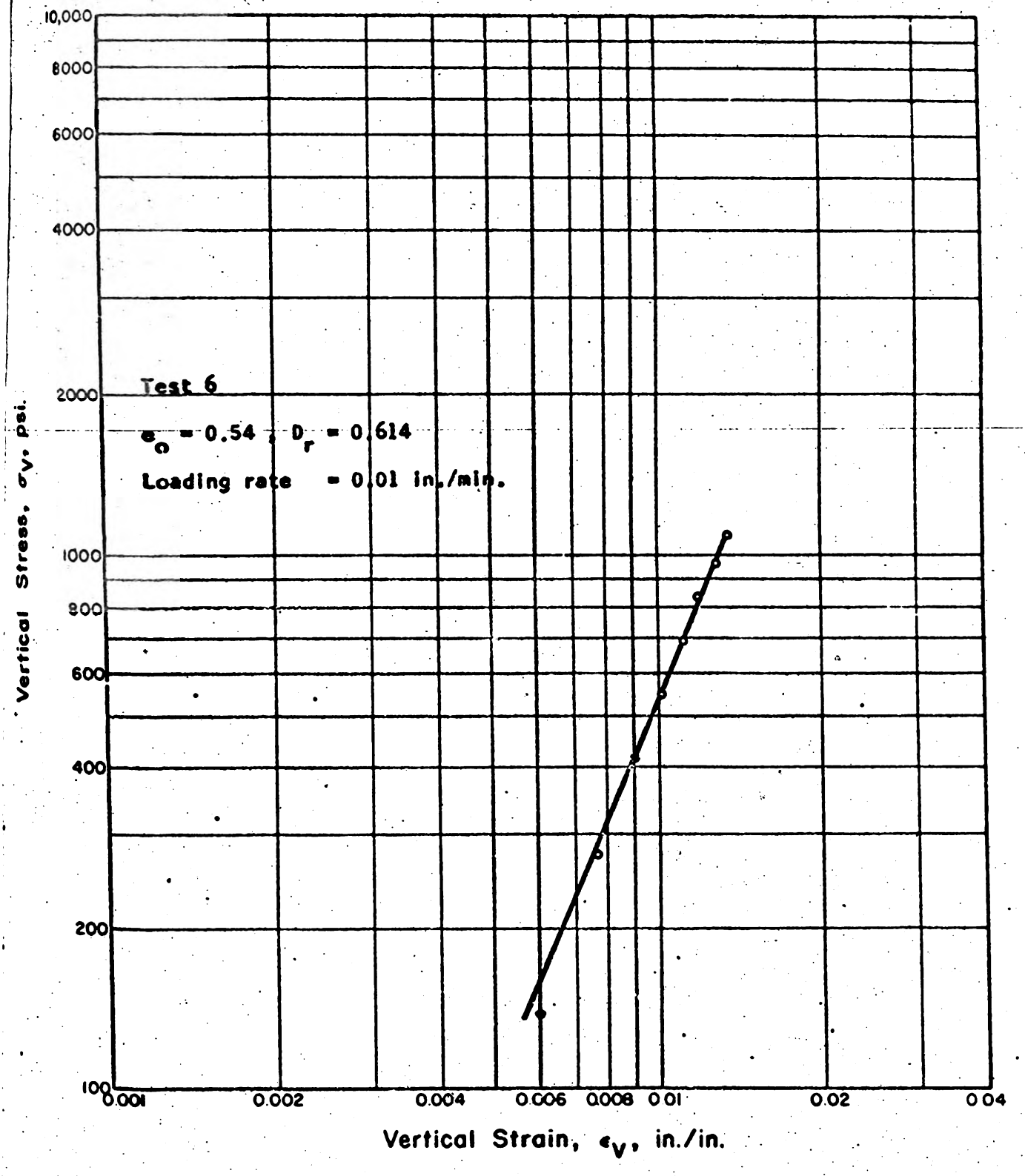

Fig. 6.34 LOGARITHMIC PLOT OF STRESS STRAIN CURVE FOR MINNESOTA SAND IN ONE-DIMENSIONAL COMPRESSION

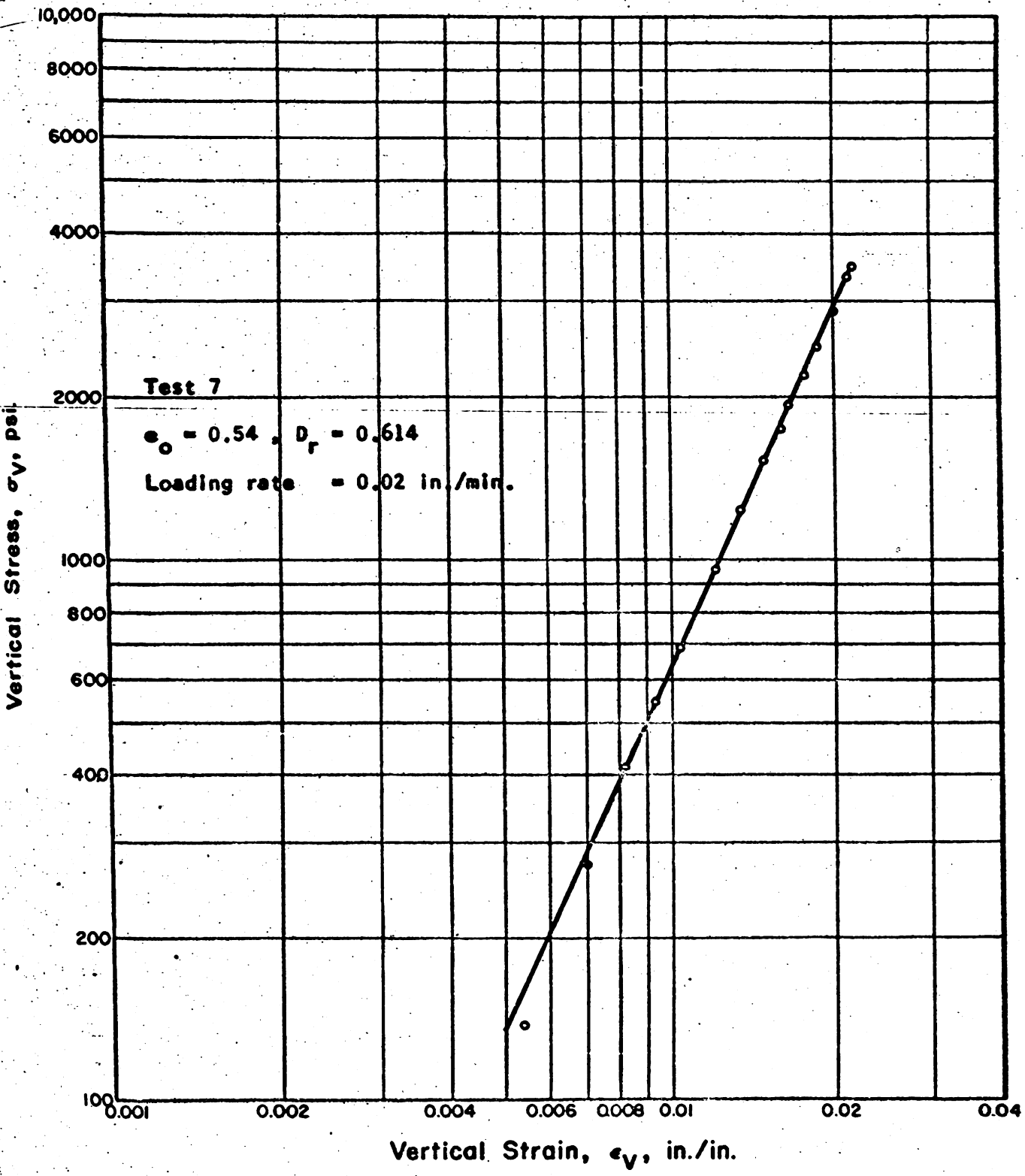

Fig. 6.35 LOGARITHMIC PLOT OF STRESS STRAIN CURVE FOR MINNESOTA SAND IN ONE-DIMENSIONAL COMPRESSION

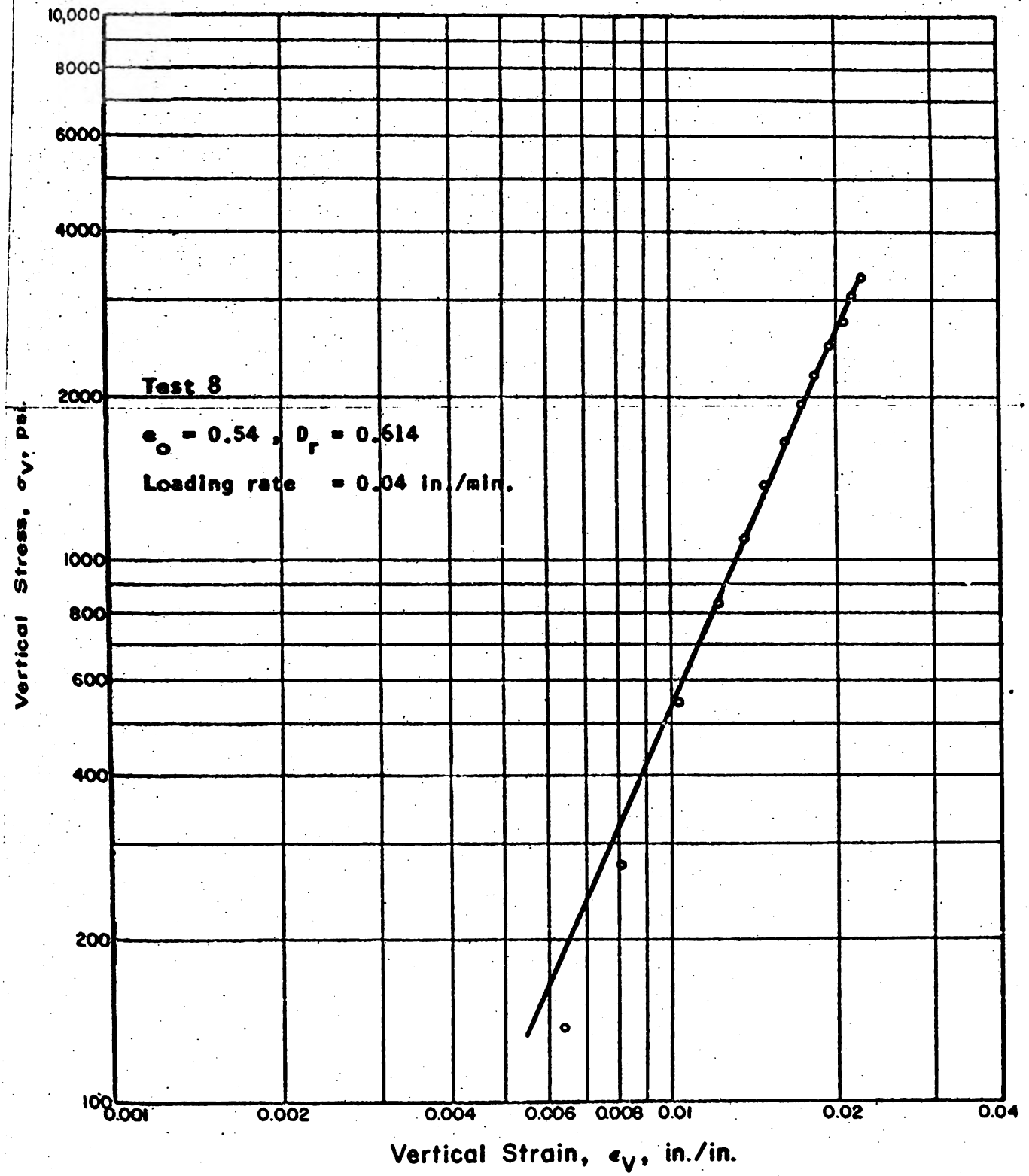

Fig. 6.36 LOGARITHMIC PLOT OF STRESS STRAIN CURVE FOR MINNESOTA SAND IN ONE-DIMENSIONAL COMPRESSION

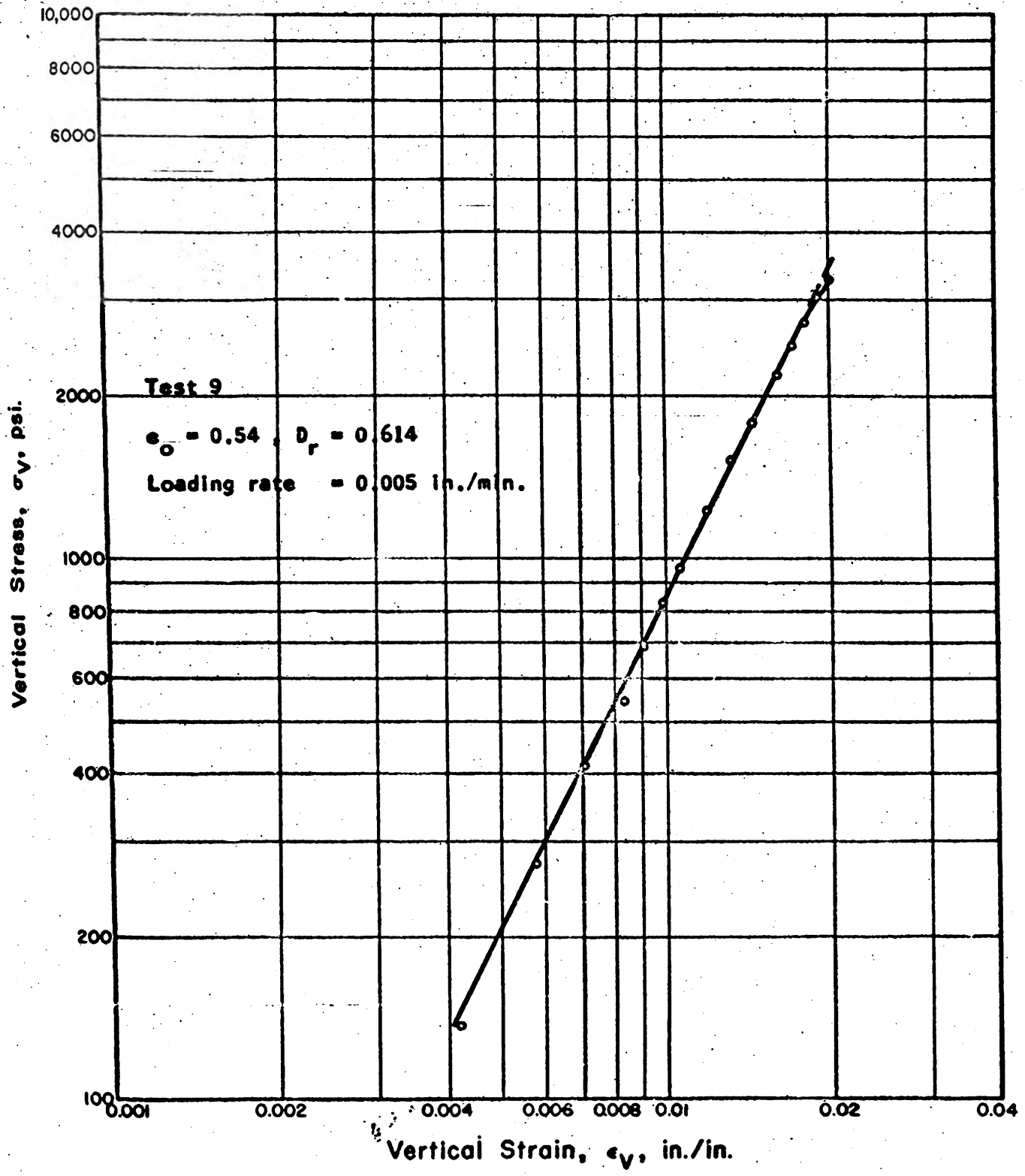

Fig. 6.37 LOGARITHMIC PLOT OF STRESS STRAIN CURVE FOR MINNESOTA SAND IN ONE-DIMENSIONAL COMPRESSION

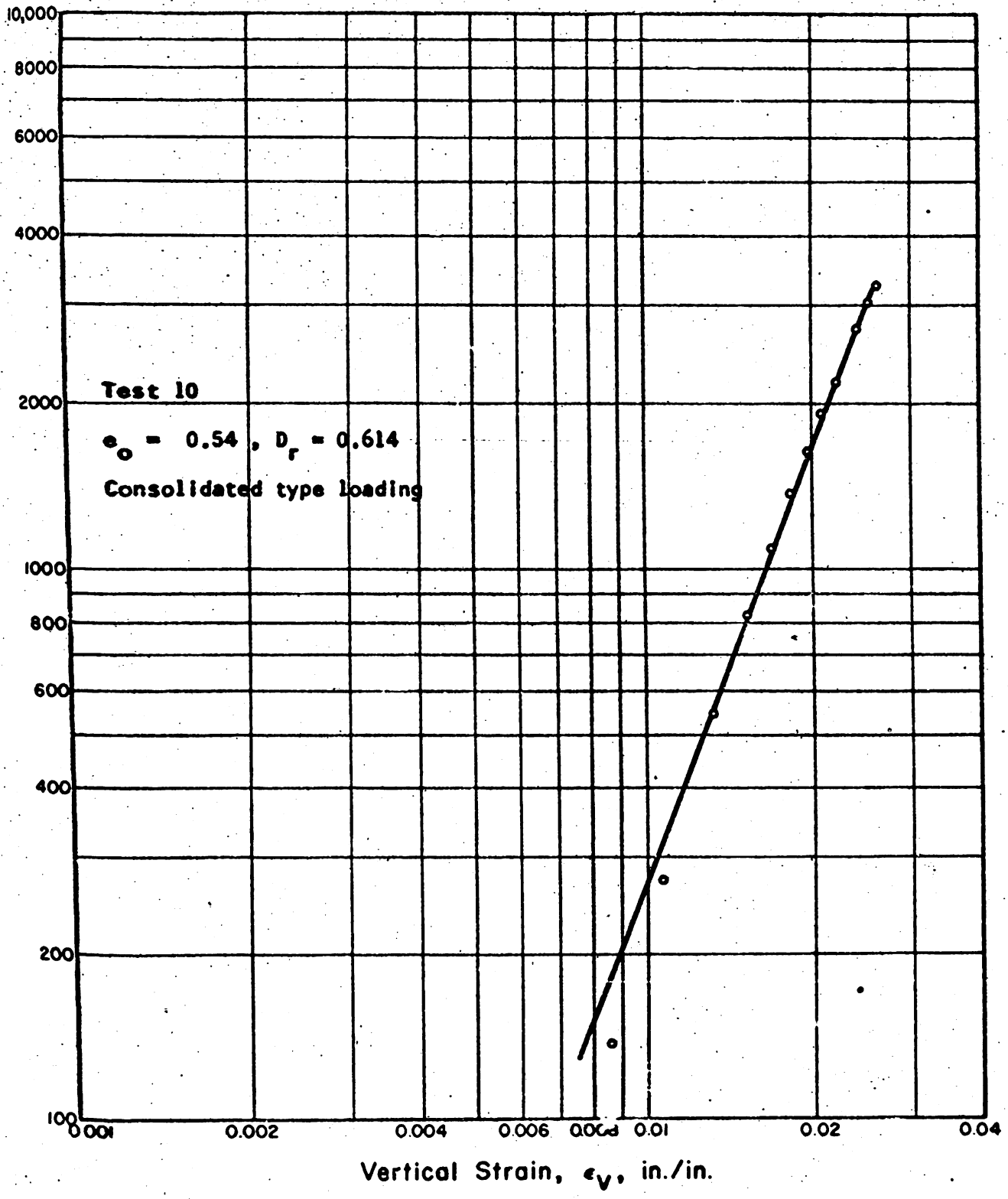

Fig. 6.38 LOGARITHMIC PLOT OF STRESS STRAIN CURVE FOR MINNESOTA SAND IN ONE-DIMENSIONAL COMPRESSION

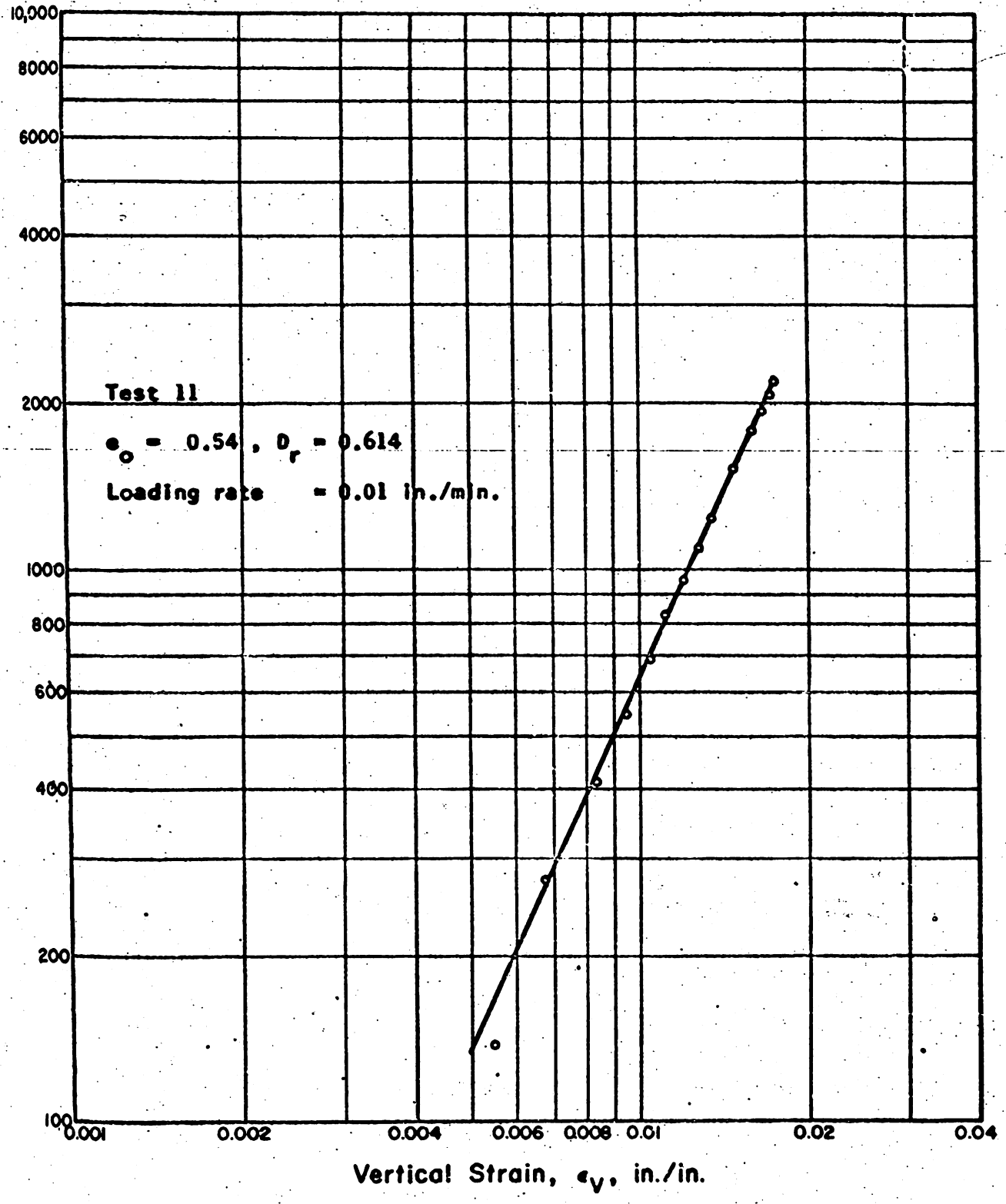

Fig. 6.39 LOGARITHMIC PLOT OF STRESS STRAIN CURVE FOR MINNESOTA SAND IN ONE-DIMENSIONAL COMPRESSION

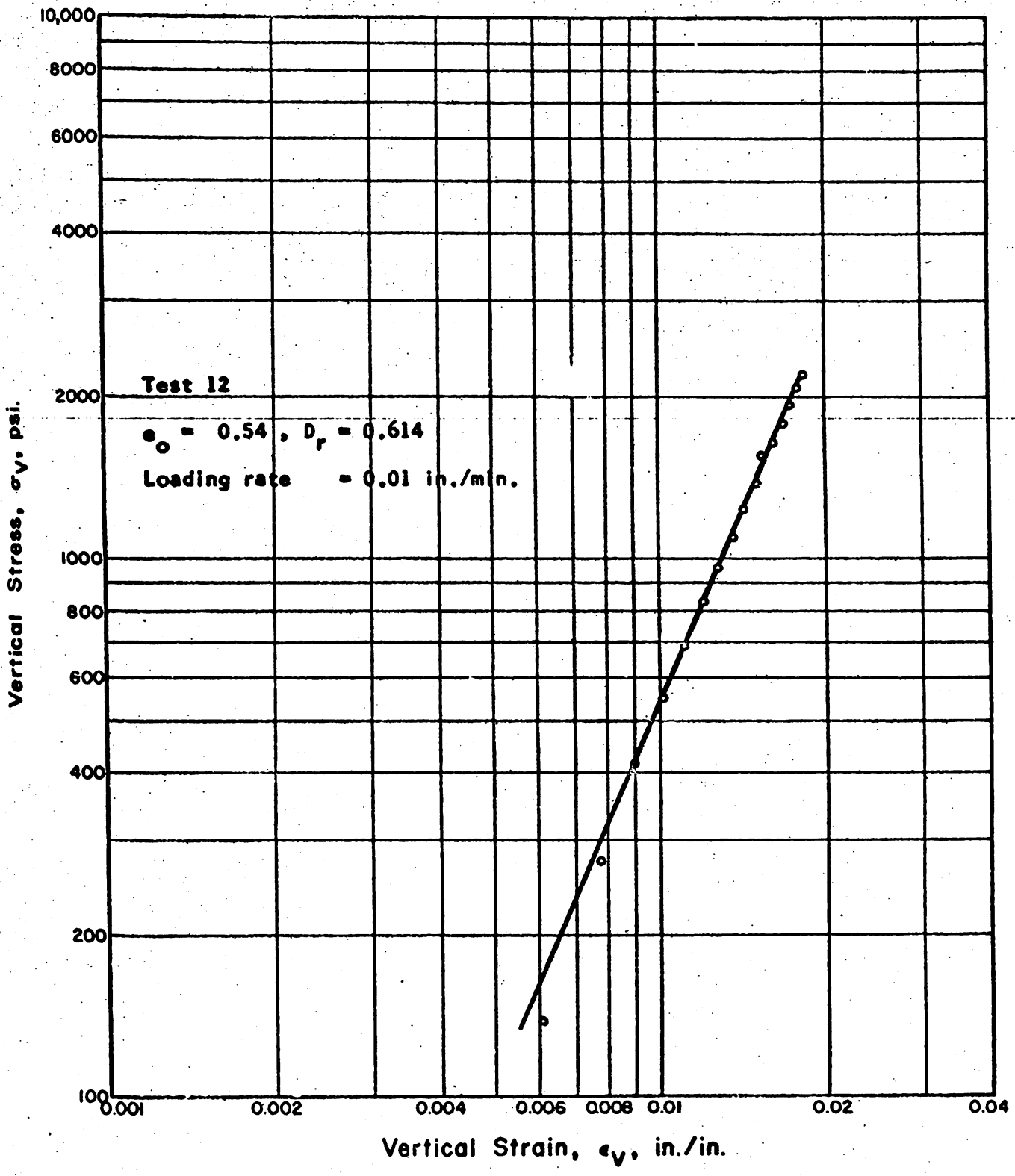

Fig. 6.40 LOGARITHMIC PLOT OF STRESS STRAIN CURVE FOR MINNESOTA SAND IN ONE-DIMENSIONAL COMPRESSION

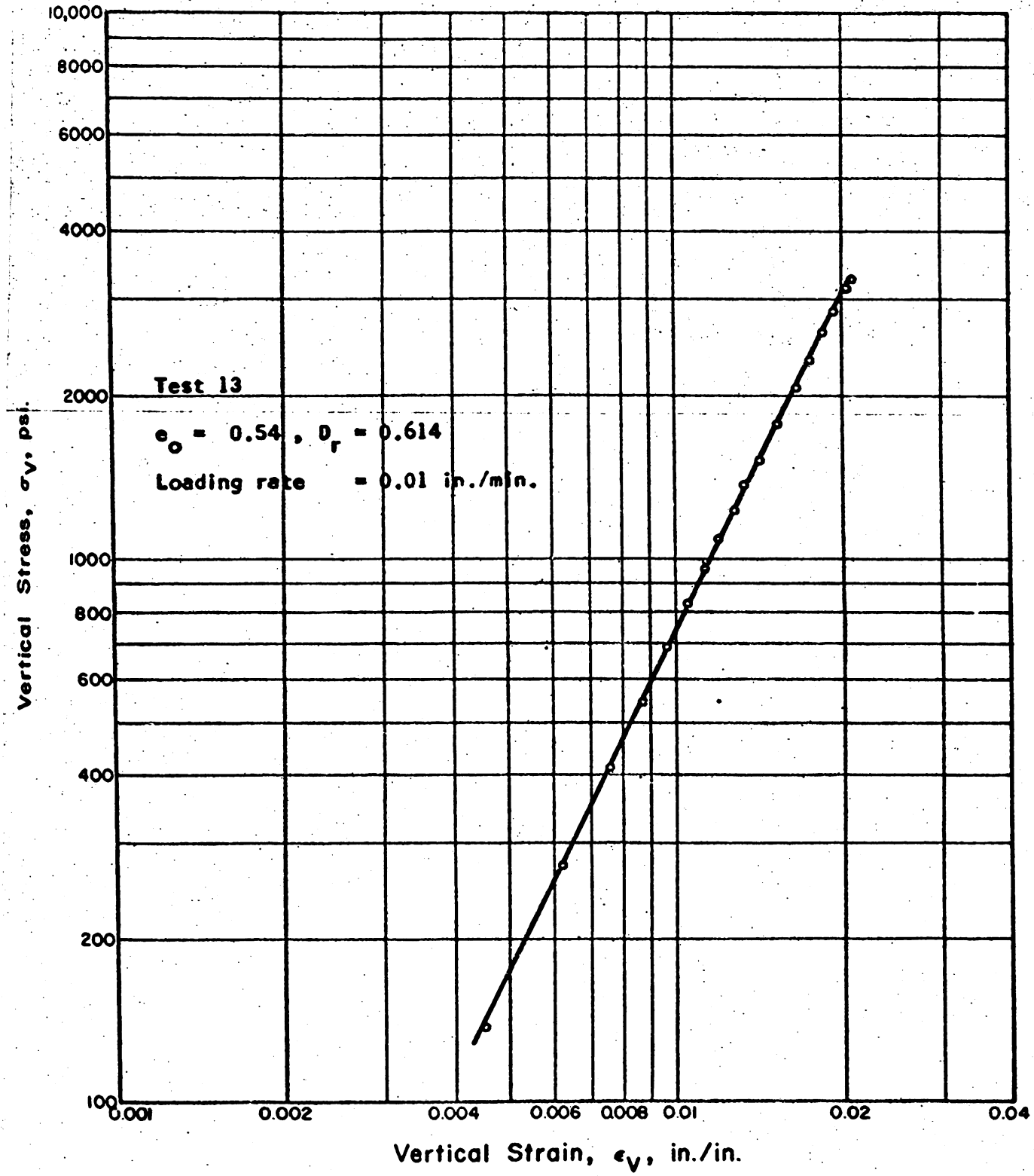

Fig. 6.41 LOGARITHMIC PLOT OF STRESS STRAIN CURVE FOR MINNESOTA SAND IN ONE-DIMENSIONAL COMPRESSION

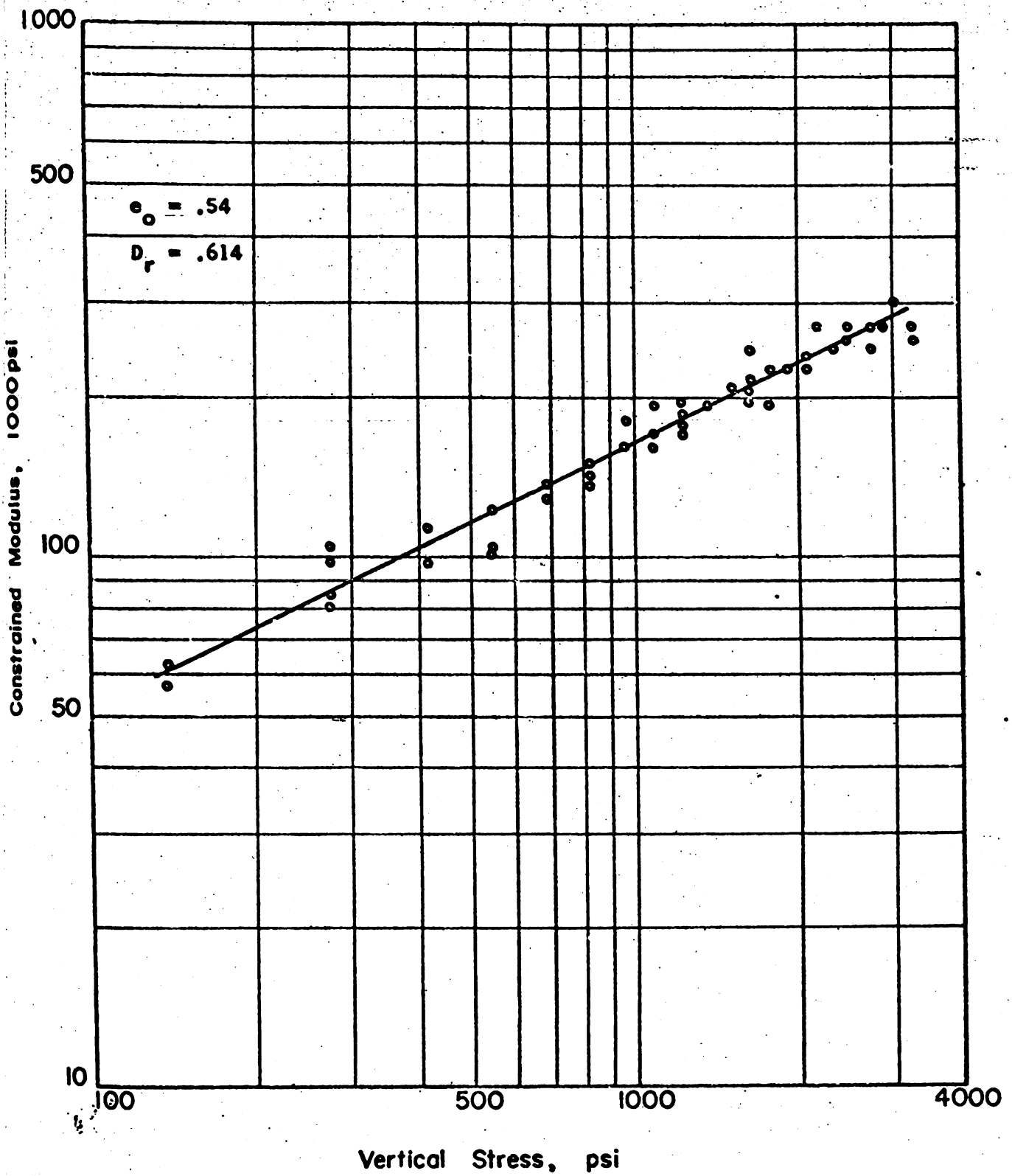

Fig. 6.42 RELATIONSHIP BETWEEN CONSTRAINED MODULUS AND VERTICAL STRESS FOR MINNESOTA SAND IN ONE-DIMENSIONAL COMPRESSION

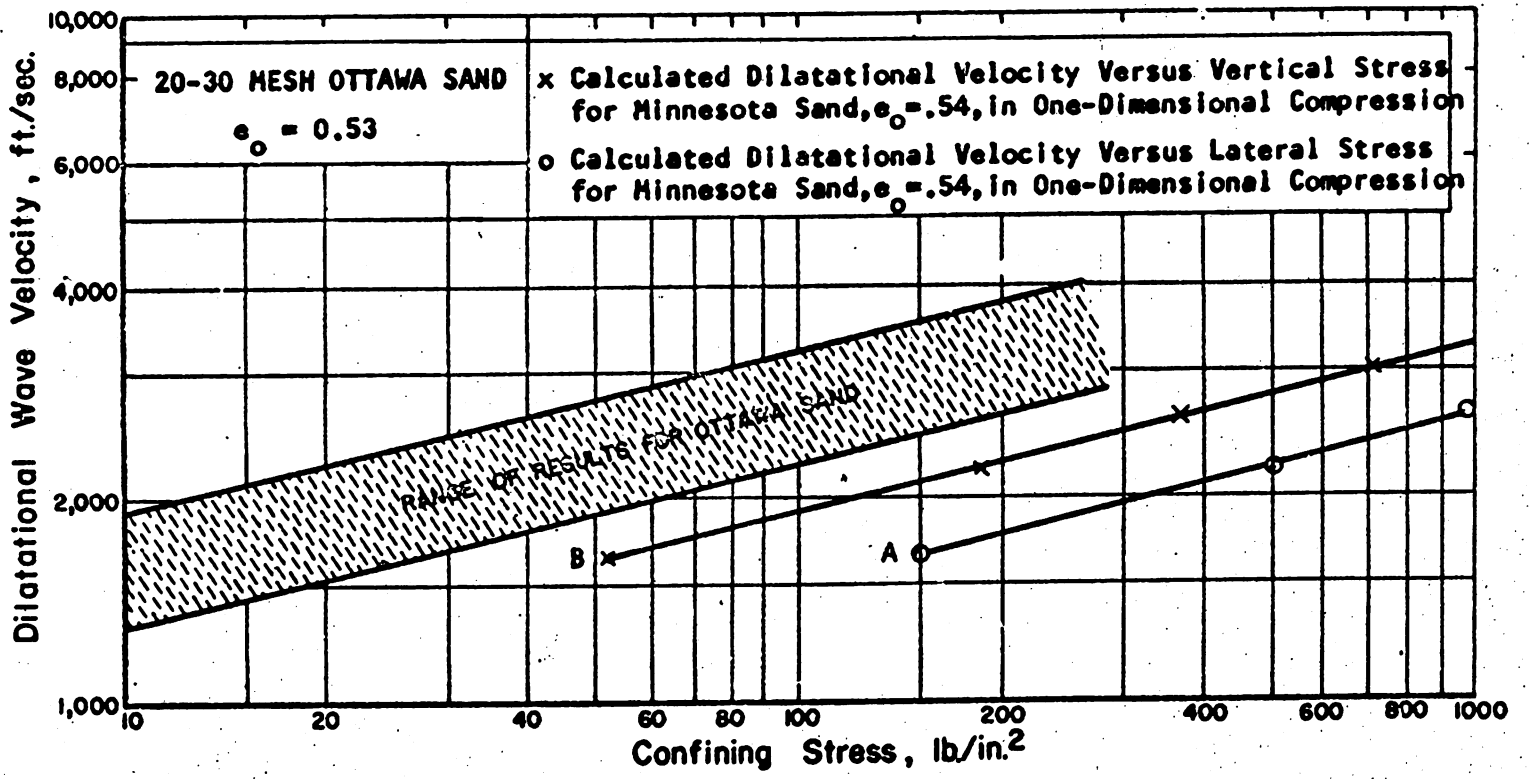

Fig. 6.43 DILATATIONAL WAVE VELOCITY VERSUS CONFINING PRESSURE FOR OTTAWA SAND AFTER WHITMAN (1962)

APPENDIX A

APPLICATION OF THE HERTZ THEORY TO THE BEHAVIOR OF A GRANULAR MEDIUM

A question of paramount importance arises in the development of a theory of granular media based on the Hertz theory, (Hertz, 1881). It must first be proven that the Hertz theory is valid in the pressure regions of interest before the theory has any usefulness. Therefore it is worthwhile to review the development of the theory here for the convenience of the reader and note simultaneously the fundamental assumptions as they arise.

The derivation given in the following is a summary of the presentation given by Timoshenko and Goodier (1951), and the assumptions are discussed by the writer in relation to applying the results to a granular medium composed of well-rounded quartz sand.

Let us first look at the pressure between two spherical bodies held in contact by a normal force. In the solution of this problem it is assumed that at the point of contact these bodies have spherical surfaces with radii R_1 and R_2 (Fig. A. 1). If there is no pressure between the bodies there is contact at only one point 0. The normal distances from the tangent plane at 0 to points such as M and N, on a meridian section of the spheres at a very small distance r from the axis z_1 and z_2, can be approximated in the following manner (Fig. A. 2):

$$z = u \tan \beta/2 \qquad 1/2\, u \tan \beta$$

$$z = 1/2\, u \,.\, u/R = u^2/2R \qquad \text{(A. 1)}$$

$$z = r^2/2R \text{ where } r^2 = u^2 \,.$$

Thus in (Fig. A. 1)

$$z_1 = \frac{r^2}{2R_1}, \text{ and } z_2 = \frac{r^2}{2R_2} \qquad \text{(A. 2)}$$

The distance between points M and N is

$$z_1 + z_2 = \frac{r^2(R_1 + R_2)}{2R_1R_2} \qquad (A.3)$$

In the particular case of contact between two spheres of equal radius, R, equation (A.3) reduces to

$$z_1 + z_2 = \frac{r^2\, 2R}{2R^2} = r^2/R \qquad (A.4)$$

If the bodies are pressed together along the normal at 0 by a force P, there will be a local deformation near the point of contact producing contact over a small surface with a circular boundary, called the surface of contact. Assuming that the radii of curvature R_1 and R_2 are very large in comparison with the radius of the surface of contact, the results obtained for a point load on a semi-infinite boundary can be applied for calculating local deformation. Let w_1 denote the displacement due to the local deformation in the direction z_1 of a point such as M on the surface of the lower ball (Fig. A.1), and w_2 denote the same displacement in the direction z_2 for a point such as N of the upper ball. If it is assumed that the tangent plane at 0 remains immovable during local compression, then, as a result of this compression, any two points of the bodies on the axes z_1 and z_2 at large distances* from 0 will approach each other by a certain amount a, and the distance between two points such as M and N will diminish by $a - (w_1 + w_2)$. If the two spheres are of equal radius, the distance between such points as M and N will diminish by $a - 2w$. If finally, as a result of local compression, the points M and N come inside the surface of contact, the relative approach of points M and N is given by

$$a - (w_1 + w_2) = z_1 + z_2 = \frac{r^2\,(R_1 + R_2)}{2R_1R_2} \qquad (A.5)$$

* Such distances that deformations due to the compression at these points can be neglected.

If the spheres have a radius $R = R_1 = R_2$ then equation (A.5) becomes

$$a = 2w = 2z = r^2/R$$

Thus

$$w = \frac{a - r^2/R}{2} \tag{A.6}$$

at any point a distance r from the center of the surface of contact.

Conditions of symmetry require that the intensity of pressure q between the bodies in contact and the corresponding deformation are symmetrical with respect to the center 0 of the surface of contact. The circle shown in Fig. A.4 represents the surface of contact, and M is a point on the surface of contact of the lower ball. The displacement of this point can be found in the following manner. For a point load on the surface of an infinite medium such as shown in Fig. A.3, the vertical deflection at a distance r from the load P is given as

$$w = \frac{P(1 - \nu^2)}{\pi E r} \tag{A.7}$$

where E is Young's modulus and ν is Poisson's ratio for the medium.

Consider Fig. A.4 where a distributed load q is shown over the circular area of radius a, and it is desired to relate the vertical displacement of point M to the distributed load q. The vertical deflection w at any point M within the loaded boundary can be found by integrating equation (A.7) over the area loaded by q to obtain

$$w = \frac{1 - \nu^2}{\pi E} \iint \frac{q d\bar{a}}{s} \tag{A.8}$$

where

$$d\bar{a} = ds \cdot d\psi \cdot s \tag{A.9}$$

Thus

$$w = \frac{(1 - \nu^2)}{\pi E} \iint q d\psi ds \tag{A.10}$$

Hence if two spherical balls of equal radii R are pressed together, at some point r the local displacement w becomes

$$2w = a - r^2/R = \frac{2(1 - \nu^2)}{\pi E} \iint q\,d\psi\,ds \qquad \text{(A. 11)}$$

The distribution of q must therefore be such that Eq. (A. 11) is satisfied. It will now be shown that this requirement is satisfied by using a pressure distribution of q over the contact surface represented by the ordinates of a hemisphere of radius a constructed on the surface of contact.

If q_o is the pressure at the center 0 of the surface of contact, then

$$q_o = \frac{k}{a} \qquad \text{(A. 12)}$$

where k is a constant factor indicating the scale of the representation of the pressure distribution. Along a chord mn the pressure q varies, as indicated in Fig. A. 4 by the dotted semicircle.

Performing the integration along the chord gives

$$\int q\,ds = \frac{q_o}{a} A \qquad \text{(A. 13)}$$

where A is the area of the semicircle indicated by the dotted line and is equal to

$$A = \frac{\pi}{2} (a^2 - r^2 \sin^2 \psi) \qquad \text{(A. 14)}$$

Substituting Eq. (A. 14) into Eq. (A. 11) yields

$$2w = a - \frac{r^2}{R} = \frac{(1 - \nu^2)}{E} \int_0^{\pi} \frac{q_o}{a} (a^2 - r^2 \sin^2 \psi)\,d\psi$$

or

$$a - \frac{r^2}{R} = \frac{q_o}{a} \frac{(1 - \nu^2)}{E} \int_0^{\pi} (a^2 - r^2 \sin^2 \psi)\,d\psi \qquad \text{(A. 15)}$$

Integrating Eq. (A. 15) yields

$$a - \frac{r^2}{R} = \frac{q_o}{a} \frac{(1 - \nu^2)}{E} \frac{\pi}{2} (2a^2 - r^2) \qquad \text{(A. 16)}$$

This equation will be satisfied for any value of r, and hence the assumed pressure distribution is the correct one if the following relations exist for the displacement a and the radius a of the surface of contact between two equal radii spheres:

$$a = \frac{q_o a \pi (1 - \nu^2)}{E} = \frac{q_o a \pi (1 - \nu)}{2\mu} \qquad \text{(A. 17)}$$

and

$$a = \frac{q_o R \pi (1 - \nu^2)}{2E} = \frac{q_o R \pi (1 - \nu)}{4\mu} \qquad \text{(A. 18)}$$

where μ is the shear modulus of the spheres.

If the volume of the pressure diagram between two spheres is defined as the normal force N between the spheres, then

$$N = \frac{q_o}{a} \cdot \frac{2}{3} \pi a^3 \qquad \text{(A. 19)}$$

Combining Eq. (A. 19) with Eq. (A. 17) and (A. 18) yields

$$a = \frac{3}{4} \frac{N(1 - \nu)}{a\mu} \qquad \text{(A. 20)}$$

$$a^3 = \frac{3}{8} \frac{RN(1 - \nu)}{\mu} \qquad \text{(A. 21)}$$

The radius of contact a may be eliminated from Eq. (A. 20) and (A. 21) to give

$$a = 2 \left[\frac{3(1 - \nu)N}{8\mu R^{1/2}} \right]^{-1/3} \qquad \text{(A. 22)}$$

Equation (A. 22) shows that the relative approach of the center of two spheres is a function of the two-thirds power of the contact force.

The normal compliance C is

$$C = \frac{da}{dN} = \frac{4}{3}\left[\frac{3(1-\nu)N}{8\mu R^{1/2}}\right]^{-1/3}\frac{3(1-\nu)}{8\mu R^{1/2}}$$

which may be simplified to

$$C = \frac{(1-\nu)}{2\mu a}$$

where a is given by

$$a = \left[\frac{3(1-\nu)NR}{8\mu}\right]^{1/3} \tag{A.24}$$

There are two key assumptions in the Hertz theory which should be discussed to justify its use in a theory of granular media.

The first of these is that described by Eqs. (A.1) where it was assumed that the deviation from a tangent plane is quadratic, i.e.

$$z = \frac{r^2}{2R} \tag{A.25}$$

The exact expression for the deviation from the tangent plane is

$$z = \frac{r^2}{2R}\,\frac{1}{1-\frac{z}{2R}} \tag{A.26}$$

Hence if $\frac{z}{R}$ is small, the quadratic approximation is reasonable.

The second assumption requires that the radius of contact be small compared to the sphere radius R. This assumption is associated with the use of the expression for the deflection resulting from a point load on an infinite medium, i.e., Equation (A.7). Essentially what is being assumed is that the curvature of the spheres beyond the contact area does not affect the stress distributions and deflections at the contacts. Clearly if the radius of contact is small, the curvature has little effect on the behavior.

The problem is to assess the validity of the Hertz theory for describing the behavior of a granular medium, namely sand, subjected to an average applied stress,

σ_{zz} in one-dimensional compression. Therefore, it is of interest to determine the range of stress within which the assumptions are reasonably correct.

In Section 3.1 it was determined that the normal contact force N_2 was related to the radius of contact by Eq. (3.1)

$$a = \left[\frac{3(1 - \nu)\, RN_2}{8\mu}\right]^{1/3} \tag{A.27}$$

The normal force, N_2, was related to the applied force, P_{zz}, in one-dimensional compression by Eq. (3.48a)

$$N_2 (1 + f) = \frac{\sqrt{2}}{8} P_{zz} \tag{A.28}$$

Furthermore it was shown that the average stress σ_{zz} is related to P_{zz} by

$$\sigma_z = \frac{P_{zz}}{8R^2} \tag{A.29}$$

Equations (A.27), (A.28) and (A.29) may be combined to give

$$\left(\frac{a}{R}\right)^3 = \frac{2^{1/3}(1 - \nu)}{8(1 + f)} \frac{\sigma_{zz}}{\mu} \tag{A.30}$$

Representative values of f, ν and μ for quartz which are applicable to sand are

$$f = 0.15$$

$$\nu = 0.20$$

$$\mu = 6 \times 10^6 \text{ psi}$$

Substitution of these values into Eq. (A.30) yields the following relation between a/R and σ_{zz}:

$$\left(\frac{a}{R}\right)^3 = 0.369 \frac{\sigma_{zz}}{\mu} \tag{A.31}$$

A numerical evaluation of equation (A.31) gives

$\frac{a}{R}$	σ_{zz}, psi
0.031	500
0.039	1,000
0.057	3,000
0.085	10,000
0.10	16,300

Thus for the stresses of interest (prior to crushing) where the theory is to be applied, the radius of contact compared to the radius of the sphere will be less than 0.04. Not only is this fairly small but there are other assumptions involved in the application of this theory to sand which may be far worse. In fact the assumption that the sand particles are spheres is more questionable, even for a well rounded quartz sand. It is also quite improbable that a uniform sand can ever be placed in the densest state because a perfectly orderly arrangement cannot be achieved.

It is concluded from the above discussion that the Hertz theory, for its expected use in this problem, is applicable for describing the behavior at points of contact between uniform, well rounded grains, below the stress level at which crushing begins. Especially if considered in the light that other assumptions used are much more at variance with reality.

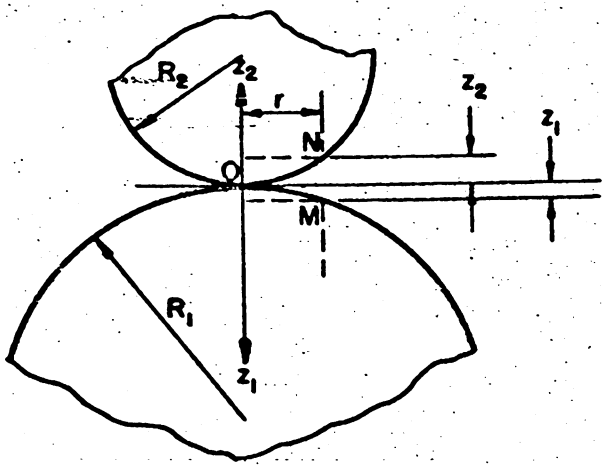

Fig. A.1 TWO UNSTRESSED SPHERES IN CONTACT

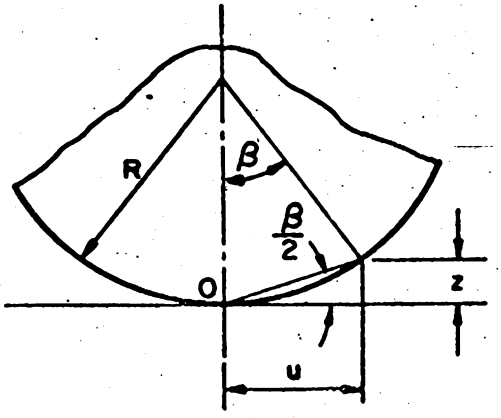

Fig. A.2 SEGMENT OF A SPHERE TANGENT TO A PLANE

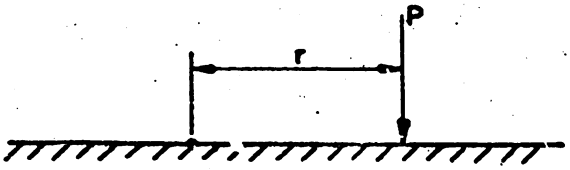

Fig. A.3 POINT LOAD ON AN INFINITE SURFACE

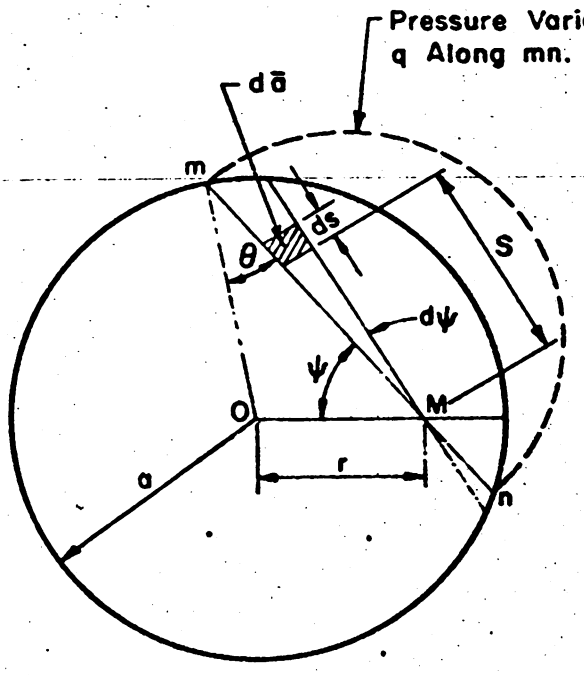

Fig. A.4 PLAN VIEW OF THE CONTACT SURFACE OF TWO SPHERES IN HERTZ CONTACT .

APPENDIX B

TRIAXIAL TESTS

A series of 44 triaxial tests were conducted on all four sands to define the variation of the drained angle of internal friction, ϕ, with the initial void ratio. Samples were set up at various initial void ratios and were sheared at confining pressure of 45 and 90 psi. The samples were 1-7/8 inches in diameter by 4 inches high.

Samples were prepared by settling the sand through water into a membrane encased in a Wykeham Farrance mold. When the sample height was approximately equal to the height of the mold the loading cap was placed on the sample and rubber bands put around the cap to secure the rubber membrane. A slight vacuum was then applied to the sample by connecting the base of the cell to a burette with a free surface about 2 feet below the center of the sample. The mold was then removed and the height of the sample measured to the nearest $\pm$ .01 inches. The cell was then placed around the sample and a confining pressure of 1.5 psi was applied. The burette was then set up at approximately the same height as the sample and an initial burette reading obtained. A confining pressure of 45 or 90 psi was then applied and another burette reading was obtained. The difference between the burette readings was taken as the volume change due to the application of the confining pressure ; the initial void ratio which is referred to in reporting these data is the void ratio computed after the full cell pressure has been applied. The samples were then sheared at a strain rate of 0.015 inches per minute and volume change measurements were made throughout the test by means of a 10 c.c. burette.

Typical stress versus strain and volume change versus strain curves are shown for dense and loose specimens of Wabash River Sands in Fig. B.1. Figure B.2 shows a typical variation of initial tangent modulus versus confining pressure for dense and loose specimens of Wabash River Sand.

The angle of internal friction versus initial void ratio curves were determined in the following manner. The conditions at failure for several samples with almost the same initial void ratio were plotted on a graph of one-half the stress difference versus one-half the sum of the major and minor principal stresses. Test results for tests 5, 8, and 10 on Wabash River Sand with initial void ratios of .52, .51, and .51, respectively are shown in Fig. B.3. The best straight line was fitted through these three points as shown and the angle of internal friction was calculated from the relationship given on Fig. B.3. The angle of internal friction obtained in this manner was plotted against the average void ratios for all three tests. This procedure was followed for all tests and the angle of internal friction versus initial void ratio relationships obtained are given in Fig. B.4.

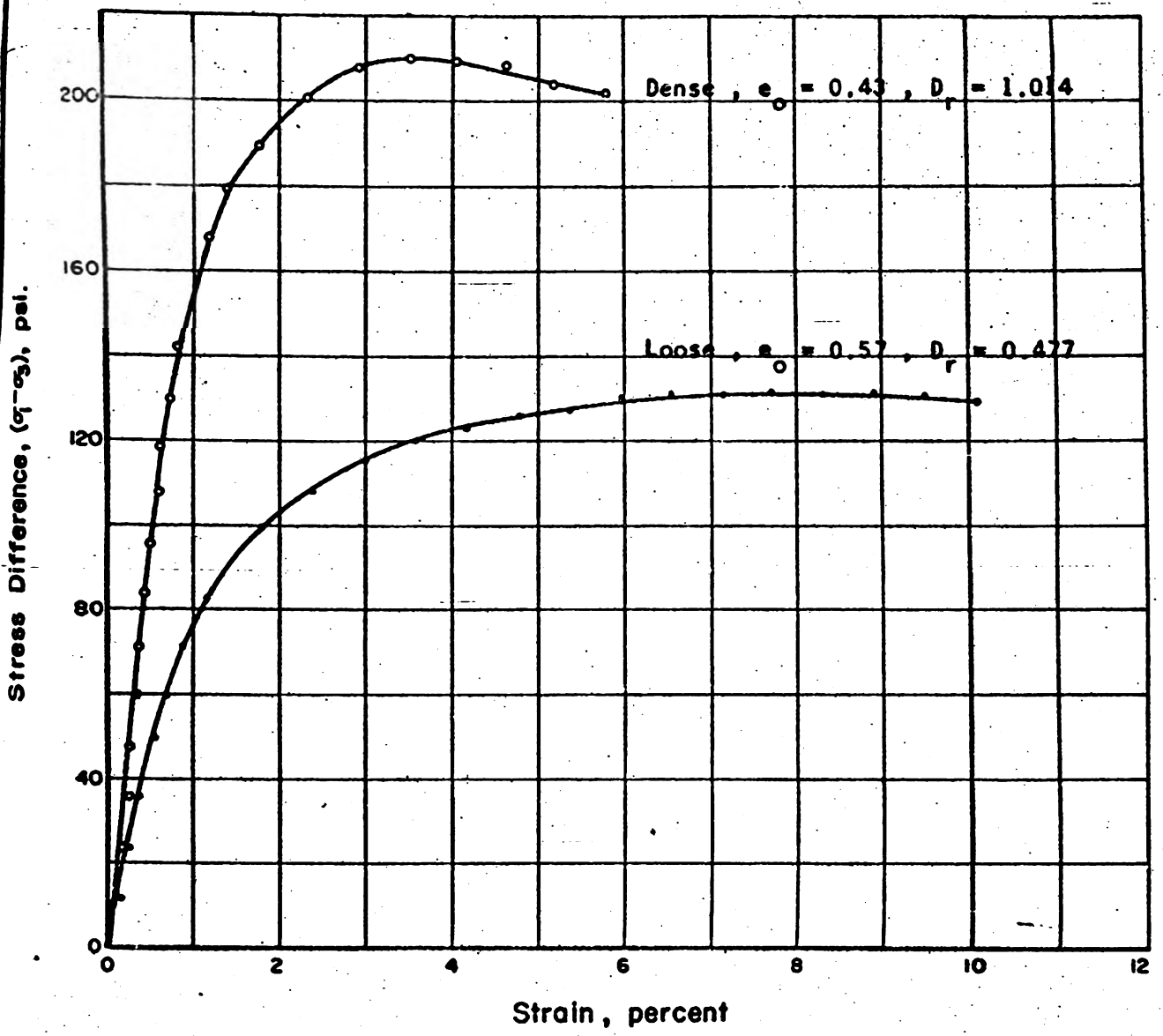

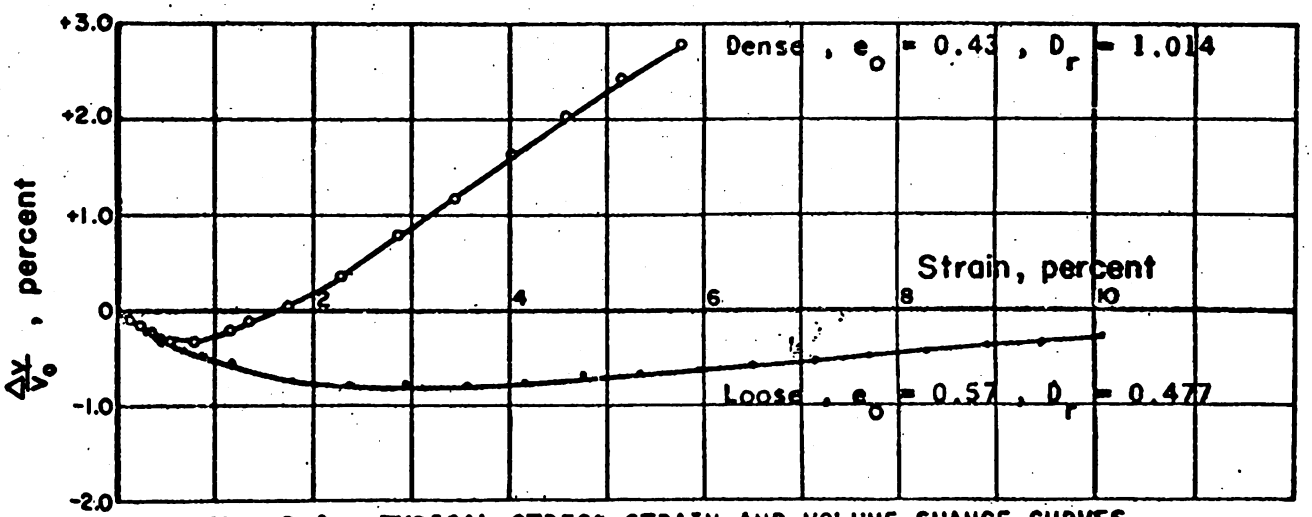

Fig. B.1 TYPICAL STRESS STRAIN AND VOLUME CHANGE CURVES FOR TRIAXIAL TESTS ON WABASH RIVER SAND

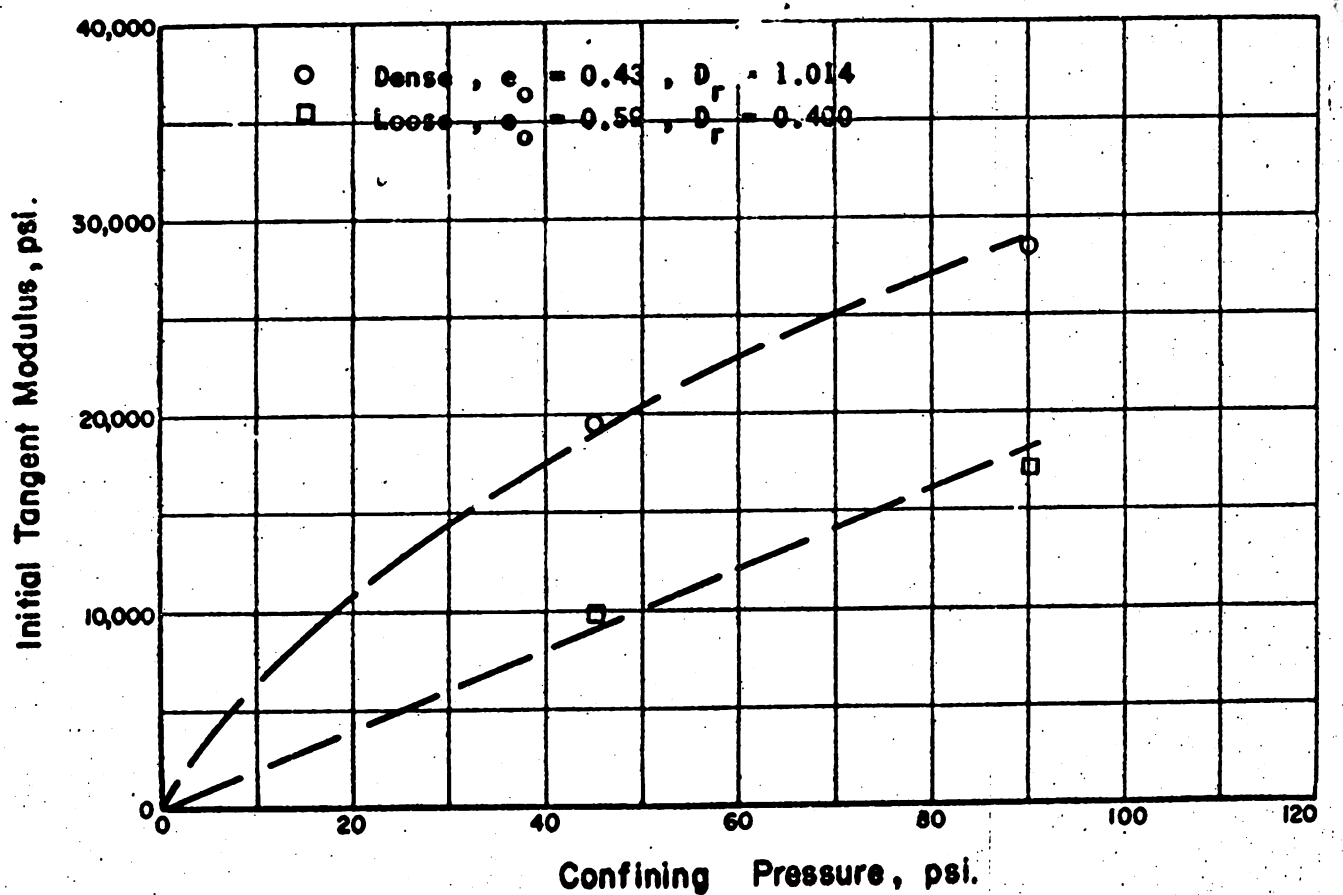

Fig. 8.2 RELATIONSHIP BETWEEN THE INITIAL TANGENT MODULUS AND CONFINING PRESSURE FOR WABASH RIVER SAND

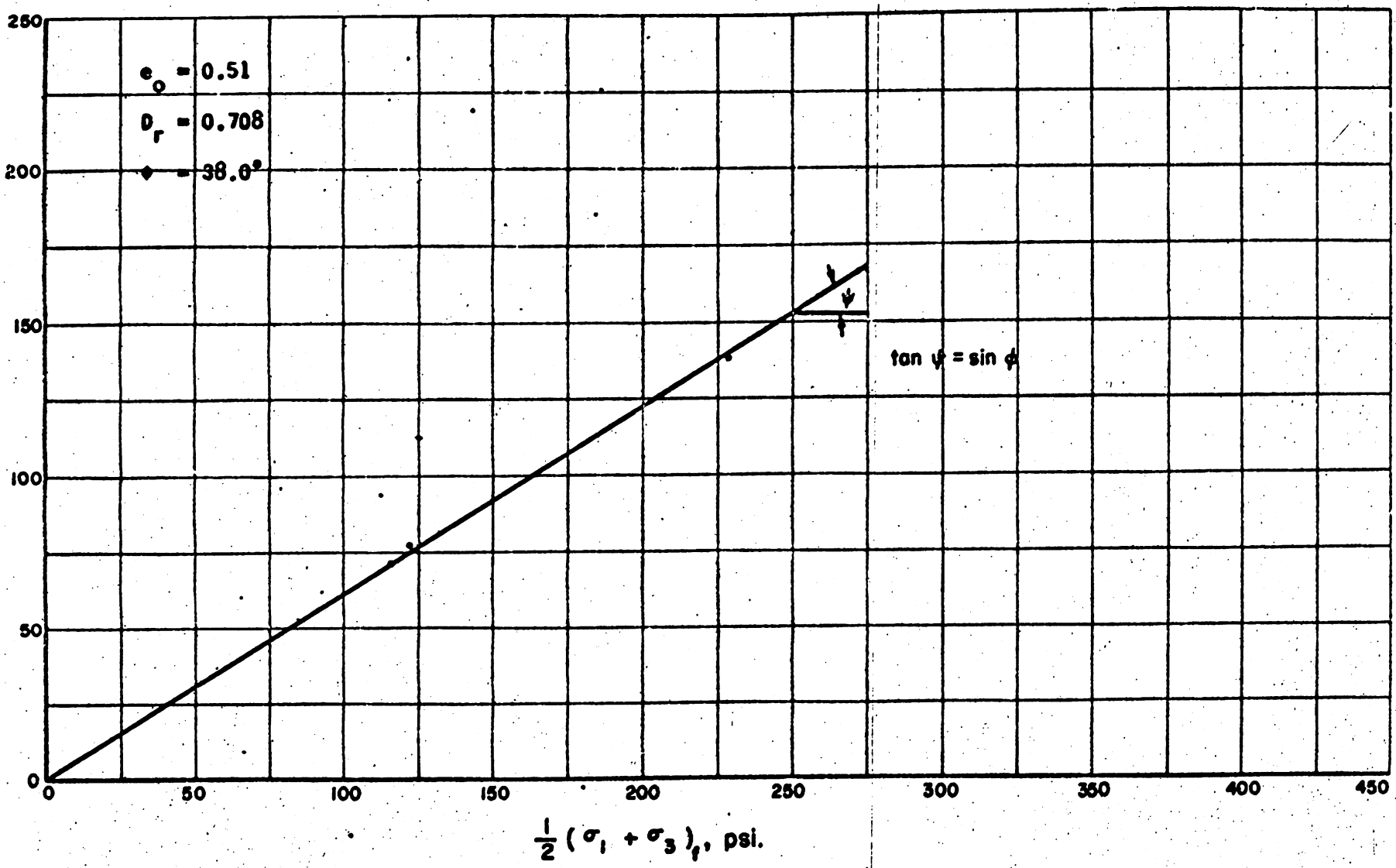

Fig. B.3 MODIFIED MOHR-COULOMB DIAGRAM FOR TRIAXIAL TESTS ON WABASH RIVER SAND

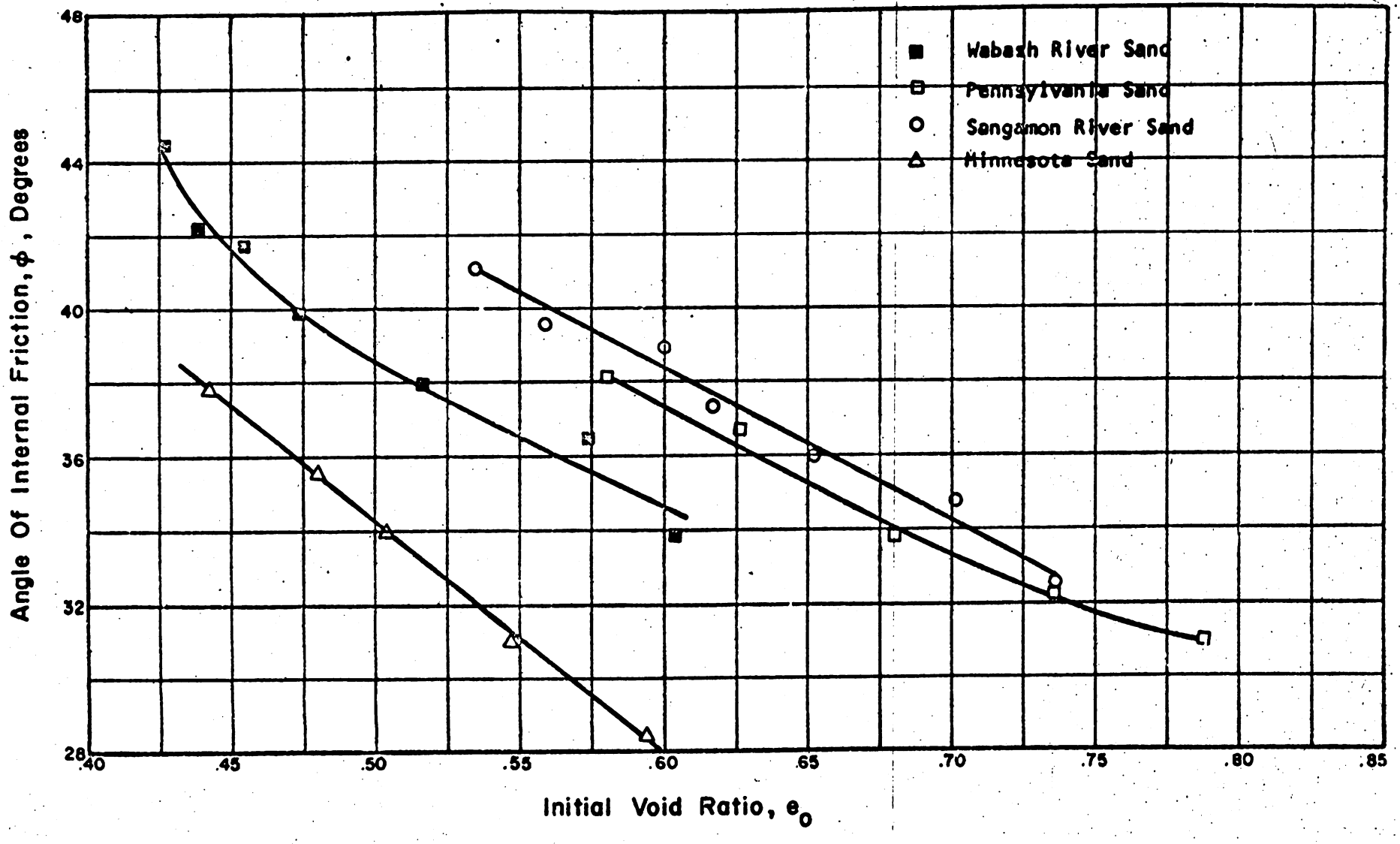

Fig. 8.4 RELATIONSHIP BETWEEN THE ANGLE OF INTERNAL FRICTION AND INITIAL VOID RATIO FOR SANDS INVESTIGATED

APPENDIX C
EVALUATION OF RING FRICTION

Several tests were conducted on Minnesota Sand to obtain an approximation of the vertical load transmitted to the ring by friction. Strain gages were placed along four axial lines at 90° intervals around the outside surface of the ring to measure axial strains. One axial line of gages consisted of four 1/4-inch gages; a second line was comprised of two 1/4-inch gages, one at the top and one at the bottom of the ring; and a one inch gage was placed at the midheight of the ring along each of the other two axial lines. Metalfilm strain gages were used and were calibrated for the effects of oil pressure by the method described in Chapter 4.

The ring friction tests were conducted on Minnesota Sand with an initial void ratio of 0.54 by loading the specimens in stress increments of 30,000 lbs. up to a maximum of 120,000 lbs. Strain gage readings were taken after a load increment was applied while the Ames dials still indicated a slight downward movement. After the sample stopped compressing the load was decreased; as the sample rebounded upward the strain gage readings were taken again. It was assumed in the analysis of this data that the frictional forces on the ring were reversed by the change in direction of movement of the testing head. The differences in the two gage readings are assumed to be due to the reversal of the frictional forces.

The test results are shown in Fig. C.1 in a graph of computed frictional load versus applied machine load. Most of the data seem to fall along line A; however, two points along line B show considerably more friction. Therefore line B will be taken as an envelope to the experimental points. The percentage of the total vertical load transferred to the ring by side friction along the envelope given by line B is 4.6 percent, which seems rather low.

A measurement of ring friction is more reliable if the total frictional load in the ring is measured. This type of measurement was made by the Norwegian Geotechnical

Institute for one-dimensional compression tests conducted on granular materials (Bjerrum, 1960). The tests were conducted in a cylinder 50 cm. in diameter and 25 cm. high. The ring friction measurements from these tests showed that the total applied vertical load should be reduced by 10 percent to account for ring friction. The ring friction in the Norwegian tests, however, would be a greater percentage than in the tests conducted on this study because the diameter to height ratio in the Norwegian tests was 2 as compared to 3.5 for tests on this investigation. A comparison between the two sets of tests, however, can be made by using the ring friction analysis presented in Chapter 4. According to this analysis the percentage of load transferred to the ring is

$$100\ (1 - \epsilon^{-2K_o\, fH/R}) \qquad \text{(C.1)}$$

where ϵ is the base of Naperian logarithms, K_o is the coefficient of earth pressure at rest, f is the coefficient of friction between the soil and the ring, and H/R is the height to radius ratio of the ring. Since the value of H/R for the Norwegian ring is 1.0 then eqn. C.1 becomes

$$.10 = 1 - \epsilon^{-2K_o f} \qquad \text{(C.2)}$$

and therefore the average value of $2K_o f$ for the granular materials tested was .106. If these same materials were tested in the device used on this study with an H/R = .572 then equation C.1 would give

$$\text{percent friction} = 1 - \epsilon^{-(.106)\,(.572)} \qquad \text{(C.3)}$$

or the percent friction would be 5.8 percent. Therefore a reasonable estimate of the error due to ring friction in the one-dimensional tests on this study is 5.8 percent.

The value of the coefficient of earth pressure at rest for the one-dimensional tests conducted on this investigation was taken as

$$\frac{\sigma_H}{\sigma_V} = K_o \qquad \text{(C.4)}$$

where σ_V is the applied machine load. Therefore if the true vertical load on the soil is reduced by 5.8 percent because of ring friction then the true value K_o is given by

$$\frac{\sigma_H}{(.942)\,\sigma_V} \qquad \text{(C.5)}$$

Therefore the true value of the coefficient of earth pressure at rest is about 6 percent higher than the value computed without correcting for ring friction.

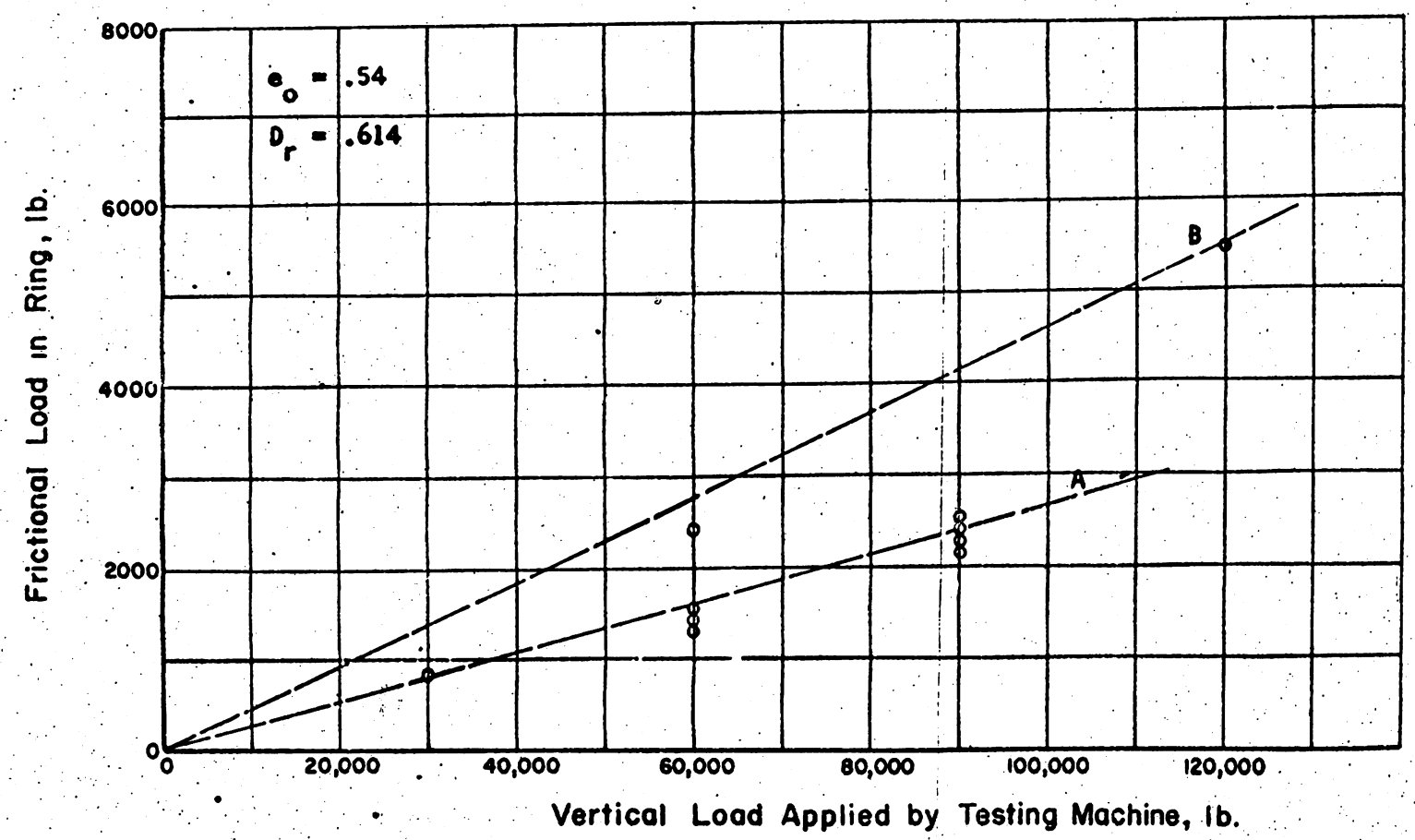

Fig. C.1 RELATIONSHIP BETWEEN MEASURED RING FRICTION LOAD AND APPLIED VERTICAL LOAD FOR MINNESOTA SAND

DISTRIBUTION

No. cys

HEADQUARTERS USAF

1 Hq USAF (AFOCE), Wash, DC 20546
1 AFOAR, Bldg T-D, Wash, DC 20333
1 AFCRL, Hanscom Fld, Bedford, Mass 01731
1 AFOSR, Bldg T-D, Wash, DC 20333

MAJOR AIR COMMANDS

AFSC, Andrews AFB, Wash 25, DC
1 (SCT)
1 AUL, maxwell AFB, Ala 36112

AFSC ORGANIZATIONS

1 RTD (RTN-W, Maj Munyon), Bolling AFB, Wash 25, DC
1 AF Msl Dev Cen (RRRT), Holloman AFB, NM 88330
1 RADC (Document Library), Griffiss AFB, NY 13442

KIRTLAND AFB ORGANIZATIONS

1 AFSWC (SWEH), Kirtland AFB, NM 87117
AFWL, Kirtland AFB, NM 87117
19 (WLL)
25 (WLRS)

OTHER AIR FORCE AGENCIES

Director, USAF Project RAND, via: Air Force Liaison Office, The RAND Corporation, 1700 Main Street, Santa Monica, Calif 90406
1 (RAND Physics Div)
1 (RAND Library)

ARMY ACTIVITIES

1 Director, Ballistic Research Laboratories (Library), Aberdeen Proving Ground, Md 21005
1 Director, US Army Waterways Experiment Sta (WESRL), P. O. Box 60, Vicksburg, Miss

DISTRIBUTION (cont'd)

No. cys	
	NAVY ACTIVITIES
1	Commanding Officer and Director, Naval Civil Engineering Laboratory, Port Hueneme, Calif
	OTHER DOD ACTIVITIES
	Chief, Defense Atomic Support Agency, Wash 25, DC
1	(Document Library, ATTN: Miss Gertrude Camp)
1	(Mr. J. Lewis)
1	Commander, Field Command, Defense Atomic Support Agency (FCAG3, Special Weapons Publication Distribution), Sandia Base, NM 87115
20	Hq Defense Documentation Center for Scientific and Technical Information (DDC), Cameron Sta, Alexandria, Va 22314
	AEC ACTIVITIES
1	Sandia Corporation (Dr. Mel Merritt), Box 5800, Sandia Base, NM 87115
1	University of California Lawrence Radiation Laboratory (Technical Information Division, ATTN: Dr. R. K. Wakerling), Berkeley 4, Calif
	OTHER
1	Office of Assistant Secretary of Defense (Civil Defense), Wash 25, DC
1	OTS, Department of Commerce, Wash 25, DC
1	Institute for Defense Analysis, Room 2B257, The Pentagon, Wash 25, DC THRU: ARPA
1	Armour Research Foundation, Illinois Institute of Technology, ATTN: Dr. Gene Sevin, 3422 South Dearborn St, Chicago 15, Ill.
1	MRD Division, General American Transportation Corporation, ATTN: Dr. Glen Neidhardt, 7501 North Natchez Ave, Niles 48, Ill
1	National Engineering Science Company, ATTN: Dr. Al Soldate, 711 South Fairoaks Ave, Pasadena, Calif
1	Shannon & Wilson, Inc., Soil Mechanics and Foundation Engineers, ATTN: Mr. Stan Wilson, 1105 North 38th St, Seattle 3, Wash

DISTRIBUTION (cont'd)

No. cys	
1	United Research Services, ATTN: Mr. Harold Mason, 1811 Trousdale Drive, Burlingame, Calif
1	University of Illinois, ATTN: Dr. N. M. Newmark, 207 Talbot Laboratory, Urbana, Ill
3	University of New Mexico, ATTN: Dr. Eugene Zwoyer, University Hill, Albuquerque, N Mex
1	University of Notre Dame, Department of Civil Engineering, ATTN: Dr. Harry Saxe, Notre Dame, Ind
1	Stanford Research Institute, ATTN: Mr. Fred Sauer, Menlo Park, Calif
1	University of Washington, ATTN: Dr. I. M. Fyfe, Seattle 5, Wash
1	Purdue University, Civil Engineering Department, ATTN: Prof G. A. Leonards, Lafayette, Ind
1	Massachusetts Institute of Technology, Department of Civil and Sanitary Engineering, ATTN: Dr. Robert Whitman, 77 Massachusetts Ave, Cambridge 39, Mass
1	Paul Weidlinger and Associates, ATTN: Dr. M. L. Baron, 770 Lexington Ave, New York 21, NY
1	University of Michigan, Department of Civil Engineering, ATTN: Prof F. E. Richart, Jr., Ann Arbor, Mich
1	University of California, Department of Civil Engineering, ATTN: Prof H. Bolton Seed, Los Angeles, Calif
1	Recan Incorporated, ATTN: Dr. Grover L. Rogers, Box 3622 MSS, Tallahassee, Fla
1	University of California, College of Engineering, ATTN: Prof C. Martin Duke, Assistant Dean, Los Angeles, Calif
1	North Carolina State College, ATTN: Dr. Ralph Fadum, Head, Dept of Civil Engineering, Raleigh, North Carolina
1	The Mitre Corporation, ATTN: Warren McCabe, P. O. Box 208, Bedford Mass
1	St. Louis University, Institute of Technology, ATTN: Dr. Carl Kisslinger, 3621 Olive St, St. Louis 8, Mo
1	United Electrodynamics, Inc., ATTN: Mr. R. Obenchain, 200 Allendale Rd, Pasadena, Calif
1	Space Technology Laboratories, Inc., ATTN: Dr. M. V. Barton, P. O. Box 95001, Los Angeles 45, Calif
1	Iowa State University, ATTN: Dr. D. F. Young, Dept of Nuclear Engineering, Ames, Iowa

DISTRIBUTION (cont'd)

No. cys	
1	Physics International Co, ATTN: Charles Godfrey, 2229 Fourth St, Berkeley 10, Calif
1	Northrop Corporation, Ventura Division, ATTN: Jack Trulio, 1515 Rancho Conejo Blvd, Newbury Park, Calif
1	Stanford Research Institute, ATTN: Dick Fowles, 333 Ravens Wood, Menlo Park, Calif
1	Official Record Copy (Capt Harry E. Auld, WLRS)

UNCLASSIFIED